

UC San Diego

UC San Diego Electronic Theses and Dissertations

Title

Transition Metal Mediated Cycloaromatization of Dienyne and Eneidyne Systems; Chromium Mediated Selective Terminal Alkene Hydrogenation; Chelated Zinc Lewis Acid Co-catalyzed Electrochemical Reduction of Carbon Dioxide by Mn Catalysts

Permalink

<https://escholarship.org/uc/item/7x87c3q1>

Author

Steger, Han

Publication Date

2020

Peer reviewed|Thesis/dissertation

UNIVERSITY OF CALIFORNIA SAN DIEGO

Transition Metal Mediated Cycloaromatization of Dienyne and Eneidyne Systems
Chromium Mediated Selective Terminal Alkene Hydrogenation
Chelated Zinc Lewis Acid Co-catalyzed Electrochemical Reduction of Carbon Dioxide by Mn
Catalysts

A dissertation submitted in partial satisfaction of the requirements for the degree Doctor of
Philosophy

in

Chemistry

by

Han Steger

Committee in charge:

Professor Joseph M. O'Connor, Chair
Professor Carlo Ballatore
Professor Seth M. Cohen
Professor Michael J. Sailor
Professor Emmanuel A. Theodorakis

2020

Copyright
Han Steger, 2020
All rights reserved.

The dissertation of Han Steger is approved, and it is acceptable in quality and form for publication on microfilm and electronically:

Chair

University of California San Diego

2020

DEDICATION

**In recognition of my dearest, royal friend and family member Photon:
A smart, brave, and lovely Australian shepherd.**

EPIGRAPH

“Always show respect to your chemicals.”

- Joseph M. O’Connor. Ph. D.

“There is no failed reaction, only failed work up.”

- Clifford P. Kubiak. Ph. D.

“I never had doubt in you. I know you will make the comeback.”

- Tommaso A. Vannelli. Ph. D.

TABLE OF CONTENTS

SIGNATURE PAGE	iii
DEDICATION	iv
EPIGRAPH.....	v
TABLE OF CONTENTS.....	vi
LIST OF FIGURES	ix
LIST OF SCHEMES.....	xv
LIST OF TABLES	xxi
LIST OF ABBREVIATIONS.....	xxiii
ACKNOWLEDGMENTS	xxiv
CURRICULUM VITA	xxvi
ABSTRACT OF DISSERTATION.....	xxix
Chapter 1 . Introduction: Transition metal complexes in activating conjugated π systems.	1
I. Classic thermal Hopf and Bergman electrocyclization.....	2
II. Lewis acid catalyzed 6 π electrocyclization.....	3
III. Ligand exchange between Ru- η^6 -Arene and RuL ₃	5
IV. Ru(η^4 -cyclobutadiene) leads to a ring expansion reaction via a Ru(η^4 -alkene) intermediate.....	7
V. Cp/Cp* [*] Ru ⁺ (NCMe) ₃ catalyzed triene electrocyclization.	9
VI. Cp* [*] Ru ⁺ (NCMe) ₃ mediated dienyne electrocyclization.....	14
VII. Cp* [*] Ru ⁺ (NCMe) ₃ mediated enediyne electrocyclization.....	16
VIII. Cr(η^6 -naphthalene) triggered Bergman cyclization under ambient temperature.	18
IX. η^6 -Coordinated iridium enables selective aromatic C-H hydroxylation.	20
X. Ru(η^4/η^6 -alkene) complexes in catalyzing alkene linear dimerization.	22
XI. Ru(0) catalyzed alkyne/diene dimerization.....	25
XII. Synthesis and pronation of Rh based η^4 diene-complexes.	29
XIII. Iron(η^4 -diene) complexes and their reactivity.....	31
XIV. References	34
Chapter 2 . Ruthenium complex mediated dienyne electrocyclization at ambient temperature and investigation mechanism.....	37
I. Introduction.....	38

II. Isolation and characterization of Cp*Ru ⁺ (η ⁶ -dienyne) intermediate of TMS substituted dienyne.	41
III. Cycloaromatization of dienyne with phenyl substrates.	45
IV. Photoactivate transition metal triggers for enediyne and dienyne cyclization.....	52
V. Attempt to mediate dienyne cyclization with an iridium complex.	55
VI. Conclusions and Future Outlook	58
VII. Experimental.....	58
VIII. Acknowledgements.	107
IX. References.....	108
Chapter 3 Ambient Temperature Cr(CO)₃(η⁶-naphthalene)-Mediated 1,3-Dien-5-yne	
Cycloaromatization.	110
I. Introduction.....	111
II. Attempts in mediating dienyne cyclization.....	114
III. Mechanistic investigation and kinetic study with Fourier-transform infrared spectroscopy (FT-IR).	118
IV. 2D-IR in determining intermediates.	125
V. Proposed Mechanism.	130
VI. Conclusions and Future work.	131
VII. Experimental.....	132
VIII. Acknowledgments.	150
IX. References.....	150
Chapter 4 . Selective Terminal C-C Double Bond Reduction of Conjugated 1,3-Dien-5-yne in Cr(CO)₃(CH₃CN)₃-Acetone Solution Under Moderate Conditions	
I. Introduction.....	153
II. Hydrogenation of 1,3-Dien-5-yne.	155
III. Investigation in hydrogenation sources.....	158
IV. Study on chromium and solvent.....	161
V. Mechanism.	162
VI. Investigation on various alkene substrates.....	163
VII. Conclusion.	164
VIII. Experimental.	165
IX. Acknowledgement.	191

X. Reference.....	191
Chapter 5 Chelated $[\text{Zn}(\text{cyclam})]^{2+}$ Lewis acid improves the reactivity of the electrochemical reduction of CO_2 by Mn catalysts with bulky bipyridine ligands.....	193
I. Introduction.....	194
II. Synthesis of Mn complex with bulky bipyridine ligand, cyclam and cyclam chelated zinc complexes.....	200
III. Cyclic voltammetry study of Zn catalyzed Mn CO_2 electroreduction system.....	203
IV. Controlled potential electrolysis (CPE) study.....	208
V. Examinations on other cyclam chelated Lewis acid with Mn catalyst.....	209
VI. Conclusions and Future Outlook.....	210
VII. Experimental.....	210
VIII. Acknowledgements.....	230
IX. References.....	230

LIST OF FIGURES

Figure 1-1: Relative electronic energies of the thermal (number above line) and protonated carbonyl group (number below line) electrocyclization pathways computed at the B3LYP/6-31G** level of theory. 1-substituted (left); 2-substituted (mid); 3-substituted (right). ⁶	4
Figure 1-2: Computational studies of Ru accelerated disrotatory triene electrocyclization.	12
Figure 2-1: X-Ray crystal structure of complex 24	43
Figure 2-2: X-Ray crystal structure of complex 35	47
Figure 2-3: Kinetic study of 40E (Top) and 40Z (Bottom) treated with 92 and NCMe-d ₃	50
Figure 2-4: Kinetic study of 40Z treated with 92 and NCMe-d ₃	72
Figure 2-5: Kinetic study of 40Z treated with 92 and NCMe-d ₃ (First 15 min after reaction started).....	73
Figure 2-6: Kinetic study of 40Z treated with 92 and NCMe-d ₃ (Last one hours before reaction is done).....	74
Figure 2-7: Kinetic study of 40Z treated with 92 and NCMe-d ₃	75
Figure 2-8 : Kinetic study of 40E treated with 92 and NCMe-d ₃ (First 15 min after reaction started).....	76
Figure 2-9: Kinetic study of 40E treated with 92 and NCMe-d ₃ (Last hour after reaction is completed).....	77
Figure 2-10: 24 ¹ H NMR spectrum (CDCl ₃ , 400 MHz).	81
Figure 2-11: 24 ¹³ C NMR spectrum (CDCl ₃ , 500 MHz).	82
Figure 2-12: 32 ¹ H NMR spectrum (CDCl ₃ , 400 MHz).	83
Figure 2-13: 32 ¹³ C NMR spectrum (CDCl ₃ , 500 MHz).	84

Figure 2-14: 35 ^1H NMR spectrum (CDCl_3 , 400 MHz).....	85
Figure 2-15: 35 ^{13}C NMR spectrum (CDCl_3 , 500 MHz).....	86
Figure 2-16: 40E ^1H NMR spectrum (CDCl_3 , 400 MHz).	87
Figure 2-17: 40E ^{13}C NMR spectrum (CDCl_3 , 500 MHz).	88
Figure 2-18: 40Z ^1H NMR spectrum (CDCl_3 , 400 MHz).	89
Figure 2-19: 40Z ^{13}C NMR spectrum (CDCl_3 , 500 MHz).	90
Figure 2-20: ^1H NMR spectrum of 49 reacting with 93 (Acetone- d_6 , 400 MHz).	91
Figure 2-21: ^1H NMR spectrum of 51 reacting with 93 (Acetone- d_6 , 400 MHz).	92
Figure 2-22: Initial ^1H NMR spectrum of competition reaction of 22 and 23 reacting with 92 . (CDCl_3 , 400 MHz).....	93
Figure 2-23: Final ^1H NMR spectrum of competition reaction of 22 and 23 reacting with 92 . (CDCl_3 , 400 MHz).....	94
Figure 2-24: Initial ^1H NMR spectrum of competition reaction of 40Z and 40E reacting with 92 . (CDCl_3 , 400 MHz).....	95
Figure 2-25 : Final ^1H NMR spectrum of competition reaction of 40Z and 40E reacting with 92 . (CDCl_3 , 400 MHz).....	96
Figure 2-26 : ^1H NMR spectrum of reaction of 53 reacting with 94 in a mole ratio of 1: 1. (Acetone- d_6 , 400 MHz).....	97
Figure 2-27 : ^1H NMR spectrum of reaction of 53 reacting with 94 in a mole ratio of 10: 1. (Acetone- d_6 , 400 MHz).....	98
Figure 3-1: X-ray crystal structure of 64 , hydrogens atoms are not shown.....	115

Figure 3-2: Proposed mechanism routes and intermediates of Cr mediated diyne electrocyclization.	118
Figure 3-3: FT-IR monitored reaction of 53 with 95 in a 10:1 mole ratio in THF.....	119
Figure 3-4: FTIR spectrum of 95 under ambient atmosphere (yellow), 95 reacting with 53 under ambient air (blue), 95 under N ₂ (green) and CrCO ₆ (red).....	120
Figure 3-5: FTIR monitored reaction of 22 with 95 in a 10:1 mole ratio in THF.	121
Figure 3-6: FTIR monitored reaction of 54 with 95 in a 10:1 mole ratio in 2,5-dimethyltetrahydrofuran.	121
Figure 3-7: Time trace of reactant 95 , intermediate and product 60 . Each component is separated with multivariate analysis for each FTIR spectrum that taken at different time points. Experimental data is then fitted with equation 1, 2, and 3, respectively. Relative concentrations of reactant (a), intermediate (b), and product(c) are plotted as a function of time.	122
Figure 3-8: Time trace of reactant 6-H, intermediate and product 6-Cr-H. Each component is separated with multivariate analysis for each FTIR spectrum that taken at different time points. Experimental data is then fitted with equation 1, 2, and 3, respectively. Relative concentrations of reactant (a), intermediate (b), and product (c) are plotted as a function of time.	125
Figure 3-9: 2D-IR spectrum cut at 1883 cm ⁻¹ fitted with Gaussian function. Intensity as a function of wavenumber. (a) Cr(CO) ₃ (η^6 -naphthalene) peak's anharmonicity is 53 cm ⁻¹ ; (b) 60 peak's anharmonicity is 54 cm ⁻¹ ; (c) One hour of reaction peak's anharmonicity is 66 cm ⁻¹	126
Figure 3-10: 2D-IR spectrum cut at 1960cm ⁻¹ fitted with Gaussian function. Intensity as a function of wavenumber. (a) Reactant peak's anharmonicity is 34 cm ⁻¹ ; (b) 60 peak's anharmonicity is 35 cm ⁻¹ ; (c) One hour of reaction peak's anharmonicity is 40 cm ⁻¹	126
Figure 3-11: Speculative mechanism of 95 mediated diyne cyclization.	130
Figure 3-12: Scheme of the 2D-IR setup in this study.	134
Figure 3-13: ¹ H NMR spectrum of 64 (CDCl ₃ , 400 MHz).....	141
Figure 3-14: ¹³ C NMR spectrum of 64 (CDCl ₃ , 500 MHz).....	142

Figure 3-15: ^1H NMR spectrum of 65 (CDCl_3 , 400 MHz).....	143
Figure 3-16: ^{13}C NMR spectrum of 65 (CDCl_3 , 500 MHz).....	144
Figure 3-17: ORTEP of 64 , SH22_a.....	145
Figure 4-1: ^1H NMR spectrum of 79 (CDCl_3 , 400 MHz).....	172
Figure 4-2: ^{13}C NMR spectrum of 79 (CDCl_3 , 500 MHz).....	173
Figure 4-3: ^1H NMR spectrum of 85 (CDCl_3 , 400 MHz).....	174
Figure 4-4: ^{13}C NMR spectrum of 85 (CDCl_3 , 500 MHz).....	175
Figure 4-5: ^1H NMR spectrum of 80 (CDCl_3 , 400 MHz).....	176
Figure 4-6: ^{13}C NMR spectrum of 80 (CDCl_3 , 500 MHz).....	177
Figure 4-7: ^1H NMR spectrum of 85 (CDCl_3 , 400 MHz).....	178
Figure 4-8: ^{13}C NMR spectrum of 85 (CDCl_3 , 500 MHz).....	179
Figure 4-9: ^1H NMR spectrum of 78 (CDCl_3 , 400 MHz).....	180
Figure 4-10: ^{13}C NMR spectrum of 78 (CDCl_3 , 500 MHz).....	181
Figure 4-11: ^1H NMR spectrum of 84 (CDCl_3 , 400 MHz).....	182
Figure 4-12: ^{13}C NMR spectrum of 84 (CDCl_3 , 500 MHz).....	183
Figure 4-13: ^1H NMR spectrum of 79-<i>d</i>₂ (CDCl_3 , 400 MHz).....	184
Figure 4-14: ^1H NMR spectrum of 85-<i>d</i> (CDCl_3 , 400 MHz).	185
Figure 4-15: ^1H NMR spectrum of 96 heating with acetone in ethyl acetate and the comparison with reference 4-methylpent-3-en-2-one.	186

Figure 4-16: ^1H NMR spectrum of 96 reacting with 1,4-CHD.	187
Figure 5-1: CO_2 content in atmosphere reported by Mauna Loa Observatory on May 12, 2019.	194
Figure 5-2: Equilibrium potential for CO_2 reduction at pH 7 (V° Vs. SHE).	195
Figure 5-3: Schematic of the molecular structure of $[\text{Mn}(\text{mes-bpy})(\text{CO})_3(\text{Br})]$ and $[\text{Mn}(\text{mes-bpy})(\text{CO})_3(\text{MeCN})]^+$	195
Figure 5-4: Left: Cyclic voltammograms (CVs) showing catalytic current for 1 mM $[\text{Mn}(\text{mesbpy})(\text{CO})_3(\text{MeCN})](\text{OTf})$ under CO_2 with added MeOH (red). This current increase is due solely to the electrocatalytic reduction of CO_2 to CO. Under N_2 with added MeOH.	196
Figure 5-5: Saveant reported CVs of TPPFe(III)Cl in DMF with various Lewis acids.	197
Figure 5-6: Saveant reported mechanism of TPPFe(III)Cl in DMF with various Lewis acids.	197
Figure 5-7: Fujita reported CV of $[\text{Ru}(\text{bpy})_2(\text{CO})\text{Cl}]^-$ in CH_3CN . Solid line: under Ar; dotted line: under CO_2 ; top: with Pr_4NClO_4 ; bottom: with LiClO_4	198
Figure 5-8: Sampson reported CVs of 1 mM $[\text{Mn}(\text{mesbpy})(\text{CO})_3(\text{MeCN})](\text{OTf})$ under CO_2 with varying concentrations of Mg^{2+} , showing electrocatalytic reduction of CO_2	198
Figure 5-9: Proposed catalytic mechanism of $[\text{Mn}(\text{mesbpy})(\text{CO})_3]$ with CO_2 and Mg^{2+} at -1.5 V versus $\text{Fc}^{+/0}$, showing an overall catalytic reaction of $2\text{CO}_2 + 2e^- \rightarrow \text{CO} + \text{CO}_3^{2-}$	199
Figure 5-10: X-Ray crystal structure of the main isomers of 5-12 (left) and 5-13 (right).	202
Figure 5-11: Left: CVs of 10 mM of 5-13 under Ar (blue), under CO_2 (red) in acetonitrile. Right: CVs of 1 mM 5-4 under CO_2 with varying concentrations of 5-13 , showing electrocatalytic reduction of CO_2	203
Figure 5-12: Left: CVs of 1 mM 5-4 with 10 mM of 5-12 under Ar (black), with 10 mM of 5-12 under CO_2 (blue). 10 mM 5-12 under CO_2 is shown in gray. Right: CVs of 1 mM 5-4 under CO_2 with free Zn^{2+} ($\text{Zn}(\text{BF}_4)_2$).	204

Figure 5-13: CVs of 1 mM 5-4 (left) or 5-5 (right) under CO ₂ with varying concentrations of 5-12 , showing electrocatalytic reduction of CO ₂	205
Figure 5-14: CVs of 1 mM 5-4 (left) and 5-5 (right) under Ar with varying concentrations of 5-12	205
Figure 5-15: CV of 1 mM of 5-5 with 30 mM of 5-12 under CO ₂ (left) and under N ₂ without a substrate (right) in 0.1 M TBAPF ₆ /MeCN at various scan rates (0.1 – 3.4 V/s).	207
Figure 5-16: CPE current density over time for 0.5 mM of 5-5 under CO ₂ with 30 mM of 5-12 . Conditions: potential = -1.6 V vs. Fc ⁺⁰	208
Figure 5-17: CVs of 1 mM Mgcyclam (top left), Bacyclam (top right) or Cacyclam (bot) under CO ₂ with varying concentrations of 5-12 , showing electrocatalytic reduction of CO ₂	209
Figure 5-18: 5-3 ¹ H NMR spectrum (CDCl ₃ , 300 MHz).....	216
Figure 5-19: 5-4 ¹ H NMR spectrum (CD ₃ CN, 300 MHz).....	217
Figure 5-20: 5-12 ¹ H NMR spectrum (CD ₃ CN, 300 MHz).....	218
Figure 5-21: 5-12 ¹⁵ N NMR spectrum (CD ₃ CN, 300 MHz).....	219
Figure 5-22: ORTEP of 5-12	220

LIST OF SCHEMES

Scheme 1-1: Proposed mechanism for thermal cycloaromatization of dienyne.....	2
Scheme 1-2: Proposed mechanism for thermal cycloaromatization of enediyne.	2
Scheme 1-3: Lewis acid catalyzed electro cyclization of 1-8 and 1-9 to yield 1-10 and 1-11 under moderate thermal conditions.....	4
Scheme 1-4: Thermal arene exchange in coordination solvent.....	5
Scheme 1-5: Equilibrium reaction of 1-12 with 1-naphthylammonium cation.	6
Scheme 1-6: The pH-controlled haptotropic rearrangement.....	6
Scheme 1-7: Ring expansion reaction triggered with Ru- η^4 -cyclobutadiene with the addition of alkene and alkyne.....	8
Scheme 1-8: Proposed mechanism for ruthenium-promoted dehydrocycloaromatizations.....	9
Scheme 1-9: Electrocyclization of 1-30ZZ , EZ and EE	9
Scheme 1-10: Observation of reactive intermediates in triene 1-30ZZ and 1-30EE cyclization promoted by CpRu ⁺ (NCMe) ₃	10
Scheme 1-11: Observation of reactive intermediates in triene 1-30EZ cyclization promoted by CpRu ⁺ (NCMe) ₃	11
Scheme 1-12: Ru catalyzed triene 1-37ZE and 1-37ZZ electrocyclization.	12
Scheme 1-13: Cp* ⁺ Ru ⁺ (NCMe) ₃ mediated dienyne cyclization.	14
Scheme 1-14: Cp* ⁺ Ru ⁺ (NCMe) ₃ triggered cycloaromatization of 1-chlorodienynes.....	14
Scheme 1-15: Cp* ⁺ Ru ⁺ (NCMe) ₃ triggered cycloaromatization of 2-methyldienynes.....	15

Scheme 1-16: Cp*Ru ⁺ (NCMe) ₃ triggered cycloaromatization of enediynes.....	16
Scheme 1-17: Isotopic study Cp*Ru ⁺ (NCMe) ₃ triggered cycloaromatization of enediynes.	17
Scheme 1-18: Proposed key intermediates in ruthenium triggered enediyne cyclization.....	17
Scheme 1-19: Bergman cyclization triggered by Cr(CO) ₃ (naphthalene) under ambient temperature.	18
Scheme 1-20: Two proposed mechanistic pathways in Cr triggered Bergman cyclization.....	19
Scheme 1-21: Proposed product when reacting with bulky terminal alkyne substituents.	19
Scheme 1-22: Synthetic cycle for oxidation of benzene to phenol.	20
Scheme 1-23: C-O bond formation via η ⁵ -cyclohexadienyl adducts.	21
Scheme 1-24: Cp*Ru(η ⁴ -diene) triggered conjugated alkene dimerization.	22
Scheme 1-25: Ru(η ⁴ -1,5-cod)(η ⁶ -1,3,5-cot) catalyzes butadiene and methyl acrylate dimerization.	22
Scheme 1-26: Cp/Cp*Ru(η ⁴ -1,5-cod) in triggering alkene/diene liner dimerization (top) and allene /conjugated ketone dimerization (bot).....	23
Scheme 1-27: Oxidative coupling mechanism of [Ru(η ⁶ -naphthalene)(η ⁴ -1,5-cod)] catalyzed alkene dimerization.....	24
Scheme 1-28: Heating Ru(η ⁴ -1,5-cod)(η ⁶ -1,3,5-cot) results the formation of Ru ²⁺ (η ⁵ -cyclooctadienyl) ₂	24
Scheme 1-29: Ru(η ⁴ -1,5-cod)(η ⁴ -cisdiene)(NCMe) complex in triggering diene dimerization (top) and diene/acrylate dimerization (bot).....	25
Scheme 1-30: Proposed mechanism of Ru(0) triggered diene/alkyne dimerization.....	26

Scheme 1-31: Proposed mechanism of two β hydride elimination pathways influenced by the addition of NCMe.	27
Scheme 1-32: Reaction between complex 1-102 and 1-104 with methyl penta-2,4-dienoate.	28
Scheme 1-33: Oxidative coupling of asymmetrical terminal alkyne with diene.	28
Scheme 1-34: Synthesis of Rh(I)(η^4 -diene) complex 1-109 and 1-111	29
Scheme 1-35: Complex 1-109 and its isomer 1-111 isomerizes differently in acidic conditions.	29
Scheme 1-36: Complex 1-114 isomerizes differently in acidic conditions.	30
Scheme 1-37: η^4 Complex 1-116 produces η^3 complex 1-117 under acidic condition.....	31
Scheme 1-38: Mechanism of η^4 Complex 1-118 produces η^3 complex 1-117 under acidic condition.	31
Scheme 1-39: Selective synthesis of Fe-2,5-dihydranisole complexes.....	32
Scheme 1-40: Selective synthesis of ester substituted Fe-cyclo-2,5-diene complexes.....	32
Scheme 1-41: Nucleophilic substitution and alkylation mediated by Fe-cyclo-2,5-diene complexes.	33
Scheme 2-1: Proposed mechanism of thermal Hopf cyclization.	38
Scheme 2-2: Proposed mechanism of thermal Bergman cyclization.	38
Scheme 2-3: Two proposed mechanism of Ru mediated Hopf cyclization.	39
Scheme 2-4: Proposed mechanism of Ru mediated Bergman cyclization.....	40
Scheme 2-5: Proposed electrocyclization of dienyne 22 and 23	41
Scheme 2-6: Synthesis of dienyne 22 from cyclohexanone.....	42

Scheme 2-7: Synthesis of dienyne 32 from cyclohexanone.....	45
Scheme 2-8: Possible products of the reaction between dienyne 23 and Cp*Ru ⁺	46
Scheme 2-9: Speculative product between dienyne 23 and 2 mole eq. Cp*Ru ⁺ (NCMe) ₃ after three days.	46
Scheme 2-10: Synthesis of 40-Z and 40-E	48
Scheme 2-11: 40-E and 40-Z undergoes electrocyclization to generate the same arene product 43	48
Scheme 2-12: Proposed mechanism of 40-E and 40-Z cyclization mediated by the Ru complex.	51
Scheme 2-13: Synthesis of 48 , 49 and 50	52
Scheme 2-14: Cp*Ru ⁺ (η ⁶ -naphthalene) complex serves as photoactivated Bergman cycloaromatization triggers.....	53
Scheme 2-15: Attempted cyclization of 48 , 49 and 50 with Cp*Ru ⁺ (η ⁶ -naphthalene).....	54
Scheme 2-16: An example of Ir complex activating: Synthetic cycle for oxidation of benzene to phenol.....	55
Scheme 2-17: Speculative product after reacting 54 with Cp*Ir ²⁺ (NCMe) ₃ in a 10:1 mole ratio.	57
Scheme 3-1: Top: Thermal Hopf/dienyne cyclization under. Bot: Thermal Bergman/enediyne cyclization.	111
Scheme 3-2: Speculative mechanism of Cp*Ru ⁺ (η ⁶ -dienyne) mediated dienyne cyclization reported by O'Connor's group. (PF ₆ - Counterions Not Shown).	111
Scheme 3-3: Bergman cyclization triggered by Cr(CO) ₃ (naphthalene) under ambient temperature.	112

Scheme 3-4: Two proposed mechanistic pathways in Cr triggered Bergman cyclization.	112
Scheme 3-5: 93 mediated electrocyclization of 49 and 54	114
Scheme 3-6: Synthesis of 62 , 63 and 93 mediated electrocyclization.	115
Scheme 3-7: 93 mediated electrocyclization of 66	116
Scheme 3-8: Cr(CO) ₃ (η^6 -dienyne) mediated electrocyclization of 32	116
Scheme 3-9: 22 and 23 failed to cyclize when reacting with Cr(CO) ₃ (η^6 -dienyne).	117
Scheme 3-10: Proposed mechanism routes and intermediates of Cr mediated dienyne electrocyclization.	118
Scheme 4-1: Dienyne cyclization triggered with Ru and Cr complex demonstrated in O'Connor lab's previous work.	153
Scheme 4-2: Alkene reduction facilitated by Cr complex in previously reported work.	154
Scheme 4-3: 96 facilitates alkene hydrogenation of 62	155
Scheme 4-4: 96 facilitates alkene hydrogenation of 22 and 32	155
Scheme 4-5: 96 facilitates alkene hydrogenation of 54	156
Scheme 4-6: 96 facilitates alkene hydrogenation of 82	156
Scheme 4-7: 96 facilitates alkene hydrogenation and tautomerization of dienyne.	157
Scheme 4-8: Synthesis of 22-d₂ and 87	158
Scheme 4-9: Hydrogenation of 22 in acetone- <i>d</i> ₆	159
Scheme 4-10: Speculative mechanism of the hydrogenation reaction of dienyne.	162

Scheme 4-11: Attempted reactions of treating 96 with other organic compounds with unsaturated carbon bonds.	163
Scheme 5-1: Synthesis of 6,6'-Dimesityl-2,2'-bipyridine.	200
Scheme 5-2: Synthesis of $[\text{Mn}(\text{mes-bpy})(\text{CO})_3(\text{Br})]$ and $[\text{Mn}(\text{mes-bpy})(\text{CO})_3(\text{MeCN})]^+$	200
Scheme 5-3: Synthesis of cyclam 5-11	201
Scheme 5-4: Synthesis of $[\text{Zn}(\text{cyclam})]^{2+}$ complexes with a variety of counterions (BF_4 , 5-12 and Tosyl, 5-13).	201

LIST OF TABLES

Table 2-1: Structure of the Cp*Ru(η^6 -dienyne) 24 and selective ^1H NMR resonances.	43
Table 2-2: Speculative product after reacting 54 with Cp*Ir $^{2+}$ (NCMe) $_3$ in a 1:1 mole ratio and selective ^1H NMR resonances.....	56
Table 2-3: Crystal data and structure refinement for 24	100
Table 2-4: Fractional Atomic Coordinates ($\times 10^4$) and Equivalent Isotropic Displacement Parameters ($\text{\AA}^2 \times 10^3$) for 24 . U_{eq} is defined as 1/3 of the trace of the orthogonalised UIJ tensor.....	101
Table 2-5: Anisotropic Displacement Parameters ($\text{\AA}^2 \times 10^3$) for 24	102
Table 2-6: Bond Lengths for 24	103
Table 2-7: Bond Angles for 24	104
Table 2-8: Hydrogen Atom Coordinates ($\text{\AA} \times 10^4$) and Isotropic Displacement Parameters ($\text{\AA}^2 \times 10^3$) for 24	106
Table 3-1: Calculated bond length (\AA) and bond angle ($^\circ$) of Cr-dienyne intermediate XIII . ..	127
Table 3-2: Calculated bond length (\AA) and bond angle ($^\circ$) of Ru-dienyne intermediate 69	128
Table 3-3: Crystal data and structure refinement for 64	146
Table 3-4: Fractional Atomic Coordinates ($\times 10^4$) and Equivalent Isotropic Displacement Parameters ($\text{\AA}^2 \times 10^3$) for 64 . U_{eq} is defined as 1/3 of the trace of the orthogonalized U_{IJ} tensor.	147
Table 3-5: Anisotropic Displacement Parameters ($\text{\AA}^2 \times 10^3$) for 64 . The Anisotropic displacement factor exponent takes the form: $-2\pi^2[h^2a^*2U_{11}+2hka^*b^*U_{12}+\dots]$	148

Table 3-6: Bond Lengths for 64	149
Table 3-7: Hydrogen Atom Coordinates ($\text{\AA} \times 10^4$) and.....	149
Table 4-1: Product yield of 78 obtained by treating 84 and $\text{Cr}(\text{NCMe})_3(\text{CO})_3$ with a variety of solvent. Reaction time: 16 h; Reaction temperature: 70 °C.....	160
Table 4-2: Hydrogenation and tautomer product yield at various reaction times.....	188
Table 4-3: Hydrogenation and tautomer product yield with various substrate to Cr mole ratios.	189
Table 4-4: Hydrogenation product yield with various hydrogen sources.....	190
Table 5-1: Result of CPE experiments with 5-12 added. Performed under CO_2 with 1 mM of cat. 5-4 or 5-5 and 30 mM of 5-12 . Potentials are reported vs. $\text{Fc}^{+/0}$	208
Table 5-2: Crystal data and structure refinement for 5-22	221
Table 5-3: Atomic coordinates ($\times 10^4$) and equivalent isotropic displacement parameters ($\text{\AA}^2 \times 10^3$) for 5-22 . $U(\text{eq})$ is defined as one third of the trace of the orthogonalized U_{ij} tensor.	222
Table 5-4: Bond lengths [\AA] and angles [$^\circ$] for 5-22	222
Table 5-5: Anisotropic displacement parameters ($\text{\AA}^2 \times 10^3$) for 5-22 . The anisotropic	228
Table 5-6: Hydrogen coordinates ($\times 10^4$) and isotropic displacement parameters ($\text{\AA}^2 \times 10^3$).....	229

LIST OF ABBREVIATIONS

Alphabetical within Category

Chemical Abbreviations

1,4 – CHD: 1, 4-cyclohexadiene
Cp: cyclopentadienyl
CP*: pentamethylcyclopentadienyl
D/-d: deuterium
DCM: dichloromethane
DMF: N,N-dimethylformamide
IPA: isopropyl alcohol

Me: methyl, -CH₃
Et: ethyl, -CH₂CH₃
NBS: N-bromosuccinimide
OAc: acetate, -OC(O)CH₃
OTf: triflate, -OS(O)CF₃
-Ph: phenyl, -C₆H₅
nPr: n-propyl, -CH₂CH₂CH₃

THF: tetrahydrofuran
TMS: trimethylsilyl

Parameter Units

Å: Angstrom
°C: degree Celsius

h: hour
Hz: Hertz
Cal: calorie
cm⁻¹ : wavenumber
eV: electron volt
K: Kelvin
L: liter
M: molar
m: meter
mol: mole
ppm: parts per million

Experimental/ Spectroscopic

ΔG^0_{rxn} : standard reaction energy
 δ : chemical shift
 η^x : x atoms π bound to metal
 λ : wavelength
 σ_{meta} : substituent constant meta
A: conformational energy
APCI: atmospheric pressure chemical ionization
COSY: correlation spectroscopy
CV: cyclic voltammetry
CPE: control potential electrolysis
d: doublet
DR: diastereomeric ratio
ESI: electrospray ionization
FT-IR: fourier transform infrared spectroscopy
2D-IR: 2-dimension infrared spectroscopy
h ν : ultraviolet radiation
J: coupling constant
KIE: kinetic isotope effect
m: multiplet
NMR: nuclear magnetic resonance spectroscopy
p: pentet
q: quartet
RDS: rate determining step
rt: room temperature
s: singlet
t: triplet
TLC: thin layer chromatography
TOF: turn over frequency
TON: turnover number
UV: ultraviolet radiation

ACKNOWLEDGMENTS

I would like to sincerely thank my thesis advisor Prof. Joseph O'Connor for his guidance throughout my Ph.D. study in his group. I would also like to thank my thesis committee members: Prof. Michael Sailor, Prof. Seth Cohen, Prof. Emmanuel Theodorakis and Prof. Carlo Ballatore for their insightful help and suggestions. Prof. Charles Perrin is thanked for his helpful discussions and advice during group meetings and conversations. Prof. Clifford Kubiak is thanked for his mentorship when I was studying in his group for the first two years at UCSD.

Dr. Curtis Moore, Dr. Milan Gembicky and Prof. Arnold Rheingold are acknowledged for acquisition of data for X-ray structures. Dr. Yongxuan Su is acknowledged for acquisition of MS data. Dr. Anthony Mrse is acknowledged for assistance with acquisition of NMR data. Prof. Kim Baldrige is acknowledged for her help in obtaining computation data. Prof. Wei Xiong is acknowledged for the guidance in IR studies. Dr. Shrinidhi Annadka is thanked for his collaboration in material presented in chapter 4.

Prof. Tommaso Vannelli and Prof. David Rider are thanked for their guidance throughout my undergraduate study and continuous support throughout my graduate career. Dr. Pengjin Qin, LiAn Wang, Yifan Li and Dr. Pauline Olsen are thanked for their support and as companions in O'Connor's lab. I also must thank all the teachers that have taught or mentored me during the past 22 years in my life.

Finally, without my family members: Arthur Steger (Father), Wen Wang (Mother), and my Australian shepherd, Photon and the Shiba inu, Yoshi's companionship and support, none of this would have been possible.

The material in Chapter 2, in part, has been published in *Organometallics* in 2017 with following authors: Qin, P.; Cope, S. K.; Steger, H.; Veccharelli, K.; Holland, L. R.; Hitt, M. D.; Moore, E. C.; Baldrige, K. K and O'Connor, M. J. The rest of the materials are currently under preparation for two publications with the following authors: Qin, P.; Steger, H.; O'Connor, M. J.; Baldrige, K. K. Cope, S. K. and Hitt, D. M. Qin, P.; Steger, H.; Baldrige, K. K.; O'Connor, M. J.

The material in Chapter 3, is currently under preparation for publication with the following authors: Steger, H.; Chen, L; Baldrige, K. K.; Xiong, W.; O'Connor, J. M. The dissertation author was the primary investigator and author of this material.

The material in Chapter 4 is currently under preparation for publication with the following authors: Steger, H.; Shrinidhi, A.; O'Connor, J. M. The dissertation author was the primary investigator and author of this material.

The material in Chapter 5, has been published in *Dalton Trans* in 2017 with the following authors: Zhanaidarova, A.; Steger, H.; Reineke, H. M.; Kubiak, C. P. The dissertation author was the primary investigator and author of this material.

CURRICULUM VITA

Education:

2015 - 2020: **Chemistry Ph.D.**
University of California San Diego
Degree received on December 2020.

2011 - 2015: **Chemistry B.S.**
Western Washington University, WA
Degree received on June 2015.

Research Experiences:

2017 – Present: **Graduate Research Assistant**
Department of Chemistry and Biochemistry,
University of California San Diego, CA
Principal Investigator: Dr. Joseph M. O'Connor
Worked on metal (Ru, Cr, Mo, W, Ir, Fe) triggered Bergman (enediynes) and Hopf (dienynes) cyclization at ambient temperature and selective alkene hydrogenation.
Key words: Organic synthesis, Organometallics, Photochemistry.

2015 - 2017: **Graduate Research Assistant**
Department of Chemistry and Biochemistry,
University of California San Diego, CA
Principal Investigator: Dr. Clifford P. Kubiak

- Worked on a chelated Zn complex as Lewis acid cocatalyst that improved reactivity of the electrochemical reduction of CO₂ by Mn catalysts with bulky bipyridine ligands.

Key words: Electrochemistry, Ligand design, CO₂ reduction.

2012 - 2015: **Undergraduate Research Assistant**
Department of Chemistry,
Western Washington University, WA
Principal Investigator:
Dr. Tommaso A. Vannelli
Dr. David A. Rider

- Worked on a surface polar gas sensing film by employing layer-by-layer self-assembly deposition on polystyrene substrate.

Key words: Surface chemistry, chemical sensing, nanoparticles.

Teaching Experiences:

Chem 6A (General Chemistry I): Fall 2015, Spring 2019, Winter 2019, Summer 2019
Chem 6B (General Chemistry II): Winter 2017
Chem 6C (General Chemistry III): Spring 2018
Chem 40A (Organic Chemistry I): Fall 2017, Fall 2018, Spring 2019

Chem 40B (Organic Chemistry II): Winter 2015, Spring 2017
Chem 7L (General Chemistry Laboratory): Fall 2015, Spring 2017
Chem 143A (Organic Chemistry Laboratory): Spring 2018

Awards and Scholarships:

Scholarships: 2014 Western Foundation Academic Excellence Scholarship
2014 American Associate of University Women Scholarship
2014 Knapman Chemistry Scholarship
2014 Multicultural Achievement Program Scholarship
2013 Knapman Chemistry Scholarship
2013 Whatcom Education Credit Union Scholarship
2011 August and Carol Radke Scholarship
2011 Leadership Advantage Annual Scholarship

Awards: 2014 WWU Research and Creative Opportunity for Undergraduates Grant
2013 WWU Research and Creative Opportunity for Undergraduates Grant
2012 WWU Most Outstanding Chemistry Student

Publications:

1. Steger, H.; Chen, L.; Xiong, W.; O'Connor, M. J. "Cr(CO)₃(η⁶-naphthalene) mediated 1,3-Dien-5-yne aromatization at ambient temperature." Manuscript under preparation.
2. Steger, H.; Shrinidhi, A.; O'Connor, M. J. "Selective Terminal C-C Double Bond Reduction of Conjugated 1,3-Dien-5-yne in Cr(CO)₃(CH₃CN)₃-Acetone Solution Under Moderate Conditions." Manuscript under preparation.
3. Qin, P.; Steger, H.; O'Connor, M. J.; Baldrige, K. K. Cope, S. K. "Ruthenium-Accelerated Cycloisomerization of Phenyl Substituted Conjugated Dienes." Manuscript under preparation.
4. Hitt, D. M. Qin, P.; Steger, H.; Baldrige, K. K.; O'Connor, M. J. "Ambient Temperature Aitken Cycloisomerization of Dienes: Partitioning between Hopf and Aitken Pathways." Manuscript submitted.
5. Qin, P.; Cope, S. K.; Steger, H.; Veccharelli, K.; Holland, L. R.; Hitt, M. D.; Moore, E. C.; Baldrige, K. K. O'Connor, M. J. "Photoactivated Transition-Metal Triggers for Ambient Temperature Ene-yne and Diene-yne Cyclization: Ruthenium-η⁶-Naphthalene Complexes." *Organometallics*. **2017**, 36, 3967-3973.
6. Zhanaidarova, A.; Steger, H.; Reineke, H. M.; Kubiak, C. P. "Chelated [Zn(cyclam)]²⁺ Lewis acid improves the reactivity of the electrochemical reduction of CO₂ by Mn catalysts with bulky bipyridine ligands." *Dalton Trans*, **2017**, 46, 12413-12416.

Presentations:

1. Chromium-triggered cyclization and selective alkene hydrogenation of conjugated dienes (Oral). 258th ACS National Meeting, San Diego, CA, August 2019.

2. Chelated Zinc cyclam as cocatalyst in electrochemical reduction of CO₂ by Mn catalyst (Oral). Southern California Inorganic Photophysics (SCIP), Catalina Island, CA, September 2016.
3. Develop a solid-state CO₂ sensor applying Layer-by-Layer deposition on unfunctionalized polystyrene (Poster). 2014 ACS Undergraduate Research Symposium, Puget Sound, WA, April 2014.

Other Scholarly Outreach and Activities:

1. O'Connor Laboratory Safety Coordinator (2018–2020).
2. Mentor in UCSD Chemistry Department ChemPAL program (2016-2017).
Reached out to incoming chemistry undergraduates and help them with schoolwork and career.
3. Mentor in ENLACE program at UCSD (2018-2019).
Mentored two high schoolers complete scientific projects in O'Connor lab. 2018 Summer and 2019 Summer.

Other Working Experiences:

2012-2015

Financial Aid Advisor

Financial Aid Services Center,
Western Washington University, WA
Supervisor: Barbara Luton

- Advised parents and students organize and prepare their financial aid packages.

2011-2014

Electronic Repair Technician

MriFixit (Blair's Repair)
424 West Bakerview Rd, Bellingham, WA
Supervisor: Jon Hooper

- Fixed mostly iPhone, iPod, Mac and PC including data recovering, virus wiping, hardware and software installing.

ABSTRACT OF DISSERTATION

Transition Metal Mediated Cycloaromatization of Dienyne and Eneidyne Systems
Chromium Mediated Selective Terminal Alkene Hydrogenation
Chelated Zinc Lewis Acid Co-catalyzed Electrochemical Reduction of Carbon Dioxide by Mn
Catalysts

by

Han Steger

Doctor of Philosophy in Chemistry

University of California San Diego 2020

Professor Joseph M. O'Connor, Chair

This work started with a thorough review on current study in activating conjugate alkene or alkyne system with metal complexes. The insightful research on various metal coordinated η^6 , η^4 and η^2 complexes provided us with concrete references in resolving metal mediated

electrocyclizations. With these studies we proposed many interesting hypotheses and investigated and produced novel research results.

In chapter 2, we continued investigating the Cp*Ru⁺L₃ triggered electrocyclization. We successfully isolated and characterized the first Cp*Ru(η^6 -dienyne) complex, which was believed to be the crucial intermediate during the electrocyclization. Further study was carried out with a focus on phenyl substituted dienyne substrates. We confirmed the coordination priority and resolved an isomerization within its mechanism. We then ameliorated the ruthenium complex with a naphthalene ligand to achieve a control on the para-diradical formation with photon activation. Lastly, we presented an interesting and unexpected result when replacing the Ruthenium metal center with Iridium in reacting with dienyne substrate.

In chapter 3, we report a chromium complex mediator, Cr(CO)₃(η^6 -naphthalene), that mediates the traditional thermal dienyne cyclization at ambient temperature. Successful cycloaromatizations were observed to proceed to moderate yield in coordination. Further mechanistic study was undertaken by monitoring $\nu(\text{CO})$ stretching via infrared (IR) spectroscopy. A speculative Cr(CO)₃(η^6 -dienyne) intermediate was observed using 2D-IR spectroscopic analysis and coanalysis.

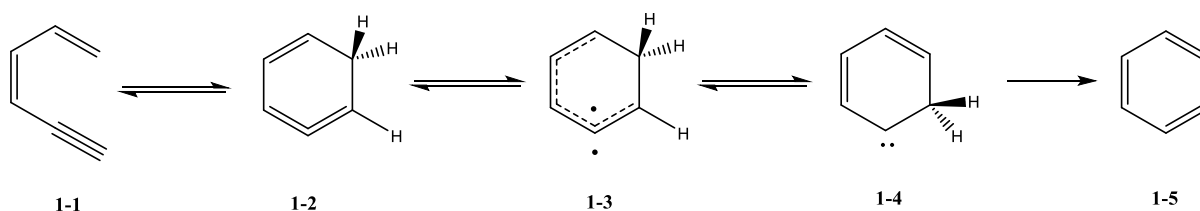
In chapter 4, we report a newly discovered alkene reduction reaction mediated by tris(acetonitrile)tricarbonylchromium in acetone. While attempting to effect chromium-mediated thermal cycloaromatization of dienyne, we discovered that, in a homogeneous tris(acetonitrile)tricarbonylchromium-acetone solution system, a highly selective reduction of a less hindered terminal alkene can be achieved without the source of hydrogen. A further mechanistic study has confirmed that hydrogen was provided by the solvent, acetone. Therefore, we present an attempt to elucidate its mechanism.

In chapter 5 reports the use of a soluble Lewis acid complex, $[\text{Zn}(\text{cyclam})]^{2+}$ (cyclam = 1,4,8,11-tetraazacyclotetradecane) as a co-catalyst coupled with $\text{Mn}(\text{Mesbpy})(\text{CO})_3\text{Br}$ (Mesbpy = 6,6'-dimesityl-2,2'-bipyridine) for the electrochemical reduction of CO_2 to CO. Utilization of the soluble chelated Lewis acid avoids the use of sacrificial additives and prevents the formation of insoluble products such as MgCO_3 or ZnCO_3 that change the thermodynamics of the CO_2 reduction. The use of soluble Lewis acids greatly improves catalysis compared to previously reported systems that used sacrificial anodes.

**Chapter 1 . Introduction: Transition metal complexes in activating
conjugated π systems.**

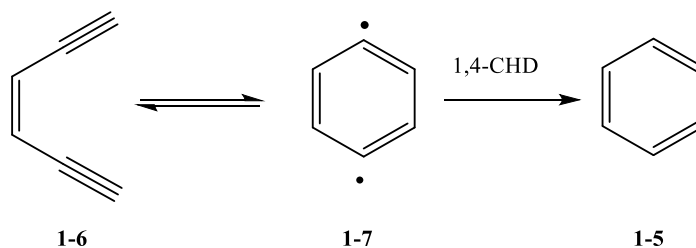
I. Classic thermal Hopf and Bergman electrocyclization.

Traditional thermal dienyne cyclization was first reported by Hopf in 1969.¹ Under a high temperature, 274 °C, dienyne cyclizes to yield aromatized benzene derivative product via an electrocyclization pathway. A commonly accepted mechanism supported by computational and experimental studies suggests that, *cis*-hexa-1,3-dien-5-yne (**1-1**) first undergoes a 6π -electrocyclization to isobenzene intermediate (**1-2**) followed by the generation of a diradical intermediate (**1-3**). Then it undergoes a [1,2] hydride shift to yield a singlet diradical intermediate (**1-4**). The final cyclized benzene product (**1-5**) is produced through a secondary [1,2] hydride shift (Scheme 1-1).²



Scheme 1-1: Proposed mechanism for thermal cycloaromatization of dienyne.

A similar cyclization, Bergman cyclization, describes a cyclization of enediyne to yield benzene product. Under a similarly high temperature, 300 °C, electrocyclization of *cis*-hexa-3-en-1,5-diyne (**1-6**) yields a benzene diradical intermediate **1-7**. With the presence of a hydrogen donor,



Scheme 1-2: Proposed mechanism for thermal cycloaromatization of enediyne.

1,4-CHD, a two-step hydrogen extraction occurs to generate the final aromatized benzene product from the enediyne substrate (Scheme 1-2).³

Although both cyclization reactions provided a reliable way to produce an aromatic product and its derivatives, a limitation of applications of thermal Hopf and Bergman cyclization remains due to the high temperature.⁴

A variety of methods for lowering the energy barrier have been studied. Transition metal containing groups that interfere with the highly delocalized system, ML_n , offer a promising potential. Nicolaou's work pointed out that reaction temperature is tightly associated with the alkyne termini distance in Bergman cyclization.⁵ A key fragment that has been mentioned repeatedly in previous literature is an $\eta^n-M-\pi$ ($n = 2, 4$ or 6) complex that significantly lowers the cyclization activation energy barrier by lowering the C_1-C_6 distance. However, we have not yet confirmed the role of $\eta^n-M-\pi$ complex is playing in Bergman/Hopf cyclization and how the coordination environment affects the reaction mechanism. Thus, the purpose of this review is to highlight the current research highlights of $\eta^n-M-\pi$ complexes and their roles in activating the conjugated π system towards a better understanding of metal mediated cyclization mechanism.

II. Lewis acid catalyzed 6 π electrocyclization.

It was demonstrated that in a conjugated triene system, the rate of electrocyclization can be varied by varying the electronics of the substituents.⁶ The activation energy barrier can be significantly lowered by having an electron withdrawing group on the substrate. Furthermore,

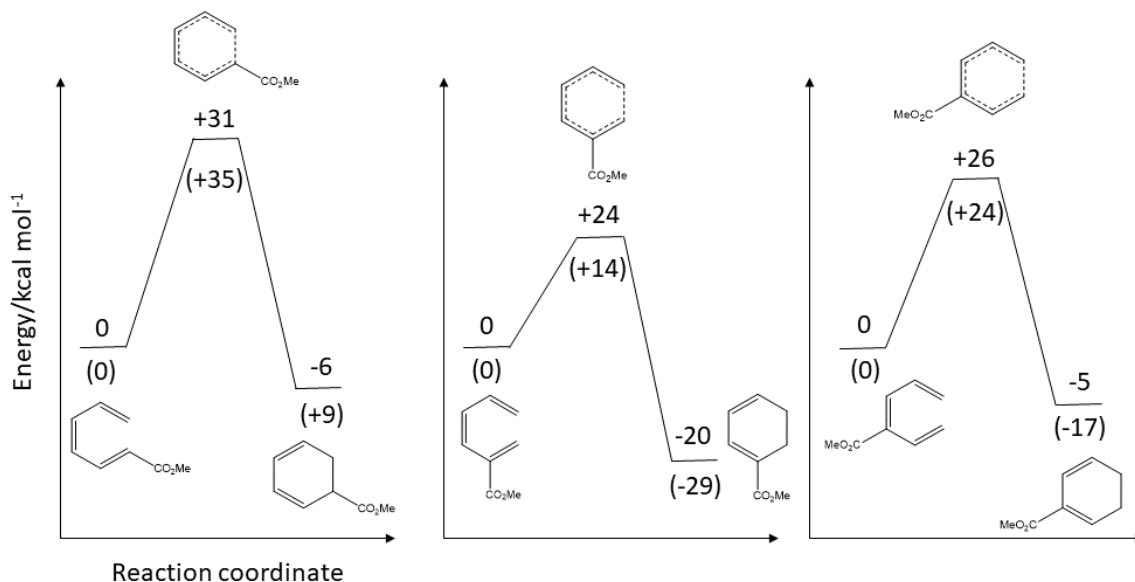
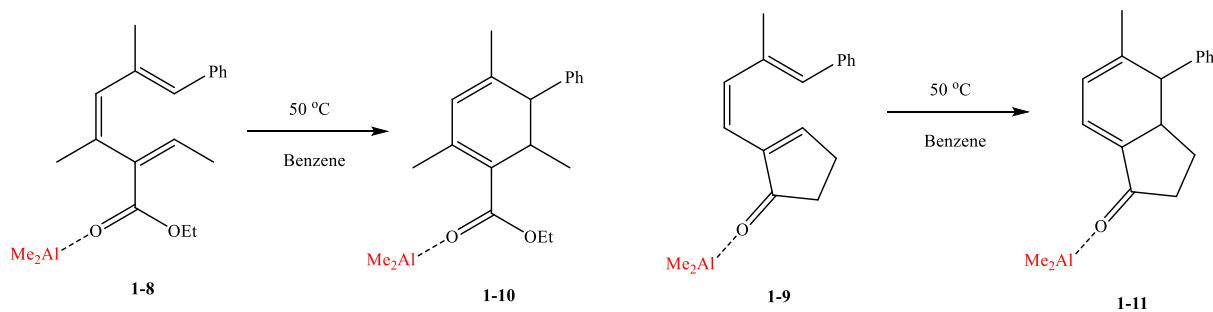


Figure 1-1: Relative electronic energies of the thermal (number above line) and pruned carbonyl group (number below line) electrocyclization pathways computed at the B3LYP/6-31G** level of theory. 1-substituted (left); 2-substituted (mid); 3-substituted (right).⁶

Bergman's group reported that a DFT calculation shows that having a methyl ester pruned on the 2-position can lower the energy barrier by 10 kcal/mol, in comparison to 1 and 3 position substitution (Figure 1-1).⁵

Using triene substrate **1-8** and **1-9** as the examples, Lewis acids accelerated the disrotatory cyclization under thermal conditions to yield **1-10** and **1-11**, respectively (Scheme 1-3). Among a variety of Lewis acids within the study, Me_2AlCl tended to give the best catalytic performance. NMR studies indicated a favorable 1:1 binding at approximately one equivalent of Me_2AlCl to **1-**

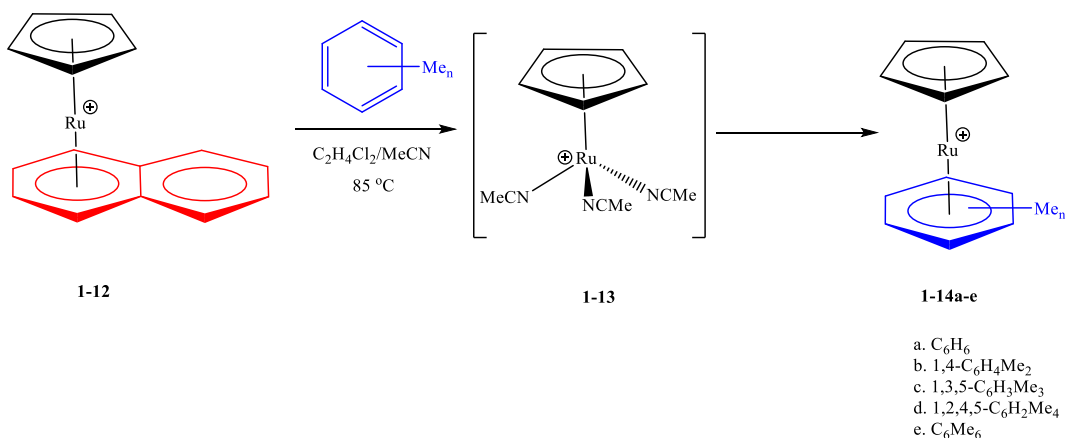


Scheme 1-3: Lewis acid catalyzed electro cyclization of **1-8** and **1-9** to yield **1-10** and **1-11** under moderate thermal conditions.

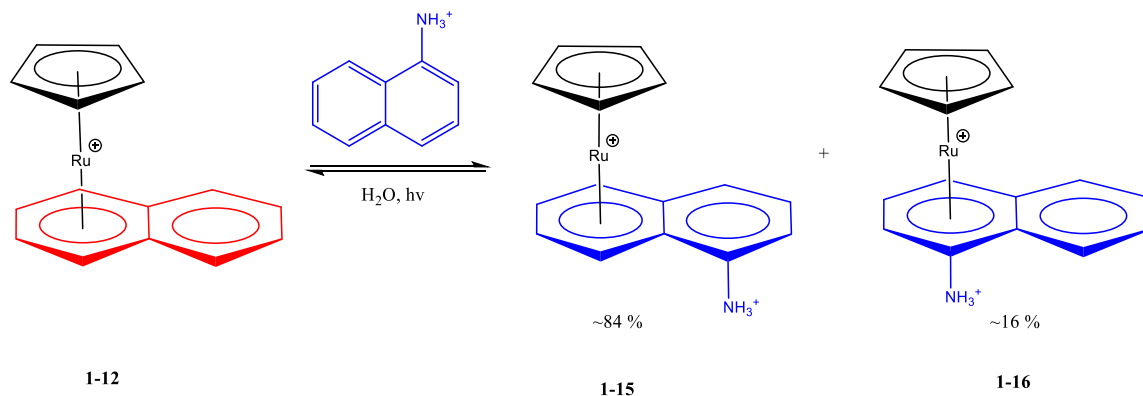
8. Under the condition of 1:1 Lewis acid to triene substrates, a rate acceleration of 13 and 55 fold were observed in the case of **1-8** and **1-9**, respectively.⁷ This study suggests that by increasing the electron withdrawing effect of the conjugated triene system, it may be possible to lower the electrocyclization energy barrier.

III. Ligand exchange between Ru- η^6 -Arene and RuL₃.

To extend the understanding of ML₃ complex in triggering electrocyclization, it is crucial to study the M(η^6 -arene) complex and its mechanism in yielding ML₃ product. CpRu⁺(η^6 -arene), as one of the most studied examples, has been used as the reference in comparison to other transition metal-arene complexes. A detailed study was reported by Kudinov's group.⁸ CpRu⁺(η^6 -naphthalene) (**1-12**) as the precursor was found to be able to convert to CpRu⁺(η^6 -benzene) under

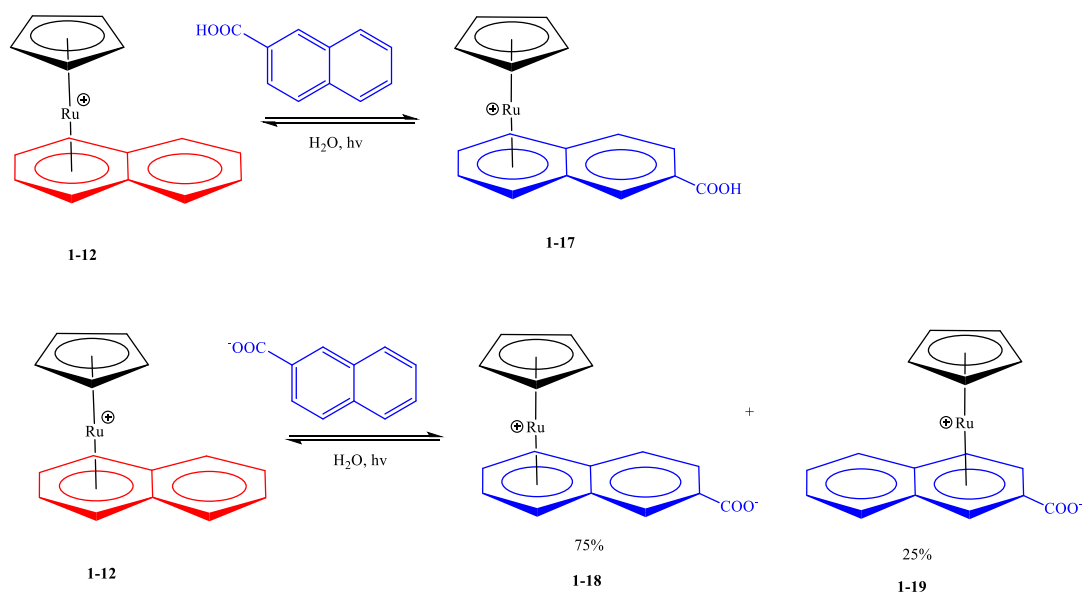


Scheme 1-4: Thermal arene exchange in coordination solvent.



Scheme 1-5: Equilibrium reaction of **1-12** with 1-naphthylammonium cation.

thermal conditions at a yield between 10-70 %. It is important to notice that naphthalene is more readily substituted than benzene, resulting from the facial irreversible η^6 to η^4 ring slippage. However, yield was significantly increased to 70-80 % when running the reaction in acetonitrile (Scheme 1-4). The mechanism suggests that short lived $\text{CpRu}^+(\text{NCMe})_3$ intermediate plays a crucial role in catalyzing arene exchange. Similar increase in percent conversion with coordination solvent was also observed in photochemical conditions: The conversion of $\text{CpRu}^+(\eta^6\text{-naphthalene})$ to $\text{CpRu}^+(\eta^6\text{-arene})$ was accelerated by coordination solvents from 10-100 %. Arene substituents

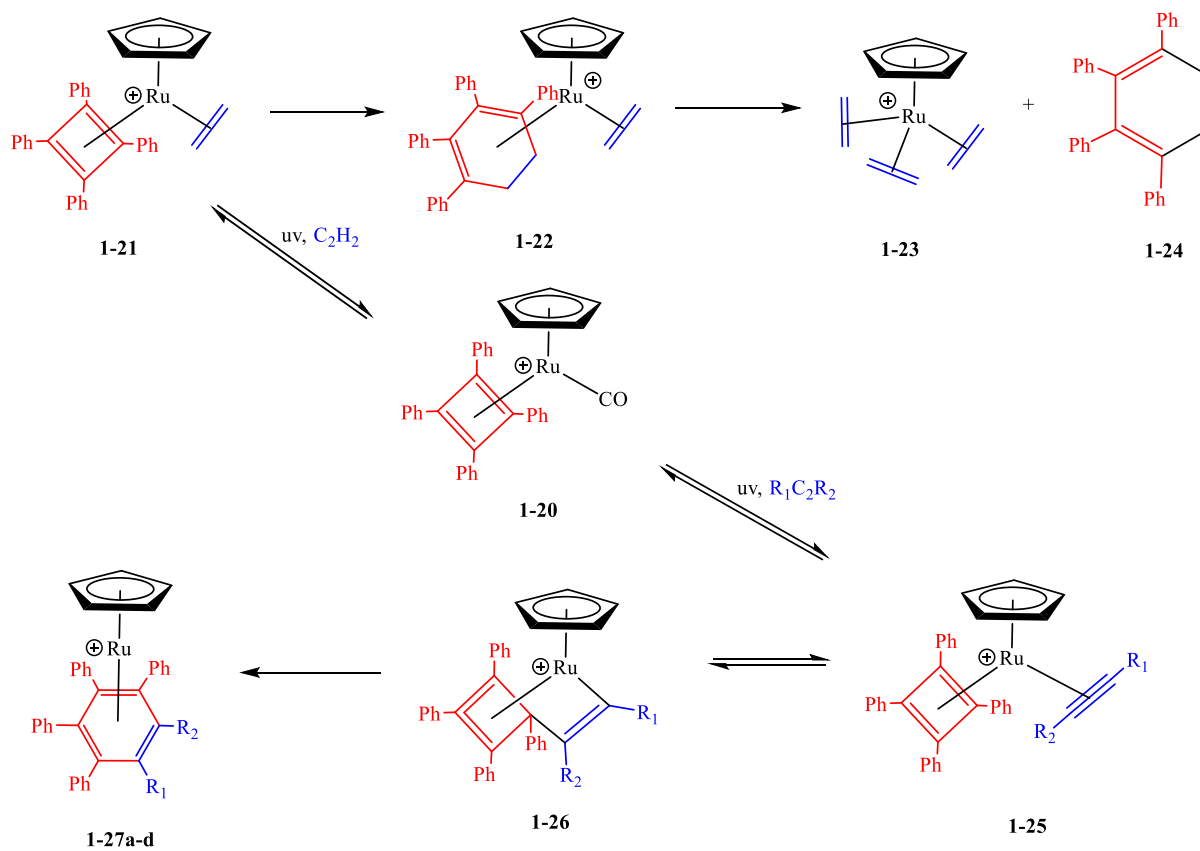


Scheme 1-6: The pH-controlled haptotropic rearrangement.

also influence the conversion in arene change. The sequence reported in Kudinov's work from fast to slow can be explained by the conflicting influence of electronic and steric effects. $1,4\text{-C}_6\text{H}_4(\text{OMe})_2 > 1,4\text{-C}_6\text{H}_4\text{Me}_2 > \text{C}_6\text{H}_6 > 1,3,5\text{-C}_6\text{H}_3\text{Me}_3 > 1,2,4,5\text{-C}_6\text{H}_2\text{Me}_4 \gg \text{C}_6\text{Me}_6$ (Scheme 1-4). The favorable donor effect of the substituent accelerates the rate but can also be overcome by the unfavorable steric hindrance. An electron-withdrawing group NH_3^+ was tested in aqueous solution to precipitate uncoordinated naphthalene. Ruthenium attached to the unsubstituted arene **1-15** was 5 times more concentrated than **1-16** (Scheme 1-5). $-\text{COOH}$ was also examined under various pH conditions. While complex **1-17** was the only product when it is protonated, deprotonated COOH to COO^- as the electron withdrawing substituent converts 25 % of **1-18** to **1-19** (Scheme 1-6). This is a rare report of metal migration between arenes influenced by pH.

IV. Ru(η^4 -cyclobutadiene) leads to a ring expansion reaction via a Ru(η^4 -alkene) intermediate.

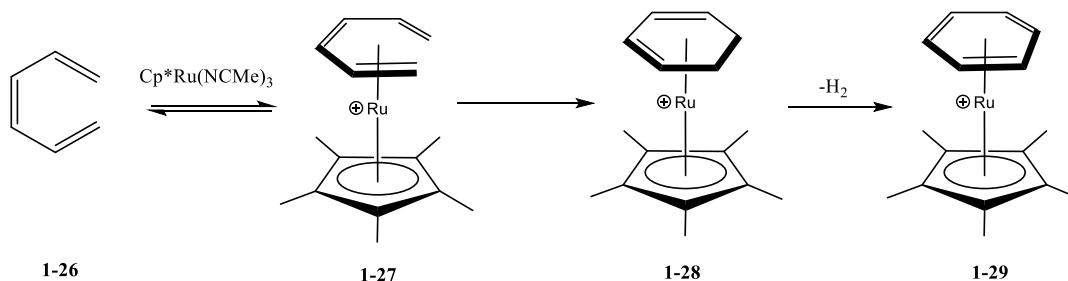
A ring expansion reaction triggered by a $\text{CpRu}^+(\eta^4\text{-cyclobutadiene})$ (**1-20**) was discussed in Thomas's work. A $\text{Ru}(\eta^4\text{-diene})$ complex was proposed as the key intermediate to yield the final aromatic product. This work presented a detailed reversible pathway to generate an η^6 from the η^4 Ru^+ precursor via photochemically induced ligand exchange. Replacing CO with ethylene under UV resulted in the formation of the η^6 intermediate (**1-21**). Ring expansion then occurred to yield the organic product (**1-24**) as well as the complex remaining as the $\text{CpRu}^+(\text{C}_2\text{H}_4)_3$ (**1-23**). Under similar conditions, ring expansion can be extended to alkynes with a mechanism that, in a similar fashion, yields a series of products (**27 a-d**).



- a. $R_1 = R_2 = \text{Ph}$
- b. $R_1 = \text{Ph}, R_2 = \text{Me}$
- c. $R_1 = R_2 = \text{Me}$
- d. $R_1 = R_2 = \text{CO}_2\text{Me}$

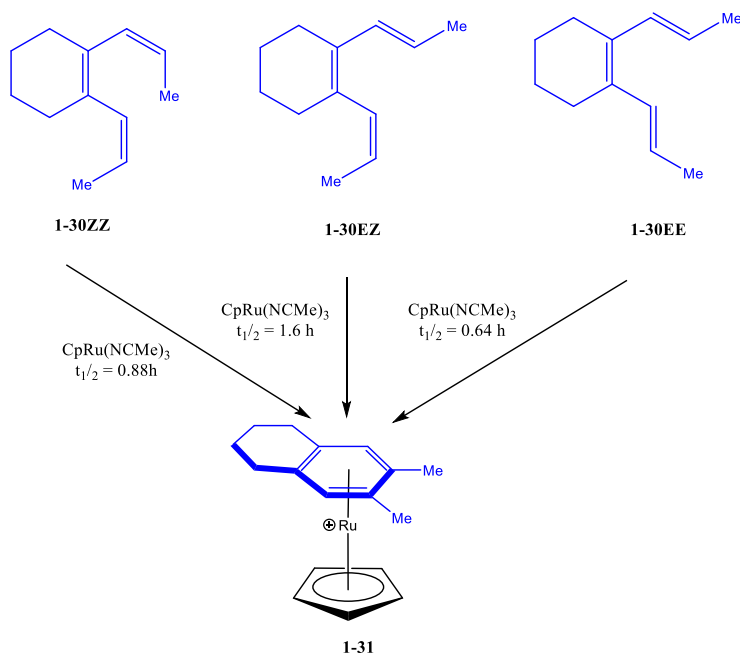
Scheme 1-7: Ring expansion reaction triggered with Ru- η^4 -cyclobutadiene with the addition of alkene and alkyne.

V. Cp/Cp*Ru⁺(NCMe)₃ catalyzed triene electrocyclization.



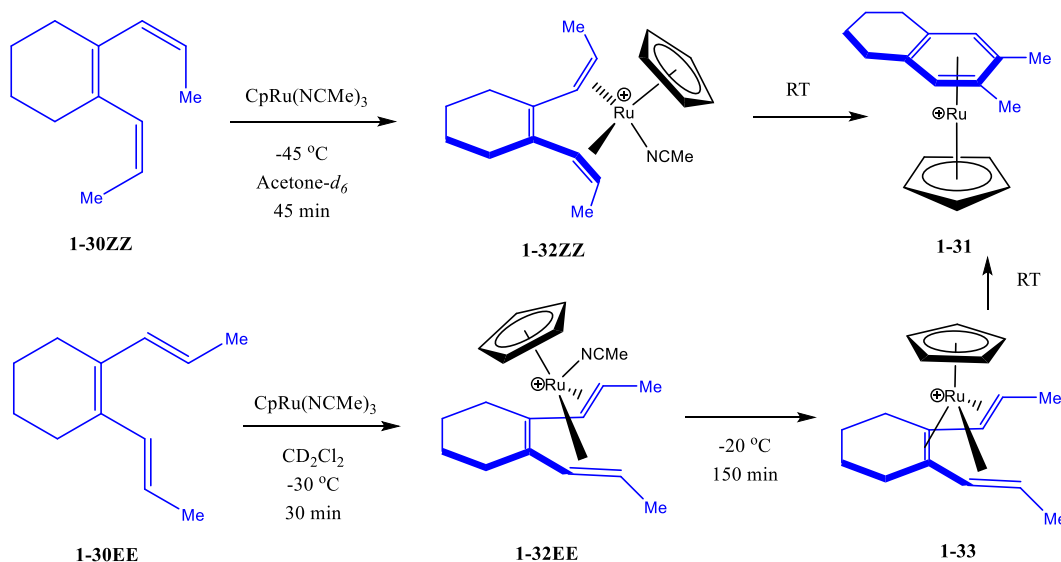
Scheme 1-8: Proposed mechanism for ruthenium-promoted dehydrocycloaromatizations.

A well-established triene electrocyclization system was reported by O'Connor's group.⁹ It was proposed in his work that a triene could undergo a similar hexahapto intermediate with Ru to lower the activation energy barrier for cyclization. The predicted mechanism suggested that the key step involves the generation of a Cp*Ru⁺(η^6 -triene) intermediate (**1-27**) then the formation of a Cp*Ru⁺(η^4 -cyclohexadiene) complex (**1-28**) followed by dehydrogenation to yield the cyclized

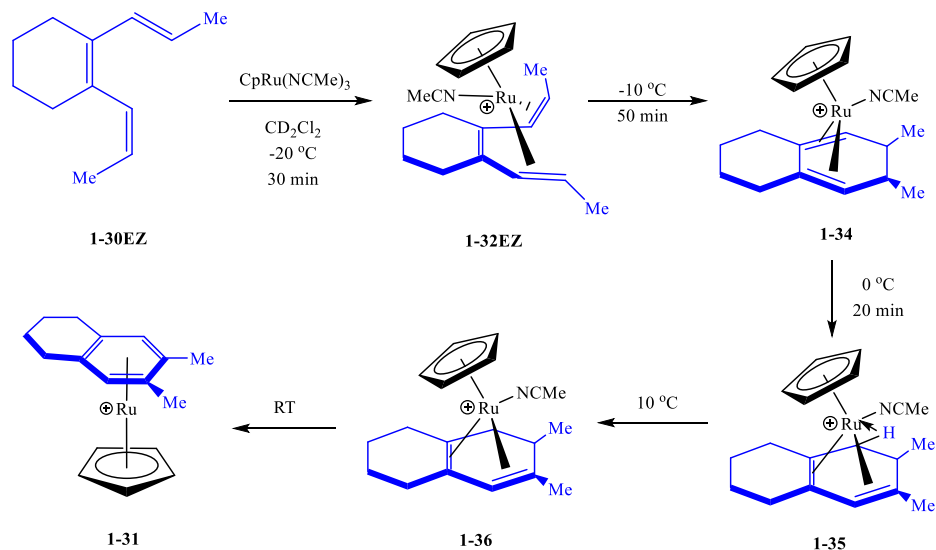


Scheme 1-9: Electrocyclization of **1-30ZZ**, **EZ** and **EE**.

product (**1-29**) (Scheme 1-8). A stereospecificity study was carried out on three triene substrates **1-30ZZ**, **1-30EE** and **1-30EZ**. Although cyclized product **1-31** was obtained in all three cases, three different half-lives for disappearance ($EZ > ZZ > EE$) observed in the kinetic study pointed to the likelihood that the rate of reaction is dependent on stereochemistry (Scheme 1-9). Predicted intermediates were observed in VT NMR experiments. **1-32ZZ**, as the only η^4 Ru-triene intermediate was observed and isolated in the case of **1-30ZZ** while **1-30EE** went through a similar η^4 complex **1-32EE** and a second stage $Ru^+(\eta^6\text{-triene})$ **1-33** to yield the product. Intermediate **1-33** was successfully isolated and characterized as the first ambient hexahapto complex of an acyclic conjugated triene (Scheme 1-10). Mechanism details were more revealing in the case of the **1-34EZ** reaction when gradually warmed from $-10\text{ }^\circ\text{C}$ to $10\text{ }^\circ\text{C}$ (Scheme 1-11). Despite the formation of the expected intermediate **1-32EZ**, at $0\text{ }^\circ\text{C}$, a ^1H NMR resonance at $\delta - 7.9$ (t, 1H, $J_{\text{HH}} = 16.0$ Hz) ppm indicated the presence of an anti-to-ring agnostic hydrogen as shown in structure **1-35**. It is notable that reacting **1-30EZ** with $\text{CpRu}^+(\text{NCMe})_2\text{CO}$ did not yield product **1-**



Scheme 1-10: Observation of reactive intermediates in triene **1-30ZZ** and **1-30EE** cyclization promoted by $\text{CpRu}^+(\text{NCMe})_3$.



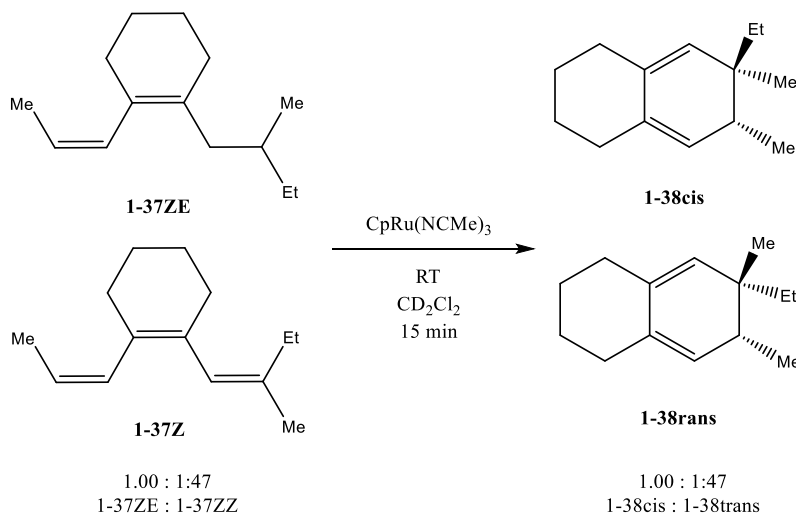
Scheme 1-11: Observation of reactive intermediates in triene **1-30EZ** cyclization promoted by $\text{CpRu}^+(\text{NCMe})_3$.

31, which indicates that the three facial coordination sites are crucial for triggering cyclization. To study the stereochemistry of ring closure, a mixture of **1-37ZE** and **1-37ZZ** at a ratio of 1:1.5 was mixed with catalytic amount of $\text{CpRu}^+(\text{NCMe})_3$ and the product **1-38cis** and **1-38trans** with a ratio of 1:1.5 consistent with the disrotatory hypothesis (scheme 1-12). The most crucial step for the



Figure 1-2: Computational studies of Ru accelerated disrotatory triene electrocyclicization.

ring closure is the generation of the hexahapto triene intermediate. The structure of **5-cp-cis** established by the BP86/Def2-TZVPP(THF) computation method is predisposed for a disrotatory electrocyclicization to produce the agnostic complex (Figure 1-2). The conversion between **5-Cp-**

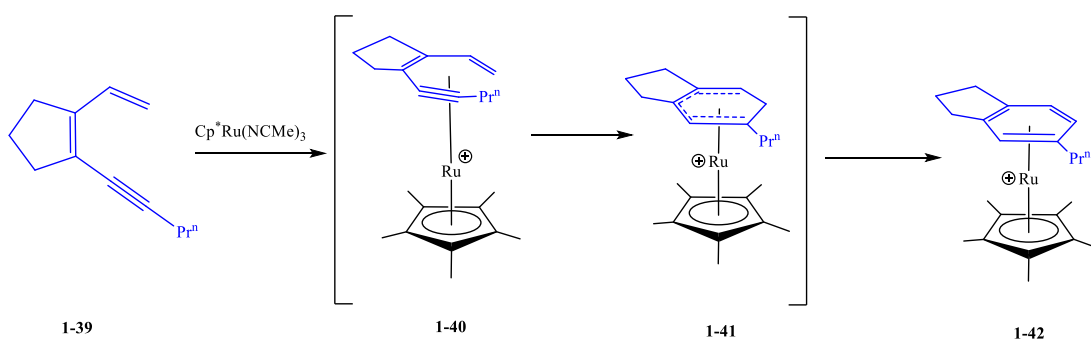


Scheme 1-12: Ru catalyzed triene **1-37ZE** and **1-37ZZ** electrocyclicization.

cis/cis and **6-Cp** was found to have an energy barrier of 17.7 kcal/mol. While thermal electrocyclization of the triene substrate has an energy barrier of 27.7 kcal/mol with a transition stage of **23-TS**. Thus, by introducing RuL_3 as mediator, the energy barrier is reduced by 10 kcal/mol when compared at the same thermal conditions.

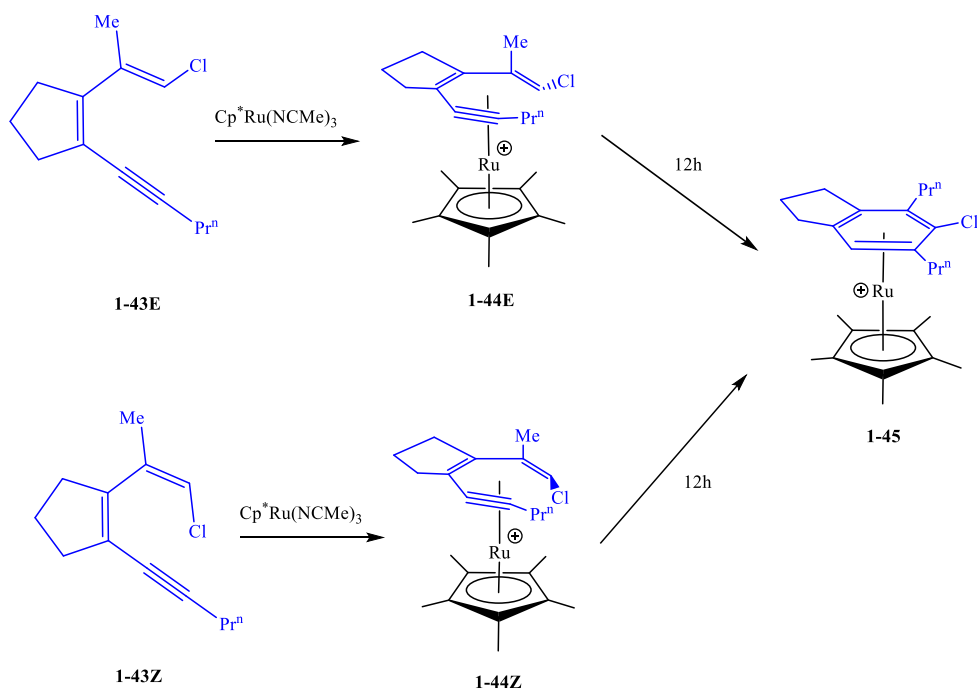
VI. $\text{Cp}^*\text{Ru}^+(\text{NCMe})_3$ mediated dienyne electrocyclization.

The first metal triggered ambient temperature Hopf cyclization was reported by O'Connor's group in 2002.¹⁰ The first example describes dienyne (**1-39**) undergoing aromatization

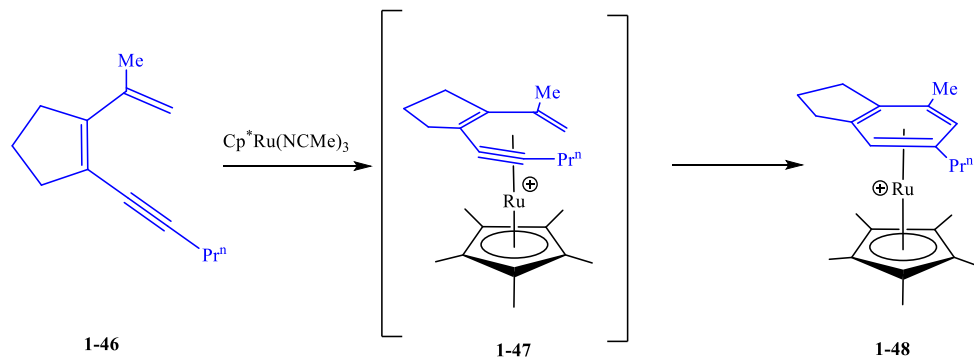


Scheme 1-13: $\text{Cp}^*\text{Ru}^+(\text{NCMe})_3$ mediated dienyne cyclization.

under ambient temperature to produce product (**1-42**) with the presence of $\text{Cp}^*\text{Ru}^+(\text{NCMe})_3$ at a 52 % yield in THF within 10 min and 96 % yield in CDCl_3 within 50 min. In this case, he predicted $\text{Cp}^*\text{Ru}^+(\eta^6\text{-dienyne})$ as a potential intermediate during the conversion. Furthermore, isomer **1-**



Scheme 1-14: $\text{Cp}^*\text{Ru}^+(\text{NCMe})_3$ triggered cycloaromatization of 1-chlorodienynes.

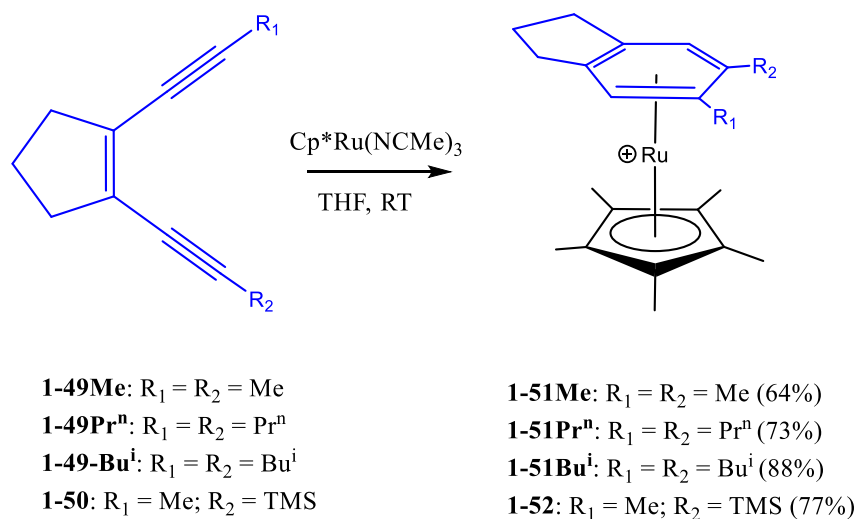


Scheme 1-15: $\text{Cp}^*\text{Ru}^+(\text{NCMe})_3$ triggered cycloaromatization of 2-methyldienynes.

43E and **1-43Z** were also treated with $\text{Cp}^*\text{Ru}^+(\text{NCMe})_3$ under the same conditions. **1-45** was isolated in both cases with a yield of 95 % and 45 %, respectively. It was notable that NMR spectroscopy analysis provided the evidence of intermediates that have distinguishable vinyl hydrogen features. The ^1H NMR resonance features at δ 2.17 and 4.89 ppm indicated the correlation of anti and syn geometry that belong to **1-44E** and **1-44Z**. The lack of the observation of coordinated acetonitrile strongly suggest that all three π bonds were involved in coordination, in which case, a $\text{Ru}^+(\eta^6\text{-dienyne})$ complex can be reasoned. The first Ru coordinated to conjugated dienyne complex was also reported by O'Connor three years later.¹¹ It was isolated by treating dienyne **1-46** with $\text{Cp}^*\text{Ru}^+(\text{NCMe})_3$ at -10 °C. It was observed that vinyl hydrogen resonances were greatly shifted due to the coordination environment. It was confirmed to be ^1H NMR resonances at δ 0.11 and 3.27 ppm for the anti and the syn vinyl hydrogens, respectively. However, it was still not confirmed by the researchers that the intermediate **1-47** lies on the direct pathway between **1-46** and **1-48**.

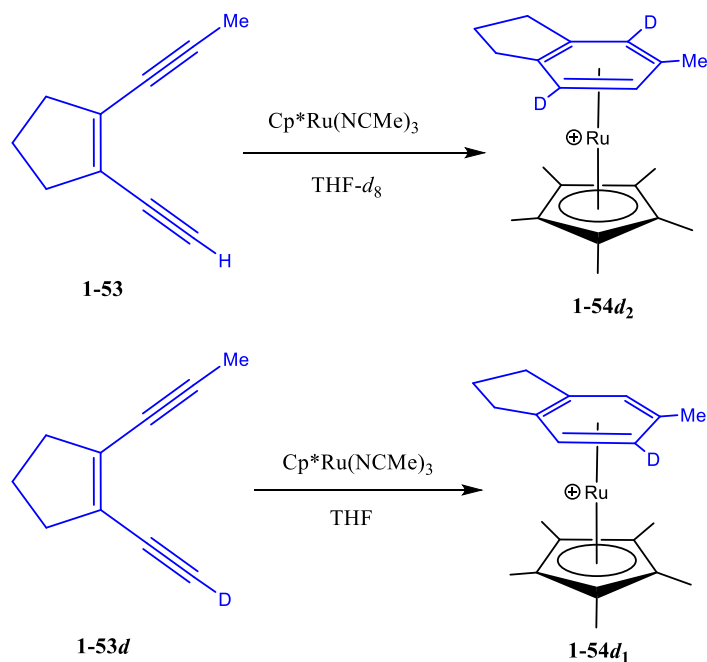
VII. Cp*⁺Ru(NCMe)₃ mediated enediyne electrocyclization.

In spite of mediating triene and dienyne aromatization under ambient temperature, O'Connor's group was also pleased to discover that Bergman (enediyne) cyclization can be triggered in a similar fashion by Cp*⁺Ru(NCMe)₃.¹² Successful cyclization reactions were



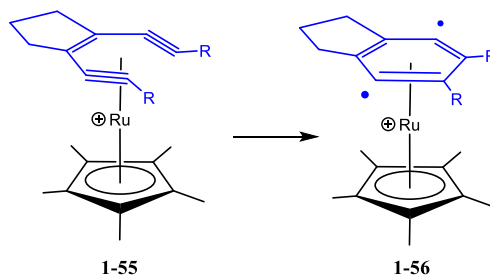
Scheme 1-16: Cp*⁺Ru(NCMe)₃ triggered cycloaromatization of enediyne.

observed in the examination of a series of enediyne substrates from **1-49** to **1-50** (Scheme 1-16). The investigation of its mechanism was initially started with an isotopic labeling study. Enediyne **1-53** was reacted with Cp*⁺Ru(NCMe)₃ in THF-*d*₈ and deuterium enrichments on C4 and C7 were observed suggesting a structure of **1-54-d₂**. In addition, reacting enediyne **1-53-d** with



Scheme 1-17: Isotopic study $\text{Cp}^*\text{Ru}^+(\text{NCMe})_3$ triggered cycloaromatization of enediynes.

$\text{Cp}^*\text{Ru}^+(\text{NCMe})_3$ under the same conditions, but within protio THF, only resulted in a deuterium enrichment on C6 (Scheme 1-17) of **1-54-d₁**. This result is consistent with the p-biradical benzene intermediate (**1-56**) that was likely generated from the $\text{Ru}^+(\eta^6\text{-enediynes})$ (**1-55**) along the reaction pathway as well as the computation result reported by Kundig's group.¹³ Furthermore, in order to achieve a spatiotemporal control for diradical formation, a photoactive ruthenium trigger,

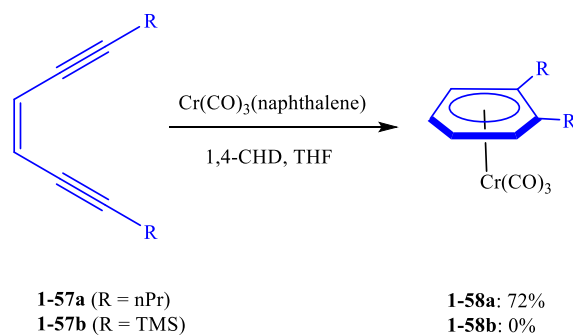


Scheme 1-18: Proposed key intermediates in ruthenium triggered enediyne cyclization.

ruthenium naphthalene was tested and resulted in a good product yield. Detailed results will be discussed in later chapters.

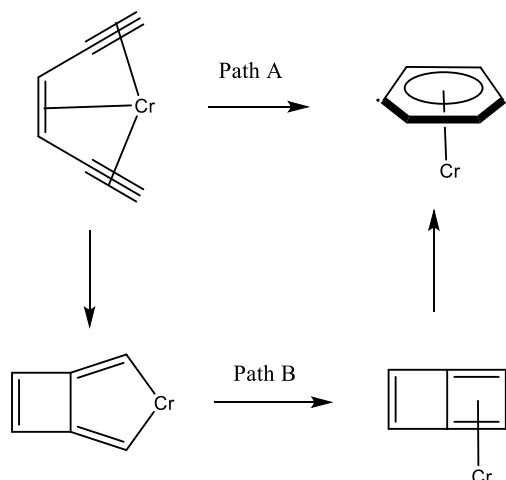
VIII. Cr(η^6 -naphthalene) triggered Bergman cyclization under ambient temperature.

Kundig and his group reported the first example of triggering Bergman cyclization with a Cr(η^6 -naphthalene)(CO)₃ under ambient temperature.¹⁴ Simple enediyne **1-57a** undergoes electrocyclicization at room temperature in the coordination solvent THF to generate **1-58a**. The



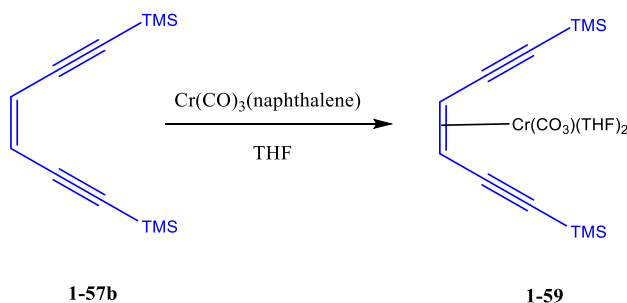
Scheme 1-19: Bergman cyclization triggered by Cr(CO)₃(naphthalene) under ambient temperature.

yield significantly improved with the addition of a hydrogen source 1,4-CHD (Scheme 1-19). This reaction was not observed in a non-coordination solvent or with bulky terminal substituents, consistent with what was discovered in my later work. Two mechanistic pathways (Scheme 1-20) were introduced in his work, while path A described a direct cyclization between C1 and C6 and B described oxidative coupling followed by reductive elimination and bond hemolysis. DFT computation method suggested that Path B is unfavorable with a comparison of 80.4 kcal/mol to 16.7 kcal/mol in activation energy barrier. Their work pointed out that the Cr(η^6 -enediyne)



Scheme 1-20: Two proposed mechanistic pathways in Cr triggered Bergman cyclization.

complex is the crucial pathway that leads to cyclization. An unreactive model diTMS (**1-57b**) was studied as a comparison. Greater NMR resonance shift towards up field of the alkene carbon relative to a slight shift of the alkyne carbons indicated that only $\text{Cr}(\eta^2\text{-alkene})$ (**1-59**) was established with two coordinated THF but alkynes remained uncoordinated (Scheme 1-21). The

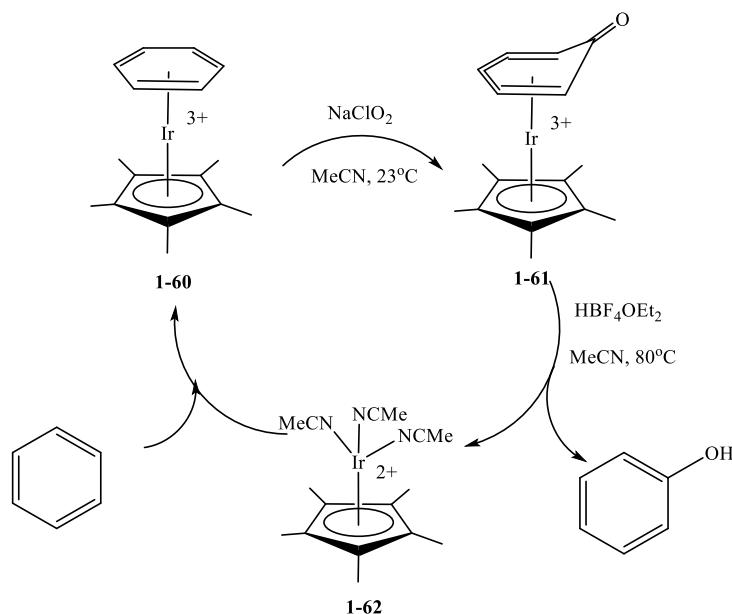


Scheme 1-21: Proposed product when reacting with bulky terminal alkyne substituents.

formation of benzene diradical intermediate was confirmed by a close match between experimental and simulated EPR spectra of the triplet p-benzyne biradical. Kundig's work demonstrated the viability of a chromium mediated variant to ruthenium presented by O'Connor's lab and its key intermediate benzyne biradical was observed to lie on the reaction pathway.

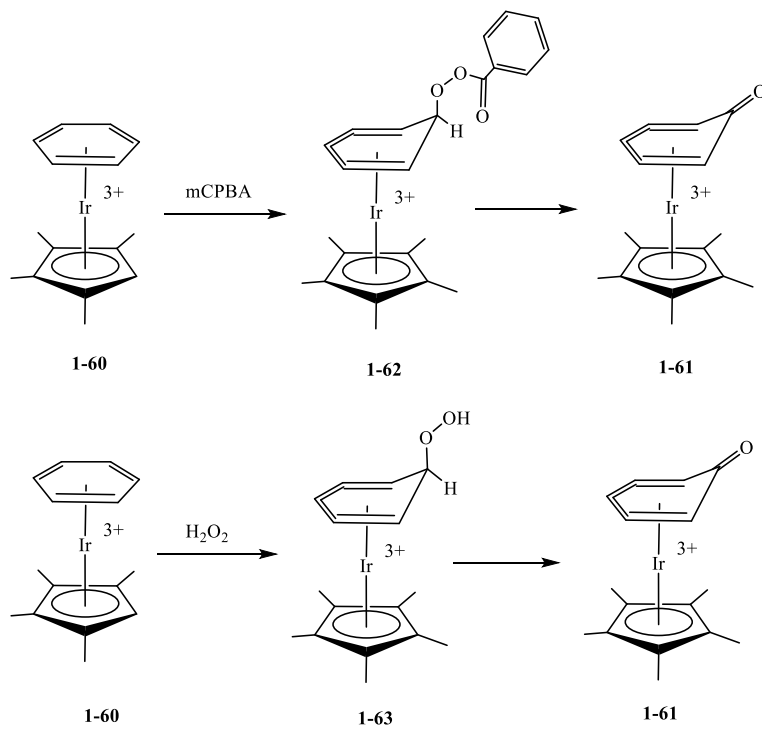
IX. η^6 -Coordinated iridium enables selective aromatic C-H hydroxylation.

Besides chromium and ruthenium, iridium also demonstrated its capability in activating tri- π systems. Reported by Ritter and coworkers, a selective C-H hydroxylation can be mediated



Scheme 1-22: Synthetic cycle for oxidation of benzene to phenol.

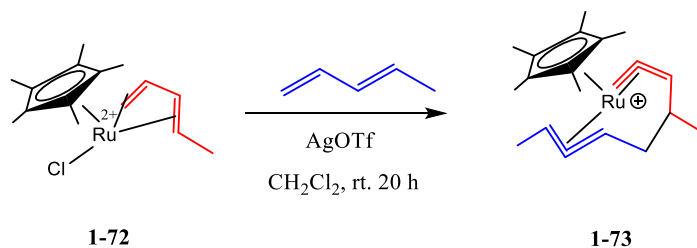
by a Cp*Ir³⁺(η^6 -arene) complex (Scheme 1-22).¹⁵ The formation of **1-61** from **1-60** mechanism suggests two general steps: nucleophilic attack followed by oxidation elimination. In a reaction analogous to that with NaClO₂, compound **1-60** was treated with mCPBA (Scheme 1-23). A noticeable up-field shifted hydrogen resonance indicated the formation of **1-62**, a Cp*Ir³⁺(η^5 -cyclohexadienyl) adduct. By treating **1-62** with H₂O₂, with the observation of **1-63**, only 5 % of **1-61** was obtained. It supports the hypothesis of a *syn* elimination in the case of NaClO₂ and mCPBA. However, the desired catalytic cycle was not obtained due to the fact that each step within the cycle involves conditions that are not compatible. While complex **1-61** requires strong acid for protonation and dissociation from iridium, it may also result the decomposition of NaClO₂. In addition to



Scheme 1-23: C-O bond formation via η^5 -cyclohexadienyl adducts.

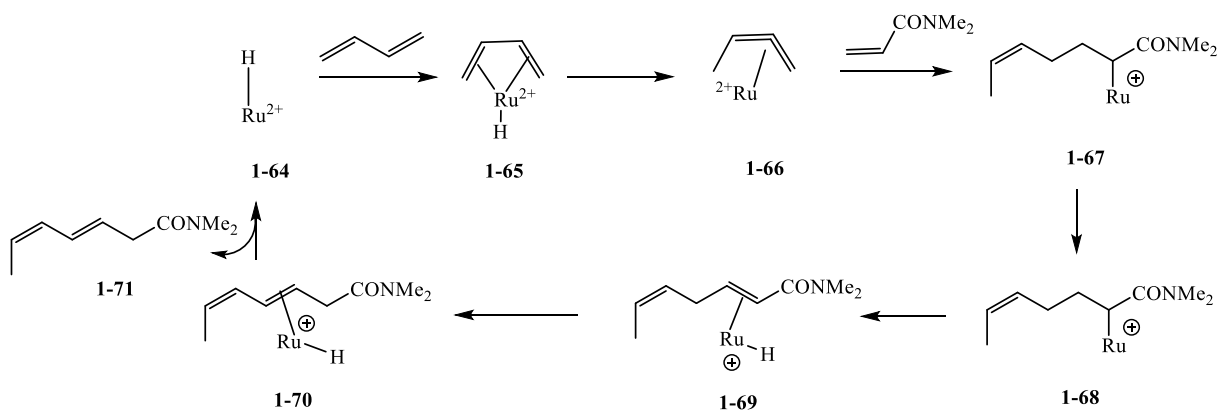
retrieve **1-60** from **1-62**, a solvent that has less coordination than acetonitrile is required to displace labile ligands with benzene.

X. Ru(η^4/η^6 -alkene) complexes in catalyzing alkene linear dimerization.



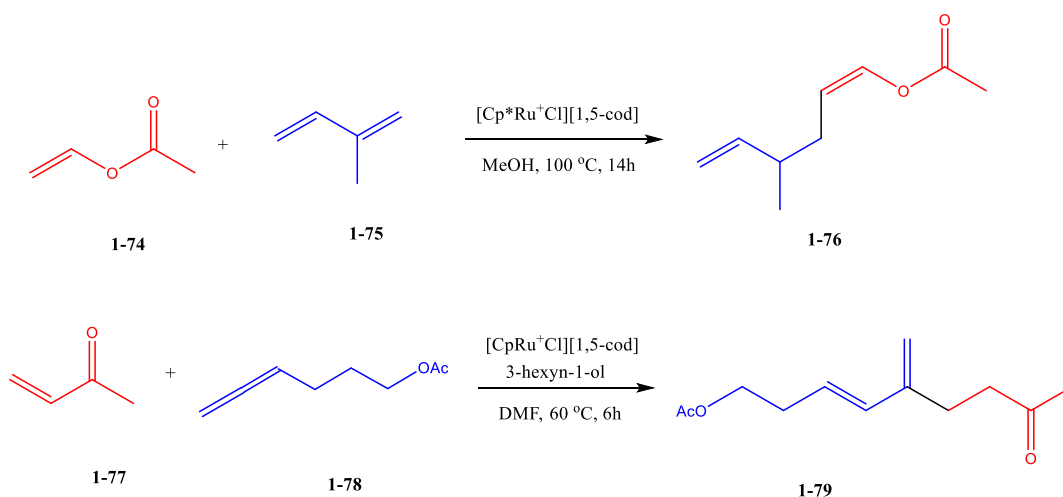
Scheme 1-24: Cp*Ru(η^4 -diene) triggered conjugated alkene dimerization.

A series of Ruthenium based diene-triene complexes demonstrated an enhanced capability in catalyzing alkene cross-dimerization. Mitsudo's chemistry showed that Ru⁺(η^4 -1,5-cod)(η^6 -1,3,5-cot) triggers dimerization of butadiene and methyl acrylate. In his proposed mechanism, a key step involves an anti-methyl Ru²⁺(η^3 -allylic) intermediate (**1-66**) that was generated from the addition of the metal hydride followed by the insertion of an acrylic acid derivative into the less hindered C-Ru bond (Scheme 1-24).¹⁶ Similar catalytic activity was also found in a cationic Ru²⁺, Cp*Ru⁺(η^4 -diene) in the presence of OTf⁻. The Ru(IV)(η^3 -allylic) complex (**1-73**) was isolated (Scheme 1-24).¹⁷ Fujiwhara and Trost also reported the successful linear cross dimerization of alkene/diene with Cp*Ru⁺(η^4 -1,5-cod) (Scheme 1-26 top).¹⁸ Allene/conjugated ketone

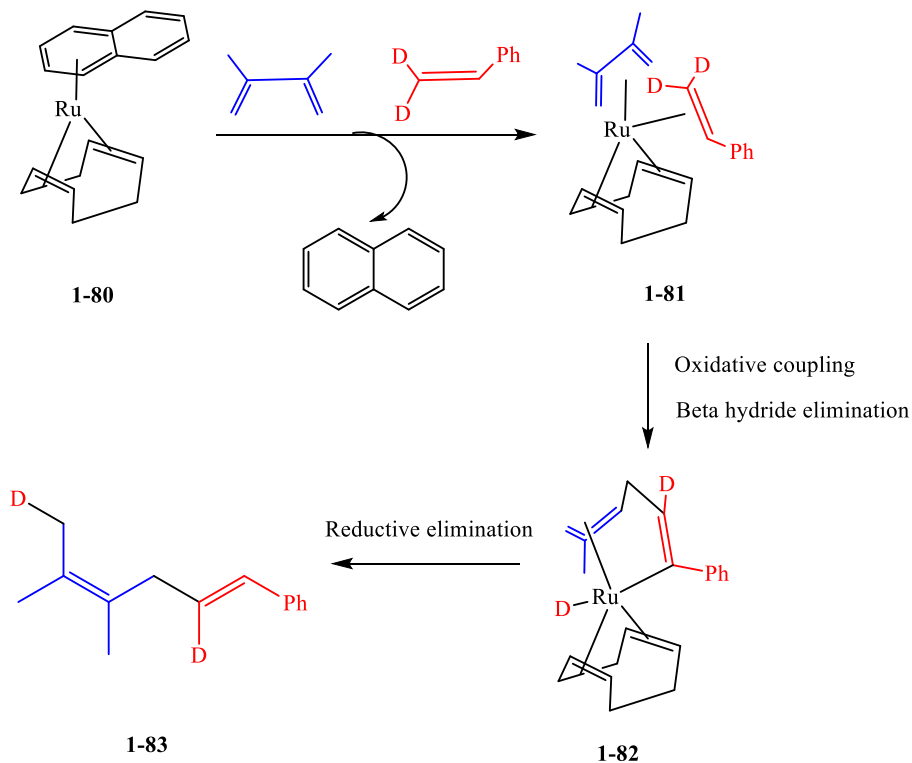


Scheme 1-25: Ru(η^4 -1,5-cod)(η^6 -1,3,5-cot) catalyzes butadiene and methyl acrylate dimerization.

dimerization with $\text{Cp}^*\text{Ru}(\eta^4\text{-1,5-cod})$ was also achieved by Trost's group, but it is worth noticing that displacing 1,5-cod with allene was difficult and thus 3-hexyn-1-ol was added as the activator (Scheme 1-26 bot).¹⁹ A slightly different mechanism involving the formation of $\text{Ru}[\eta^2\text{-alkene}][\eta^4\text{-diene}]$ was reported by Hirano. $\text{Ru}(\eta^6\text{-naphthalene})(\eta^4\text{-1,5-cod})$ readily dissociates naphthalene to open up three facial vacancy sites, which allow the 4π (diene) and 2π (alkene) to coordinate. The resulting intermediate **1-81** was observed at $-80\text{ }^\circ\text{C}$.²⁰ Intermediate **1-81** continuously undergoes oxidative coupling followed by a β hydride elimination to yield the intermediate **1-82**. It subsequently yields product **1-83** via reduction elimination (Scheme 1-27). This was confirmed by observing the deuterium enrichment on the internal alkyl group. However, in Misuto's work, when naphthalene was replaced with $(\eta^6\text{-1,3,5-cot})$, it was easier to dissociate the 1,5-cod ligand to generate the Ru^{2+} hydride complex.²¹ Interestingly, Pertici reported that $\text{Ru}(\eta^4\text{-1,5-cod})(\eta^6\text{-1,3,5-}$

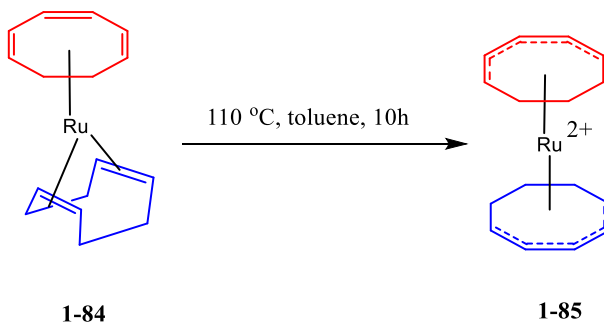


Scheme 1-26: $\text{Cp}/\text{Cp}^*\text{Ru}(\eta^4\text{-1,5-cod})$ in triggering alkene/diene liner dimerization (top) and allene /conjugated ketone dimerization (bot).

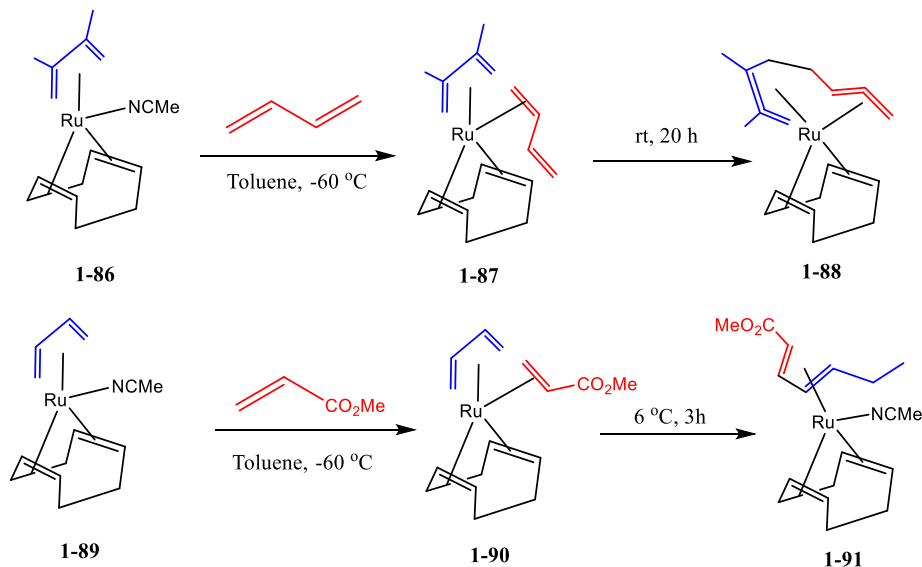


Scheme 1-27: Oxidative coupling mechanism of $[\text{Ru}(\eta^6\text{-naphthalene})(\eta^4\text{-1,5-cod})]$ catalyzed alkene dimerization.

cot) rapidly converts to $\text{Ru}^{2+}(\eta^5\text{-cyclooctadienyl})_2$ under thermal conditions.²² Oxidative coupling at the $\text{Ru}(0)$ center was again observed in Hirano's work when replacing one coordination site with a labile NCMe ligand. The 4π (diene) and 2π (alkene) intermediate was again observed through proton NMR spectroscopy at -60°C (Scheme 1-29 top).²³ A similarly fashioned intermediate



Scheme 1-28: Heating $\text{Ru}(\eta^4\text{-1,5-cod})(\eta^6\text{-1,3,5-cot})$ results the formation of $\text{Ru}^{2+}(\eta^5\text{-cyclooctadienyl})_2$



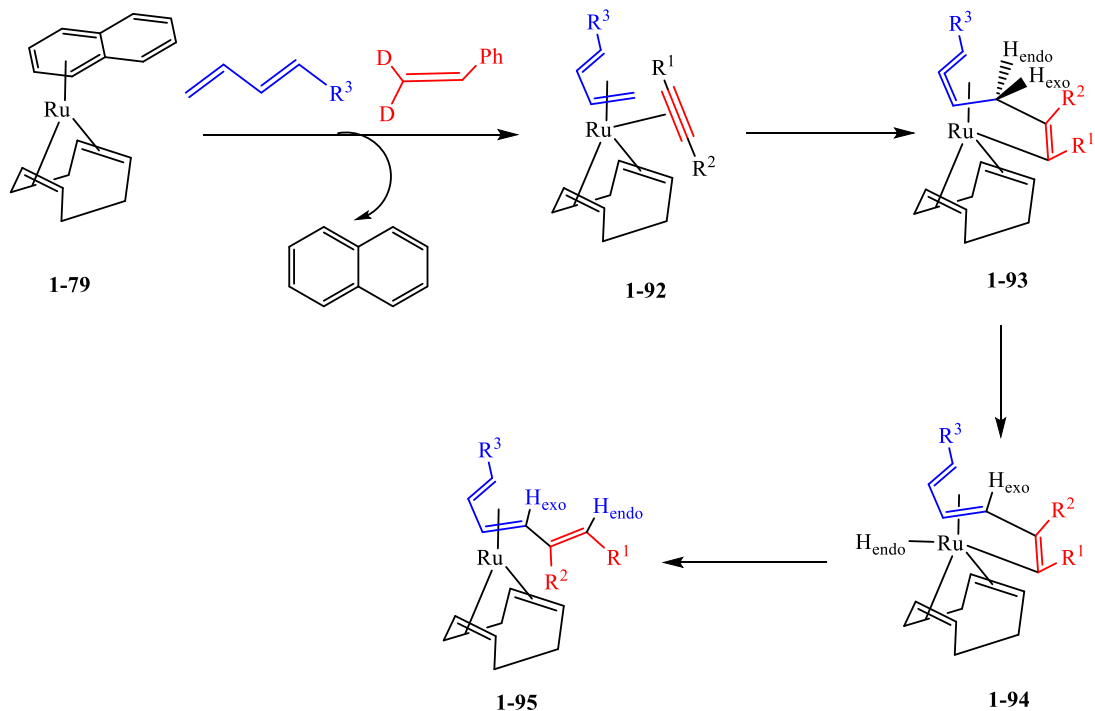
Scheme 1-29: Ru(η^4 -1,5-cod)(η^4 -cisdiene)(NCMe) complex in triggering diene dimerization (top) and diene/acrylate dimerization (bot).

between diene and acrylate was isolated as well (Scheme 1-29 bot).²⁴ These two examples again provided strong evidence of Ru(η^4 -cisdiene) and Ru(η^2 -alkene) oxidative coupling at the Ru(0) center.

XI. Ru(0) catalyzed alkyne/diene dimerization.

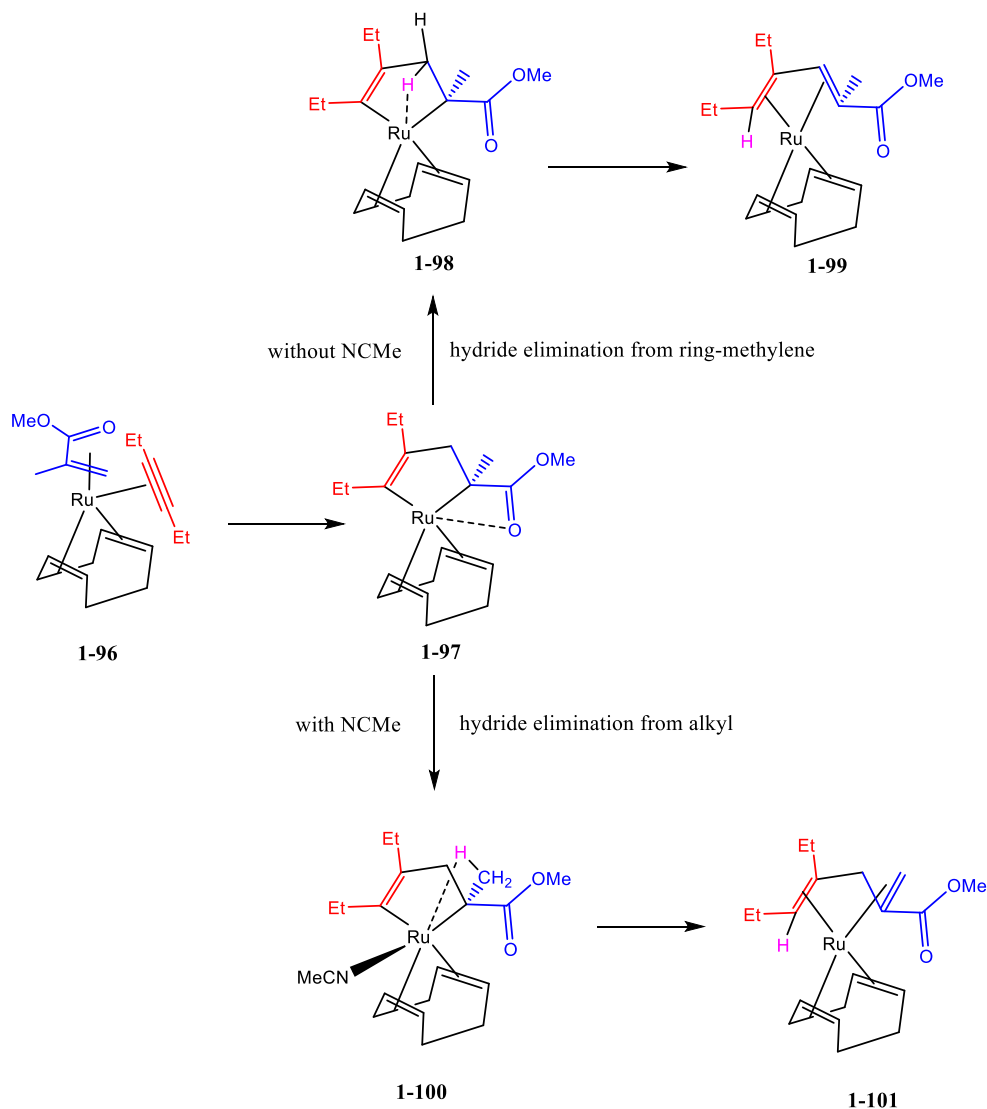
Furthermore, Ru(0) complexes demonstrated an excellent potential in catalyzing alkyne/diene dimerization and its chemistry has been extensively studied. Its mechanism is very similar to what has been demonstrated in alkene/diene dimerization. With Ru(η^6 -naphthalene)(η^4 -1,5-cod) (**1-79**) as the precursor, the dissociation of naphthalene allows three facial coordination sites to bind cis-diene and terminal alkyne as 4 π and 2 π electron donor, respectively (**1-92**). Oxidative coupling then took place to generate the η^3 : η^1 Ru²⁺ complex (**1-93**). β hydride

elimination that favors the H_{endo} occurred to yield intermediate **1-94** followed by reductive elimination to give the final dimerized product **1-95**.²⁵ Furthermore, its regioselectivity can be monitored via directing a different β hydride elimination pathway by the addition of a coordination



Scheme 1-30: Proposed mechanism of Ru(0) triggered diene/alkyne dimerization.

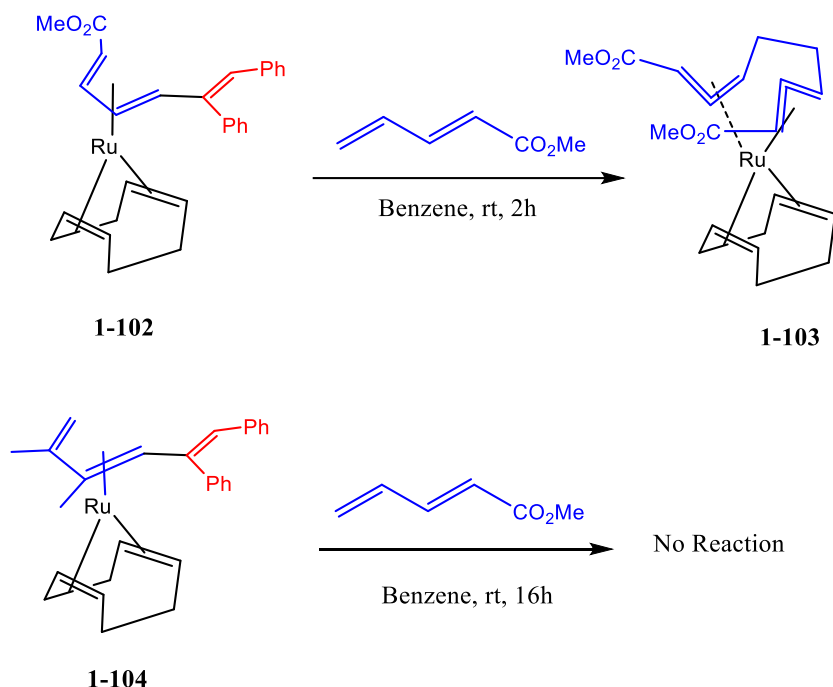
solvent. Without NCMe, β hydride elimination occurred via ring methylation followed by reductive elimination to generate product **1-99**. With the presence of NCMe, the α -alkyl group approaches the metal center to allow a hydride elimination from α alkyl. Thus, product **1-99** was



Scheme 1-31: Proposed mechanism of two β hydride elimination pathways influenced by the addition of NCMc.

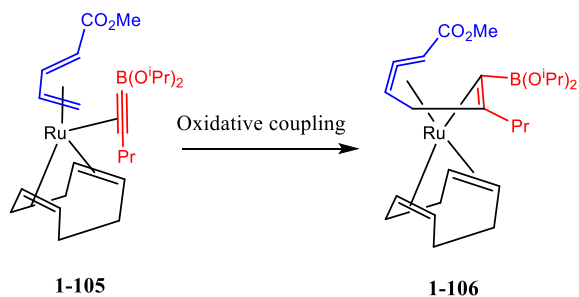
generated instead of **1-101**.²⁶ It is also worth noting that the reactivity and lability of the Ru-diene complex can be varied. Continuously treating the complex **1-102** with methyl penta-2,4-dienoate in benzene for 2 h resulted in the formation of the dimerized product and complex **1-103**, where **1-103** is the product between the cis η^4 -(methyl penta-2,4-dienoate) and the trans η^4 -(methyl penta-2,4-dienoate). However, reacting complex **1-104** with methyl penta-2,4-dienoate in benzene for

16 h did not produce any new products. This result demonstrated that **1-104** was not likely to undergo a ligand exchange and that explains the inert nature of some conjugated dienes.



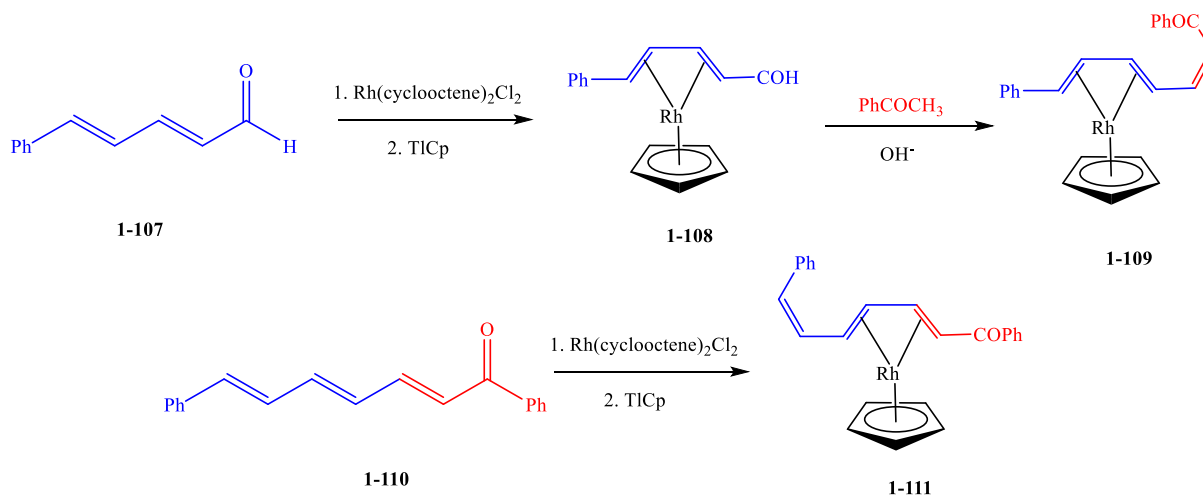
Scheme 1-32: Reaction between complex **1-102** and **1-104** with methyl penta-2,4-dienoate.

The region selectivity of the asymmetrical terminal alkyne was also exhaustively studied by Hirano's group.²⁷ The oxidative coupling resultant complex shows that the electron-withdrawing groups favor the external position, which allows it to approach the electron rich α position (Scheme 1-33).



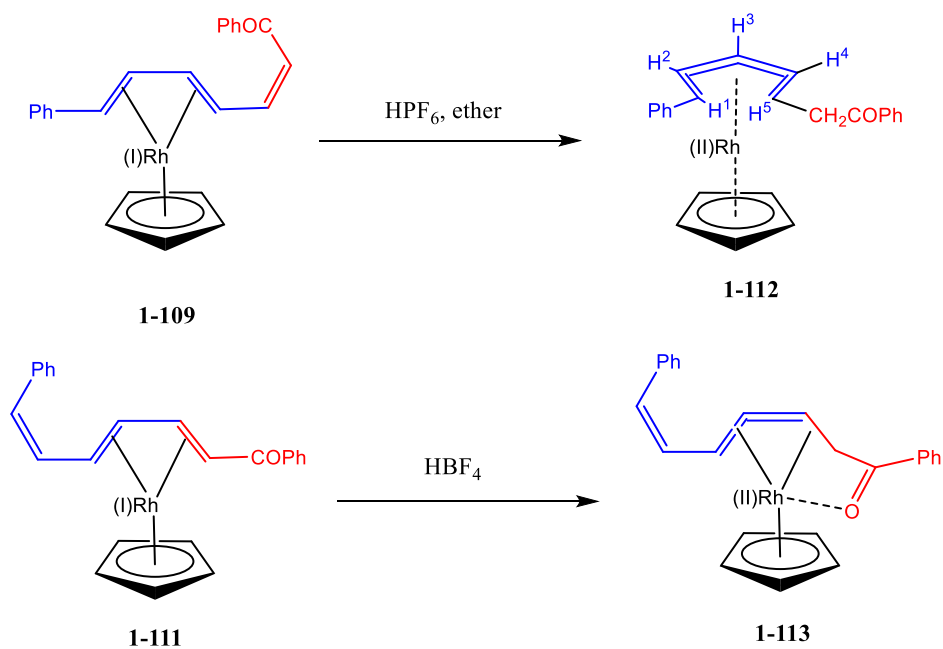
Scheme 1-33: Oxidative coupling of asymmetrical terminal alkyne with diene.

XII. Synthesis and protonation of Rh based η^4 diene-complexes.

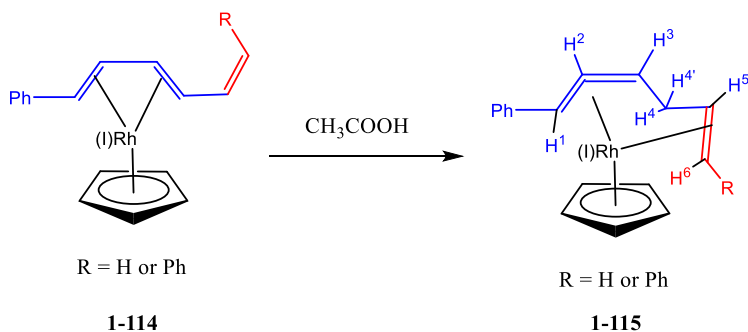


Scheme 1-34: Synthesis of Rh(I)(η^4 -diene) complex **1-109** and **1-111**.

A η^4 -Rh⁺ (I) complex reported in Powell's chemistry shows an interesting isomerization reactivity.²⁸ Compound **1-109** and its isomer **1-111** were synthesized via the methods shown in scheme 1-33. Treating complex **1-109** with HPF₆ yielded a protonated η^5 complex **1-112**. Its structure



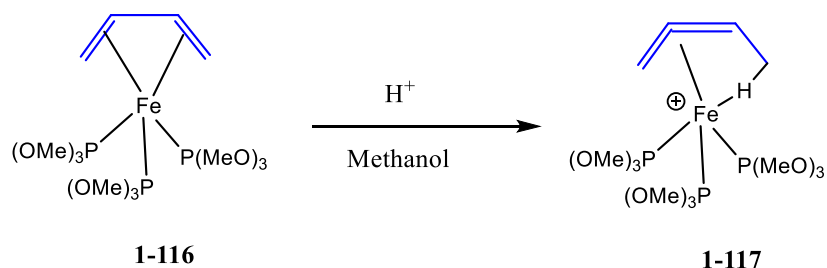
Scheme 1-35: Complex **1-109** and its isomer **1-111** isomerizes differently in acidic conditions.



Scheme 1-36: Complex **1-114** isomerizes differently in acidic conditions.

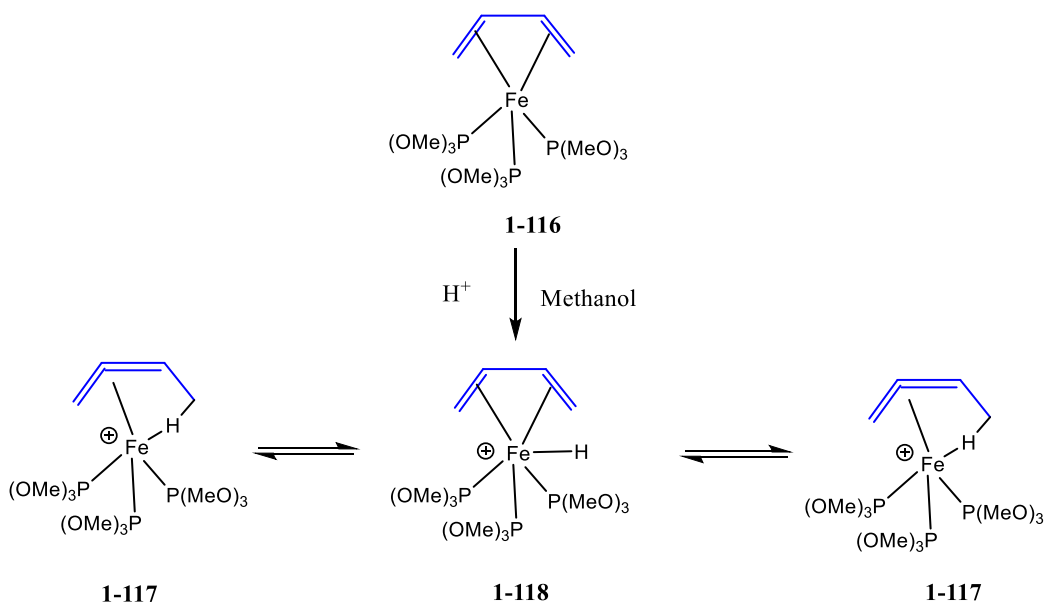
was confirmed with NOE experiments where irradiating H₄ (dd, δ 5.83 ppm) resulted in a H₃ resonance (t, δ 6.72 ppm) collapse to a doublet and H₅ resonance (m, δ 3.61 ppm) to a triplet with no effect on H₁. In addition, ¹³C NMR spectrum revealed that the coupling constant of ¹⁰³Rh-terminal C_{1,5} (10.2 Hz) was greater than the ¹⁰³Rh-inner ¹³C_{2,3,4} (6.1 Hz) (Scheme 1-34 top). However, complex **1-111** protonated differently under acidic conditions.²⁹ An η^3 -Rh²⁺ complex was observed with the acyl oxygen coordinated to the Rh center. Such an η^4 to η^5 transformation has been previously reported, the Rh-O coordination environment was supported by IR absorption of the CO stretching. The suggested uncoordinated acyl carbonyl exhibits an absorption at 1642 cm⁻¹ while in this experiment it was weakened to 1584 cm⁻¹. Powell also reported a complex **1-114**, which is similar to complex **1-109** that undergoes η^4 to η^5 protonation in a different manner. With the presence of CF₃COOH, complex **1-114** isomerizes where protonation occurred at C₄ and C₅=C₆ coordinates to the Rh²⁺ center. Proton NMR spectrum indicated a magnetic inequivalence of H₄ and H₄' with a coupling constant of $J_{HH} = 13.1$ Hz. The C-Rh coordination environment was identified by ¹³C NMR spectroscopy, where C₁, C₂, C₃, C₅, C₆ all exhibited a C-Rh coupling between 4-16 Hz, C₄ remained in its singlet resonance.³⁰

XIII. Iron(η^4 -diene) complexes and their reactivity.

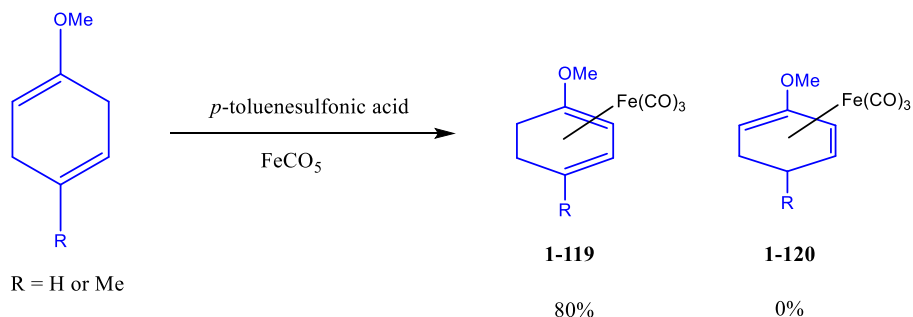


Scheme 1-37: η^4 Complex **1-116** produces η^3 complex **1-117** under acidic condition

Attention to iron(η^4 -diene) complexes was brought to us by Ittel's work on Fe(P(OMe)₃)₃(η^4 -butadiene) complexes.³¹ The addition of tetrafluoroboric acid to a solution of Fe(P(OMe)₃)₃(η^4 -butadiene) (**1-116**) in methanol caused the solution to be darkened. As iron coordinated vinyl hydrogens usually exhibit ¹H NMR resonance between δ 5.5 and 5.0 ppm, the resonance at δ 5.92 ppm under room temperature was interpreted as exchange of the

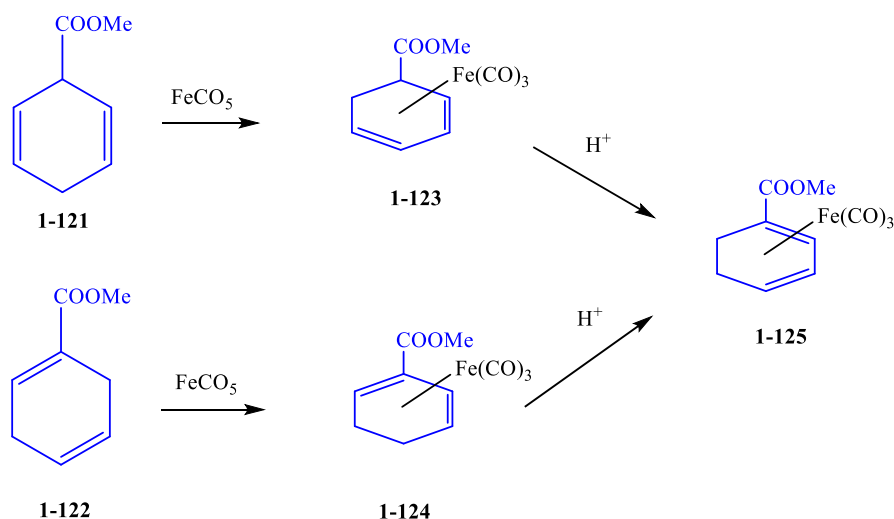


Scheme 1-38: Mechanism of η^4 Complex **1-118** produces η^3 complex **1-117** under acidic condition.



Scheme 1-39: Selective synthesis of Fe-2,5-dihydroanisole complexes.

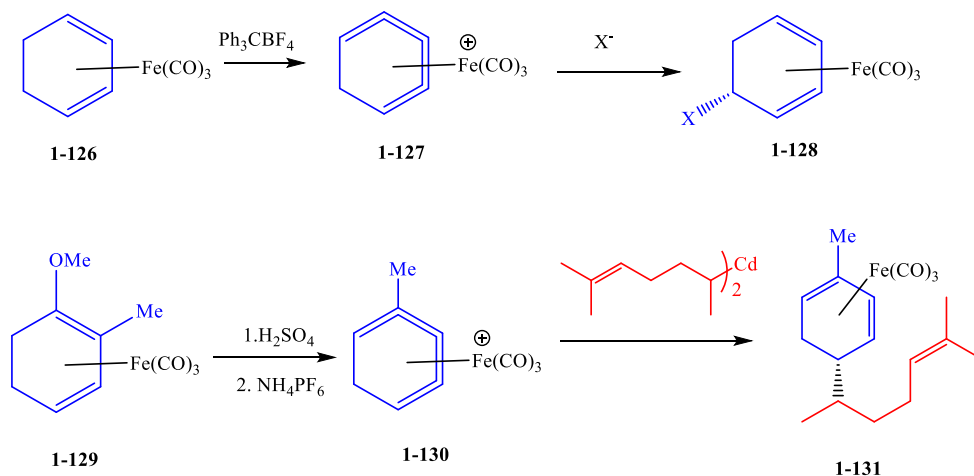
coordinated hydrogen atoms and the other two uncoordinated hydrogen atoms resulting from methyl rotation. At -100 °C, the singlet methyl peak turned into three resonances with one resonance located at 15.2 ppm, attributed to the bridging hydrogen atom which indicated the rotation was frozen at this temperature. Thus, the structure of complex **1-117** was confirmed. Its mechanism was further confirmed with an isotopic study of a cyclooctadiene complex. With a deuterium enrichment, the remaining hydrogen atoms were given a resonance shift. The intensity of the shifted peaks relative to the unshifted vinyl peaks was calculated to be 3:1,



Scheme 1-40: Selective synthesis of ester substituted Fe-cyclo-2,5-diene complexes.

which indicated the formation of the compounds **1-117** through a mechanism in scheme 1-37. This observation confirms that this Fe complex achieves coordination saturation through bonding to an aliphatic hydrogen atom.

Synthesis and reactions of Fe-cyclodiene were also studied. Peterson's group reported that adding a catalytic amount of *p*-toluenesulfonic acid significantly increases the selectivity of the product from 4-methyl-2,5-dihydroanisole or 2,5-dihydroanisols (equation 1-38).³² Synthetic selectivity in ester substituted cyclodiene was also discussed. Treating substrate **1-121** with pentacarbonyliron remains ester group sp³ hybridized (**1-123**) while treating compound **1-122** under the same conditions led to the formation of complex **1-124**. Refluxing both **1-124** and **1-123** with the presence of methanolic sulfuric acid results in the isomerization of **1-125** (Scheme 1-39).³³



Scheme 1-41: Nucleophilic substitution and alkylation mediated by Fe-cyclo-2,5-diene complexes.

Nucleophilic substitution with most simple nucleophiles can be achieved with this group of complexes.³⁴ It was also reported by Birch that a clean alkylation occurs with these cadmium reagents.³⁵

XIV. References.

1. Hopf, H.; Musso, H. *Angew. Chem. Int.* **1969**, *8*, 680-680. "Preparation of Benzene by Pyrolysis of cis- and trans-1,3-Hexadien-5-yne".
2. Prall, M.; Kruger, A.; Schreiner, P. R.; Hopf, H. *Chem. Eur. J.* **2001**, *7*, 4386-4394. "The Cyclization of Parent and Cyclic Hexa-1,3-dien-5-yne: A Combined Theoretical and Experimental Study".
3. Bergman, R. G. *Acc. Chem. Res.* **1972**, *6*, 25-31. "Reactive 1,4-Dehydroaromatics".
4. Scott, L. T.; Cheng, P. C.; Hashemi, M. M.; Bratcher, M. S.; Meyer, D. T.; Warren, H. B. *J. Am. Chem. Soc.* **1997**, *119*, 10963-10968. "Colarinnulene. A Three-Step Synthesis".
5. Nicolaou, K. C.; Zuccarello, G.; Riemer, C.; Estevez, V. A.; Dai, W.-M. *J. Am. Chem. Soc.* **1992**, *114*, 7360-7371. "Design, synthesis, and study of simple monocyclic conjugated enediynes. The 10-membered ring enediyne moiety of the enediyne anticancer antibiotics".
6. Guner, V. A.; Houk, K. N.; Davies, I. W. *J. Org. Chem.* **2004**, *69*, 8024-8028. "Computational Studies on the Electrocyclizations of 1-Amino-1,3,5-hexatrienes".
7. Karslyan, E. E.; Perekalin, D. S.; Petrovskii, P. V.; Borisova, A. O.; Kudinov, A. R. *Russ. Chem. Bull.* **2009**, *58*, 585-588. "Photochemical arene exchange in the naphthalene complex [CpRu(η^6 -C₁₀C₈)]⁺".
8. Crocker, M.; Green, M.; Orpen, A. G.; Thomas, D. M. *J. Chem. Soc., Chem. Commun.* **1984**, 1141-1144. "The synthesis, structure, and reactivity of cationic η^4 -cyclobutadiene-ruthenium complexes; formation of the trisethylene(η -cyclopentadienyl)ruthenium cation".
9. Qin, P.; Wang, L.; O'Connor, J. M.; Baldrige, K. K.; Li, Y.; Burak, T.; Chen, J.; Rheingold, A. L. *Angew. Chem. Int., Ed.* **2020**, *59*, 17958-17965. "Transition-Metal Catalysis of Triene 6π Electrocyclization: The π -Complexation Strategy Realized".
10. O'Connor, J. M.; Friese, S.; Tichenor, M. *J. Am. Chem. Soc.* **2002**, *124*, 3506-3507. "Ruthenium-Mediated Cycloaromatization of Acyclic Enediynes and Dienynes at Ambient Temperature".
11. O'Connor, J. M.; Friese, S. J.; Rodgers, B. L.; Rheingold, A. L.; Zakharov, L. *J. Am. Chem. Soc.* **2005**, *127*, 9346-9347. "An η^6 -Dienyne Transition-Metal Complex".
12. O'Connor, J. M.; Friese, S. J.; Rodgers, B. L. *J. Am. Chem. Soc.* **2005**, *127*, 16342-16343. "A Transition-Metal-Catalyzed Enediyne Cycloaromatization".

13. Perrin, C. L.; Rodger, B. L.; O'Connor, J. M. *J. Am. Chem. Soc.* **2007**, 129, 4795-4799. "Nucleophilic Addition to a *p*-Benzyne Derived from an Eneidyne: A New Mechanism for Halide Incorporation into Biomolecules".
14. Ylijoki, K. E. O.; Lavy, S.; Fretzen, A.; Kundig, P. E.; Berclaz, T.; Bernardinelli, G.; Besnard, C. *Organometallics*. **2012**, 31, 5396-5404. "A Synthetic and Mechanistic Investigation of the Chromium Tricarbonyl-Mediated Masamune–Bergman Cyclization. Direct Observation of a Ground-State Triplet *p*-Benzyne Biradical".
15. D' Amato, E. M.; Neumann, C. N.; Ritter, T. *Organometallics*. **2015**, 34, 4626-4631. "Selective Aromatic C-H Hydroxylation Enabled by η^6 -Coordination to Iridium (II)".
16. Mitsudo, T.; Zhang, S.; Kondo, T.; Watanabe, Y. *Tetrahedron Lett.* **1992**, 33, 341–344. "Ruthenium complex-catalyzed selective syntheses of 3,5-dienoic acid derivatives by coupling of 1,3-dienes or allylic carbonates with acrylic compounds".
17. Itoh, K.; Masuda, K.; Fukahori, T.; Nakano, K.; Aoki, K.; Nagashima, H. *Organometallics*. **1994**, 13, 1020–102. "Stoichiometric and catalytic dimerization of conjugated dienes with (C5R5)Ru(diene)⁺".
18. Fujiwhara, M.; Nishikawa, T.; Hori, Y. *Org. Lett.* **1999**, 1, 1635–1637. "Ruthenium-Catalyzed Regioselective Codimerization of Enol Acylates with 2-Substituted-1,3-butadienes".
19. Trost, B. M.; Pinkerton, A. B. *J. Am. Chem. Soc.* **1999**, 121, 4068–4069. "A Ruthenium-catalyze two-component addition to form 1,3-dienes".
20. Hirano, M.; Ueda, T.; Komine, N.; Komiya, S.; Nakamura, S.; Deguchi, H.; Kawauchi, S. *J. Organomet. Chem.* **2015**, 797, 174–184. "Mechanistic insights into catalytic linear cross-dimerization between conjugated dienes and styrenes by a ruthenium(0) complex".
21. Mitsudo, T.; Suzuki, T.; Zhang, S.W.; Imai, D.; Fujita, K.; Manabe, T.; Shiotsuki, M.; Watanabe, Y.; Wada, K.; Kondo, T. *J. Am. Chem. Soc.* **1999**, 121, 1839–1850. "Novel Ruthenium Complex-Catalyzed Dimerization of 2,5-Norbornadiene to Pentacyclo[6.6.0.0^{2,6}.0^{3,13}.0^{10,14}]tetradeca-4,11-diene Involving".
22. Pertici, P.; Vitulli, G.; Paci, M.; Porri, L. *Dalton Trans.* **1980**, 1961–1964. "A new synthetic method for the preparation of cyclo-olefin ruthenium complexes".
23. Hirano, M.; Inoue, H.; Okamoto, T.; Ueda, T.; Komine, N.; Komiya, S.; Wang, X. Q.; Bennett, M. A. *New J. Chem.* **2013**, 37, 3433–3439. "Cross-dimerisation between different cisoid-and transoid-1,3-dienes at a ruthenium (0) center".
24. Hirano, M.; Arai, Y.; Hamamura, Y.; Komine, N.; Komiya, S. *Organometallics*. **2012**, 31, 4006–4019. "Stoichiometric and Catalytic Cross Dimerization between Conjugated Dienes

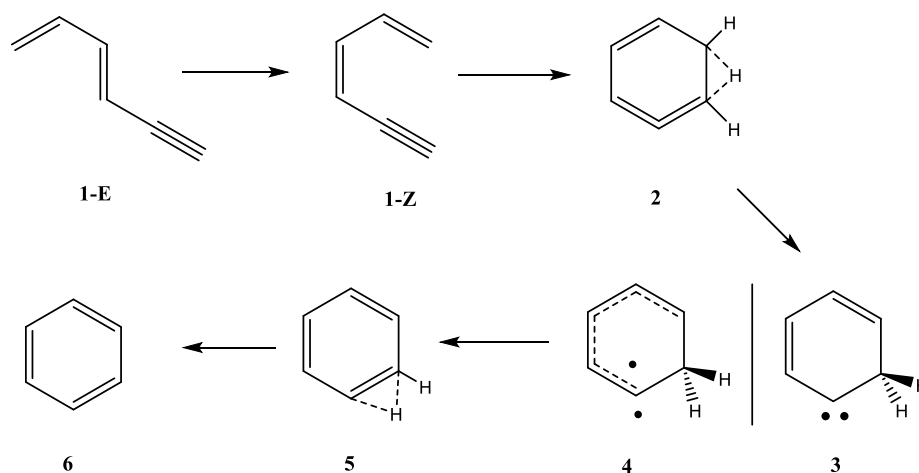
and Conjugated Carbonyl by a Ruthenium (0) Complex: Straightforward Access to Unsaturated Carbonyl Compounds by an Oxidative Coupling Mechanism”.

25. Kiyota, S.; In S.; Saito, R.; Komine, N.; Hirano M. *Organometallics*. **2016**, 35, 4033-4043. “Ru (0)-Catalyzed Direct Coupling of Internal Alkynes with Conjugated Dienes: An Efficient Access to Conjugated trienes”.
26. Kiyota, S.; In, S.; Komine, N.; Hirano, M. *Chem. Lett.* **2017**, 46, 1040–1043. “Regioselectivity Control by Added MeCN in Ru (0)-catalyzed Cross-dimerization of Internal Alkynes with Methyl Methacrylate”.
27. Hirano, M.; Kuramochi, A.; Shimada, K.; Komine, N.; Kiyota, S.; Westcott S. A. *Chem. Commun.* **2019**, 55, 10527-10530. “Catalytic cross-dimerisation giving reactive borylated polyenes toward cross-coupling”.
28. Powell, P.; *Journal of Organometallic Chemistry*. **1983**, 244, 393-399. “Diene and dienyl complexes of transition elements: VI. The protonation of two isomeric (η^5 -cyclopentadienyl)-(η^4 -1,7-diphenylheptatrien-1-one) rhodium (I) complexes”.
29. Powell, P.; *Journal of Organometallic Chemistry*. **1981**, 206, 229-237. “Diene and dienyl complexes of transition elements: II. The protonation of η diaryldienone (η -cyclopentadienyl)-rhodium (I) and -iridium (I) complexes”.
30. Powell, P.; *Journal of Organometallic Chemistry*. **1984**, 266, 307-311. “Diene and dienyl complexes of transition elements: IX. Formation of (1–3:5–6) η -hexadienyl- η^5 -cyclopentadienylrhodium cations by protonation of η^4 -triene complexes”.
31. Ittel, S. D.; Van - Catledge, F. A.; Jesson, J. P. *J. Am. Chem. Soc.* **1979**, 101, 6905-6911. “Protonation of iron diene tris(phosphite) complexes”.
32. Peterson. A. J. *Acc. Chem. Res.* **1980**, 13, 463-469. “Tricarbonyl (diene) iron complexes: synthetically useful properties”.
33. Birch. A. J.; Peterson, A. J. *Perkin Trans.* **1978**, 638.
34. Ireland, R. E.; Brown. G. G. Stanford, R. H.; McKenzie, T. C. *J. Org. Chem.* **1974**, 39.
35. Birch. A. J.; Peterson, A. J. *Tetrahedron Lett.* **1975**, 3617.

Chapter 2 . Ruthenium complex mediated dienyne electrocyclization at ambient temperature and investigation mechanism.

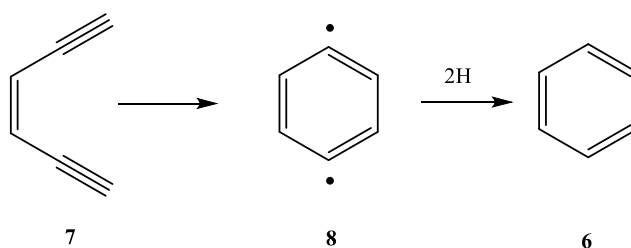
I. Introduction.

Bergman and Hopf cyclization have provided added a valuable new method for synthesizing benzene derivative products, first reported in the early 1970s.¹⁻⁵ Hopf cyclization describes a thermal electrocyclicization of a *Z*-1,3-dien-5-yne (**1-Z**) at high temperature (> 274 °C). Hopf reasoned a mechanistic pathway where the thermal conditions trigger the isomerization from **1-E** to **1-Z**, followed by the formation of an isobenzene intermediate **2**. Then a [1,2] hydride shift occurs to generate the singlet or the triplet carbene **3** or **4**, respectively. The arene product **6** is given by a secondary [1,2] hydride shift from the previous carbene structures (Scheme 2-1).^{6,7}



Scheme 2-1: Proposed mechanism of thermal Hopf cyclization.

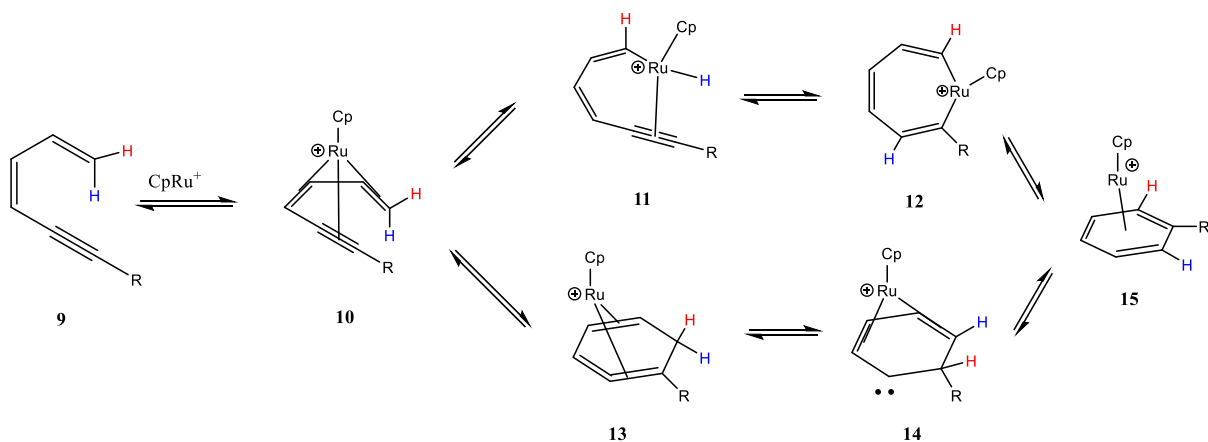
On the other hand, a similar electrocyclicization of 3-en-1,5-diyne (**7**) to form benzene was reported by Bergman. In this case, **7** with the presence of hydrogen source (toluene, 1-4 CHD, etc.)



Scheme 2-2: Proposed mechanism of thermal Bergman cyclization.

at high temperature (~300 °C) generates the symmetrical para-benzene diradical intermediate followed by the hydrogen extraction from the hydrogen source. Heat in this case, is crucial to overcome the high electrocyclization energy barrier to yield the product (Scheme 2-2).¹

As stated, the thermal conditions in these two reactions limit their applications in synthesis. Substrates likely undergo polymerization or decomposition at such high temperatures.⁸ To address this drawback, various methods including photon triggering,⁹ addition of Lewis acid¹⁰ or applying metal catalysts¹¹ were investigated. O'Connor's group has done a thorough examination in mediating such reactions with Cp/Cp*Ru⁺L₃ complexes under moderate conditions. In his work, both Bergman and Hopf cyclization reactions can be achieved at ambient temperature.¹²⁻¹⁴

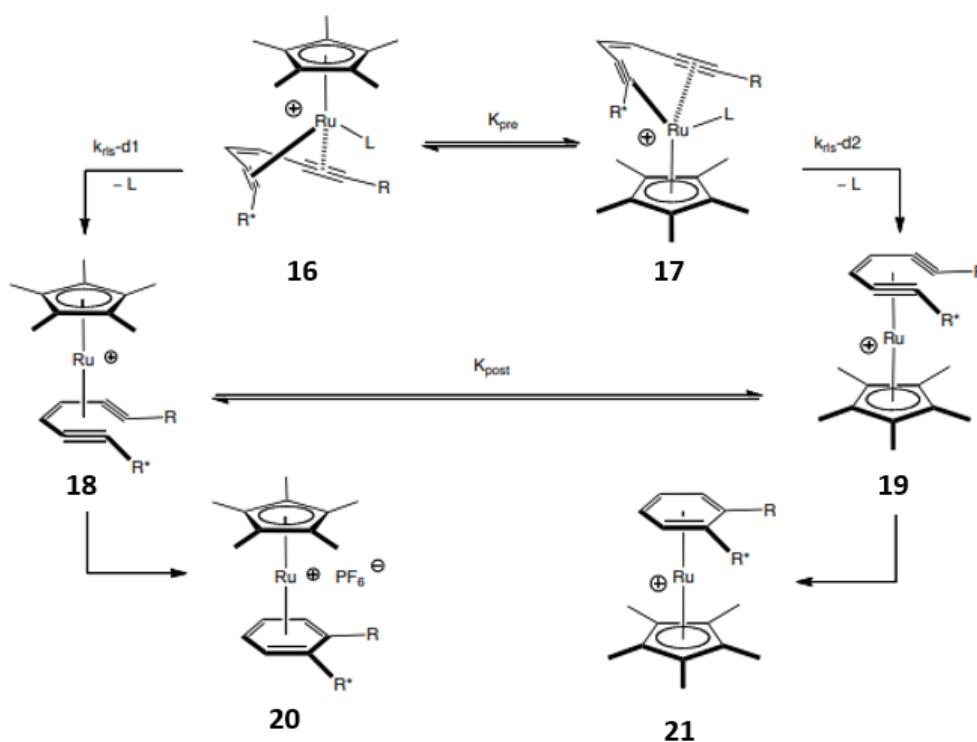


Scheme 2-3: Two proposed mechanisms of Ru mediated Hopf cyclization.

In his proposed mechanism pathways, the Cp*Ru⁺(η^6 -diene) (**10**) is the crucial intermediate in both speculative mechanistic routes. One pathway describes the ruthenium center inserting between the terminal C-H bond of the alkene to form **11**. It would then undergo a [1,5] hydride shift as the ruthenium continuously inserts the alkyne to form **12**. The arene product is generated via a reductive elimination. The ruthenacycloheptatriene structure **12** was proposed in previously reported Ru mediated arene synthesis.¹⁵ The other pathway begins with the formation

of a $\text{CpRu}^+(\eta^4\text{-isobenzene})$ (**13**), followed by a [1,2] hydride to generate the carbene structure **14** then a secondary [1,2] hydride shift to yield the final product. The product can also be obtained via a [1,5] shift from the **13** as shown in the thermal pathway.¹⁶

Bergman cyclization was also successfully achieved under similar conditions with the presence of hydrogen donors. $\text{Cp}^*\text{Ru}^+(\eta^4\text{-enediyne})(\text{solvent})$ complexes (**16** and **17**) were firstly established. The loss of the third ligand would yield the $\text{Cp}^*\text{Ru}^+(\eta^6\text{-enediyne})$ complexes (**18** and **19**). The favorability in forming **18** and **19** is affected by the steric interactions between the alkyne substituents and the Cp^* . Lastly, cyclization occurred by going through the para-benzene diradical intermediates to produce diastereomers **20** and **21** as the products¹⁷.

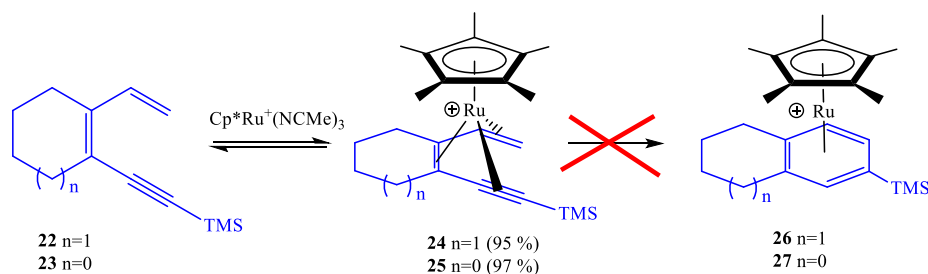


Scheme 2-4: Proposed mechanism of Ru mediated Bergman cyclization.

The purpose of my work is to continue the in-depth mechanistic study of the dienyne cyclization and extend the scope of the generality with various substrates. The system was then further modified with $\text{Cp}^*\text{Ru}^+(\eta^6\text{-naphthalene})$ to achieve a handy control over the biradical formation during Bergman cyclization as well as a metal-complex precursor that is high stable with respect to moisture and ambient air. Lastly, an examination was carried out on an iridium complex.

II. Isolation and characterization of $\text{Cp}^*\text{Ru}^+(\eta^6\text{-dienyne})$ intermediate of TMS substituted dienyne.

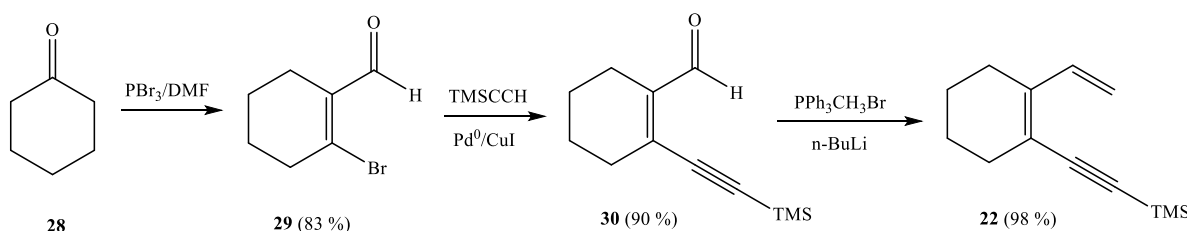
Although O'Connor cyclization has been successful and provided an advancement in the synthesis of a variety of dienyne substrates, it was not possible to obtain the same reaction for substrates **22** and **23** to form the cyclized products **26** and **27** (Scheme 2-5). We presume that the activation energy barrier is significantly increased due to the steric conjunction resulting from the bulky trimethylsilyl substituents on the alkyne. Based on the speculated mechanism (Scheme 2-5), it is reasonable to propose that although the cyclization was prohibited, the formation of the



Scheme 2-5: Proposed electrocyclization of dienyne **22** and **23**.

Cp* $\text{Ru}^+(\eta^6\text{-dienyne})$ structure (**24** and **25**) should not be affected by the substituent bulkiness. In another words, it was possible to isolate and characterize the Cp* $\text{Ru}^+(\eta^6\text{-dienyne})$ structure and thus provide a concrete reference and model for further understanding in its mechanism¹⁸.

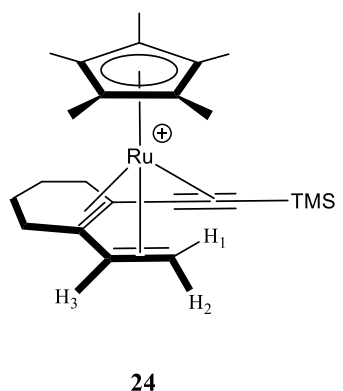
Dienyne **22** was synthesized by first running a Vilsmeier-Haack reaction with cyclohexanone, dimethylformimide (DMF) and tribromide phosphorus (PBr_3), followed by a Sonogashira coupling reaction with trimethylsilylacetylene, then a Wittig reaction with methyltriphenylphosphonium bromide (Scheme 2-6). Dienyne **23** was synthesized with the same



Scheme 2-6: Synthesis of dienyne **22** from cyclohexanone.

protocol with cyclopentanone as the starting material. The purified dry substrate **22** was then mixed with $[\text{Cp}^*\text{Ru}^+(\text{NCMe})_3][\text{PF}_6]$ (**92**) in a 1:1 mole ratio in anhydrous CDCl_3 containing 1,3,5-tri-tert-butylbenzene as the internal standard. Once the reaction reached completion, high vacuum was applied to remove all the volatiles. ^1H NMR spectra of the resulting reaction mixture did not exhibit any resonances between δ 4.0 to 7.0 ppm that can support the formation of the arene product **26**. However, three distinguishable resonances each integrated to one hydrogen were presented: δ 0.87 (dd, $J_{\text{HH}} = 11.2$ Hz, $^1J_{\text{HH}} = 2.4$ Hz), 3.45 (dd, $J_{\text{HH}} = 9.2$ Hz, $^1J_{\text{HH}} = 2$ Hz) and δ 4.96 (t, $J_{\text{HH}} = 10.4$ Hz). Due to the fact that only one resonance belongs to the TMS substrate was presented and no free or coordinated acetonitrile resonances were detected, we believe the observed structure

Table 2-1: Structure of the Cp*Ru(η^6 -dienyne) **24** and selective ^1H NMR resonances.

	Reonance	Shift (ppm)	Coupling (Hz)
	H ₁	0.87	11.2
	H ₂	3.45	9.2
	H ₃	4.96	10.4
	TMS	0.36	-
	Cp*	1.81	-

was the Cp*Ru⁺(η^6 -dienyne) (**24**) and those three hydrogen resonances were contributed by the three unique vinyl hydrogens H₁, H₂ and H₃ that were presented in the structure shown in Table 2-1, the dramatic up field shift in the comparison to those in **22** were caused by the ruthenium center coordination. The integration of each resonance as referenced to the internal standard gave a yield

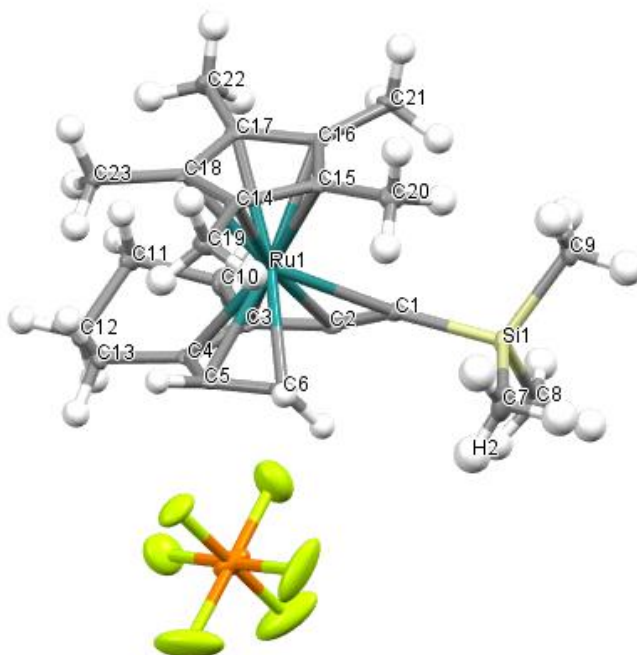


Figure 2-1: X-Ray crystal structure of complex **24**.

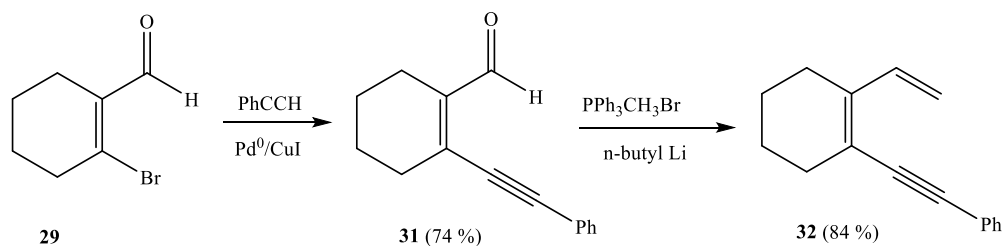
of 95.1 %. Similar resonance features were observed when reacting **23** with **92** under similar conditions.

To obtain more evidence about the structure to support our hypothesis, we attempted to grow single crystals for X-ray crystal diffraction analysis. The completed reaction mixture was concentrated to the maximum concentration under high vacuum and 3 volume eq. anhydrous hexanes was then distilled on top of the solution and fully mixed at ambient temperature in the dark. After three days we obtained crystals for analysis. It was clearly shown that the structure was identical to **24** as we proposed. The Ru-C bonds were the longest between Ru-C₁ and Ru-C₄ (2.42 and 2.30 Å), but the remaining Ru-C bonds were almost identical. As expected, there was no evidence showing that a bond was formed between C₁ and C₆.

To further understand the coordination environment, we also performed a competition reaction by reacting **22** and **23** with **92** in a mole ratio of 1: 1: 0.5. Surprisingly, 53 % of **23** was consumed while only 23 % of **22** were reacted in the formation of the products. It was still unclear to us what resulted in this difference in rate. We proposed that the coordination of the ruthenium may have relieved the ring strain in **23** resulting in a much more energetically favorable intermediate.

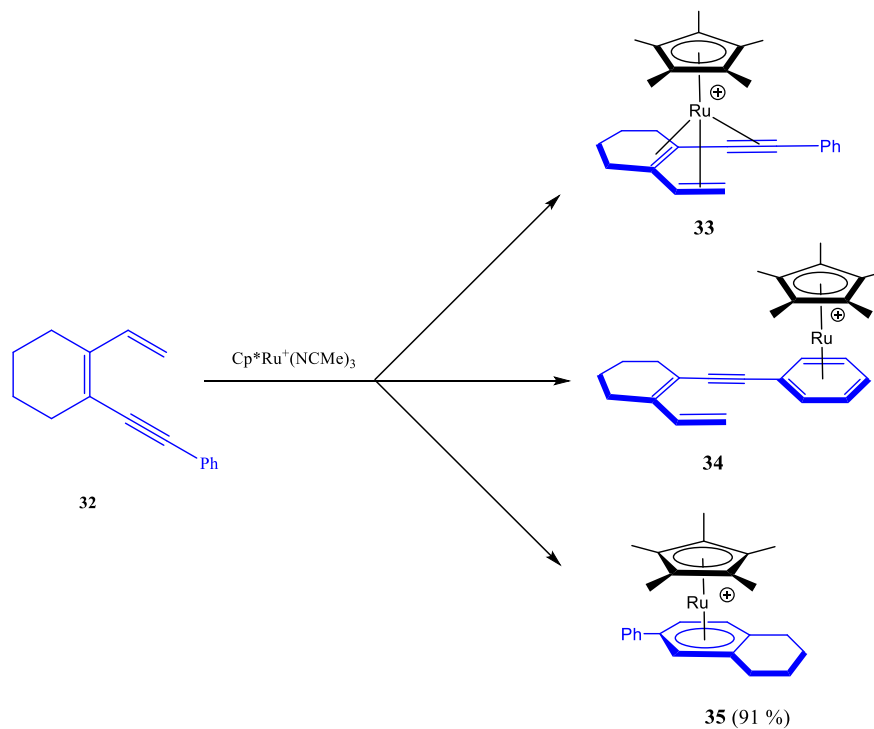
III. Cycloaromatization of dienyne with phenyl substrates.

Further investigation raised an interesting question as to whether the presence of phenyl will affect the coordination of the ruthenium center and compete with the cyclization reaction.¹⁹ To address this question dienyne **32** was synthesized as show in scheme 2-7. Reaction with **92** was carried out in a J. Young NMR tube and monitored by ¹H NMR spectroscopy. Substrate **32** was allowed to react under inert atmosphere with Cp*⁺Ru(NCMe)₃ until completion in anhydrous CDCl₃. The product was then crushed out with diethyl ether and washed through a clog of zeolite



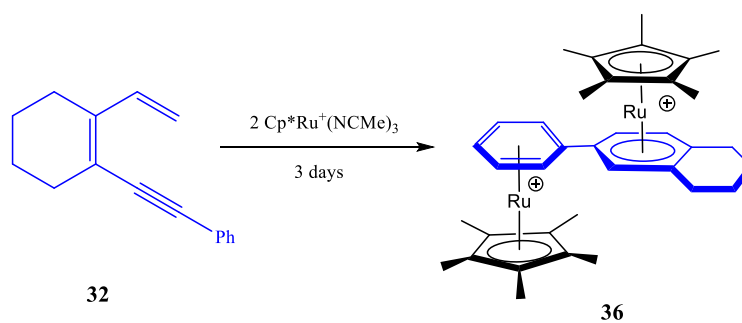
Scheme 2-7: Synthesis of dienyne **32** from cyclohexanone.

with DCM. The isolated yellow solid exhibited ¹H NMR resonances at δ 5.86 (d, $J_{\text{HH}} = 6.4$ Hz, 1H), 6.08 (s, 1H), 6.27 (d, $J_{\text{HH}} = 6$ Hz, 1H). In comparison with the Cp*⁺Ru(η^6 -dienyne) characterized in the previous section, we can eliminate the possibility of the hexahepto structure **33**. It was also not likely that the ruthenium center was coordinating to the phenyl substitute to form **34** due to the fact that one of the proton resonances exhibited as a singlet (the expected split pattern of **34** would be two doublet and one triplet) which left the last possibility that the compound we obtained was the cyclized arene product **35**. To further verify our findings, a crystal was obtained by dissolving the complex in minimal acetone and crystalized via vaper diffusion with



Scheme 2-8: Possible products of the reaction between dienyne **23** and Cp^*Ru^+ .

hexanes. Unfortunately, accurate bond lengths or angles could not be analyzed due to the poor quality of the crystal, but some notable features are still worth mentioning: First, the Ru center was coordinated to the substituted phenyl substrates and second, the substituted phenyl was rotated to the same plane as the dienyne, to minimize the steric conjunction. When mixing 2 mole eq. of Ru complex and 1 mole eq. of the substrate, we observed the resonances belonging to **35** appeared within the first 24 hours. Continuing the reaction resulted additional resonances within the



Scheme 2-9: Speculative product between dienyne **23** and 2 mole eq. $\text{Cp}^*\text{Ru}^+(\text{NCMe})_3$ after three days.

aromatic region after the removal of any organic products, which suggests that the excess ruthenium may have coordinated to the substituted phenyl to generate **36** (Scheme 2-9).

Substrate **40E** and **40Z** were synthesized to study the general selectivity during the cyclization (Scheme 2-10). **40Z** was synthesized following a similar protocol as **32** but the Sonogashira coupling was modified by running in a propyne saturated benzene/TEA solution then reacting the product **39** with phenyltriphenylphosphoniumbromide via a Wittig reaction. The coupling constant of the two vinyl hydrogen resonances was only 12 Hz, indicating that the product was a cis isomer. **40E** isomer was synthesized by stirring **41** in DCM with 0.1 mole eq. of I₂ to

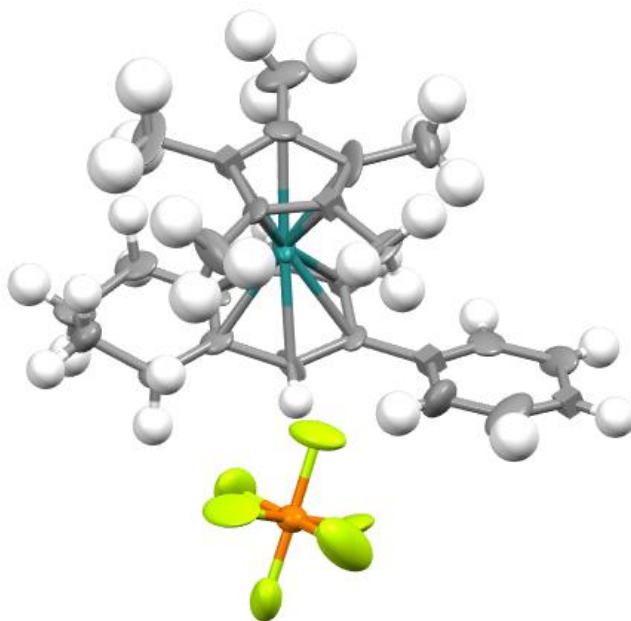
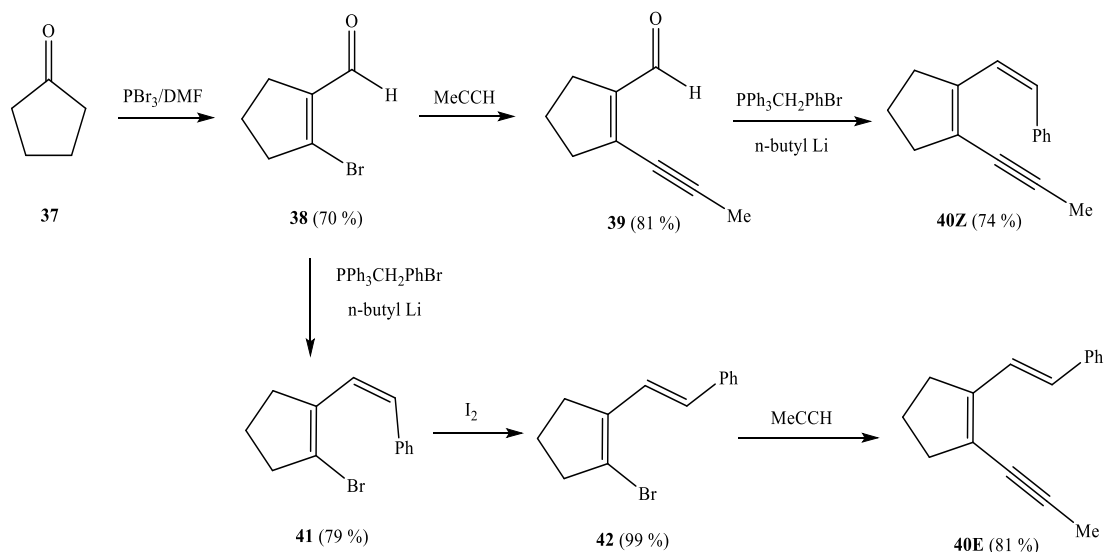


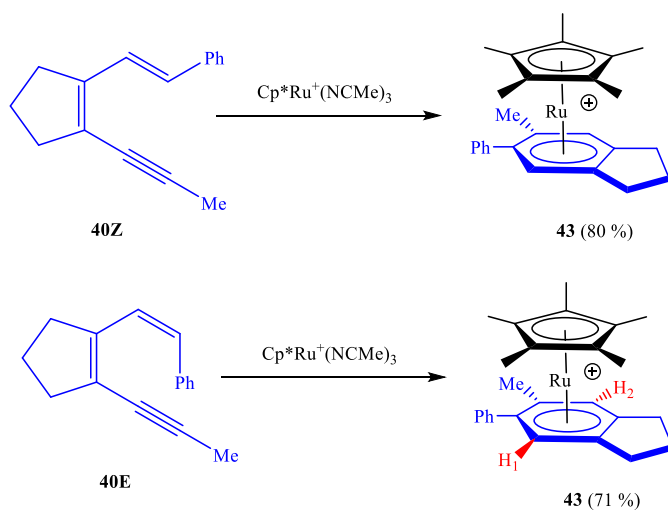
Figure 2-2: X-Ray crystal structure of complex **35**.



Scheme 2-10: Synthesis of **40-Z** and **40-E**.

trigger isomerization and allowed to react for 3 days, followed by a Wittig reaction with phenyltriphenylphosphoniumbromide. ^1H NMR spectrum showed the coupling constant of the vinyl hydrogens was 16 Hz, indicating the formation of the trans isomer.

The reaction of **40E** and **40Z** with **92** successfully yielded the same cyclized arene products. After reacting with **92** in CDCl_3 for 1 h, product in both cases exhibited two resonances at δ 5.03



Scheme 2-11: **40-E** and **40-Z** undergoes electrocyclization to generate the same arene product **43**.

and 5.17 ppm signed to H₁ and H₂, indicating that both reactions generated the same product with an asymmetrical structure that has two unique arene hydrogens presented (scheme 2-11).

Since the same product and intermediate were obtained in both cases, we believed an isomerization must occur during the cyclization. To verify our hypothesis, we carried out a competition reaction with **40E** and **40Z** and **92** in a J. Young. NMR tube containing internal standard (1,3,5-tri-tert-butylbenzene) dissolved in CDCl₃ in a mole ratio of 13: 15: 1. One hour later, we observed consumption of **40E** and **40Z** was 3.1 % and 2.1 %, respectively. We proposed that the yield difference was a result of kinetic difference which was caused by isomerization. Thus, we continued the investigation with a kinetic study.

The mole ratio of two reactants **40E**, **40Z** and **92** were 15: 1 in order to reach the reaction completion. 750 mole eq. of acetonitrile were added for the purpose of retardation. The tube was frozen at -78 °C prior to recording the initial NMR spectrum. The monitoring immediately started once the tube was warmed to 23 °C. ¹H NMR spectrum was continuously taken every 1.5 min for 1 h after reaction starts; every 5 min for the second hour and every 10 min for the 3rd hour. The

concentration of **92** was monitored based on the integration of Cp* resonances at δ 1.6 relative to the internal standard resonance and $\ln[\text{Cp}^*\text{Ru}^+]$ was plotted vs. time.

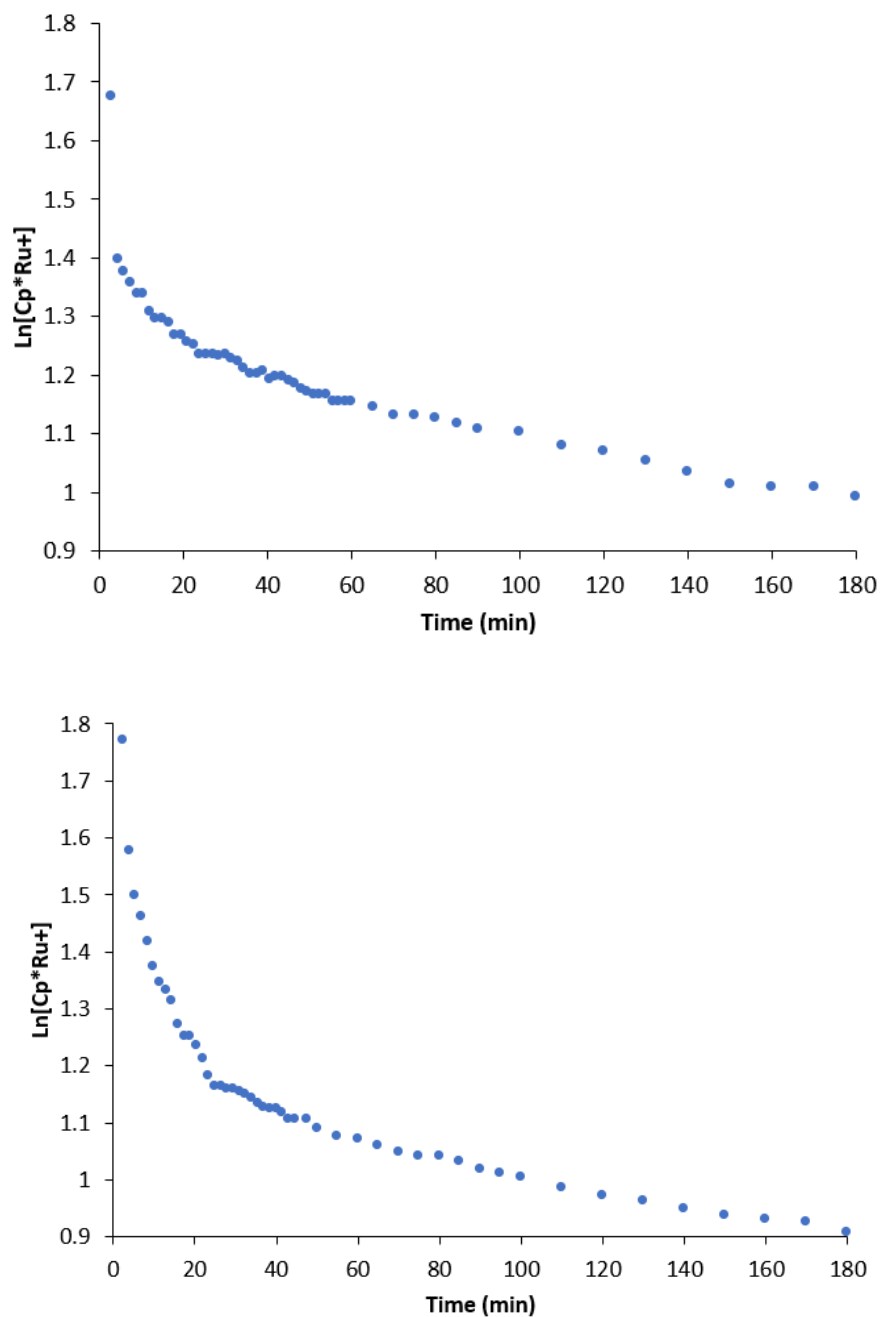
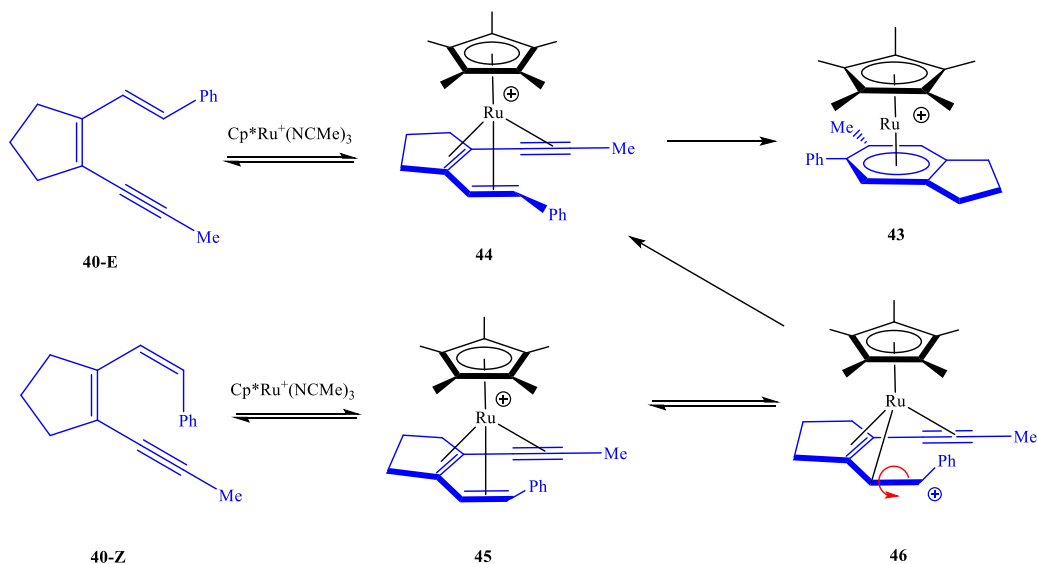


Figure 2-3: Kinetic study of 40E (Top) and 40Z (Bottom) treated with **92** and NCMe-d₃.

It was not surprising to us that the reaction rate eventually reached the same equilibrium after 90 min, (-1.1×10^{-3} for **40Z** and -1.4×10^{-3} for **40E**) as the cyclization was expected to be the rate determining step in our proposed mechanism. However, during the first 15 min, the ruthenium complex in **40Z** sample experienced a rapid consumption before reaching the same disappearing rate as **40E** while such a consumption was not observed in the case of **40E**. Both substrates were expected to generate **44** as the phenyl substrate points away from the alkyne to reduce the steric conjunction. Such a structure can be directly achieved by the coordination of ruthenium to the **40-E**. However, isomerization is required in the case of **40Z**.



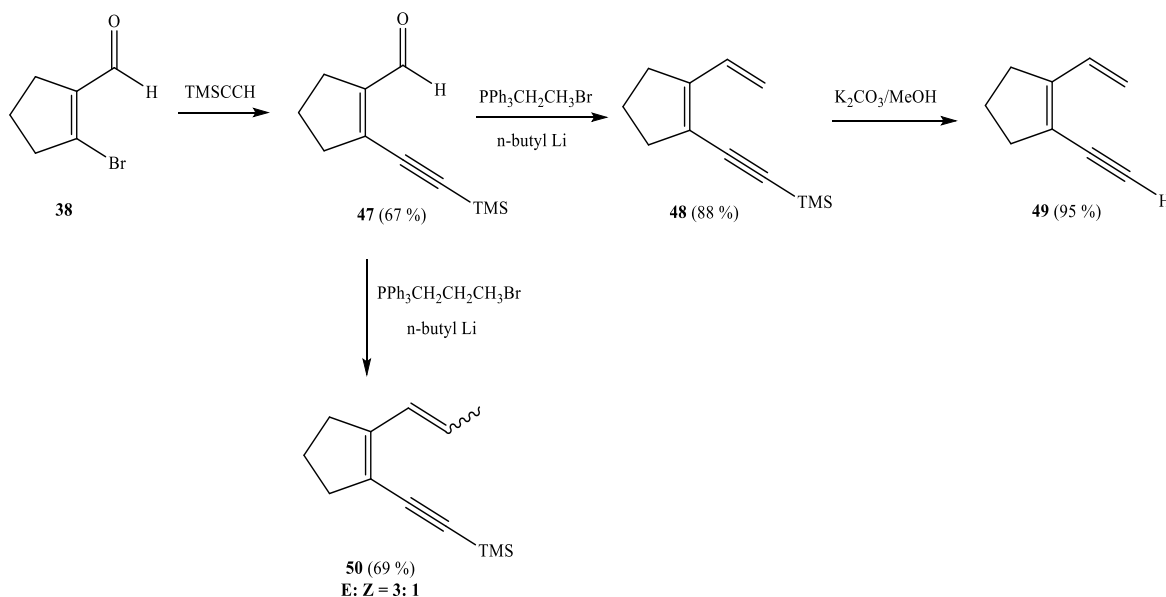
Scheme 2-12: Proposed mechanism of **40-E** and **40-Z** cyclization mediated by the Ru complex.

In our hypothesis, **45** was firstly generated with the coordination of ruthenium. Then ruthenium inserts to the internal alkene carbon, allows the cation to migrate onto the terminal alkene carbon and results a reduced C=C bond as shown in **46**. Such carbocation is expected to be stabilized via resonance with the presence of the phenyl substitute. The reduction resulted alkane bond then could freely rotate for a trans-conformation. **44** now can be achieved by regenerating the alkene (Scheme 2-12). This work proposed a selective isomerization that could occur during

the cyclization when activation energy barrier is increased with the presence of a bulky substrate, which further revealed its mechanism.

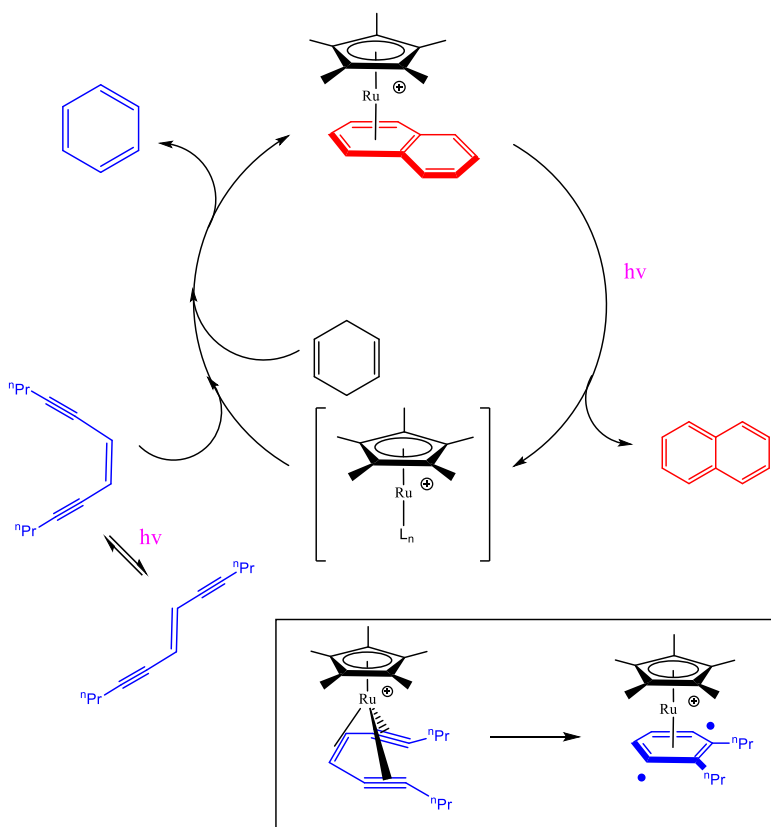
IV. Photoactivate transition metal triggers for enediyne and dienyne cyclization

Although ambient temperature Bergman cyclization can be achieved with **92**, the spatiotemporal control of diradical formation suitable for initiating free radical polymerization reactions and induce tumor cell death in biological systems remained as a challenge.^{20, 21} To address this shortcoming, O'Connor's group has developed the first generation of photoactivated metal complex to photochemically mediate the cyclization.



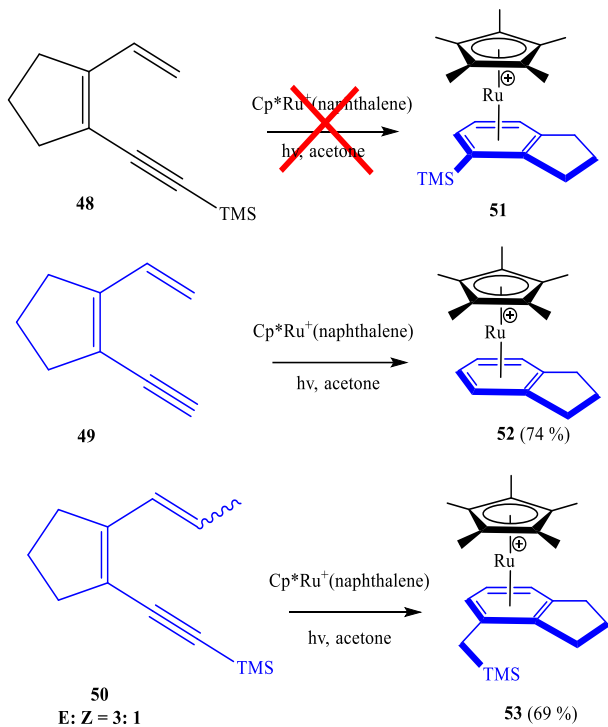
Scheme 2-13: Synthesis of **48**, **49** and **50**.

Based on Kudinov's report, $[\text{Cp}/\text{Cp}^*\text{Ru}^+(\eta^6\text{-naphthalene})][\text{PF}_6]$ complexes (**1-12**) undergo efficient ligand exchange between naphthalene and arene, as about 5-fold faster rate for naphthalene photodissociation relative to benzene dissociation.²² Thus, we seek $[\text{Cp}^*\text{Ru}^+(\eta^6\text{-$



Scheme 2-14: $\text{Cp}^*\text{Ru}^+(\eta^6\text{-naphthalene})$ complex serves as photoactivated Bergman cycloaromatization triggers.

$[\text{Cp}^*\text{Ru}^+(\eta^6\text{-naphthalene})][\text{PF}_6]$ (**93**) as a promising photoactive precursor. The presence of light serves two purposes: First it triggers the photodissociation of the arene ligand from its precursor. Second, it mediates the photoisomerization of any E-enediynes conformer to its Z conformer (Scheme 2-14). Prior to my work, it was demonstrated that a rich ruthenium center with coordination solvent (acetone or THF) would provide superior performance, relatively. Thus, the system of **93** in acetone has been focused on in this study.²³

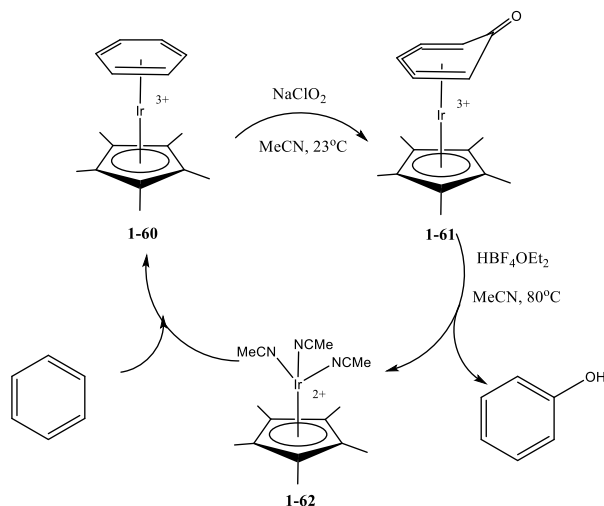


Scheme 2-15: Attempted cyclization of **48**, **49** and **50** with $\text{Cp}^*\text{Ru}^+(\eta^6\text{-naphthalene})$.

A variety of dienyne substrates were examined under similar conditions (Scheme 2-15). **48** was synthesized as shown in scheme 2-12 and **49** was synthesized by performing a desilylation on **48**. We were pleased to observe that **93** triggers **49** with the presence of light giving the formation of the cyclized product **52** at a yield of 60 %. **50** was able to produce the arene product **53** at a yield of 55 %. However, **48** under similar condition did not yield product **51** due to steric contraction which is consistent with what was mentioned in section I.

V. Attempt to mediate diyne cyclization with an iridium complex.

Iridium also demonstrated its capability in activating tri- π systems. Reported by Ritter and coworkers, a selective C-H hydroxylation can be mediated by $\text{Cp}^*\text{Ir}^{3+}(\eta^6\text{-arene})$ complex (Scheme 2-16).²⁵



Scheme 2-16: An example of Ir complex activating: Synthetic cycle for oxidation of benzene to phenol.

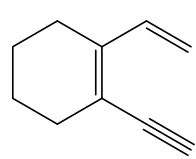
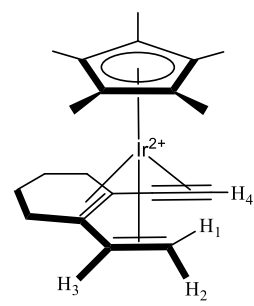
The candidate was chosen to be the $\text{Cp}^*\text{Ir}^{2+}(\text{NCMe})_3$ (**94**) in order to mimic the ruthenium system that has been well studied by our group. The complex was synthesized with a modification on the protocol given by Wu's group.²⁵ $(\text{Cp}^*\text{Ir}^{3+}\text{Cl}_2)_2$ dissolved anhydrous acetonitrile was mixed with AgBF_4 containing acetonitrile solution. AgCl white precipitate formed immediately. The reaction was stirred at ambient temperature for 2 hours until no more precipitate formed. The crude reaction mixture was then filtered and dried under vacuum, resulting in the product, a light yellow solid.

The reactions between the **94** and diyne substrates were surprising and fascinating. Mixing **54** and **94** in acetone-*d*₆ resulted an immediate color change from light yellow to dark

purple. However, such rapid color change was not observed in the reaction with **22**. 1,3,5-tri-tert-butylbenzene was not used as the internal standard in this case, because a rapid coordination between Ir center and the arene was observed. It was also confirmed that unreacted AgBF₄ or any AgCl impurity does not react with dienyne substrates.

The ¹H NMR spectrum of completed **54** and **94** reaction mixture exhibited four hydrogen resonances between δ 6.0 to 6.5 ppm that were not observed in the starting material ¹H NMR spectrum. 24 h of reaction yielded 80 % product while it remained unchanged during the next seven days. The reaction tube was then placed under high vacuum to remove all volatiles. The product remained stable when fresh acetone-*d*₆ was distilled into the tube. The ¹H NMR spectrum after distillation did not give any possible resonance that could be recognized as free or coordinated acetonitrile. Thus, we believe that the coordination that happened between the Ir center and the

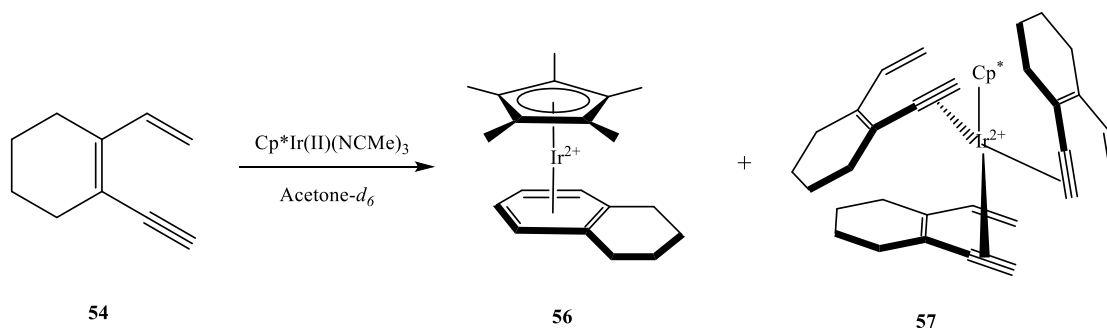
Table 2-2: Speculative product after reacting **54** with **94** in a 1:1 mole ratio and selective ¹H NMR resonances.

 <p>54</p>	$\xrightarrow[\text{Acetone-}d_6]{\text{Cp}^*\text{Ir(II)(NCMe)}_3}$	 <p>55 (85 %)</p>	<table border="0"> <thead> <tr> <th style="text-align: left;">Reaonance</th> <th style="text-align: left;">Shift (ppm)</th> </tr> </thead> <tbody> <tr> <td>H₁</td> <td>6.29</td> </tr> <tr> <td>H₂</td> <td>6.47</td> </tr> <tr> <td>H₃</td> <td>5.94</td> </tr> <tr> <td>H₄</td> <td>6.51</td> </tr> <tr> <td>Cp*</td> <td>1.78</td> </tr> </tbody> </table>	Reaonance	Shift (ppm)	H ₁	6.29	H ₂	6.47	H ₃	5.94	H ₄	6.51	Cp*	1.78
Reaonance	Shift (ppm)														
H ₁	6.29														
H ₂	6.47														
H ₃	5.94														
H ₄	6.51														
Cp*	1.78														

dienyne was likely a hexahepto coordination as shown in **55**. The four resonances we observed could be signed to the three vinyl hydrogens and the alkyne hydrogen δ 5.94, 6.29, 6.47 and 6.51 ppm. The coordination between Ir center and the alkyne would greatly reduce the electron density of the triple bond and cause alkyne to behave in an sp² like character, so it was reasonable to observe that the alkyne hydrogen experienced a similar shielding environment as the vinyl

hydrogens. The isolation including purification and crystallization of this speculative complex **54** is still in progress. We do not believe the cyclized product was observed in this reaction.

To our great surprise, running the reaction between **54** and **94** in a mole ratio of 10: 1 gave a very different ^1H NMR spectrum. Those four resonances in the previous study were not observed, instead resonances at δ 5.10 (d, 1H, $J_{\text{HH}} = 10.8$ Hz), 5.23(d, 1H, $J_{\text{HH}} = 19.2$ Hz) and 6.59 (dd, 1H, $J_{\text{HH}} = 10.4$ Hz, $J_{\text{HH}} = 16.8$ Hz) ppm behaved in a very similar pattern to the starting materials but with a slight up-field shift. We propose in the case of a 10: 1 reaction, it was unlikely for the hexahepto structure to establish but a Ir center coordinated to three **54** via the alkyne shown in **57**,



Scheme 2-17: Speculative product after reacting **54** with $\text{Cp}^*\text{Ir}^{2+}(\text{NCMe})_3$ in a 10:1 mole ratio.

which could have resulted from the high concentration of excess diene. However, this complex did not survive after the high vacuum, indicating that the coordination between the Ir center and the diene was much weaker. After the applied vacuum, only one product was left, that showing resonances at δ 5.09 (s, 2H) and 5.68 (s, 2H) ppm, integration as the reference to the Cp^* peak in a ratio of 1: 1: 8. This integration suggests that the cyclized product (**57**) shown in the figure was possibly obtained. The current work still focuses on isolating and purifying the intermediates and the product we observed in this study.

VI. Conclusions and Future Outlook

In this work we described an in-depth study of ruthenium mediated dienyne electrocyclization. The characterization of **24** gave us a reliable reference and model for any possible ruthenium coordinated dienyne complex. The study of phenyl substituted dienyne **32**, **40E**, **40Z** reaction with ruthenium revealed a selectivity and isomerization during the cyclization. A photoactive precursor **93** exhibited an excellent performance not just in Bergman cyclization but also the Hopf cyclization. The investigation of iridium also yielded an encouraging result that may provide a different perspective in solving its mechanism. Future work in this project will focus on isolating and characterizing the speculative products.

VII. Experimental

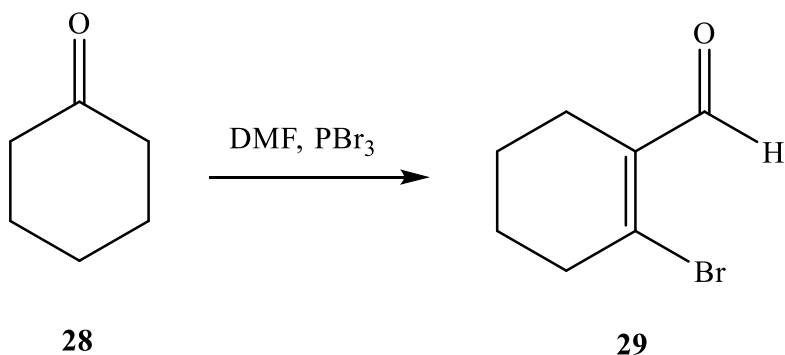
1. General procedures

Standard Schlenk technique or a nitrogen-filled glovebox are applied in all NMR reactions between dienyne substrates and metal complexes. Flash column chromatographic purifications were performed using silica gel (60 Å, particle size 43-60 um, 230-400 mesh, EMD Chemicals). ¹H and ¹³C NMR spectra were recorded on Varian Mercury 400 MHz or Varian VX 500 MHz instruments. ¹H and ¹³C NMR chemical shifts (δ) are reported in parts per million (ppm). Spectra were referenced to the residual solvent peak. Chloroform-*d* was dried by refluxing with CaH₂ overnight and acetone-*d*₆ was dried over activated molecular sieves followed by distillation under

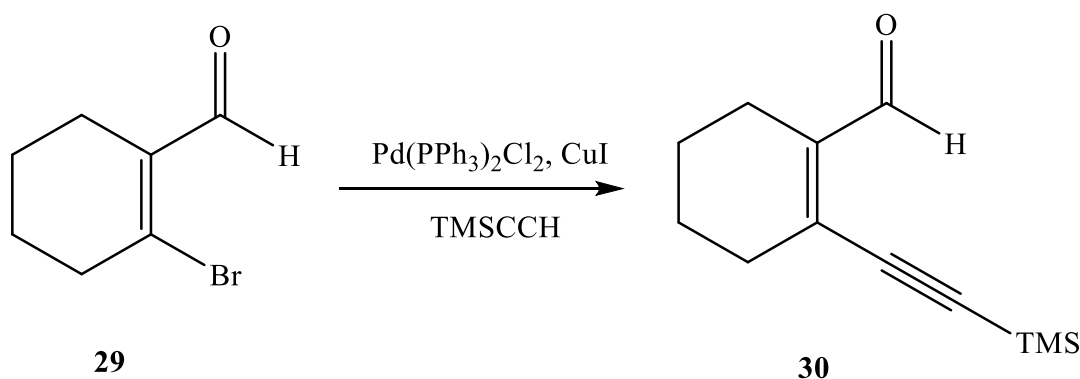
static vacuum. NMR reactions were performed in 5 mm J. Young NMR tubes equipped with a Teflon needle valve.

2. Synthesis and Characterization Data

2-bromocyclohex-1-ene-1-carbaldehyde (29): To a solution of DMF (13.0 ml, 167.9 mmol) in chloroform (80 mL), PBr_3 (15.4 mL, 152.8 mmol) was added dropwise at 0 °C. The mixture was stirred for 60 min, and then cyclohexanone (5.0 g, 50.9 mol) was added. The solution was stirred for another 16 h., and the content was poured to a 300 mL water, neutralized with solid NaHCO_3 and extracted with dichloromethane. The extract was washed with brine, dried over anhydrous MgSO_4 and concentrated under reduced pressure. The residue was purified through flash silica gel column (95:5, hexanes / EtOAc) to afford compound **29** as light yellow oil (8.0 g, 42.4 mmol, 83 %). ^1H NMR (400 MHz, CDCl_3) δ : 1.58 – 1.67 (m, 4H, $-\text{CH}_2-$), 2.19 - 2.38 (m, 4H, $-\text{CH}_2-$), 10.15 (s, 1H, CHO). The product exhibited an identical spectroscopic property to those reported in literature.

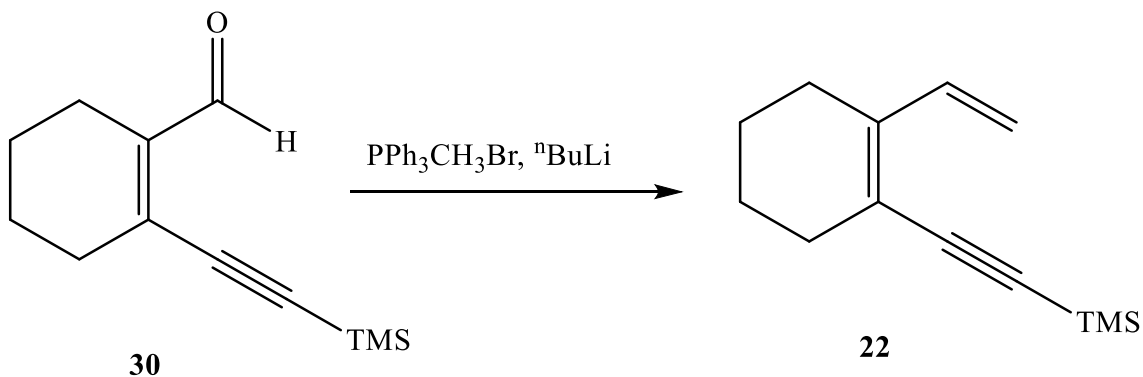


2-((trimethylsilyl)ethynyl)cyclohex-1-ene-1-carbaldehyde (30): To a triethylamine / benzene (1:1, 70 mL) solution of compound of **29** (6 g, 31.5 mmol), PdCl₂(PPh₃)₂ (0.8 g, 1.14 mmol) and CuI (0.29 g, 1.52 mmol) were added at 23 °C. The mixture was stirred under pressurized argon for 20 min before addition of trimethylsilylacetylene (6.43 g, 63.0 mmol). The solution was stirred for 12 h and concentrated in vacuo. The mixture was then diluted with DCM and extracted with ether (100 mL x 2). The organic substract was then washed with 1 M aq. HCl (100 mL x 2) / H₂O (100 mL x 2) / brine (100 mL x 2), dried over anhydrous MgSO₄ and concentrated under reduced pressure. The residue was purified through a silica gel column (98: 2, hexanes / EtOAc) to afford compound **30** as yellow oil (5.8 g, 28.4 mmol, 90 %). ¹H NMR (400 MHz, CDCl₃) δ: 0.18 (s, 9H, TMS), 1.71 - 1.74 (m, 4H, -CH₂-), 1.96 – 2.23 (m, 4H, -CH₂-), 10.18 (s, 1H, CHO). The product exhibited an identical spectroscopic property to those reported in literature.



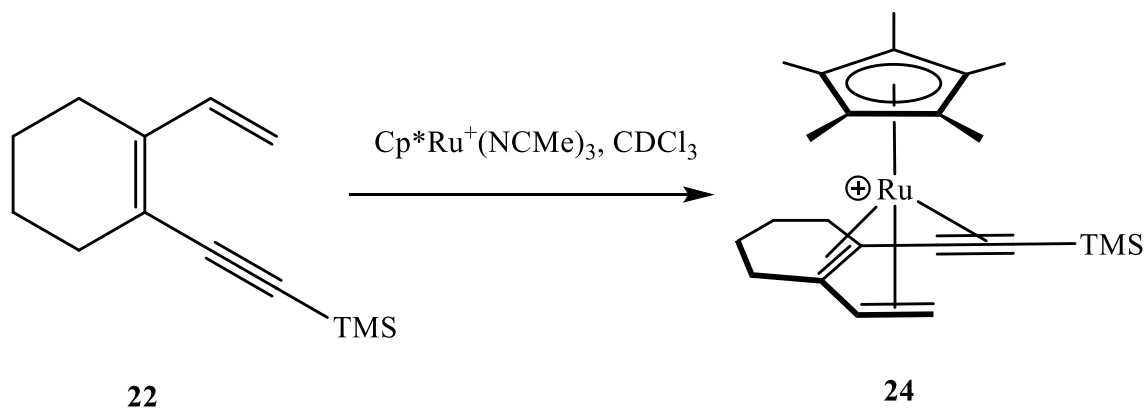
Trimethyl((2-vinylcyclohex-1-en-1-yl)ethynyl)silane (22): N-Butyllithium (5.79 mL, 13.9 mmol, 2.4 M in hexanes) was added dropwise to a stirring mixture of methyltriphenylphosphonium bromide (5.47 g, 15.3 mmol) in anhydrous THF (70 mL) at -78 °C. The solution then was stirred at 23 °C for 1 h followed by the addition of **30** (2 g, 9.7 mmol). After

stirring at 23 °C for 1h, the reaction was quenched with sat. aq. NH₄Cl (200 mL) and extracted with Et₂O (2 x 200 mL, 1 x 100 mL). The organic extract was washed with H₂O (3 x 200 mL) / brine (3 x 100 mL), dried over anhydrous MgSO₄, concentrated and purified by flash column chromatography (hexanes) to afford **22** as colorless oil (1.94 g, 9.5 mmol, 98 %). ¹H NMR (400 MHz, CDCl₃) δ: 0.21 (s, 9H, TMS), 1.60 - 1.63 (m, 4H, -CH₂-), 2.52 – 2.56 (m, 4H, -CH₂-), δ 7.17 - 7.24 (dd, 1H, *J*_{HH}= 17.6 Hz, *J*_{HH} = 11.2 Hz, vinyl H), 5.25 (d, 1H, *J*_{HH} = 17.0 Hz, vinyl H), δ 5.15 (d, 1H, 11.2 Hz, vinyl H). The product exhibited an identical spectroscopic property to those reported in literature.

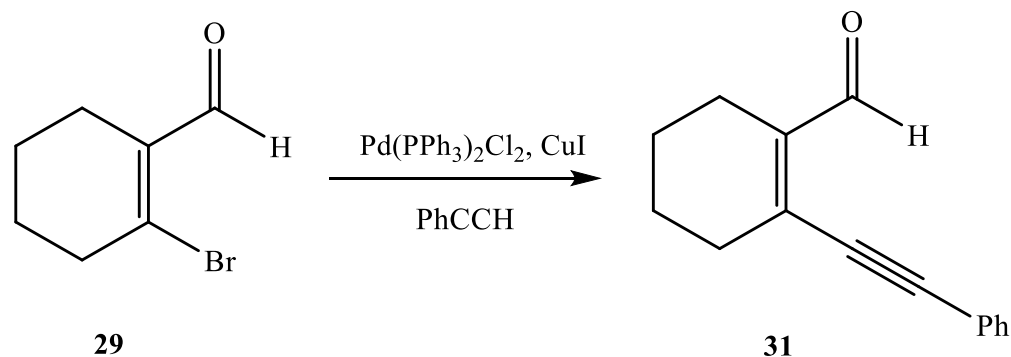


[(η^5 -C₅Me₅)Ru⁺(η^6 -trimethyl((2-vinylcyclohex-1-en-1-yl)ethynyl)silane)]PF₆ (24**):**
 [(η^5 -C₅Me₅)Ru⁺(NCMe₃)]PF₆ (**92**) (8.2 mg, 0.016 mmol), **22** (3.7 mg, 0.018 mmol), and 1,3,5-tri-tert-butylbenzene (internal standard) were placed in an oven-dried J. Young tube. Anhydrous CDCl₃ (1.1 mL) was distilled into the tube. After reacting at room temperature for 45 min (23 °C), volatiles were removed under high vacuum and fresh anhydrous CDCl₃ was distilled into the tube. The reaction was able to reach completion after 30 min in fresh CDCl₃ and give a yield of 9.4 mg of **24** in 95.1 %. ¹H NMR (CDCl₃, 400 MHz) δ: 0.36 (s, 9H, TMS), 0.87 (dd, *J*_{HH} = 11.2 Hz, *J*_{HH}

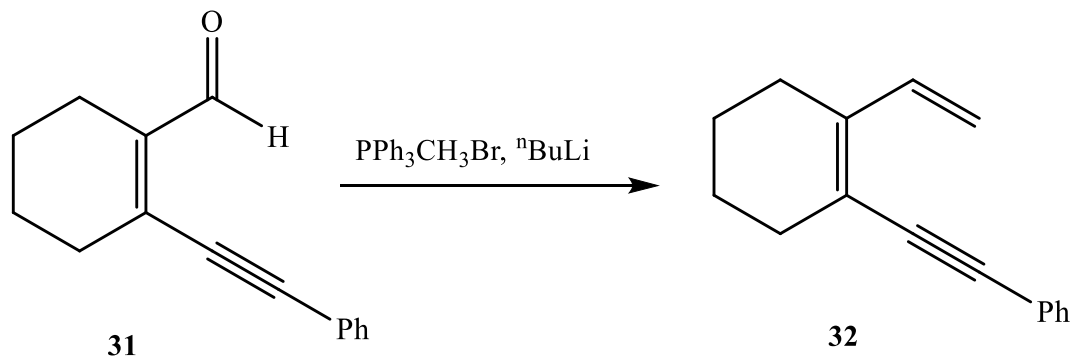
= 2.4 Hz, 1H, vinyl H), 1.81 (s, 9H, Cp*), 2.49 - 2.57 (m, 1H, CH₂), 2.66 - 2.73 (m, 1H, CH₂), 3.02 - 3.09 (dt, 1H), 3.45 (dd, $J_{\text{HH}} = 9.2$ Hz, $J_{\text{HH}} = 2$ Hz, 1H, vinyl H) and 4.96 (t, $J_{\text{HH}} = 10.4$ Hz, 1H, vinyl H). ¹³C NMR (CDCl₃, 500 MHz) δ : 0.5 (TMS), 10.1 (CH₃Cp*), 20.8, 21.2, 27.3, 38.0 (CH₂), 60.5, 87.9 (alkyne C), 90.9, 93.3, 95.1, 118.7 (vinyl C) and 97.9 (Cp*).



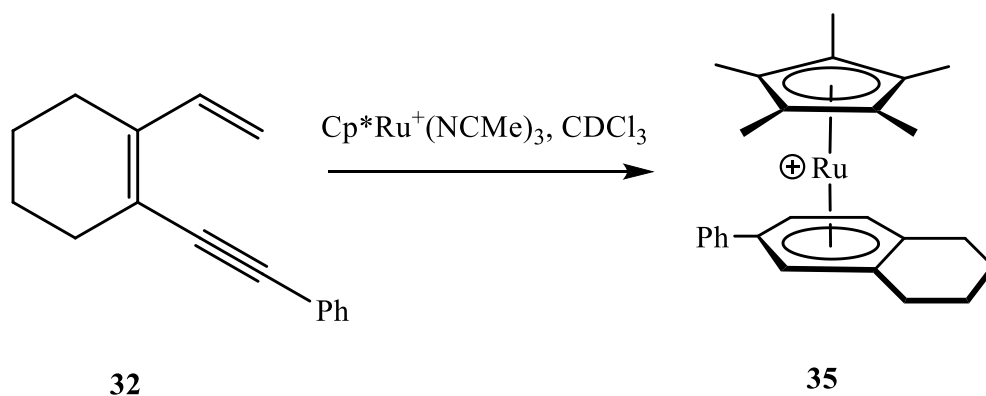
2-(phenylethynyl)cyclohex-1-ene-1-carbaldehyde (31): To a triethylamine/benzene (1:1, 70 mL) solution of compound of **29** (6 g, 31.5 mmol), PdCl₂(PPh₃)₂ (0.8 g, 1.14 mmol) and CuI (0.29 g, 1.52 mmol) were added at 23 °C. The mixture was stirred under pressurized argon for 20 min before addition of phenylacetylene (6.4 g, 63.0 mmol). The solution was stirred for 12 h and concentrated in vacuo. The mixture was then diluted with DCM and extracted with ether (100 mL x 2). The organic substract was then washed with 1 M aq. HCl (100 mL x 2) / H₂O (100 mL x 2) / Brine (100 mL x 2), dried over anhydrous MgSO₄ and concentrated under reduced pressure. The residue was purified through silica gel column (98:2, hexanes / EtOAc) to afford compound **31** as red oil (4.9 g, 23.3 mmol, 74 %). ¹H NMR (400 MHz, CDCl₃) δ : 1.73 - 1.78 (m, 4H, -CH₂-), 2.01 - 2.41 (m, 4H, -CH₂-), 7.29 - 7.47 (m, 5H, Ph), 10.15 (s, 1H, CHO). The product exhibited an identical spectroscopic property to those reported in literature.



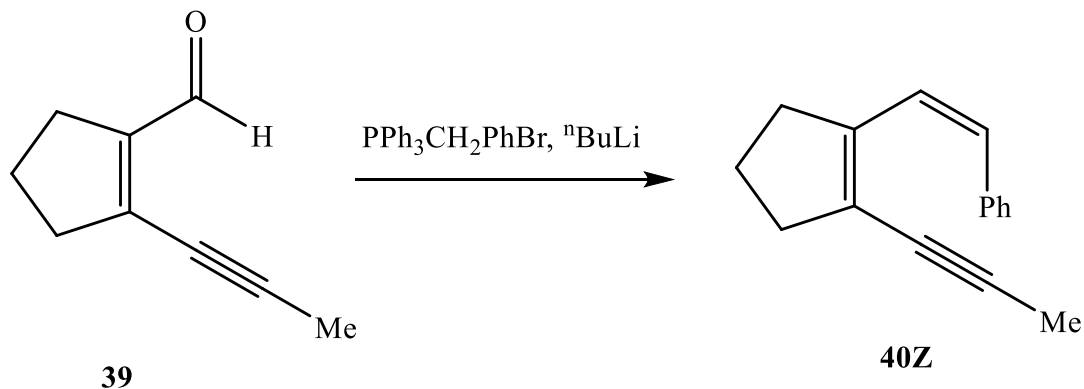
((2-vinylcyclohex-1-en-1-yl)ethynyl)benzene (32): A 2.5 M solution of n-butyllithium (7.25 mL, 18.1 mmol) in THF was added dropwise to a stirring solution of methytriphenylphosphonium bromide (6.75 g, 18.9 mmol) in 90 mL of argon saturated THF at -78 °C. After stirring for 1 h while warming up to 23 °C, **31** (2.56 g, 12.2 mmol) was added dropwise into the reaction mixture and following by stirring for 1 h. The solution was then quenched with sat. aq. NH₄Cl (100 mL) and extracted with Et₂O (2 x 60 mL). The organic extracts were washed with H₂O (2 x 80 mL) and brine (80 mL), dried over MgSO₄, concentrated, and purified by flash silica column chromatography (hexanes) to afford **32** as clear oil (2.14 g, 10.3 mmol, 84 %). IR (NaCl): 2197 cm⁻¹ (C≡C), 1614 cm⁻¹ (C=C), 1597 cm⁻¹ (Ph). ¹H NMR (400 MHz, CDCl₃) δ: 7.29 – 7.47 (m, 5H, Ph), 7.17 - 7.24 (dd, 1H, *J*_{HH} = 17.6 Hz, *J*_{HH} = 11.2 Hz, vinyl H), 5.28 (d, 1H, *J*_{HH} = 17.2 Hz, vinyl H), 5.12 (d, 1H, *J*_{HH} = 11.2 Hz, vinyl H), 2.29 – 2.38 (m, 4H, CH₂), 1.66 - 1.71 (m, 4H, -CH₂). ¹³C NMR (500 MHz, CDCl₃) δ: 22.0, 22.4, 24.5, 30.8 (CH₂), 89.5, 94.3 (C≡C), 113.1, 120.0, 123.7, 127.9 (C=C), 128.3, 131.3, 137.0, 140.1 (Ph). HRMS (EI): Calcd for (C₁₆H₁₆) = 208.1315, found: 208.1317.



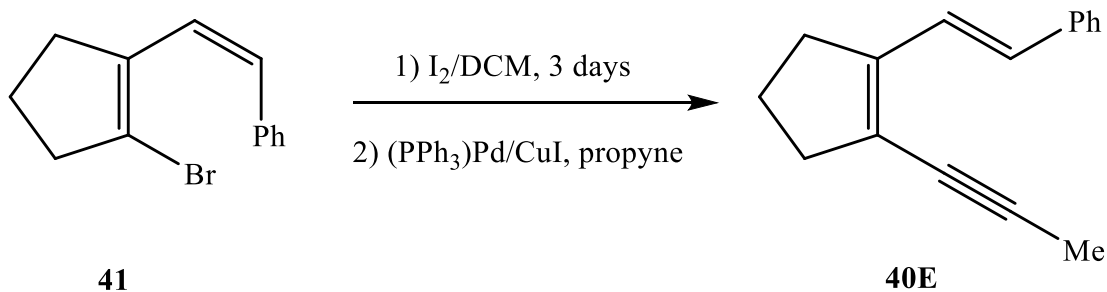
$[(\eta^5\text{-C}_5\text{Me}_5)\text{Ru}^+(\eta^6\text{-6-phenyl-1,2,3,4-tetrahydronaphthalene})]\text{PF}_6$ (**35**) **32** (5.2 mg, 0.025 mmol) and **92** (8.0 mg, 0.015 mmol) were weighted into an oven dried J. Young tube. 1.1 mL of anhydrous CDCl_3 was then distilled into the tube through the high vacuum line. The reaction mixture was then transferred to a 20 mL vial after 45 min at ambient temperature. 10 mL of Et_2O was added to the solution to precipitate out the product. The mixture was then filtered through a plug of Celite and rinsed with Et_2O (3 x 3 mL). The Celite was then rinsed with DCM (3 x 3 mL) which was collected into a fresh vial. All volatiles were removed to give the product **35** as a yellow powder (8.0 mg, 0.013 mol, 91 %). Product ^1H NMR (400 MHz, CDCl_3) δ : 1.69 (s, 15H, Cp*), 1.81-1.94 (m, 2H), 2.42 - 2.54 (m, 2H), 2.78 - 2.86 (m, 2H), 5.86 (d, $J_{\text{HH}} = 6.4$ Hz, 1H), 6.08 (s, 1H), 6.27 (d, $J_{\text{HH}} = 6$ Hz, 1H), 7.49 - 7.65 (m, 5H, Ph). ^{13}C NMR (500 MHz, CDCl_3) δ : 131.6, 130.3, 129.5, 126.7, 101.6, 101.2, 100.0, 94.7, 87.6, 84.1, 83.6, 26.3, 25.6, 21.7, 21.6, 9.7. HRMS (ESI): Calculated for ($\text{C}_{26}\text{H}_{31}\text{Ru}^+$): 445.1471. Found: 445.1472.



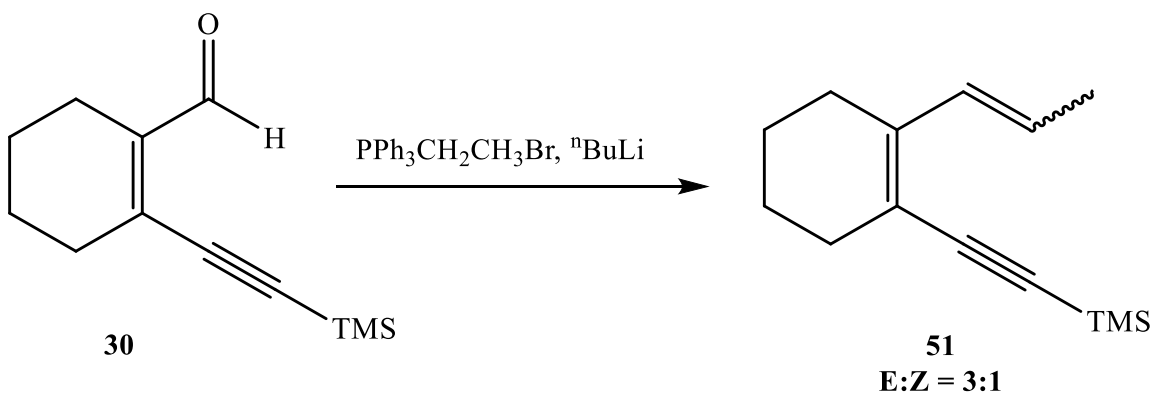
(Z)-2-(2-(prop-1-yn-1-yl)cyclopent-1-en-1-yl)vinyl)benzene (40Z): N-Butyllithium (5.6 mL, 2.4 M in hexanes, 13.4 mmol) was added dropwise to a stirring mixture of benzyltriphenylphosphonium bromide (6.07 g, 14 mmol) in anhydrous THF (200 mL) at -78 °C. After 1 h while warming up to 23 °C, **39** (1.5 g, 11.2 mmol) was added and the reaction mixture was then stirred for 1 h at 23 °C, quenched with sat. aq. NH_4Cl solution and extracted with Et_2O . The organic layer was then washed with brine (1 x 200 mL), dried with anhydrous MgSO_4 , concentrated, and purified by flash column chromatography (hexanes) to afford product **40Z** as light-yellow oil (1.72 g, 8.3 mmol, 74 %). ^1H NMR (CDCl_3 , 400 MHz) δ : 1.70 - 1.76 (m, 2H, - CH_2 -), 2.07 (s, 3H, - CH_3), 2.06 - 2.21 (m, 2H, - CH_2 -), 2.41 - 2.46 (m, 2H, - CH_2 -), 6.58 - 6.61 (d, $J_{\text{HH}} = 12$ Hz, 1H, vinyl H), 6.65 - 6.68 (d, $J_{\text{HH}} = 12$ Hz, 1H, vinyl H), 7.26 - 7.30 (5H, m, Ph). ^{13}C NMR (CDCl_3 , 500 MHz) δ : 4.9, 22.3, 31.0, 32.0, 37.6, 93.3, 123.6, 124.0, 126.6, 127.4, 128.6, 130.1, 137.6, 145.8. HRMS (APCI-MS) for $\text{C}_{16}\text{H}_{17}$: calculated 209.1325; found 209.1326.



(E)-2-(2-(prop-1-yn-1-yl)cyclopent-1-en-1-yl)vinyl)benzene (40-E): **41** (1.0 g, 4.0 mmol) was stirred in DCM with I₂ (50.0 mg, 0.20 mmol) for 3 days then filtered. Propyne was bubbled through a mixture of Pd(PPh₃)₄ (0.2 g, 0.16 mmol) and CuI (0.07 g, 0.035 mmol) in Net₃/Benzene (1:1, 60 mL) at 23 °C for 30 min. Isomerized dienyne **42** (1.0 g, 4.0 mmol) was then added dropwise and the mixture was allowed to stir under propyne atmosphere for 3h. The mixture was then concentrated, diluted with H₂O (80 mL), and extracted with Et₂O (3 x 100 mL). The organic extract was washed with brine and dried over anhydrous MgSO₄, concentrated, and purified by flash column chromatography (hexanes) to afford **40E** as white solid (0.71 g, 3.44 mmol, 81 %). ¹H NMR (CDCl₃, 400 MHz) δ: 1.94 (p, 2H, -CH₂-), 2.11 (s, 3H, -CH₃), 2.58 - 2.63 (m, 4H, -CH₂-), 6.47 - 6.51 (d, *J*_{HH} = 16 Hz, 2H, vinyl H), 7.24-7.51 (5H, m, Ph). ¹³C NMR (CDCl₃, 500 MHz) δ: 5.0, 22.3, 32.0, 37.6, 93.3, 123.6, 124.0, 126.6, 127.4, 128.6, 130.1, 137.6, 145.8. HRMS (APCI-MS) for C₁₆H₁₇: calculated 209.1325; found 209.1325.



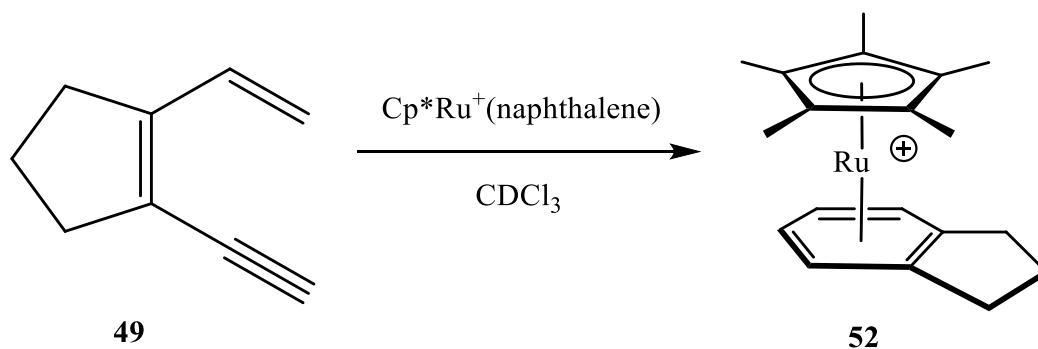
Trimethyl((2-(prop-1-en-1-yl)cyclohex-1-en-1-yl)ethynyl)silane (51): N-Butyllithium (5.79 mL, 13.9 mmol, 2.4 M in hexanes) was added dropwise to a stirring mixture of ethyltriphenylphosphonium bromide (5.68 g, 15.3 mmol) in anhydrous THF (70 mL) at -78 °C. The solution then was stirred at 23 °C for 1 h followed by the addition of **30** (2 g, 9.7 mmol). After stirring at 23 °C for 1h, the reaction was quenched with sat. aq. NH₄Cl (200 mL) and extracted with Et₂O (2 x 200 mL, 1 x 100 mL). The organic extract was washed with H₂O (3 x 200 mL) / brine (3 x 100 mL), dried over anhydrous MgSO₄, concentrated and purified by flash column chromatography (hexanes) to afford **51** as colorless oil (1.45 g, 6.69 mmol, 69 %). ¹H NMR δ: 0.58 (s, 9H, E TMS), 0.61 (s, 9H, Z TMS), 1.55 – 1.67 (m, 8H, E/Z -CH₂), 1.77 (dd, *J*_{HH} = 7.5 Hz, *J*_{HH} = 1.5 Hz, 3H, Z-CH=CHCH₃), 1.82 (d, *J*_{HH} = 7.0 Hz, 3H, E-CH=CHCH₃), 2.15 – 2.25 (m, 4H, E-CH₂), 2.26 – 2.32 (m, 4H, Z-CH₂), 5.51 (dq, *J*_{HH} = 11.5 Hz, *J*_{HH} = 7.0 Hz, 1H, Z-CH=CHCH₃), 5.73 (dq, *J*_{HH} = 15.6 Hz, *J*_{HH} = 7.0 Hz, 1H, E-CH=CHCH₃), 6.28 (app. d, *J*_{HH} = 12.5 Hz, 1H, Z-CH=CHCH₃), 6.79 (d, *J*_{HH} = 16.0 Hz, 1H, E-CH=CHCH₃). The product exhibited an identical spectroscopic property to those reported in literature.



(η^5 -pentamethylcyclopentadienyl)(η^6 -indane)ruthenium(II) hexafluorophosphate

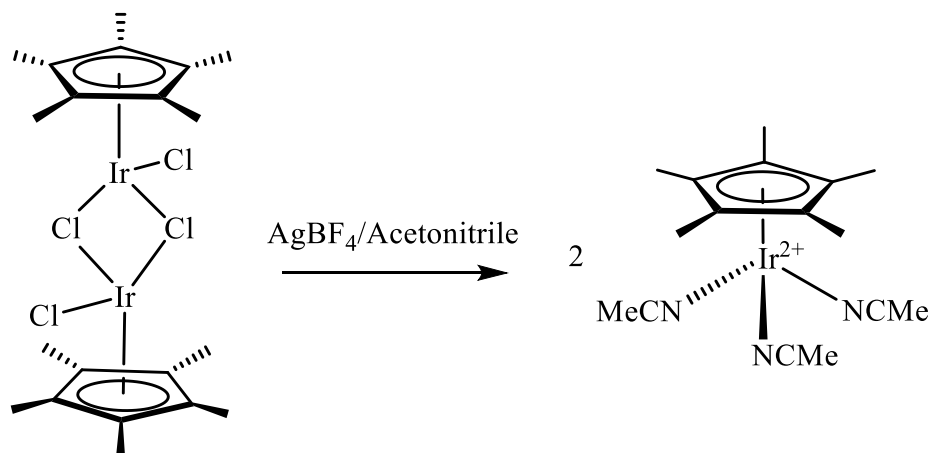
(52): Dienyne **49** (3.1 mg, 0.025 mmol), [Cp**Ru*⁺(η^6 -naphthalene)][PF₆] (**93**) (36 mg, 0.073 mmol)

and 1,3,5-tri-*tert*-butylbenzene (internal standard) were added to a J. Young NMR tube. After the NMR tube was frozen by liquid nitrogen and then placed under vacuum, 0.75 ml of CDCl₃ was distilled into the NMR tube. The resulting solution was subsequently degassed using 3 cycles of freeze/pump/thaw/degas. Then the NMR tube was sealed by propane flame. An initial ¹H NMR spectrum was taken immediately. The NMR tube was placed in Rayonel photochemical reactor centered at 254 nm and the reaction was monitored by ¹H NMR spectroscopy. After 24 hours, the **49** peaks were no longer present and new ¹H NMR resonances for **52** were observed at δ : 1.97 ppm (s, 15H, Cp*), 2.65 - 2.72 (m, 2H), 2.88 - 2.94 (m, 2H), 5.88 (bs, 2H), 6.04 (bs, 2H). Percent yield was calculated from integration of the internal standard relative to the methylene H on the 5 membered ring resonance of **52** at 5.88 ppm. (60.2 % yield).



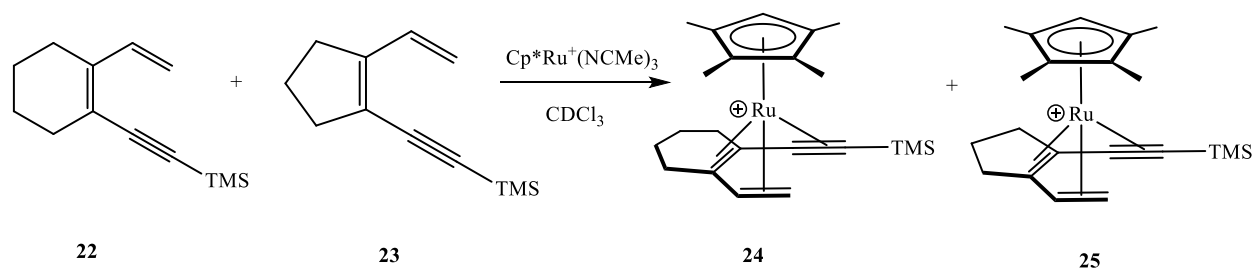
(η^5 -pentamethylcyclopentadienyl) iridium (II) trisacetonitrile tetrafluoroborate (94**):**

Pentamethylcyclopentadienyl iridium dichloride dimer (50 mg, 0.06 mmol) dissolved in 2 mL anhydrous acetonitrile and silver tetrafluoroborate (45 mg, 0.23 mmol) dissolved in 1 mL anhydrous acetonitrile were mixed. The solution turned into light yellow and AgCl precipitation started forming rapidly. After 1 h stirring under inert atmosphere, the mixture was filtered and dried under vacuum overnight. ¹H NMR resonances for **52** were observed at δ : 1.63 (s, 15H, Cp*), 2.11 (s, 9H, NCMe).

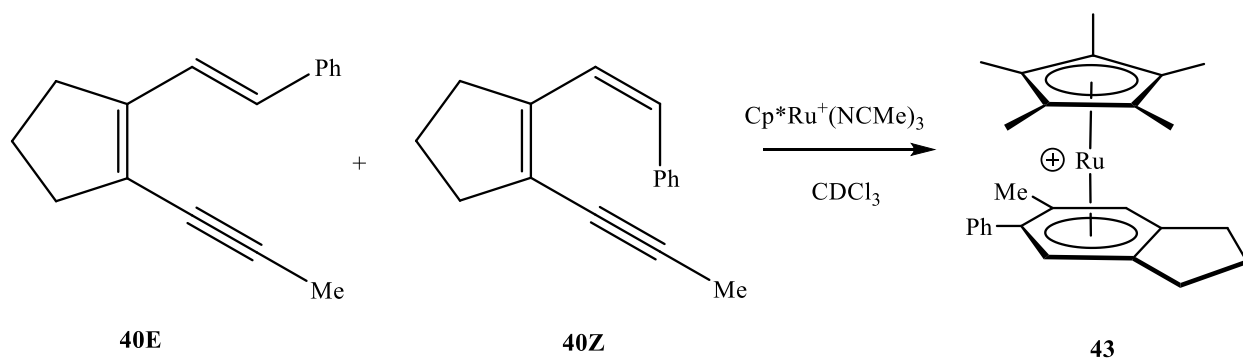


3. NMR reactions

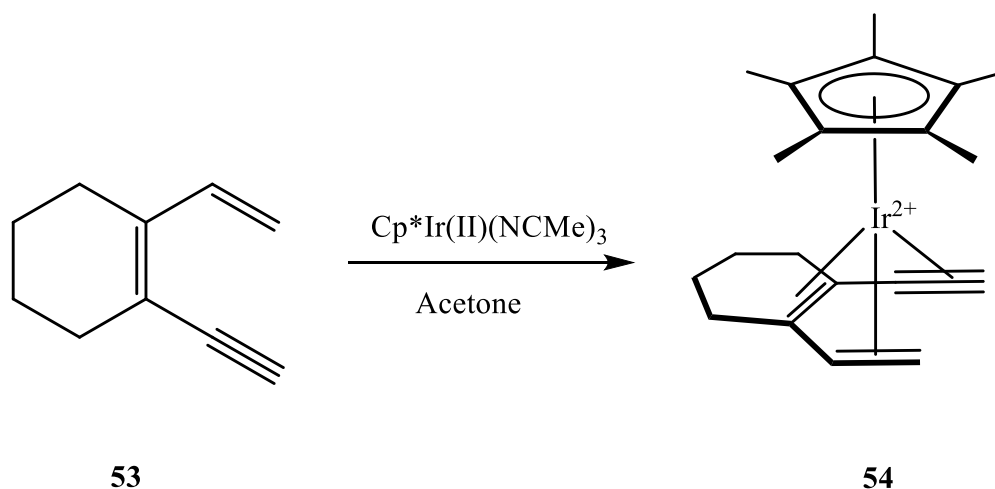
Competition reaction between 22 and 23 with 92: **23** (10 mg, 0.051 mmol), **22** (10 mg, 0.048 mmol) and 1,3,5-tri-*tert*-butylbenzene (internal standard) were placed in an oven-dried J. Young NMR tube. Anhydrous CDCl_3 (0.8 mL) was distilled into the tube and an initial ^1H NMR spectrum was taken. All volatiles were then removed under high vacuum and **92** (2.2 mg, 0.04 mmol) was added. Fresh anhydrous CDCl_3 (0.8 mL) was then distilled into the tube. After 1 h at ambient temperature, the reaction reached completion and a final spectrum was taken. Yield was calculated based on the integration of the starting material vinyl hydrogen resonances at δ : 6.85 (**23**) and 7.11 (**22**) relative to the internal standard resonance. Yield calculation indicates that 8 % of **23** and 4 % of **22** were consumed to form product **25** and **24** in a ratio of 2:1, respectively.



Competition reaction between 40E and 40Z with 92: **40E** (10.1 mg, 0.048 mmol), **40Z** (12.3 mg, 0.059 mmol) and 1,3,5-tri-*tert*-butylbenzene (internal standard) were placed in an oven-dried J. Young tube. Anhydrous CDCl_3 (0.48 mL) was distilled into the tube and an initial ^1H NMR spectrum was taken. All volatiles were then removed under high vacuum and **92** (2.0 mg, 0.004 mmol) was added. Fresh anhydrous CDCl_3 (0.48 mL) was then distilled into the tube. After 12 h at room temperature (23 °C), the reaction was able to reach completion and a final spectrum was taken. Yield was calculated based on the integration of the starting material vinyl hydrogen resonances at δ 6.67 (**40Z**) and 6.49 (**40E**) relative to the internal standard resonance. Yield calculation indicates that 3.1 % of **40E** and 2.1 % of **40Z** were consumed to form **43**.



Reaction between 54 and Cp*Ir(II)(NCMe)₃: **54** (1.25 mg, 0.01 mmol) and tetramethyl silane were placed in an oven-dried J. Young tube. Anhydrous acetone-*d*₆ (0.7 mL) was distilled into the tube and an initial ¹H NMR spectrum was taken. The tube was then brought into a N₂ filled glove box, **94** (5.0 mg, 0.009 mmol) was added to the solution. After 12 h, 3 days and 7 days at room temperature (23 °C), ¹H NMR spectrum were taken. Yield was calculated based on the integration of the product vinyl hydrogen resonances at δ: 5.94, 6.29, 6.47 and 6.51 relative to the internal standard resonance. Yield calculation indicates that yield was 50 %, 70 %, 80 % at 12 h, 3 days and 7 days of reaction period.



Kinetic study of 40Z with 92: **92** (2.0 mg, 0.004 mmol, 1eq) was added to an oven-dried J. Young tube. **40Z** (13.2 mg, 0.06 mmol, 15 eq) was then added on to the wall of the tube to avoid contact with **92**. After the addition of acetonitrile-*d*₃ (127 mg, 3.1 mmol, 750 eq), the tube was immediately frozen at – 78 °C and acetone-*d*₆ (0.6 mL) was distilled under a high vacuum. An initial ¹H NMR spectrum was taken after all reactants were dissolved while the tube started

warming up to 23 °C. ^1H NMR spectrum was continuously taken every 1.5 min for 1 h after reaction starts; every 5 min for the second hour and every 10 min for the 3rd hour. The concentration of **92** was monitored based on the integration of Cp* resonances δ 1.6 relative to the internal standard resonance and $\ln[\text{Cp}^*\text{Ru}^+]$ was plotted vs. time.

Overall plot over 3 hours

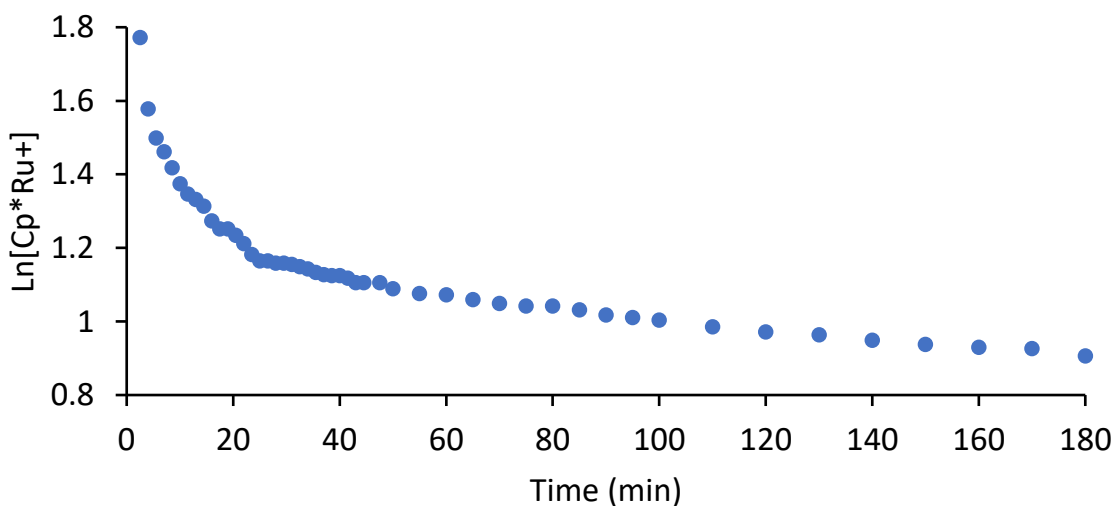


Figure 2-4: Kinetic study of 40Z treated with **92** and $\text{NCMe-}d_3$.

(First 15 min – establishing hexahepto equilibrium)

Time (min)	2.5	4	5.5	7	8.5	10	11.5	13	14.5
Ln[Cp*Ru]	1.77	1.58	1.50	1.46	1.41	1.37	1.34	1.33	1.31

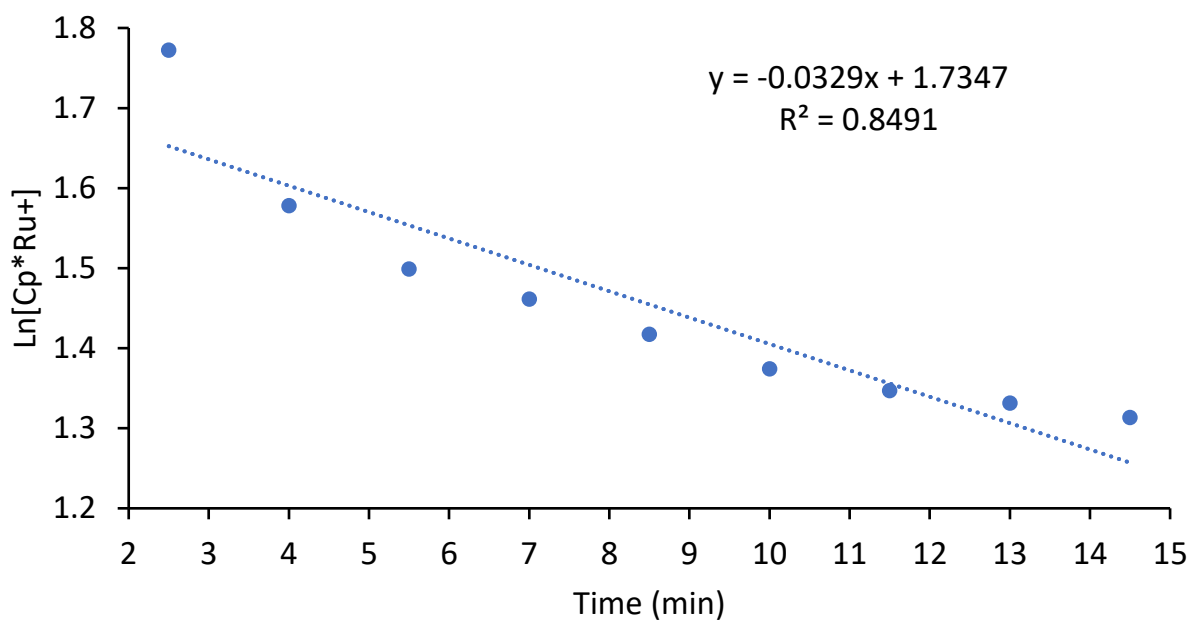


Figure 2-5: Kinetic study of 40Z treated with 92 and NCMe- d_3 (First 15 min after reaction started).

Time (min)	100	110	120	130	140	150	160	170	180
Ln[Cp*Ru]	1.00	0.98	0.97	0.96	0.95	0.94	0.93	0.92	0.90

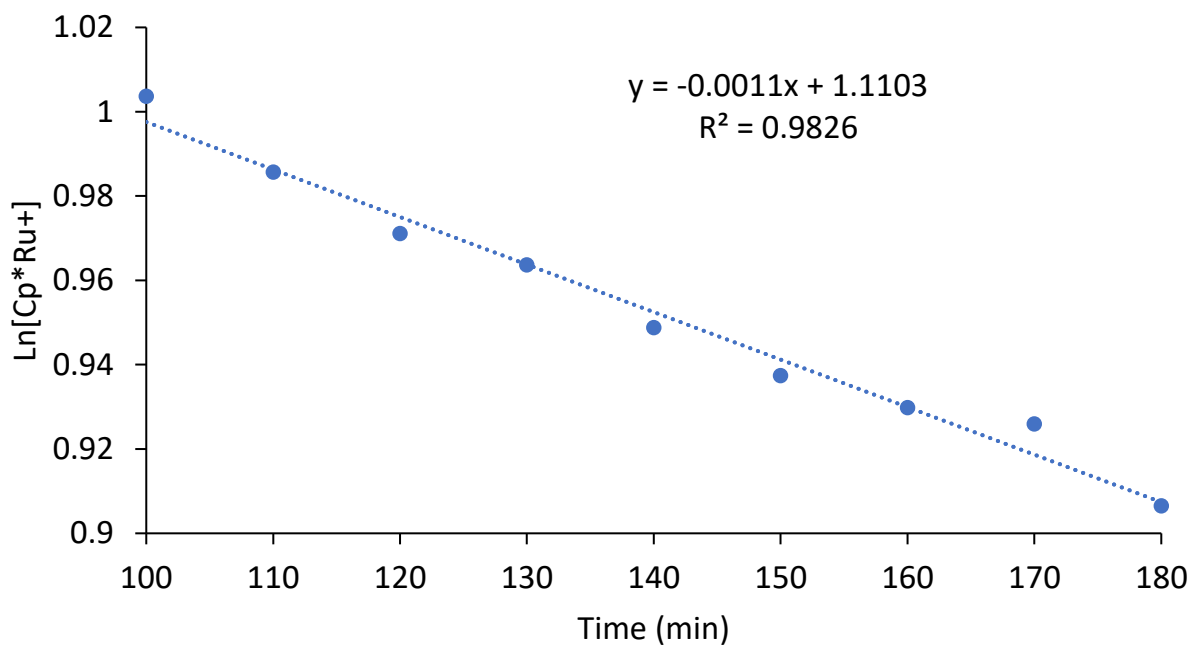


Figure 2-6: Kinetic study of 40Z treated with 92 and NCMe- d_3 (Last one hours before reaction is done).

Kinetic study of 40-E with 92: 92 (2.1 mg, 0.004 mmol, 1eq) was added to an oven-dried J. Young tube. 40E (13.0 mg, 0.06 mmol, 15 eq) was then added on to the wall of the tube to avoid

contact with the Ru complex. After the addition of acetonitrile- d_3 (133 mg, 3.1 mmol, 750 eq), the tube was immediately frozen at $-78\text{ }^\circ\text{C}$ and acetone- d_6 (0.6 mL) was distilled in under high vacuum. An initial ^1H NMR spectrum was taken after all reactants were dissolved while the tube was warming up to $23\text{ }^\circ\text{C}$. ^1H NMR spectrum was continuously taken every 1.5 min for 1 h after reaction starts; every 5 min for the second hour and every 10 min for the 3rd hour. The concentration of **92** was monitored based on the integration of Cp* resonances at δ 1.6 relative to the internal standard resonance and $\ln[\text{Cp}^*\text{Ru}^+]$ was plotted vs. time.

Overall plot over 3 hours

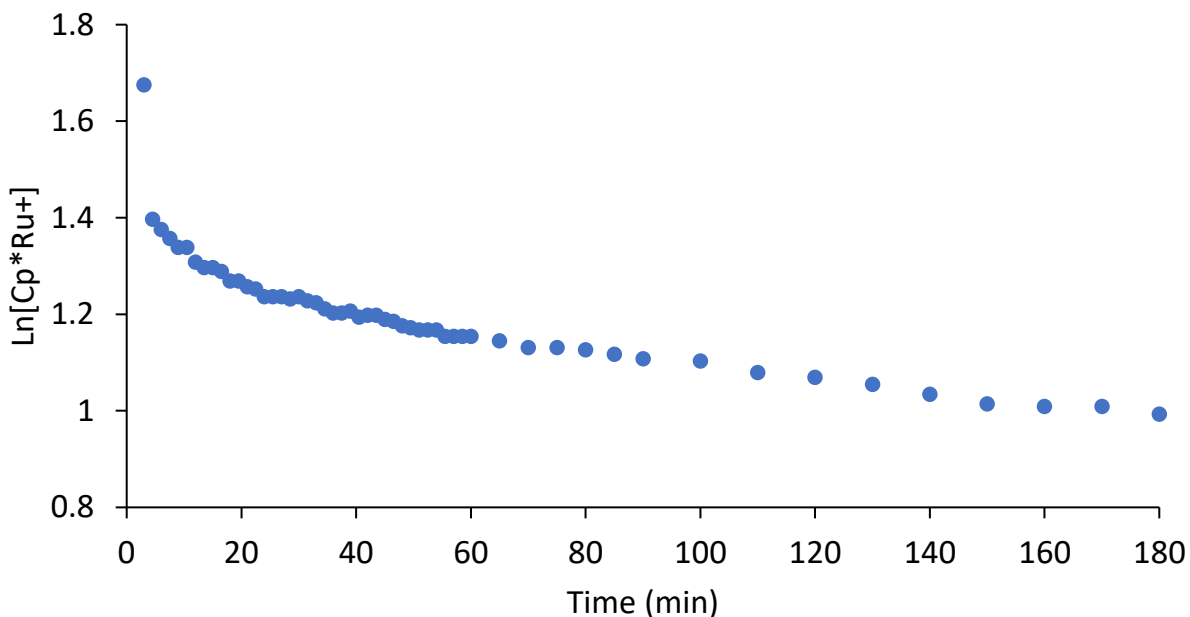


Figure 2-7: Kinetic study of 40Z treated with 92 and NCMe- d_3 .

First 15 min – establishing eda-6 equilibrium

Time (min)	3	4.5	6	7.5	9	10.5	12	13.5	15
Ln[Cp*Ru]	1.68	1.40	1.38	1.36	1.34	1.34	1.31	1.30	1.30

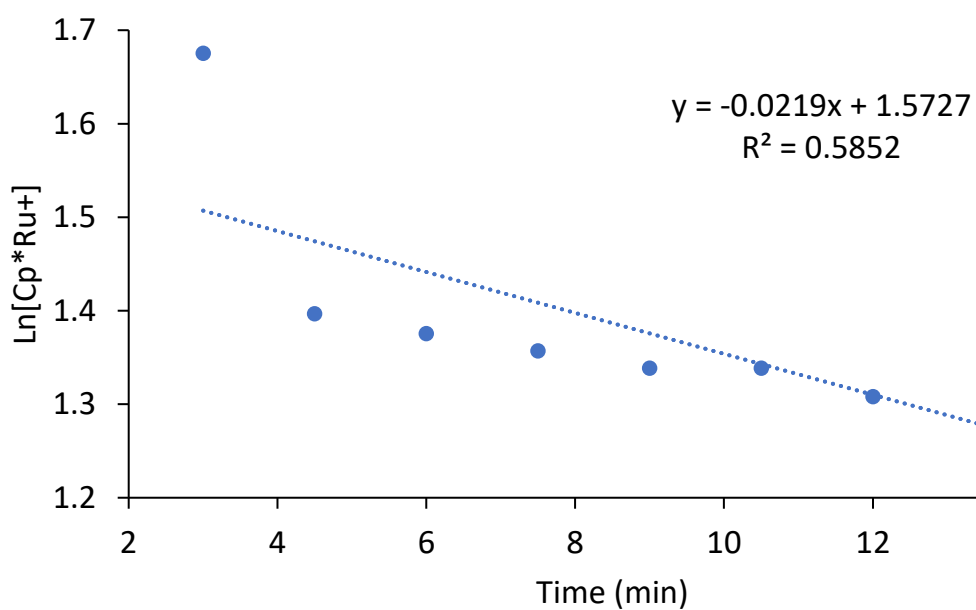


Figure 2-8 : Kinetic study of **40E** treated with **92** and NCMe-d_3 (First 15 min after reaction started).

(last 1h – cyclization to form the product)

Time (min)	100	110	120	130	140	150	160	170	180
Ln[Cp*Ru]	1.10	1.08	1.07	1.05	1.03	1.01	1.01	1.01	1.0

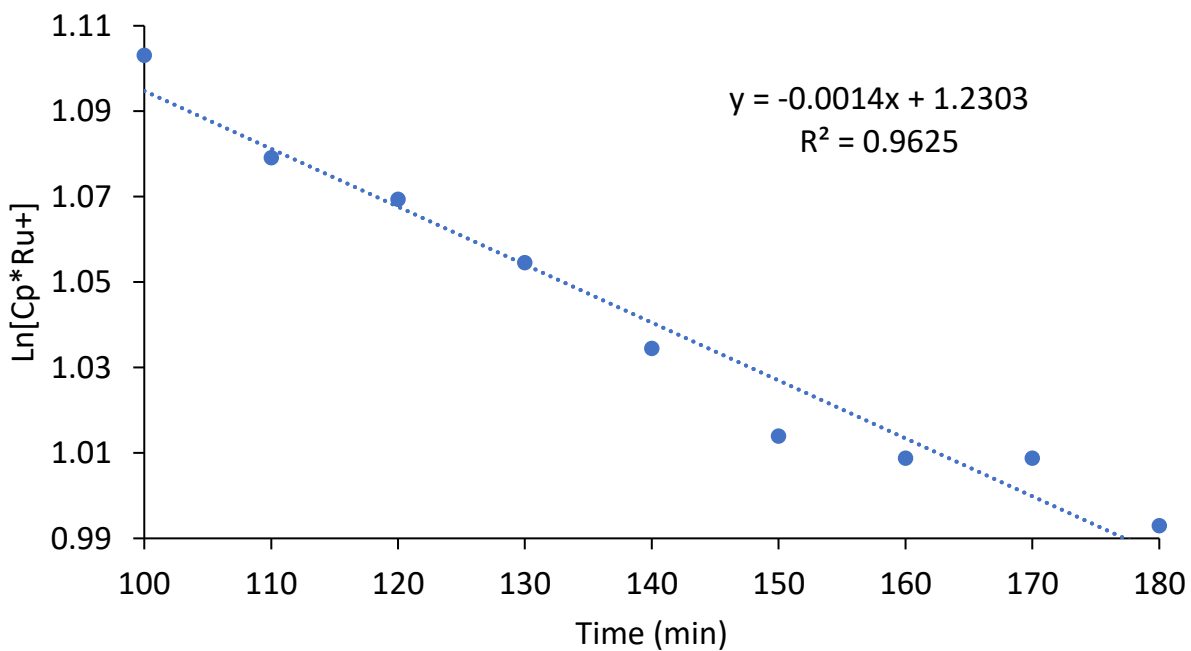
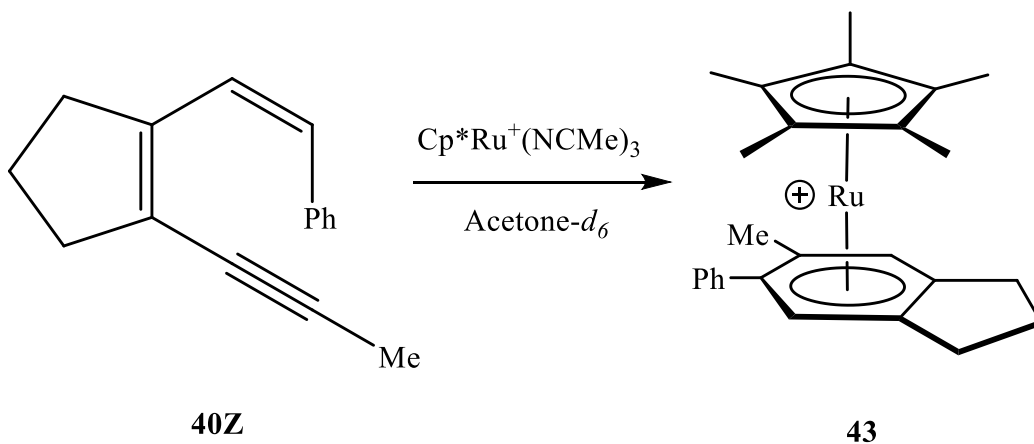


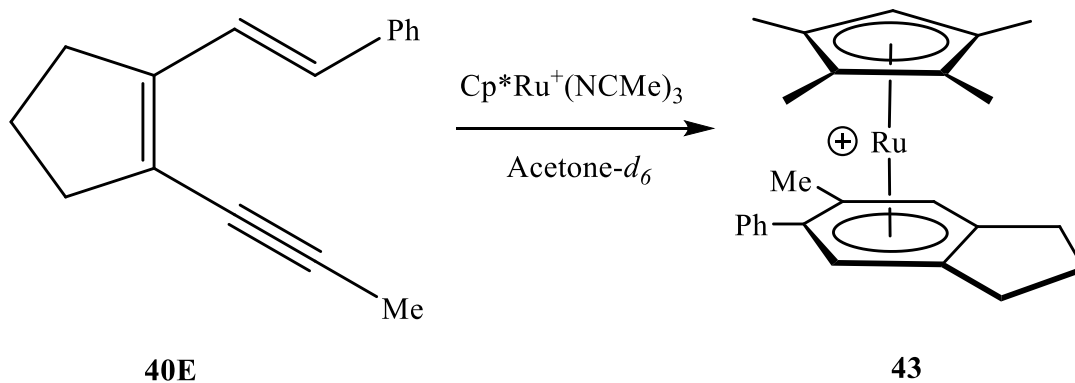
Figure 2-9: Kinetic study of **40E** treated with **92** and NCMe-*d*₃ (Last hour after reaction is completed).

Dienyne 40-Z reacting with 92: 40Z (2.1 mg, 0.01 mmol) and 1,3,5-tri-tert-butylbenzene (internal standard) were placed in an oven-dried J. Young tube. Anhydrous acetone- d_6 (0.40 mL) was distilled into the tube and an initial ^1H NMR spectrum was taken. All volatiles were then removed under high vacuum and **92** (4.0 mg, 0.008 mmol) was added. Fresh anhydrous acetone- d_6 (0.48 mL) was then distilled into the tube. Another ^1H NMR spectrum was taken after 1 h at room temperature (23 °C). The intermediate resonances were observed at δ 5.18 (d, 1H, $J_{\text{HH}} = 8$ Hz, vinyl H), 5.04 (d, 1H, $J_{\text{HH}} = 8$ Hz vinyl H) with a yield of 31 %; The product resonances were observed at δ 6.16 (s, 1H, arene H) and 6.23 (s, 1H, arene H) with a yield of 7.8 %.



Dienyne 40-E reacting with 92: 40E (2.8 mg, 0.013 mmol) and 1,3,5-tri-tert-butylbenzene (internal standard) were placed in an oven-dried J. Young tube. Anhydrous acetone- d_6 (0.40 mL) was distilled into the tube and an initial ^1H NMR spectrum was taken. All volatiles were then removed under high vacuum and **92** (4.3 mg, 0.008 mmol) was added. Fresh anhydrous acetone-

d_6 (0.4 mL) was then distilled into the tube. Another ^1H NMR spectrum was taken after 1 h at room temperature (23 °C). The intermediate resonances were observed at δ : 5.18 (d, 1H, $J_{\text{HH}} = 8$ Hz, vinyl H), 5.04 (d, 1H, $J_{\text{HH}} = 8\text{Hz}$ vinyl H) with a yield of 19 %; The product resonances were observed at δ : 6.16 (s, 1H, arene H) and 6.23 (s, 1H, arene H) with a yield of 89.0 %.



4. ^1H and ^{13}C NMR Spectroscopic Data.

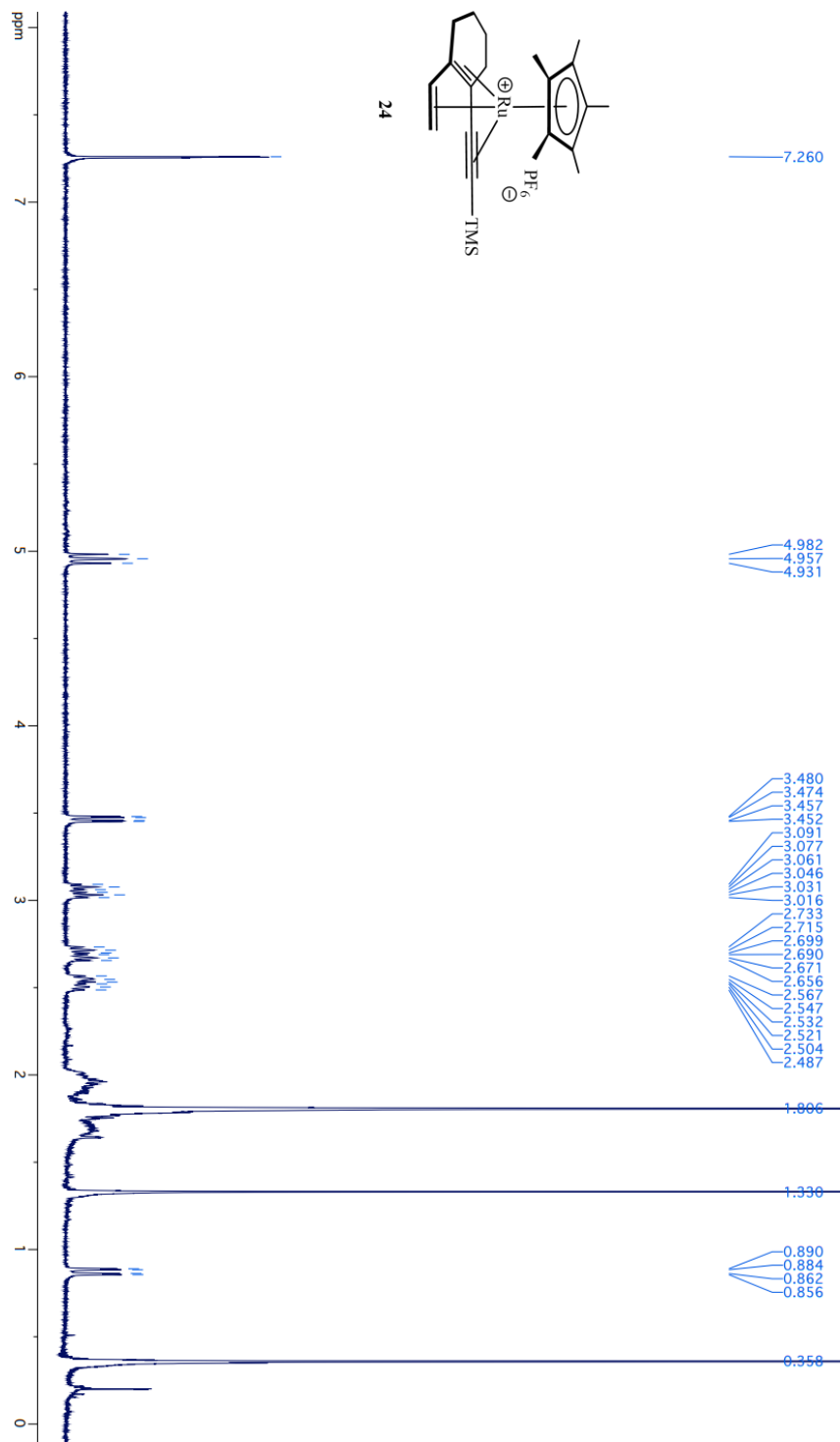


Figure 2-10: **24** ^1H NMR spectrum (CDCl_3 , 400 MHz).

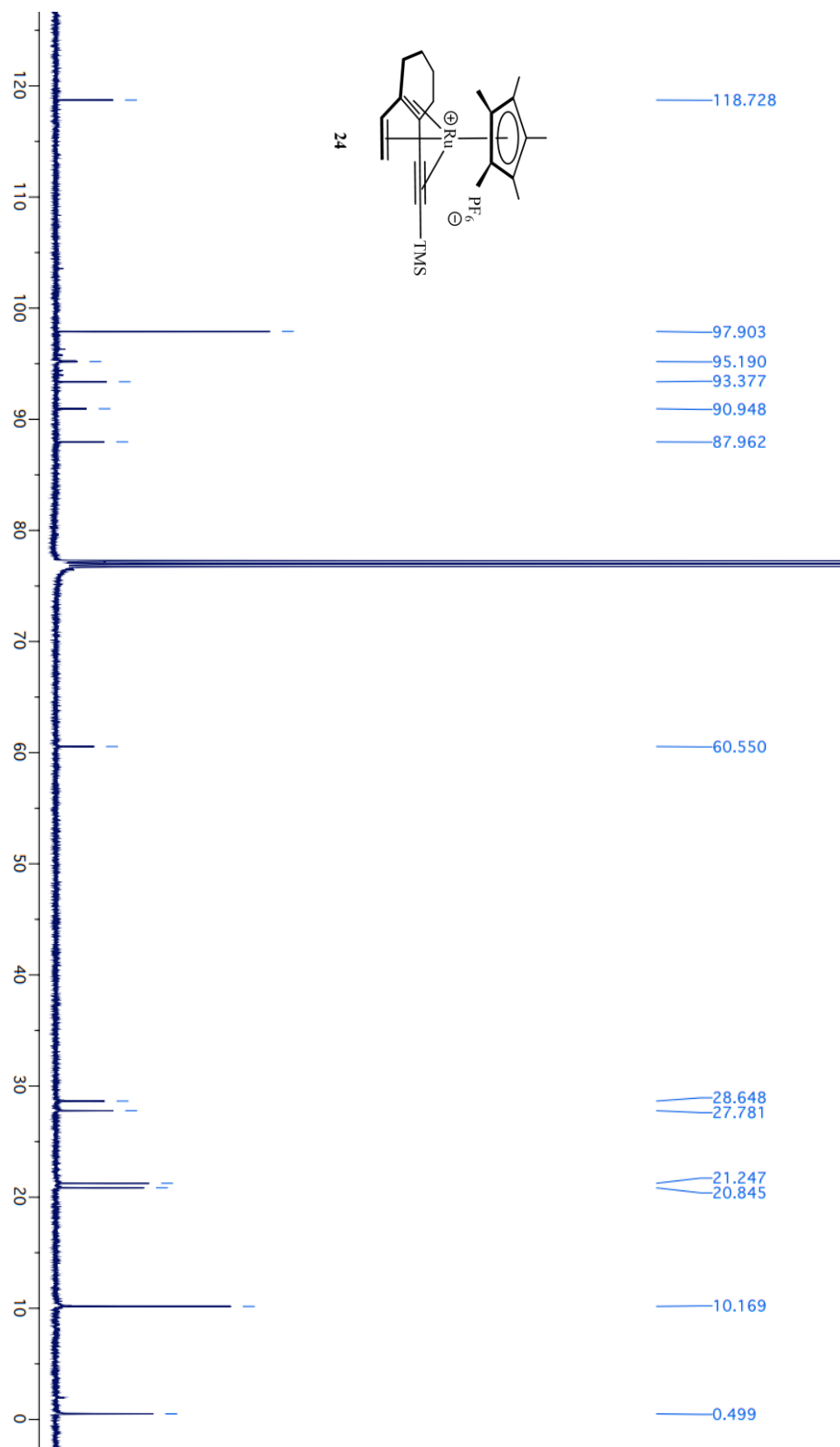


Figure 2-11: **24** ^{13}C NMR spectrum (CDCl₃, 500 MHz).

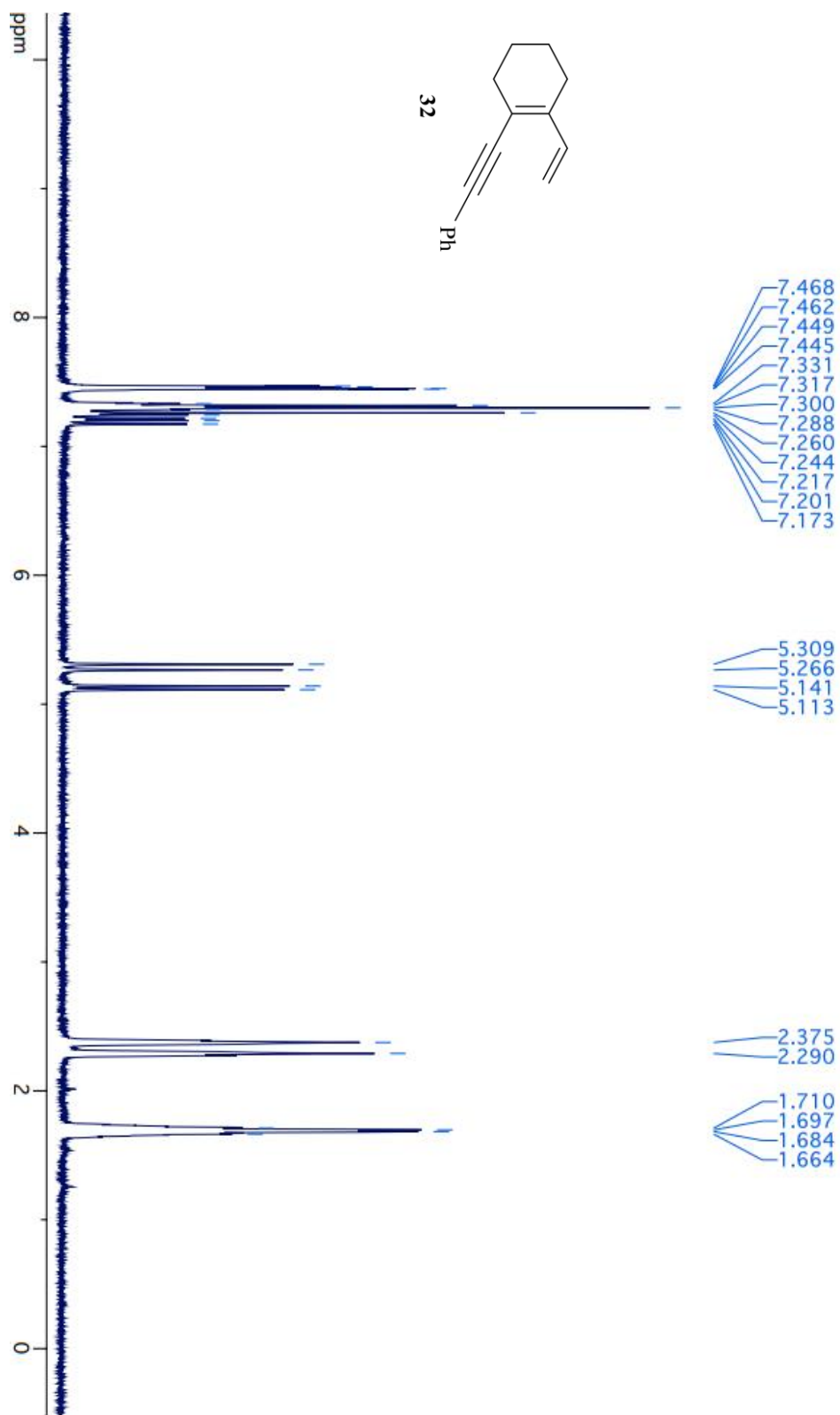


Figure 2-12: 32 ¹H NMR spectrum (CDCl₃, 400 MHz).

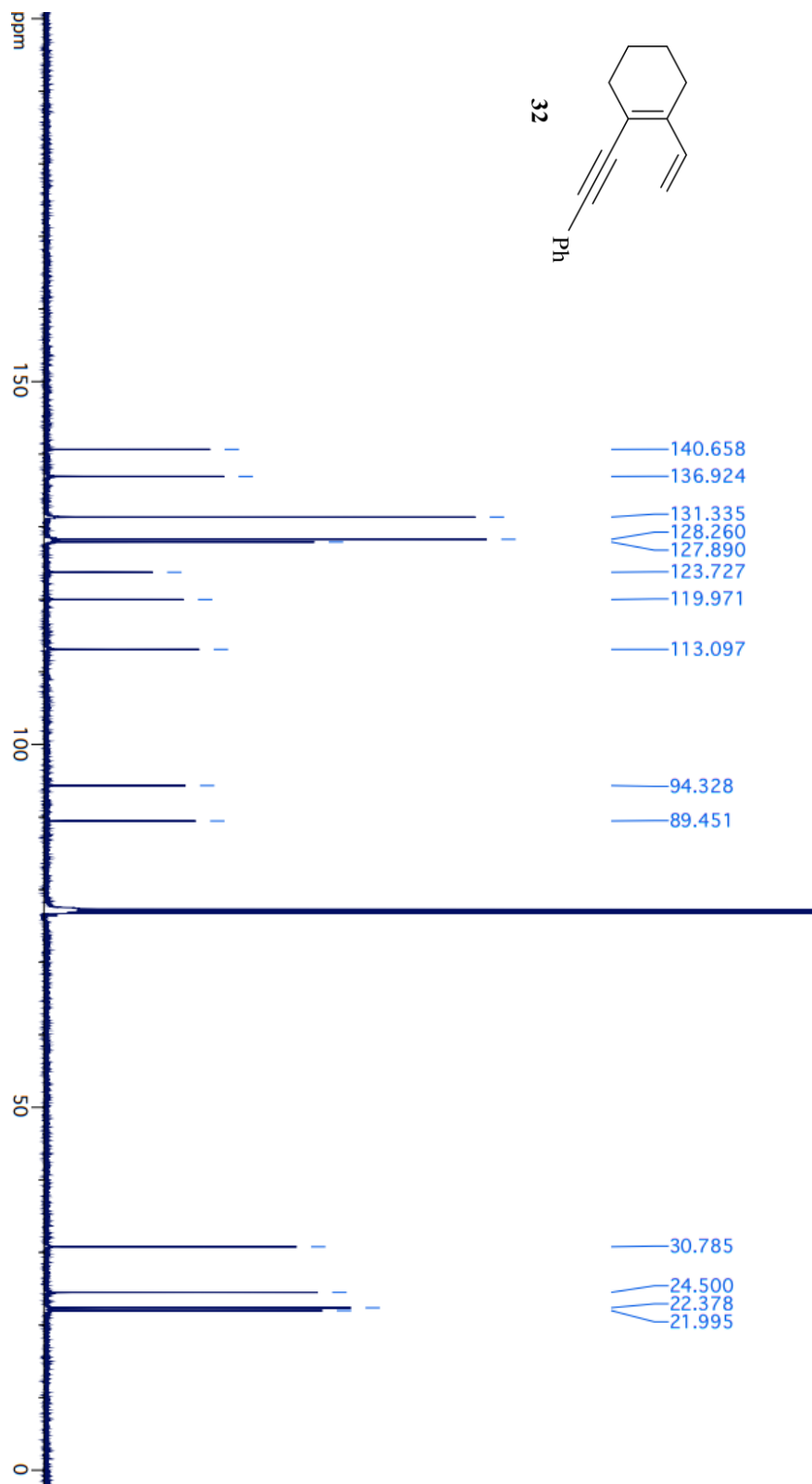


Figure 2-13: 32 ^{13}C NMR spectrum (CDCl_3 , 500 MHz).

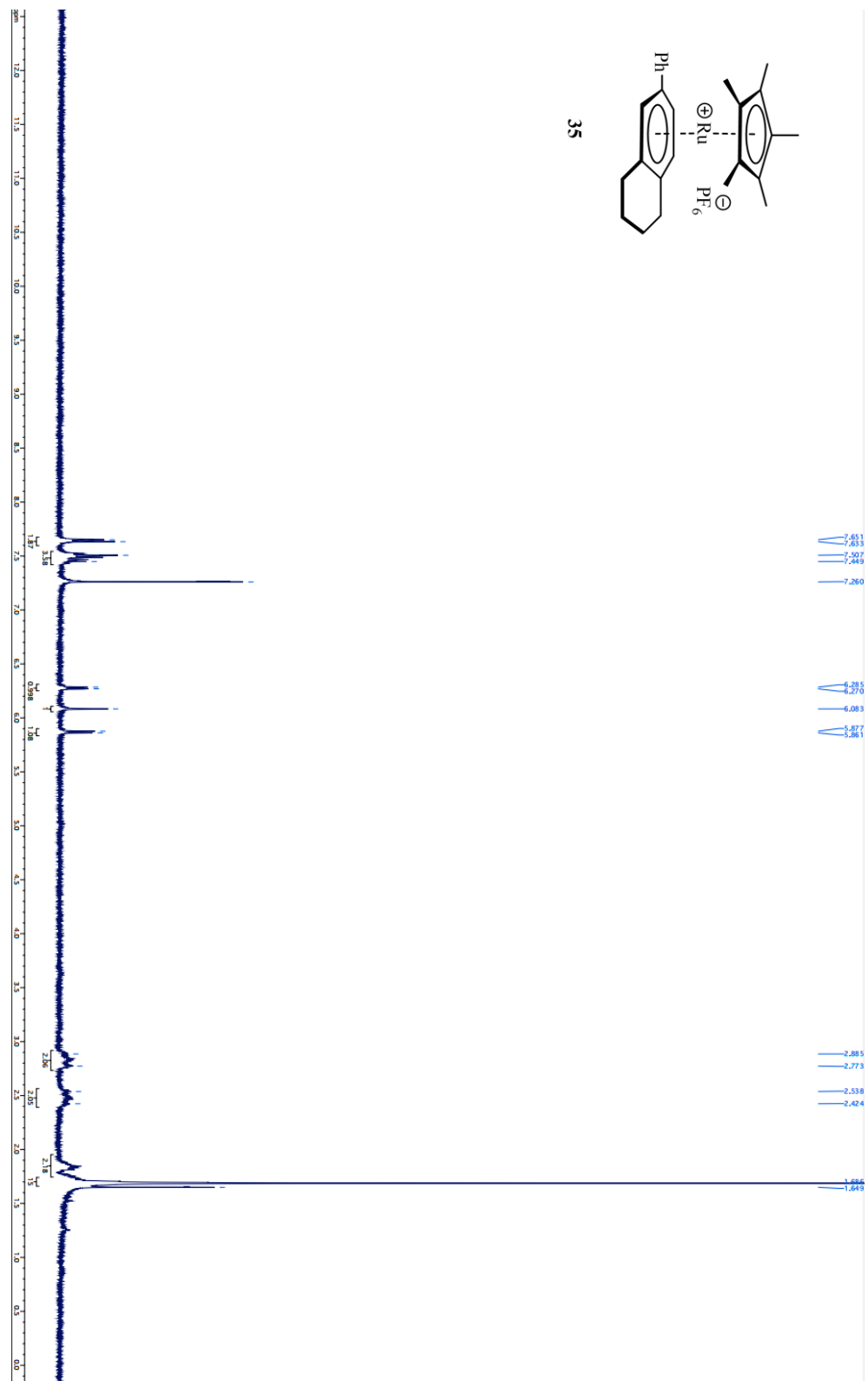


Figure 2-14: 35 ¹H NMR spectrum (CDCl₃, 400 MHz).

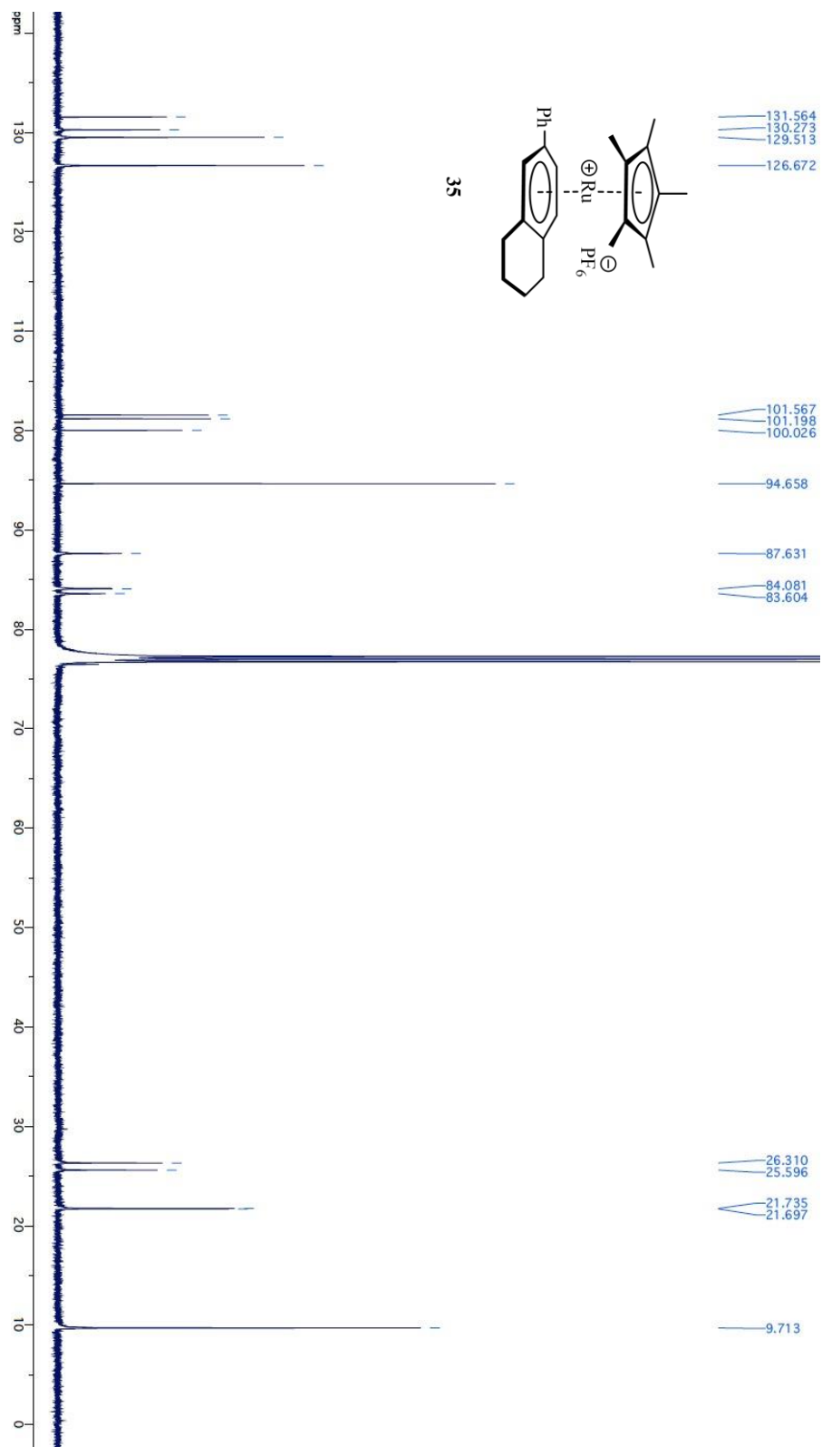


Figure 2-15: ¹³C NMR spectrum (CDCl₃, 500 MHz).

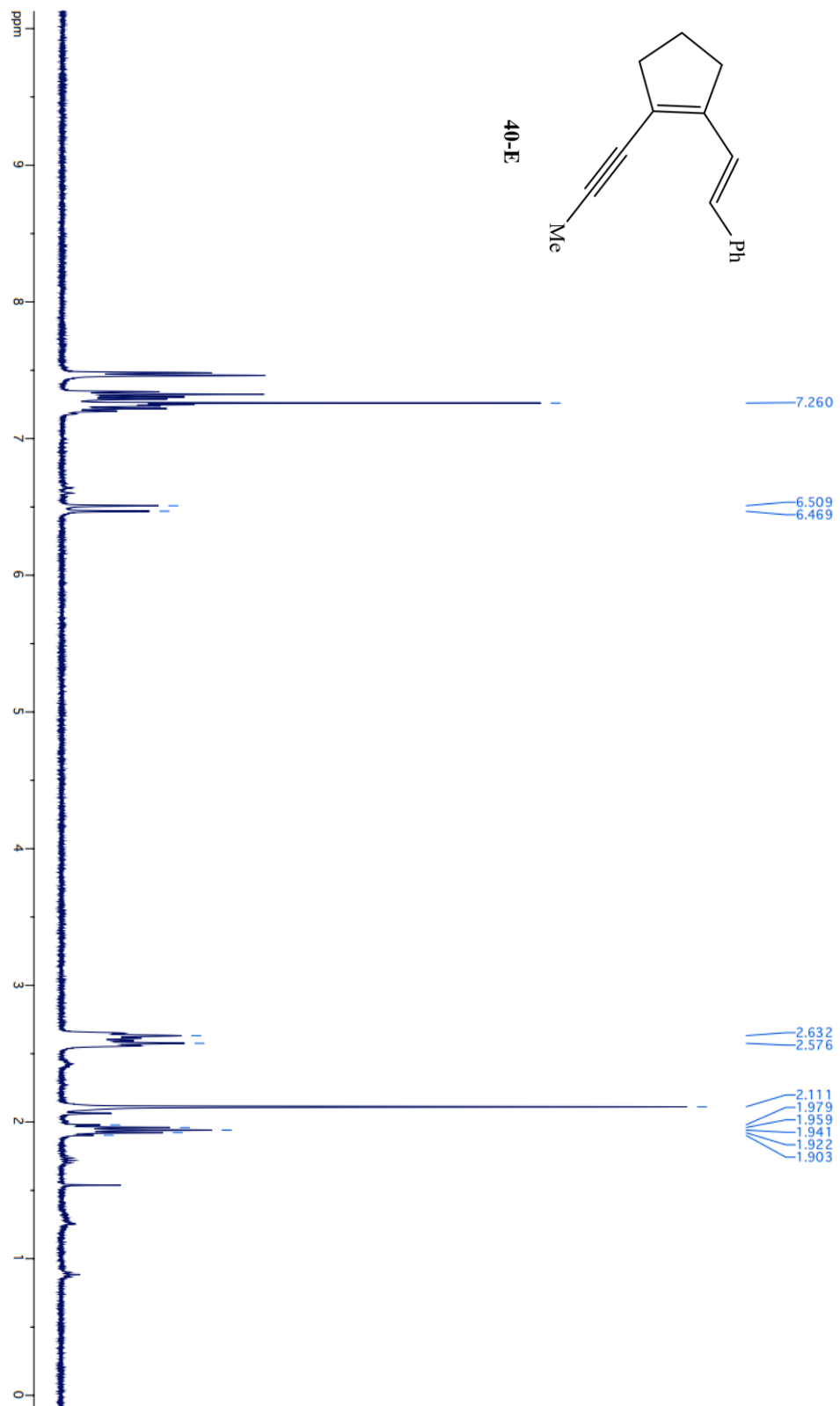


Figure 2-16: 40E ^1H NMR spectrum (CDCl_3 , 400 MHz).

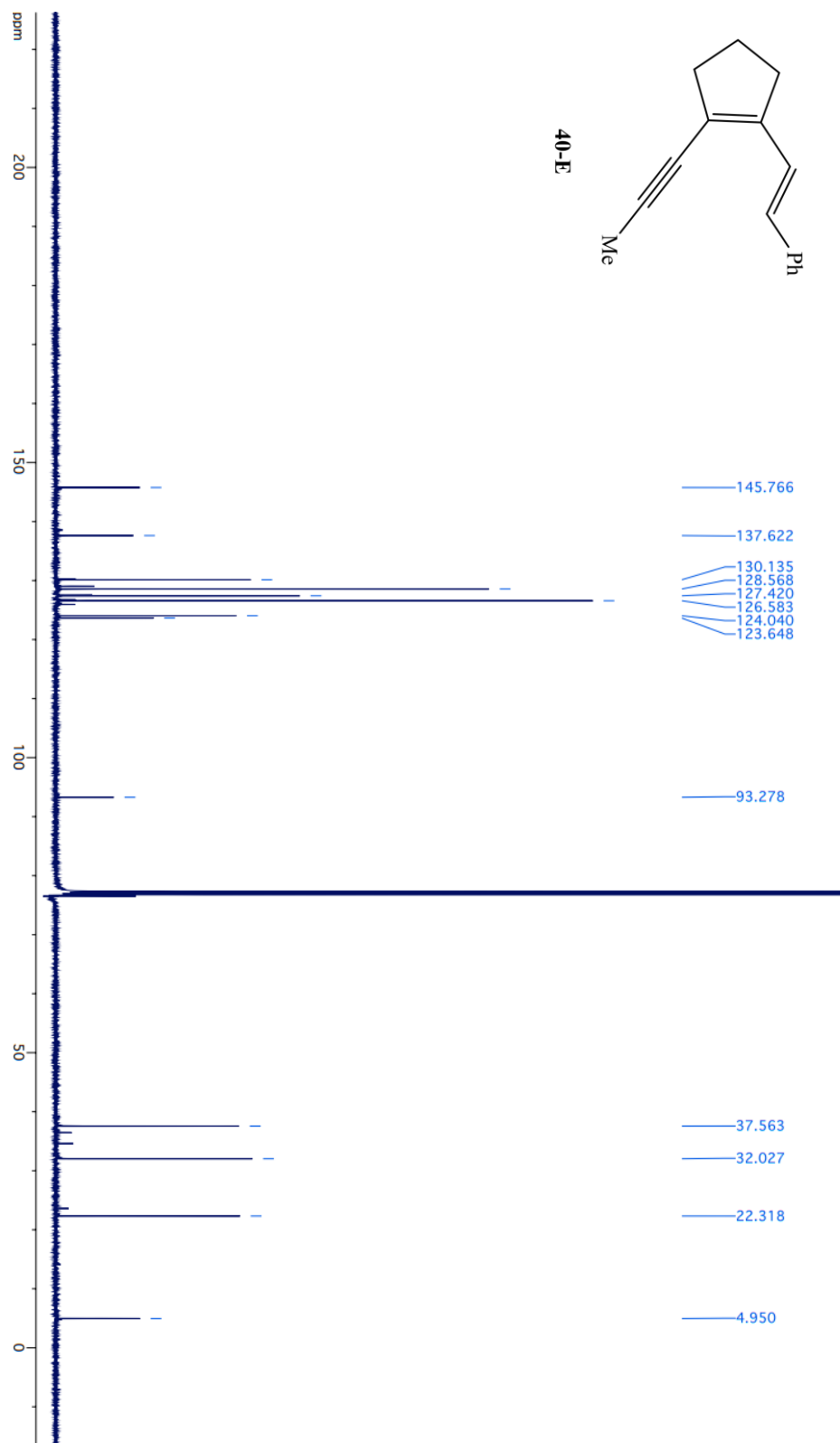


Figure 2-17: 40E ^{13}C NMR spectrum (CDCl₃, 500 MHz).

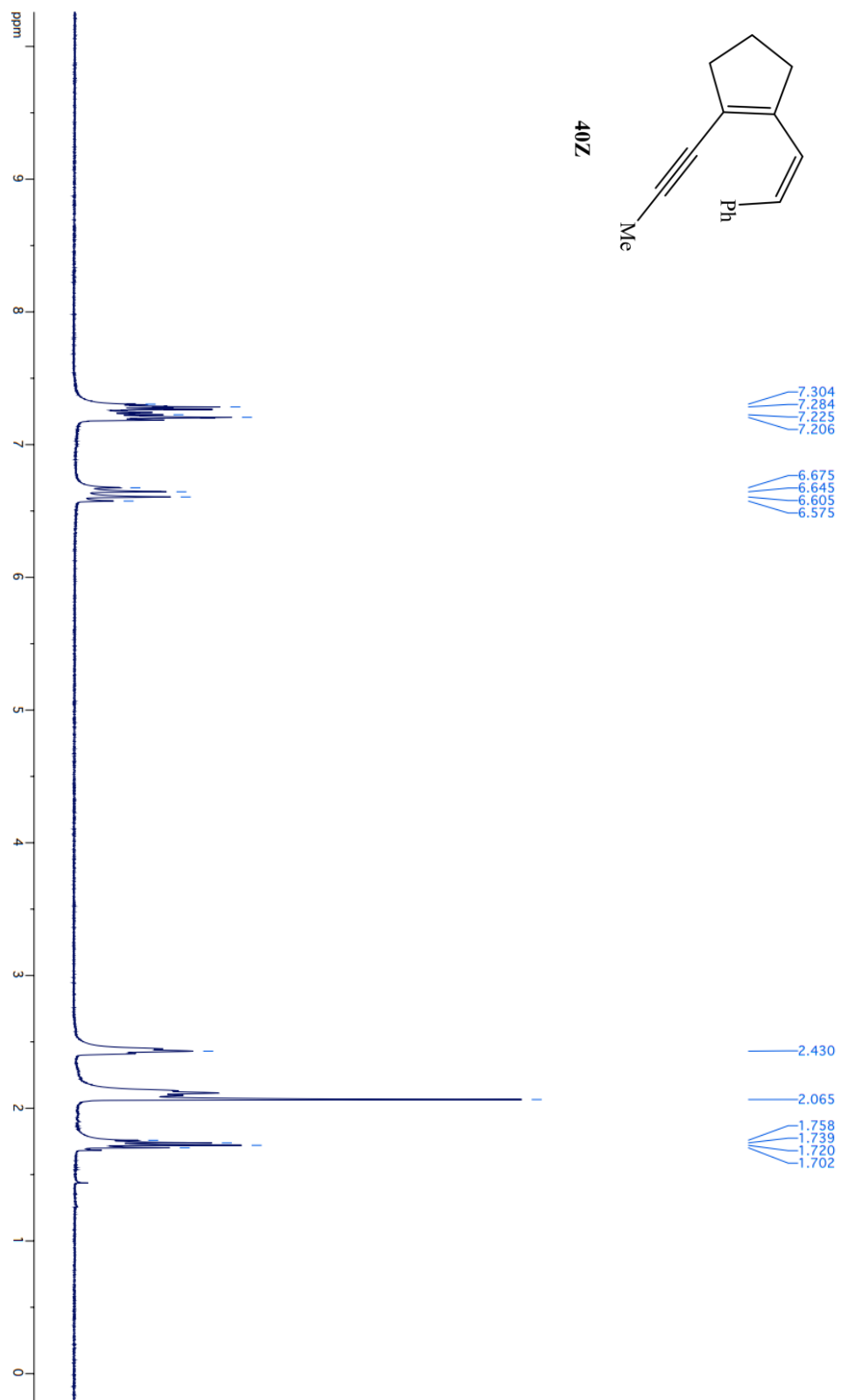


Figure 2-18: **40Z** ^1H NMR spectrum (CDCl_3 , 400 MHz).

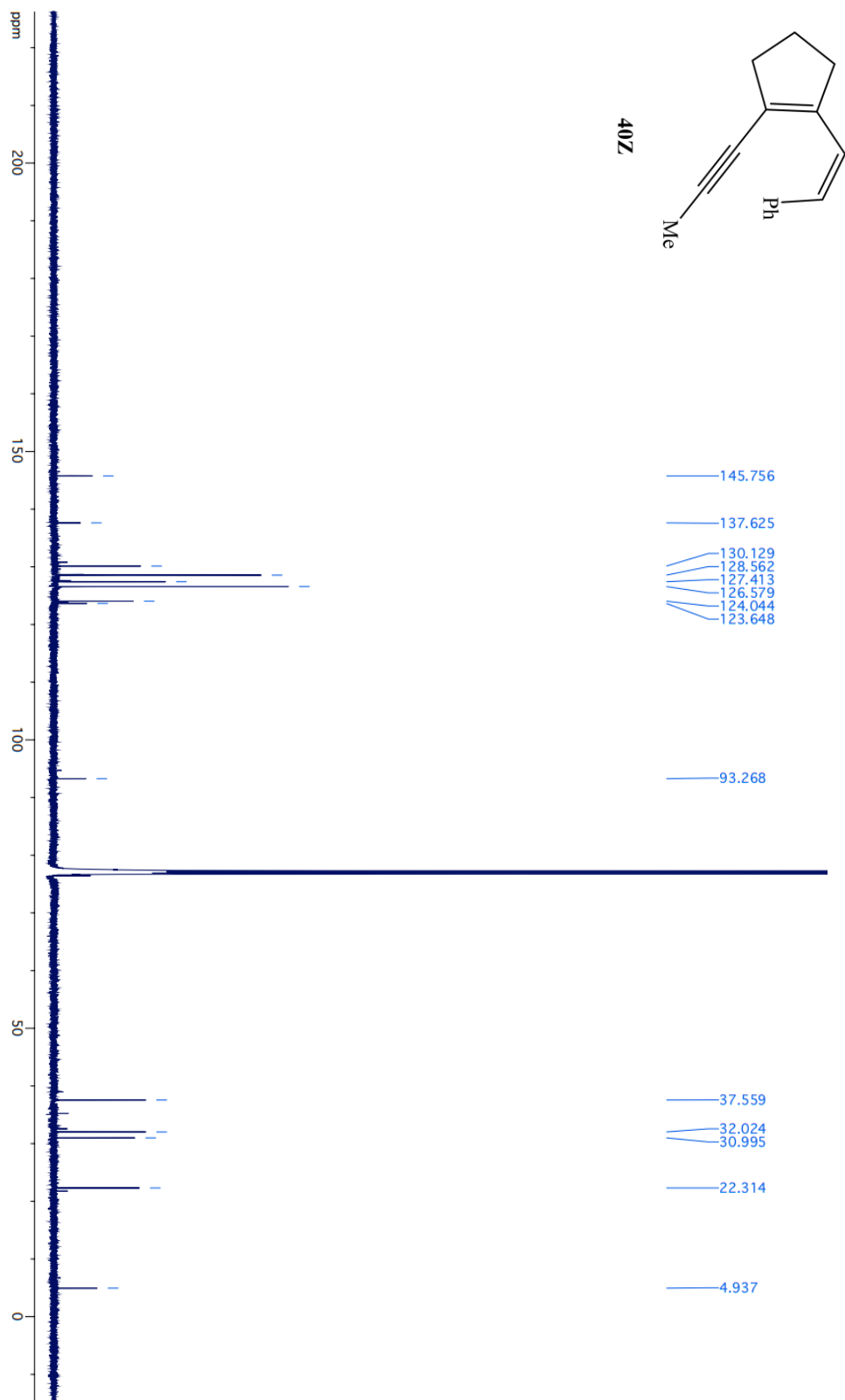


Figure 2-19: 40Z ¹³C NMR spectrum (CDCl₃, 500 MHz).

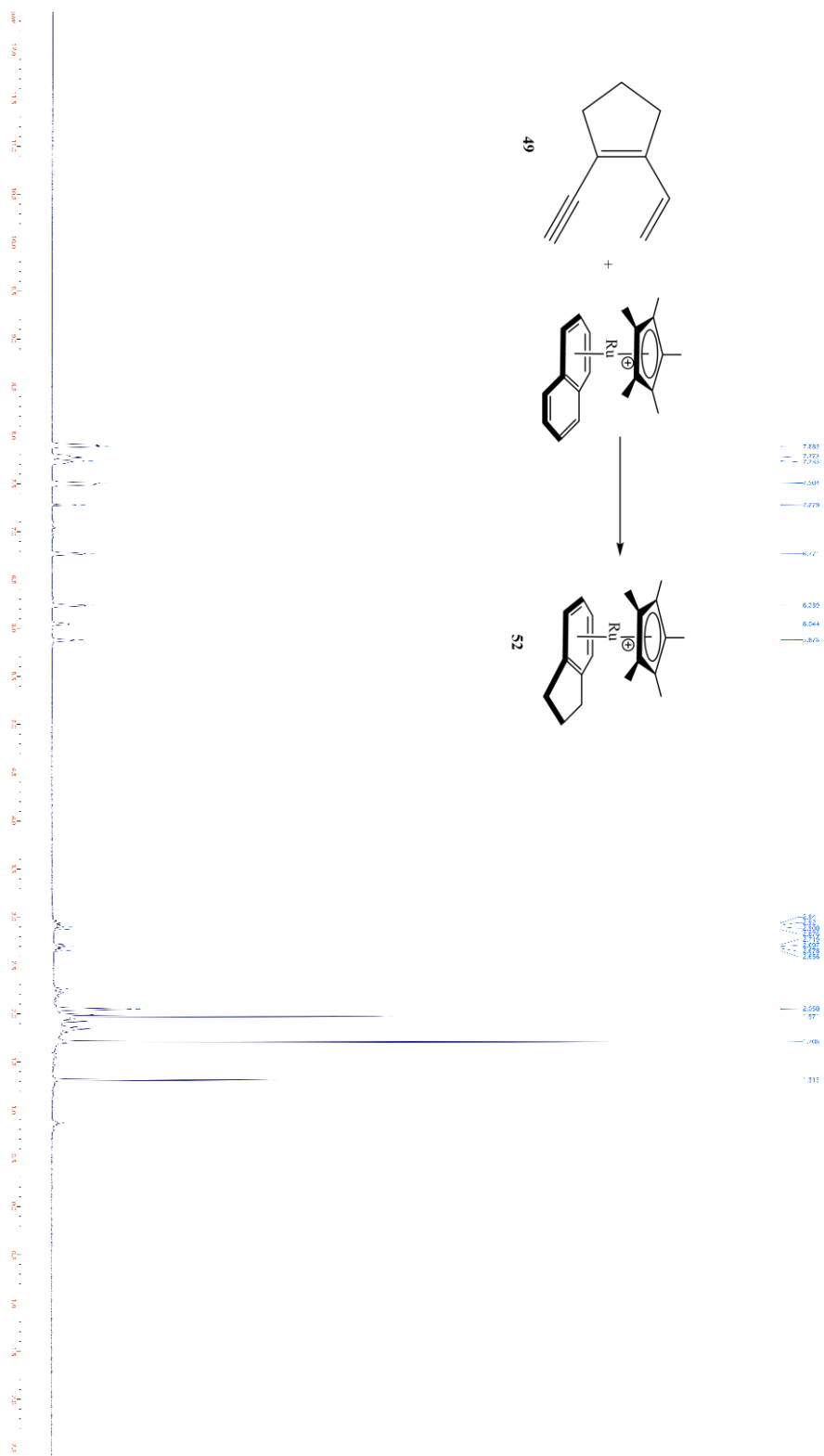


Figure 2-20: ^1H NMR spectrum of **49** reacting with **93** ($\text{Acetone-}d_6$, 400 MHz).

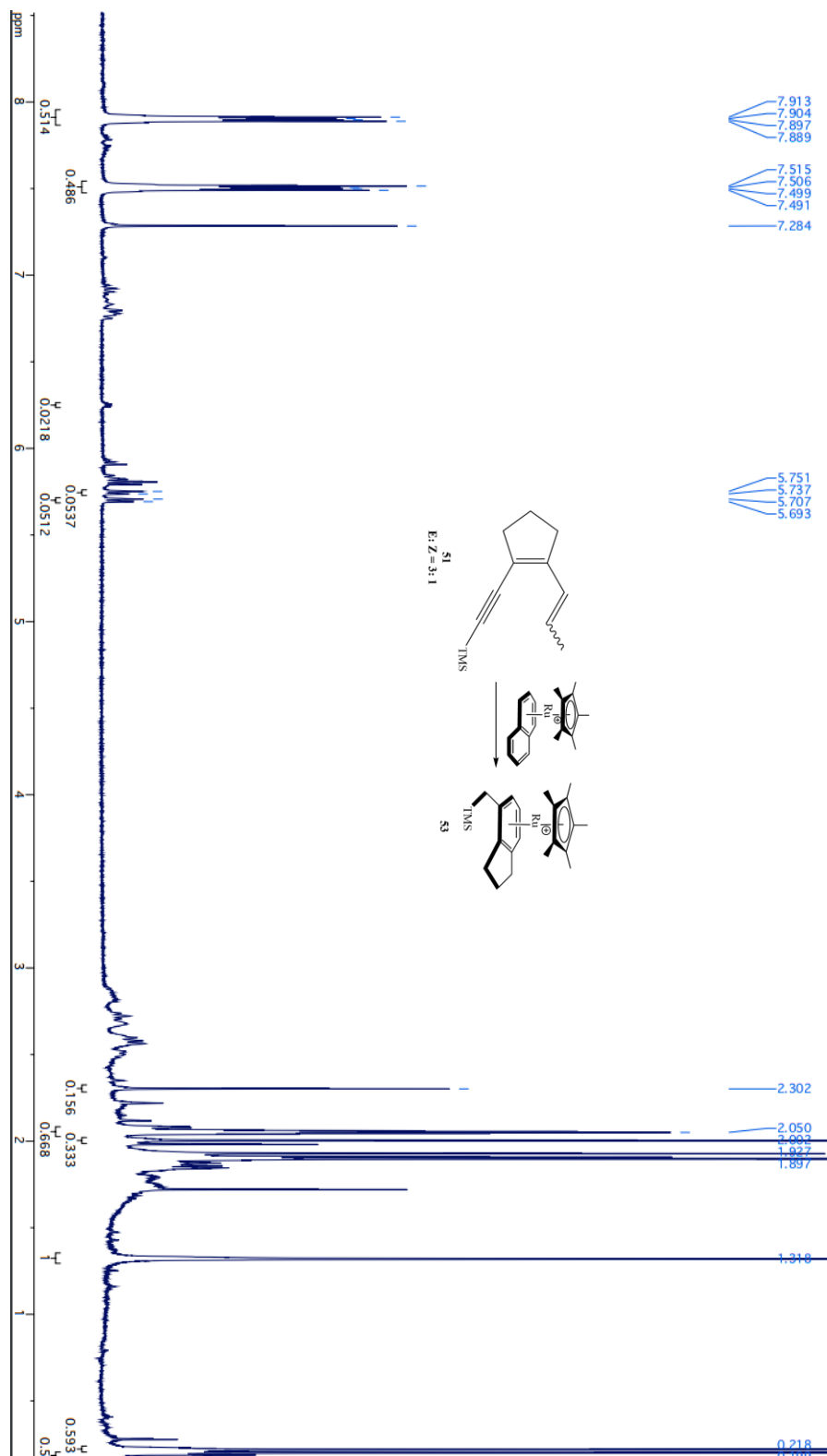


Figure 2-21: ^1H NMR spectrum of **51** reacting with **93** ($\text{Acetone-}d_6$, 400 MHz).

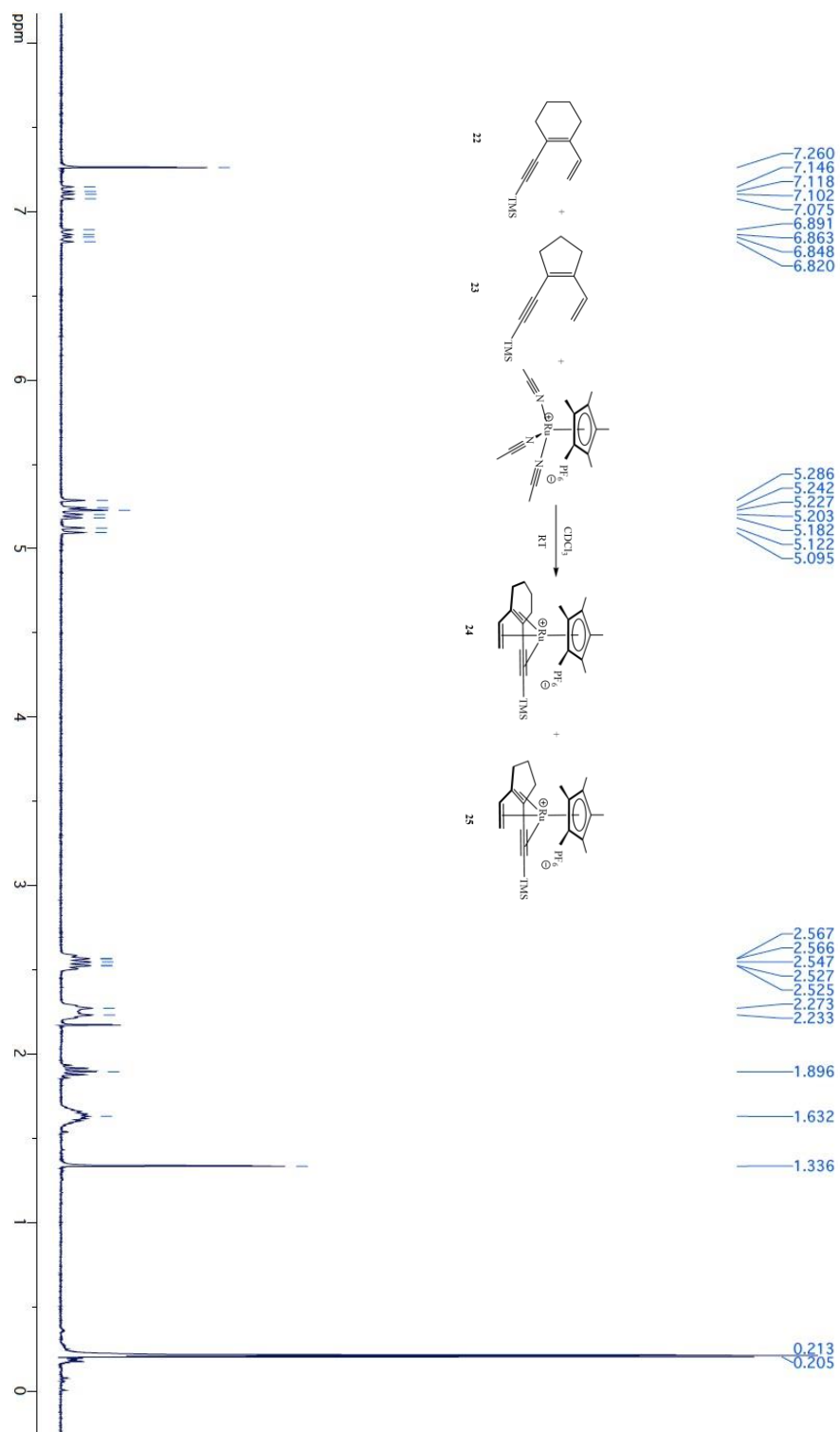


Figure 2-22: Initial ^1H NMR spectrum of competition reaction of **22** and **23** reacting with **92**. (CDCl₃, 400 MHz).

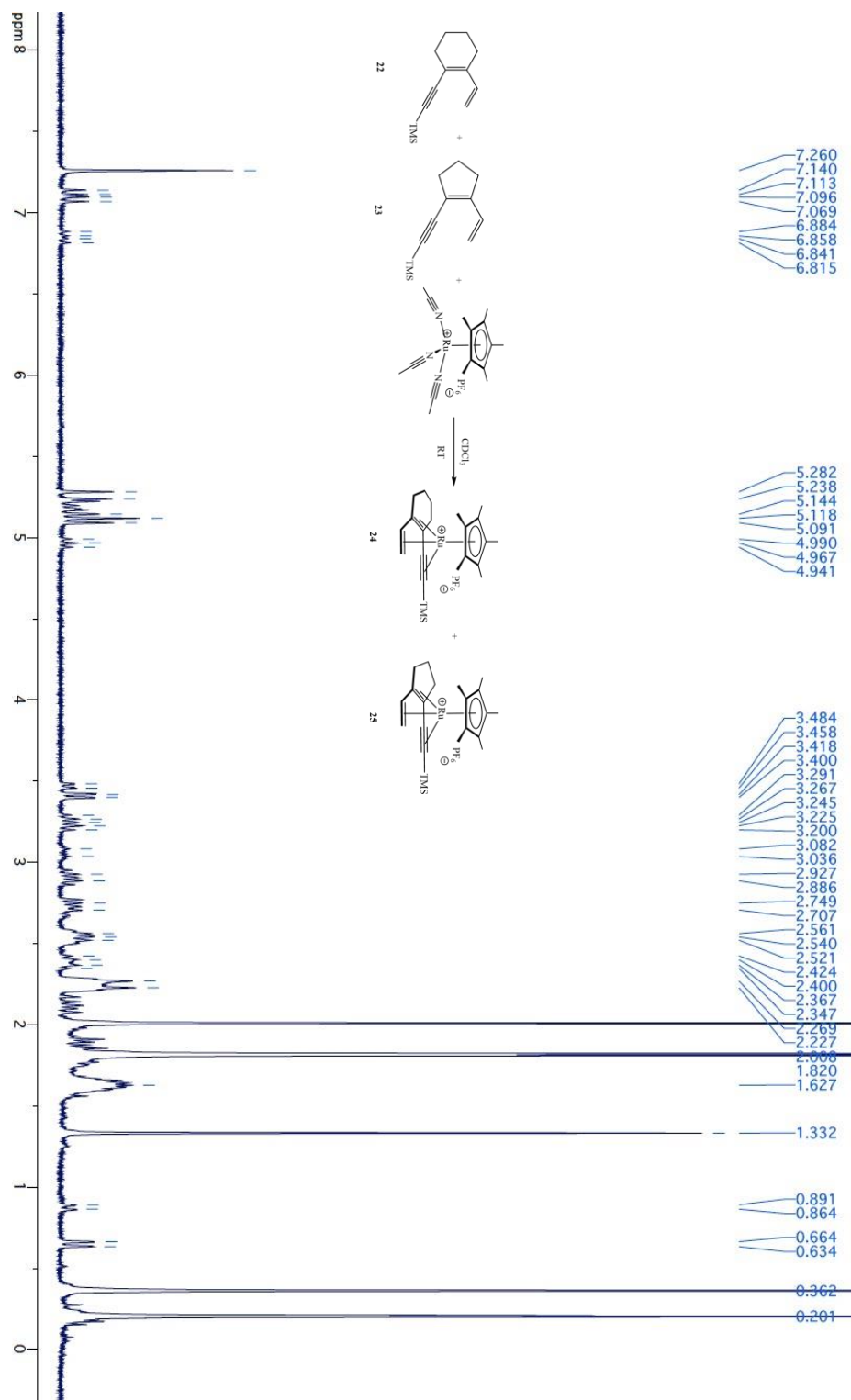


Figure 2-23: Final ¹H NMR spectrum of competition reaction of **22** and **23** reacting with **92**. (CDCl₃, 400 MHz).

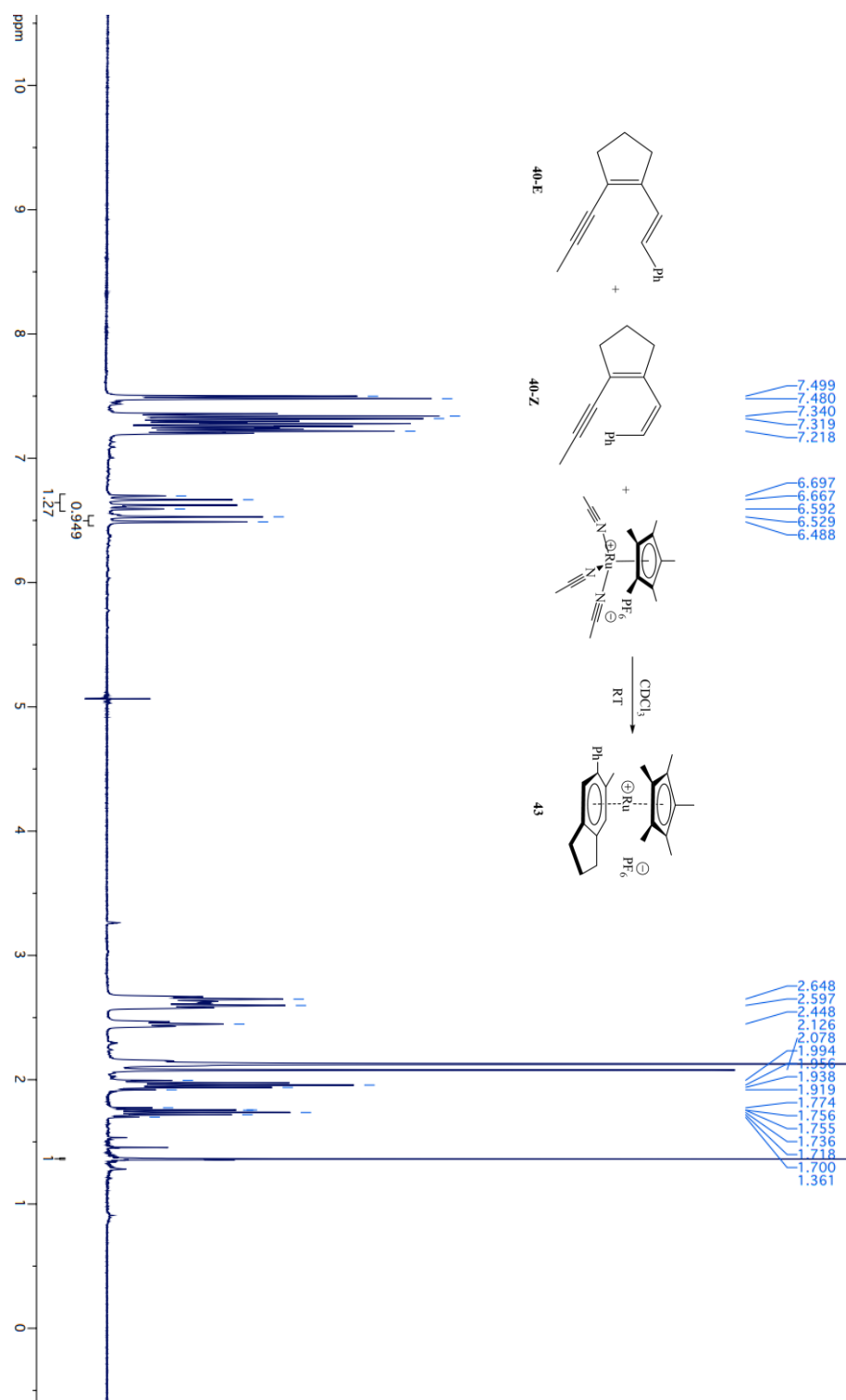


Figure 2-24: Initial ^1H NMR spectrum of competition reaction of **40Z** and **40E** reacting with **92**. (CDCl_3 , 400 MHz).

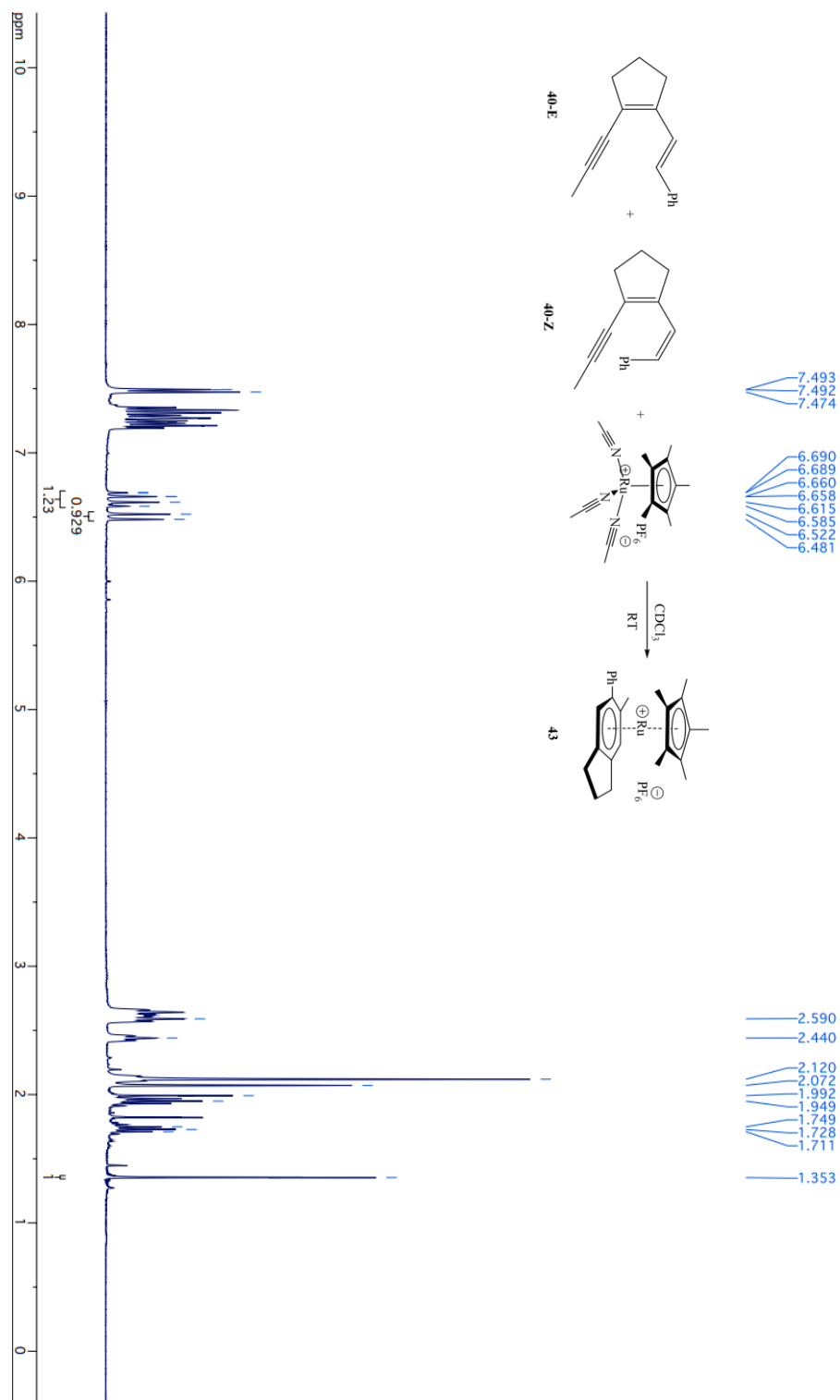


Figure 2-25 : Final ¹H NMR spectrum of competition reaction of **40Z** and **40E** reacting with **92**. (CDCl₃, 400 MHz).

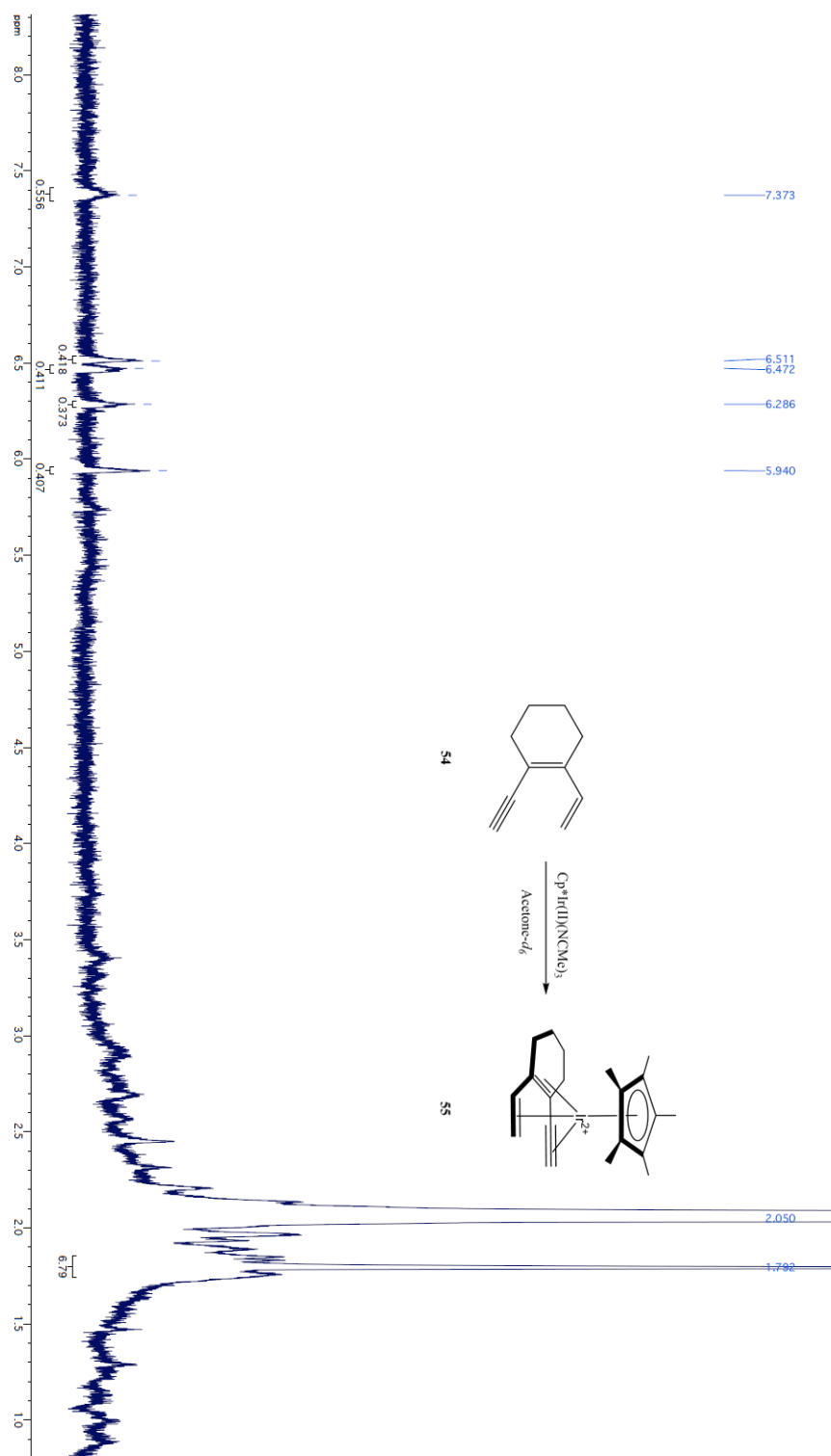


Figure 2-26 : ^1H NMR spectrum of reaction of **53** reacting with **94** in a mole ratio of 1: 1. (Acetone- d_6 , 400 MHz).

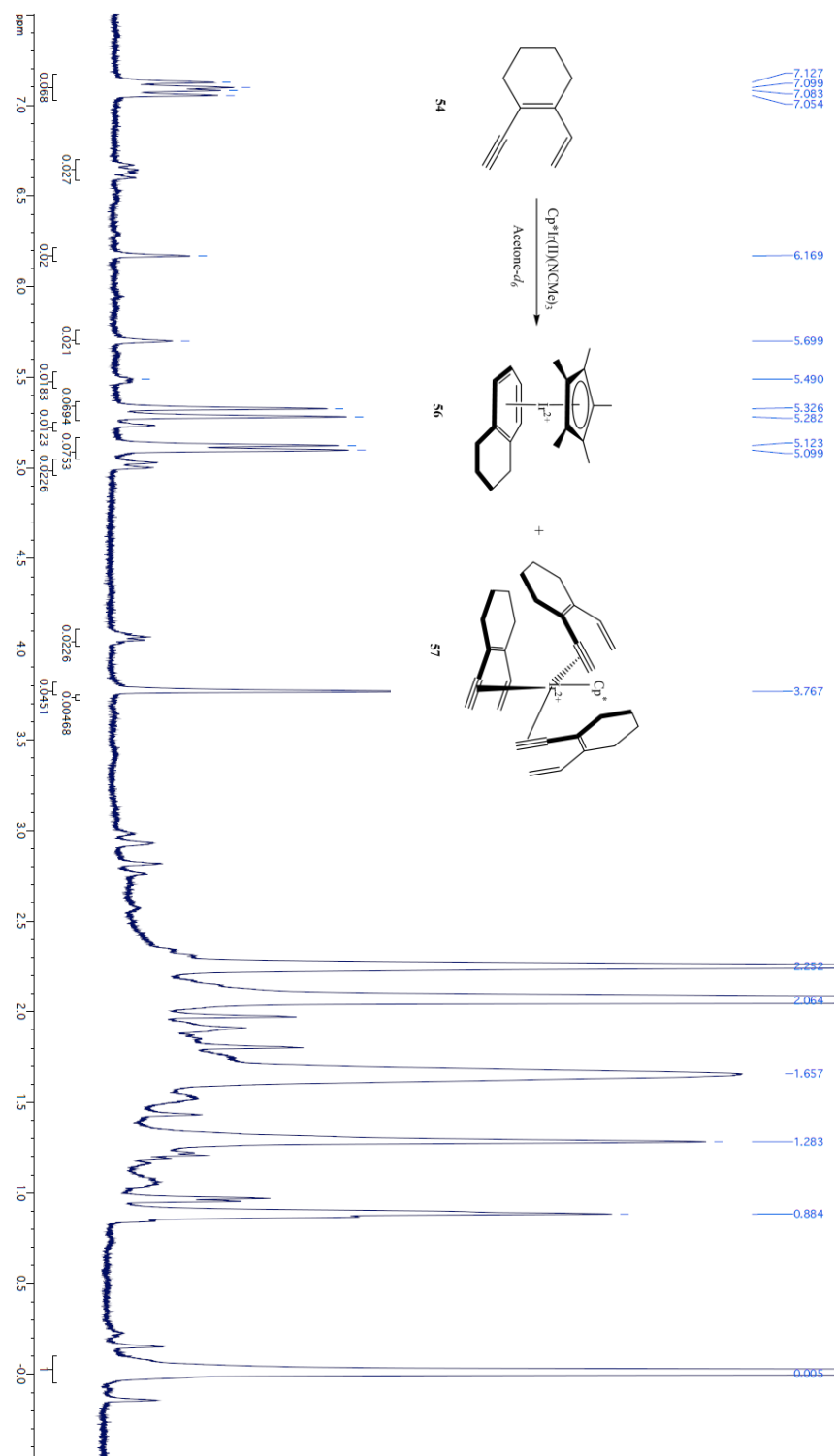


Figure 2-27 : ^1H NMR spectrum of reaction of **53** reacting with **94** in a mole ratio of 10: 1. ($\text{Acetone-}d_6$, 400 MHz).

5. X-ray Crystallographic Summary for Complex 24.

General Experimental for X-ray Structure Determinations.

The single crystal X-ray diffraction studies were carried out on a Bruker Kappa APEX-II CCD diffractometer equipped with molybdenum K α radiation ($\lambda = 0.71073 \text{ \AA}$). The crystals were mounted on a cryoloop with paratone oil and data were collected under a nitrogen gas stream at 100 K using ω and φ scans. Data were integrated and scaled using the Bruker SAINT software program. Solution by direct methods (SHELXS) produced a complete phasing model consistent with the proposed structure. All non-hydrogen atoms were refined anisotropically by full-matrix least squares (SHELXL-97). All hydrogen atoms were placed using a riding model. Their positions were constrained relative to their parent atom using the appropriate HFIX command in SHELXL-97. Crystallographic data and structure refinement parameters are summarized in the supporting information.

Table 2-3: Crystal data and structure refinement for **24**.

Identification code	eda6
Empirical formula	C ₂₃ H ₃₅ F ₆ PRuSi
Formula weight	585.64
Temperature/K	100.0
Crystal system	orthorhombic
Space group	Pbca
<i>a</i> /Å	15.262(8)
<i>b</i> /Å	16.786(9)
<i>c</i> /Å	19.768(10)
α /°	90
β /°	90
γ /°	90
Volume/Å ³	5064(5)
<i>Z</i>	8
ρ_{calc} /cm ³	1.536
μ /mm ⁻¹	0.783
F(000)	2400.0
Crystal size/mm ³	0.29 × 0.27 × 0.07
Radiation	MoK α (λ = 0.71073)
2 Θ range for data collection/°	4.12 to 51.43
Index ranges	-18 ≤ <i>h</i> ≤ 18, -20 ≤ <i>k</i> ≤ 20, -19 ≤ <i>l</i> ≤ 24
Reflections collected	33112
Independent reflections	4817 [<i>R</i> _{int} = 0.0861, <i>R</i> _{sigma} = 0.0582]
Data/restraints/parameters	4817/0/297
Goodness-of-fit on F ²	1.006
Final <i>R</i> indexes [<i>I</i> ≥ 2 σ (<i>I</i>)]	<i>R</i> ₁ = 0.0347, <i>wR</i> ₂ = 0.0592
Final <i>R</i> indexes [all data]	<i>R</i> ₁ = 0.0654, <i>wR</i> ₂ = 0.0679
Largest diff. peak/hole / e Å ⁻³	0.43/-0.41

Table 2-4: Fractional Atomic Coordinates ($\times 10^4$) and Equivalent Isotropic Displacement Parameters ($\text{\AA}^2 \times 10^3$) for **24**. Ueq is defined as 1/3 of the trace of the orthogonalised UIJ tensor.

Atom	x	y	z	U(eq)
Ru1	2239.5(2)	4147.2(2)	4236.4(2)	8.27(7)
Si1	4023.6(6)	3893.5(5)	5737.4(5)	14.1(2)
C1	3593.4(19)	4108.6(19)	4870.0(16)	11.8(7)
C2	3663.4(18)	4041.7(17)	4250.9(17)	11.3(7)
C3	3414.6(19)	4027.0(19)	3559.4(15)	11.3(7)
C4	2791(2)	3461.8(18)	3322.0(16)	13.0(7)
C5	2263(2)	2976.8(18)	3756.2(16)	14.3(7)
C6	2359(2)	2877.7(18)	4459.3(16)	14.9(7)
C7	3454(2)	3005(2)	6074.5(18)	25.9(9)
C8	5212(2)	3707(2)	5598.1(18)	20.8(8)
C9	3882(2)	4751(2)	6316.7(17)	23.4(9)
C10	3820(2)	4632(2)	3091.0(16)	16.6(8)
C11	3306(2)	4743(2)	2438.3(16)	17.2(8)
C12	3146(2)	3932(2)	2124.3(16)	19.4(8)
C13	2561(2)	3426(2)	2578.1(15)	17.5(8)
C14	853.4(19)	4291.3(18)	4453.5(16)	11.9(7)
C15	1355.6(19)	4634.5(18)	4987.6(16)	11.3(7)
C16	1849(2)	5296.4(18)	4703.4(16)	10.1(7)
C17	1644(2)	5355.6(19)	4004.7(16)	11.7(7)
C18	1050(2)	4713.0(18)	3839.1(16)	11.1(7)
C19	198(2)	3630(2)	4526.0(18)	18.0(8)
C20	1302(2)	4425(2)	5721.0(16)	18.0(8)
C21	2425(2)	5854.2(19)	5083.2(16)	16.5(7)
C22	1947(2)	6002.2(18)	3536.8(16)	17.5(8)
C23	643(2)	4565(2)	3165.2(16)	15.4(8)
P1	5247.7(6)	2214.8(6)	2904.1(5)	26.4(3)
F1	4246.5(12)	2418.1(13)	2760.5(10)	30.2(5)
F2	5001.4(15)	1993.1(18)	3663.2(12)	65.3(9)
F3	5424.9(16)	3116.4(14)	3117.9(12)	47.5(7)
F4	6246.4(14)	2007.8(16)	3044.4(15)	68.1(9)
F5	5485.3(14)	2445.8(14)	2140.5(11)	40.5(6)
F6	5074.3(16)	1321.7(14)	2681.9(17)	69.0(9)

Table 2-5: Anisotropic Displacement Parameters ($\text{\AA}^2 \times 10^3$) for **24**.

Atom	U ₁₁	U ₂₂	U ₃₃	U ₂₃	U ₁₃	U ₁₂
Ru1	8.41(12)	8.06(13)	8.34(12)	-0.22(12)	0.49(12)	0.16(11)
Si1	13.4(5)	17.9(5)	11.0(5)	0.8(4)	-2.5(4)	0.1(4)
C1	10.1(16)	10.3(17)	15.0(18)	0.5(16)	-0.2(13)	0.5(14)
C2	4.3(14)	9.6(17)	20.1(18)	-1.9(17)	1.3(15)	-0.1(12)
C3	8.2(16)	14.8(19)	10.9(17)	-1.0(14)	1.8(13)	4.7(14)
C4	12.1(16)	13.0(17)	14.0(17)	-3.1(14)	2.0(15)	6.5(15)
C5	11.3(17)	8.6(17)	23.0(19)	-7.1(14)	-0.7(16)	3.3(15)
C6	15.6(18)	8.2(17)	21.0(18)	0.7(14)	2.8(15)	1.7(14)
C7	25(2)	35(2)	18(2)	10.4(18)	-5.3(17)	-5.0(18)
C8	17.3(19)	20(2)	25(2)	-2.4(17)	-3.5(16)	1.0(15)
C9	20.2(19)	35(2)	15.0(19)	-6.5(17)	-6.0(16)	5.7(17)
C10	16.3(18)	23(2)	10.3(18)	0.5(16)	1.4(15)	-0.6(15)
C11	16.6(19)	21(2)	13.7(18)	5.6(16)	2.8(15)	3.1(15)
C12	21.0(18)	28(2)	8.7(17)	-1.0(15)	-1.3(15)	7.2(16)
C13	17.6(18)	22(2)	13.0(17)	-8.9(16)	-3.7(15)	6.1(15)
C14	7.6(15)	10.1(18)	18.0(18)	-0.2(14)	0.8(13)	4.1(13)
C15	9.4(17)	11.2(18)	13.3(18)	-1.1(14)	3.4(14)	3.7(14)
C16	8.6(16)	9.6(17)	12.2(17)	-5.4(14)	1.3(14)	4.7(13)
C17	10.7(17)	10.9(18)	13.6(17)	-1.1(14)	2.6(14)	5.7(14)
C18	7.2(16)	11.4(18)	14.7(18)	0.4(15)	-0.6(14)	6.7(13)
C19	12.2(18)	15.5(19)	26(2)	1.3(16)	2.5(15)	-0.8(15)
C20	19.5(18)	18.5(18)	16.0(18)	1.4(16)	5.0(16)	2.2(14)
C21	20.1(18)	7.7(16)	21.7(18)	-3.0(16)	2.3(14)	1.1(15)
C22	23.9(19)	12(2)	16.9(18)	2.1(15)	-1.7(15)	0.8(15)
C23	15.5(18)	16.3(19)	14.3(19)	0.3(15)	-5.8(15)	1.4(15)
P1	16.3(5)	23.5(6)	39.3(7)	16.0(5)	1.9(5)	0.6(4)
F1	15.6(11)	40.7(13)	34.1(13)	14.7(11)	3.1(10)	8.3(10)
F2	32.9(14)	114(2)	49.3(16)	59.0(17)	-8.5(13)	-12.6(15)
F3	55.5(16)	39.7(15)	47.4(16)	-7.9(13)	-0.9(13)	-14.8(13)
F4	17.9(13)	69.8(19)	117(2)	58.1(19)	-1.2(14)	0.2(13)
F5	41.5(14)	45.9(15)	34.2(14)	-0.5(12)	16.6(11)	-9.4(12)
F6	44.3(16)	18.6(13)	144(3)	3.0(16)	25.1(17)	-2.6(12)

Table 2-6: Bond Lengths for 24.

Atom	Atom	Length/Å	Atom	Atom	Length/Å
Ru1	C1	2.417(3)	C6	C5	1.407(4)
Ru1	C2	2.181(3)	C10	C11	1.522(4)
Ru1	C3	2.247(3)	C11	C12	1.516(5)
Ru1	C4	2.302(3)	C13	C12	1.524(5)
Ru1	C5	2.182(3)	C14	C19	1.501(4)
Ru1	C6	2.184(3)	C15	C14	1.426(4)
Ru1	C14	2.172(3)	C15	C20	1.494(4)
Ru1	C15	2.167(3)	C16	C15	1.455(4)
Ru1	C16	2.220(3)	C16	C17	1.419(4)
Ru1	C17	2.269(3)	C16	C21	1.488(4)
Ru1	C18	2.195(3)	C17	C22	1.499(4)
Si1	C1	1.871(3)	C18	C14	1.437(4)
Si1	C7	1.850(4)	C18	C17	1.447(4)
Si1	C8	1.861(3)	C18	C23	1.491(4)
Si1	C9	1.852(3)	P1	F1	1.591(2)
C2	C1	1.234(4)	P1	F2	1.591(3)
C3	C2	1.419(4)	P1	F3	1.595(3)
C3	C10	1.507(4)	P1	F4	1.588(2)
C4	C3	1.424(4)	P1	F5	1.600(2)
C4	C5	1.431(4)	P1	F6	1.584(3)
C4	C13	1.513(4)			

Table 2-7: Bond Angles for 24.

Atom	Atom	Atom	Angle/°	Atom	Atom	Atom	Angle/°
C2	Ru1	C1	30.58(11)	C3	C2	Ru1	73.87(17)
C2	Ru1	C3	37.35(12)	C2	C3	Ru1	68.79(17)
C2	Ru1	C4	66.75(12)	C2	C3	C4	120.5(3)
C2	Ru1	C5	85.20(12)	C2	C3	C10	118.1(3)
C2	Ru1	C6	80.48(12)	C4	C3	Ru1	73.89(17)
C2	Ru1	C16	109.44(11)	C4	C3	C10	121.4(3)
C2	Ru1	C17	118.32(11)	C10	C3	Ru1	129.3(2)
C2	Ru1	C18	149.82(12)	C3	C4	Ru1	69.67(17)
C3	Ru1	C1	67.91(11)	C3	C4	C5	123.9(3)
C3	Ru1	C4	36.45(11)	C3	C4	C13	120.2(3)
C3	Ru1	C17	106.24(11)	C5	C4	Ru1	66.89(17)
C4	Ru1	C1	94.64(11)	C5	C4	C13	115.4(3)
C5	Ru1	C1	100.80(12)	C13	C4	Ru1	134.3(2)
C5	Ru1	C3	69.33(12)	C4	C5	Ru1	76.00(18)
C5	Ru1	C4	37.11(11)	C6	C5	Ru1	71.25(18)
C5	Ru1	C6	37.62(12)	C6	C5	C4	126.9(3)
C5	Ru1	C16	165.35(12)	C5	C6	Ru1	71.13(18)
C5	Ru1	C17	136.33(12)	C3	C10	C11	113.1(3)
C5	Ru1	C18	104.33(12)	C12	C11	C10	108.7(3)
C6	Ru1	C1	78.33(12)	C11	C12	C13	110.7(3)
C6	Ru1	C3	88.04(12)	C4	C13	C12	114.4(3)
C6	Ru1	C4	68.90(11)	C15	C14	Ru1	70.60(17)
C6	Ru1	C16	141.86(12)	C15	C14	C18	108.3(3)
C6	Ru1	C17	161.17(12)	C15	C14	C19	125.9(3)
C6	Ru1	C18	124.32(12)	C18	C14	Ru1	71.63(17)
C14	Ru1	C1	137.15(12)	C18	C14	C19	125.7(3)
C14	Ru1	C2	167.71(13)	C19	C14	Ru1	125.9(2)
C14	Ru1	C3	154.83(12)	C14	C15	Ru1	71.02(18)
C14	Ru1	C4	124.53(12)	C14	C15	C16	107.5(3)
C14	Ru1	C5	101.66(12)	C14	C15	C20	126.4(3)
C14	Ru1	C6	98.65(12)	C16	C15	Ru1	72.64(17)
C14	Ru1	C16	63.86(11)	C16	C15	C20	125.7(3)
C14	Ru1	C17	63.28(11)	C20	C15	Ru1	127.6(2)
C14	Ru1	C18	38.43(11)	C15	C16	Ru1	68.65(17)
C15	Ru1	C1	100.79(12)	C15	C16	C21	126.3(3)
C15	Ru1	C2	129.96(12)	C17	C16	Ru1	73.47(18)
C15	Ru1	C3	159.91(12)	C17	C16	C15	108.4(3)
C15	Ru1	C4	162.65(12)	C17	C16	C21	125.2(3)
C15	Ru1	C5	130.41(12)	C21	C16	Ru1	126.7(2)

Table 2-7: Bond Angles for 24. Continued.

Atom	Atom	Atom	Angle/°	Atom	Atom	Atom	Angle/°
C15	Ru1	C6	106.40(12)	C16	C17	Ru1	69.69(18)
C15	Ru1	C14	38.38(11)	C16	C17	C18	107.8(3)
C15	Ru1	C16	38.71(11)	C16	C17	C22	125.7(3)
C15	Ru1	C17	63.35(12)	C18	C17	Ru1	68.31(17)
C15	Ru1	C18	64.32(12)	C18	C17	C22	126.4(3)
C16	Ru1	C1	92.15(11)	C22	C17	Ru1	130.4(2)
C16	Ru1	C3	122.69(12)	C14	C18	Ru1	69.94(17)
C16	Ru1	C4	149.20(11)	C14	C18	C17	107.9(3)
C16	Ru1	C17	36.84(11)	C14	C18	C23	125.9(3)
C17	Ru1	C1	118.09(11)	C17	C18	Ru1	73.91(18)
C17	Ru1	C4	115.76(11)	C17	C18	C23	126.0(3)
C18	Ru1	C1	154.74(11)	C23	C18	Ru1	126.3(2)
C18	Ru1	C3	119.08(12)	F1	P1	F3	90.38(13)
C18	Ru1	C4	103.76(12)	F1	P1	F5	89.84(12)
C18	Ru1	C16	63.28(12)	F2	P1	F1	89.51(12)
C18	Ru1	C17	37.77(11)	F2	P1	F3	90.69(16)
C7	Si1	C1	108.71(15)	F2	P1	F5	179.26(16)
C7	Si1	C8	112.05(17)	F3	P1	F5	88.94(13)
C7	Si1	C9	110.42(17)	F4	P1	F1	179.67(18)
C8	Si1	C1	103.82(15)	F4	P1	F2	90.63(14)
C9	Si1	C1	112.06(15)	F4	P1	F3	89.91(15)
C9	Si1	C8	109.64(16)	F4	P1	F5	90.02(14)
Si1	C1	Ru1	141.25(16)	F6	P1	F1	89.60(13)
C2	C1	Ru1	64.05(18)	F6	P1	F2	90.04(17)
C2	C1	Si1	149.4(3)	F6	P1	F3	179.27(17)
C1	C2	Ru1	85.4(2)	F6	P1	F4	90.10(15)
C1	C2	C3	159.1(3)	F6	P1	F5	90.33(15)

Table 2-8: Hydrogen Atom Coordinates ($\text{\AA}\times 10^4$) and Isotropic Displacement Parameters ($\text{\AA}^2\times 10^3$) for **24**.

Atom	<i>x</i>	<i>y</i>	<i>z</i>	U(eq)
H11	1694.19	2790.75	3560.94	17
H6	2939.2	2692.28	4619.23	18
H6'	1861.83	2628.08	4700.79	18
H1	3653.57	2901.57	6537.55	39
H2	3586.96	2543.06	5789.18	39
H3	2820.65	3099.66	6075.45	39
H4	5285.74	3307.68	5240.8	31
H5	5477.11	3510.73	6017.86	31
H7	5499.49	4203.86	5462.28	31
H8	4173.02	4637.05	6747.82	35
H9	4141.57	5227.74	6112.83	35
H10	3255.87	4841.41	6395.92	35
H18	3859.02	5149.88	3328.36	20
H19	4423.71	4460.97	2978.47	20
H16	3640.75	5082.78	2121.08	21
H17	2739.76	5007.4	2535.14	21
H14	3712.81	3657.32	2055	23
H15	2863.2	3998.85	1677.09	23
H12	2596.69	2864.44	2426.44	21
H13	1946.57	3602.2	2520.43	21
H20	332.14	3318.56	4932.07	27
H21	-391.87	3856.7	4565.87	27
H22	224.85	3284.24	4127.29	27
H23	1206.88	3849.9	5768.51	27
H24	1850.26	4573.14	5945.9	27
H25	813.29	4713	5929.47	27
H26	2714.15	5567.31	5452.7	25
H27	2071.02	6288.92	5270.05	25
H28	2868.44	6073.66	4777.18	25
H29	1652.48	6502.32	3653.4	26
H30	2582.43	6070.02	3581.95	26
H31	1805.43	5856.94	3069.36	26
H32	127.16	4906.84	3111.57	23
H33	1067.99	4684.55	2808.09	23
H34	465.29	4004.75	3133.11	23

VIII. Acknowledgements.

The material in Chapter 2, in part, has been published in *Organometallics* in 2017 with following authors: Qin, P.; Cope, S. K.; Steger, H.; Veccharelli, K.; Holland, L. R.; Hitt, M. D.; Moore, E. C.; Baldrige, K. K and O'Connor, M. J. The rest of the materials are currently under preparation for two publications with the following authors: Qin, P.; Steger, H.; O'Connor, M. J.; Baldrige, K. K. Cope. S. K. and Hitt, D. M. Qin, P.; Steger, H.; Baldrige, K. K.; O'Connor, M. J.

IX. References.

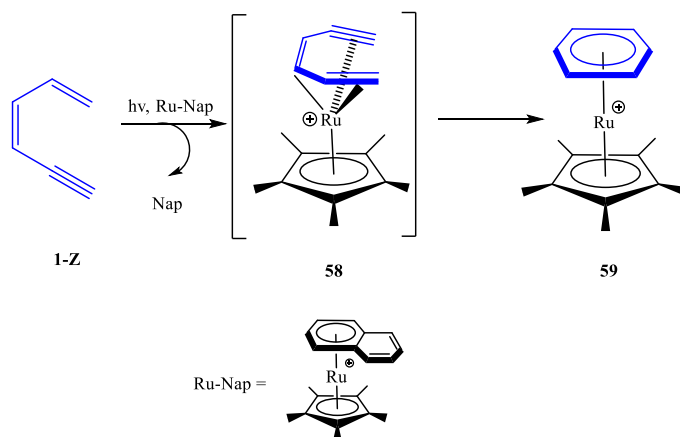
1. Bergman, R. G. *Acc. Chem. Res.* **1972**, 6, 25-31. "Reactive 1,4-Dehydroaromatics".
2. Hopf, H.; Musso, H. *Angew. Chem. Int.* **1969**, 8, 680-680. "Preparation of Benzene by Pyrolysis of cis- and trans-1,3-Hexadien-5-yne".
3. Yang, X.; Li, Z.; Ma, J.; Hu, A. *Langmuir*. **2010**, 26, 11244-11248. "Synthesis of Ultrathin Mesoporous Carbon through Bergman Cyclization of Enediyne Self-Assembled Monolayers in SBA-15".
4. Mandal, S.; Basak, A. *Tetrahedron Letters*. **2009**, 50, 3641-3644. "Aza Hopf cyclization: synthesis and reactivity of cyclic azadieneynes".
5. Hopf, H.; Berger, H.; Zimmermann, G.; Jones, P. G. *Angew. Chem. Int.* **1997**, 36, 1187-1190. "Formation of Isobenzenes by Thermal Isomerization of 1,3-hexadiene-5-yne Derivatives".
6. Prall, M.; Kruger, A.; Schreiner, P. R.; Hopf, H. *Chem. Eur. J.* **2001**, 7, 4386-4394. "The Cyclization of Parent and Cyclic Hexa-1,3-dien-5-yne: A Combined Theoretical and Experimental Study".
7. Litovitzm, A. E.; Carpenter, B. K.; Hopf, H. *Org. Lett.* **2005**, 7, 507-510. "Computational Investigation of the Reactivity of a Hexadienyne Derivative".
8. Scott, L. T.; Cheng, P. C.; Hashemi, M. M.; Bratcher, M. S.; Meyer, D. T.; Warren, H. B. *J. Am. Chem. Soc.* **1997**, 119, 10963-10968. "Colarnulene. A Three-Step Synthesis".
9. Kaplan, L.; Walch, S.P.; Wilzbach, K.E. *J. Am. Chem. Soc.* **1968**, 90, 5646-5647. "Photolysis of Benzene Vapor at 1849 Å. Formation of a cis-1,3-Hexadien-5-yne".
10. Bishop, L. M.; Barbarow, J. E.; Bergman, R. G.; Trauner, D. *Angew. Chem. Int.* **2008**, 29, 8100-8103. "Catalysis of 6- π Electrocyclizations".
11. Zhang, L.; Sun J.; Kozmin, S. A. *Adv. Syn. & Cat.* 348, **2006**, 2271-2269. "Gold and Platinum Catalysis of Enyne Cycloisomerization".
12. Hitt, D. M.; O'Connor, J. M. *Chem. Rev.* **2011**, 111, 7904-7922. "Acceleration of Conjugated Dienyne Cycloaromatization".
13. O'Connor, J. M.; Friese, S.; Tichenor, M. *J. Am. Chem. Soc.* **2002**, 124, 3506-3507. "Ruthenium-Mediated Cycloaromatization of Acyclic Enediynes and Dienynes at Ambient Temperature".
14. O'Connor, J. M.; Friese, S. J.; Rodgers, B. L.; Rheingold, A. L.; Zakharov, L. *J. Am. Chem. Soc.* **2005**, 127, 9346-9347. "An η^6 -Dienyne Transition-Metal Complex".

15. Yamamoto, Y.; Ogawa, R.; Itoh, K. *J. Am. Chem. Soc.* **2001**, 123, 6189-6190. "Significant Chemo- and Regioselectivities in the Ru(II)-Catalyzed [2+2+2] Cycloaddition of 1,6-Dienynes with Dicyanides".
16. Friese, S.; PhD. Dissertation, University of California, San Diego **2004**.
17. Hitt, D.; PhD. Dissertation, University of California, San Diego **2011**.
18. Hitt, D. M.; Qin, P.; Steger, H.; Baldrige, K. K.; Rheingold, A. L.; O'Connor, J. M. "Ambient Temperature Aitken Cycloaromatization of Dienynes: Partitioning Between Hopf and Aitken Pathways." manuscript in preparation.
19. Qin, P.; Steger, H.; O'Connor, J. M.; Baldrige, K. K.; Cope, S. K. "Chemoselective ruthenium-accelerated cycloisomerization of conjugated dienynes." manuscript in preparation.
20. Wang, Y.; Chen, S.; Hu, A. *Top. Curr. Chem.* **2017**, 375, 1– 30. "Construction of Polyarylenes with Various Structural Features via Bergman Cyclization Polymerization".
21. John, J. A.; Tour, H. M. *J. Am. Chem. Soc.* **1994**, 116, 5011-5012. "Synthesis of Polyphenylenes and Polynaphthalenes by Thermolysis of Eneidyne and Dialkynylbenzenes".
22. Karslyan, E. E.; Perekalin, D. S.; Petrovskii, P. V.; Borisova, A. O.; Kudinov, A. R. *Russ. Chem. Bull.* **2009**, 58, 585–588. "Photochemical arene exchange in the naphthalene complex $[\text{CpRu}(\eta^6\text{-C}_{10}\text{C}_8)]^+$ ".
23. Qin, P.; Cope, S. K.; Steger, H.; Veccharelli, K. M.; Holland, R. L.; Hitt, D. M.; Moore, C. E.; Baldrige, K. K.; O'Connor, J. M. *Organometallics*. **2017**, 36, 3967-3973. "Photoactivated Transition-Metal Triggers for Ambient Temperature Eneidyne and Dienyne Cyclization: Ruthenium- η^6 -Naphthalene Complexes."
24. D'Amato, E. M.; Neumann, C. N.; Ritter, T. *Organometallics*. **2015**, 34, 4626-4631. "Selective Aromatic C-H Hydroxylation Enabled by η^6 -Coordination to Iridium (II)".
25. Zhu, F.; Li, Y.; Wang, Z.; Wu, X. *Angew. Chem. Int.* **2016**, 55, 14151-14154. "Iridium-Catalyzed Carbonylative Synthesis of Chromenones from Simple Phenols and Internal Alkynes at Atmospheric Pressure".

**Chapter 3 Ambient Temperature Cr(CO)₃(η^6 -naphthalene)-Mediated
1,3-Dien-5-ynes Cycloaromatization.**

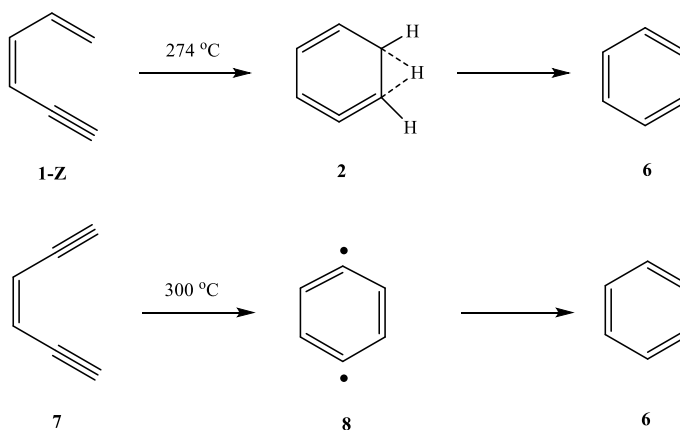
I. Introduction.

Since the initial report in 1969,^{1,2} dienyne/enediyne cyclization has generated significant interest and provided promising new applications to the current synthetic methodology.^{3,4} However, high activation energy barrier of the thermal dienyne/enediyne cyclization requires high reaction temperature (~300 °C) (Scheme 3-2).^{1,2,5} To address this drawback, our laboratory has



Scheme 3-2: Speculative mechanism of Cp*Ru⁺(η^6 -dienyne) mediated dienyne cyclization reported by O'Connor's group. (PF₆ - Counterions Not Shown).

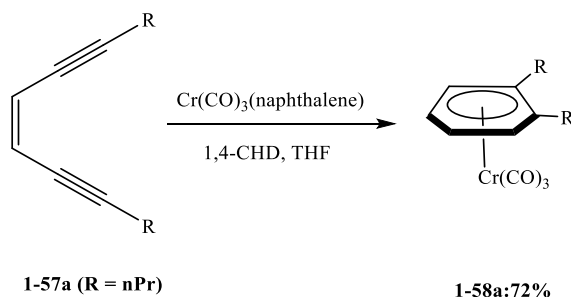
examined a variety of ruthenium complexes with three facial coordination sites and successfully triggered the cyclization at ambient temperature with excellent yields (Scheme 3-1).⁶⁻⁸ However, considering the lack of stability with respect to oxygen and moisture as well as the high cost of



Scheme 3-1: Top: Thermal Hopf/dienyne cyclization under. Bot: Thermal Bergman/enediyne cyclization.

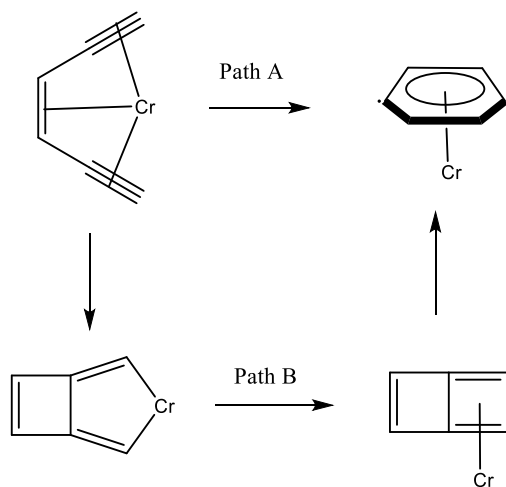
ruthenium, we investigated the possibility of triggering the diene/enediyne cyclization by using more cost-efficient transition metal complexes. The reactivity of hexahepto chromium complexes coordinated to the unsaturated carbon-carbon bonds has been extensively studied.⁹⁻¹¹

Kundig and his group reported the first example of triggering Bergman cyclization with a $\text{Cr}(\text{CO})_3(\eta^6\text{-naphthalene})$ (**95**) complex at ambient temperature (Scheme 3-3). Substrate **1-57a**



Scheme 3-3: Bergman cyclization triggered by $\text{Cr}(\text{CO})_3(\text{naphthalene})$ under ambient temperature.

undergoes electrocyclization under room temperature in the coordination solvent THF. The yield



Scheme 3-4: Two proposed mechanistic pathways in Cr triggered Bergman cyclization.

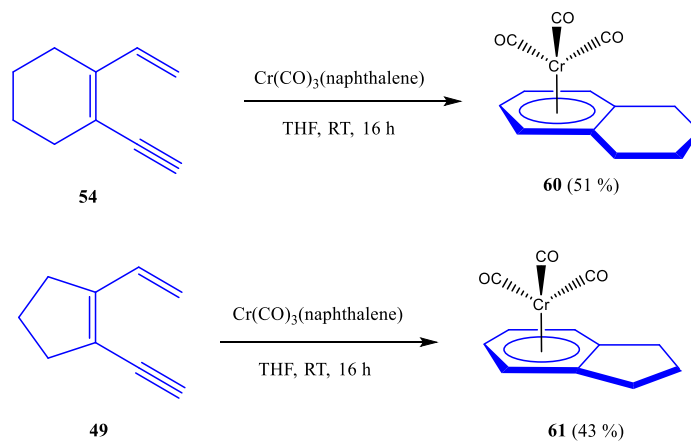
significantly improved with the addition of a hydrogen source 1,4-CHD (Scheme 3-3). This reaction was not observed in a non-coordination solvent or with a bulky terminal substituent. Two

mechanistic pathways (Scheme 3-4) were introduced in his work, while path A described a direct cyclization between C1 and C6 and B described oxidative coupling followed by reductive elimination and bond hemolysis. DFT computation methods suggested that Path B is unfavorable, with a comparison of 80.4 kcal/mol to 16.7 kcal/mol in activation energy barrier. Their work pointed out that the $\text{Cr}(\text{CO})_3(\eta^6\text{-enediyne})$ complex is the crucial pathway that leads to cyclization. The formation of a benzene diradical intermediate was confirmed by a good match between experimental and simulated EPR spectra of the triplet p-benzyne biradical. Kundig's work demonstrated the viability of a chromium mediated variant to ruthenium presented by O'Connor's lab and its key intermediate benzyne biradical was observed to lie on the reaction pathway.

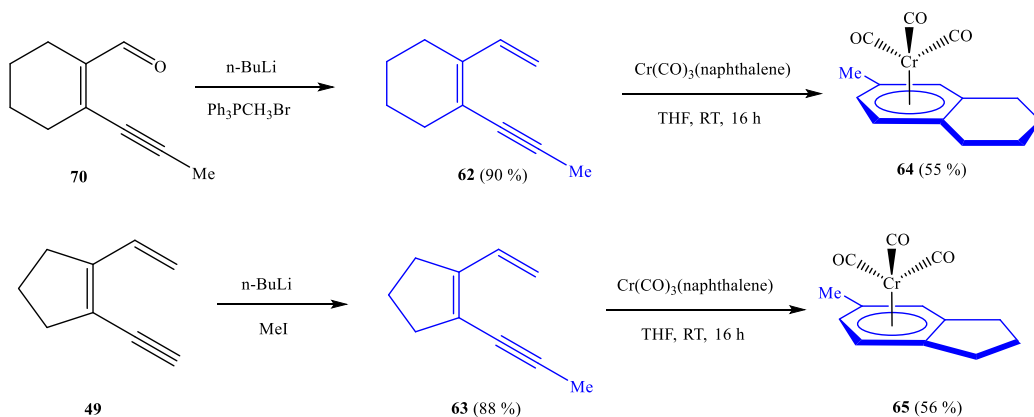
Encouraged by his work, we were excited to examine the capability with **95** in dienyne cyclization. Although the two cyclizations undergo different pathways, we believe that the hexahepto is the crucial intermediate in both electro cyclizations. Thus, we are expecting to see a Hopf cyclization that can be triggered with **95**.

II. Attempts in mediating dienyne cyclization.

Previously reported by our group, $[\text{Cp}^*\text{Ru}^+(\eta^6\text{-naphthalene})][\text{PF}_6]$ (**93**) undergoes photon triggered naphthalene dissociation in coordinating solvent. A speculative intermediate $[\text{Cp}^*\text{Ru}^+(\eta^6\text{-dienyne})]\text{PF}_6$ was then formed followed by the cyclization of dienyne.¹³ In comparison to **93**, arene dissociation of **95** occurs without the presence of a photon. Thus, a $\text{Cr}(\text{CO})_3(\eta^6\text{-dienyne})$ intermediate can be reasoned and likely leads to the successful cyclization. Our study began with treating dienyne **54** with $\text{Cr}(\text{CO})_3(\eta^6\text{-dienyne})$ in THF. After 16 hours, a product that exhibits an identical spectroscopic property to those previously reported was isolated via chromatography and was identified as **60**, which was obtained in a yield of 51 %. The reaction of **49** and $\text{Cr}(\text{CO})_3(\eta^6\text{-naphthalene})$ led to the formation of the product **61**, which was isolated at a 43 % yield. Our study expanded in scope beyond simple dienynes to bulkier substrates. Dienyne



Scheme 3-5: **93** mediated electrocyclization of **49** and **54**.



Scheme 3-6: Synthesis of **62**, **63** and **93** mediated electrocyclization.

62 and **63** were synthesized by performing a methylation on **53** and **49**, respectively. Under the same conditions, arene products **64** and **65** were obtained at a yield of 55 % and 56 %, respectively. Crystallization was successfully performed on **64** and an X-ray crystal structure was obtained (Figure 3-1). The crystal structure in Figure 3-1 indicated the C1-C6 distance (1.421 Å) is identical to the C3-C4 distance (1.417 Å) which proved the bond formation between C1 and C6. It was also obvious that the bond distances between Cr center to C1, C2, C5 and C6 (2.20 to 2.23 Å) are slightly shorter than the distance between the Cr center to C3 and C4 (2.24 to 2.25 Å). This

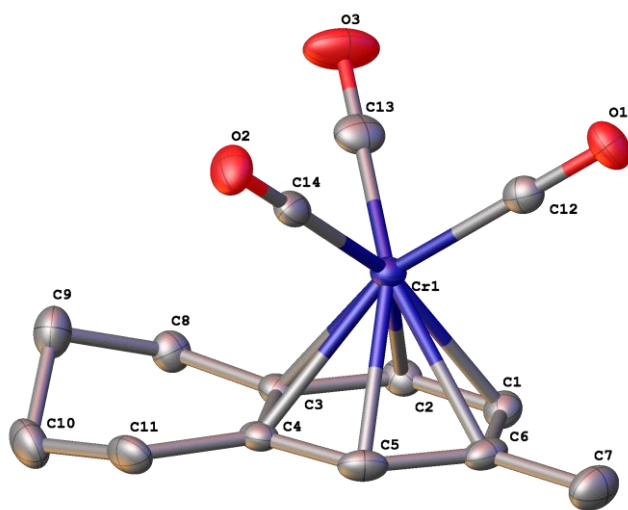
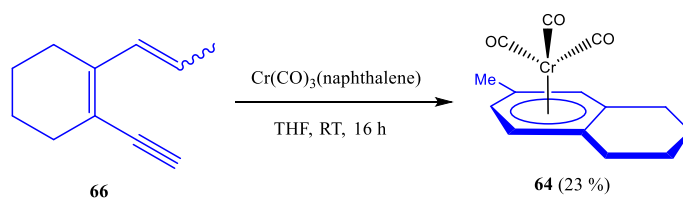


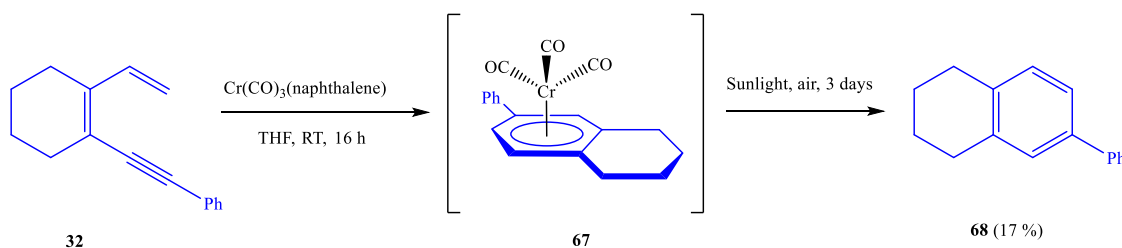
Figure 3-1: X-ray crystal structure of **64**, hydrogens atoms are not shown.

difference in bond length was likely because the cyclohexane ring caused rigidity of the C3-C4 bond. **64** could also be synthesized using a different dienyne substrate, **66** by treating it with **95** under similar conditions, but the yield (23 %) was considerably lower. We speculated that the cause of the lower yield was that only one isomer was suitable to produce the cyclization, but we have not yet investigated its mechanism.



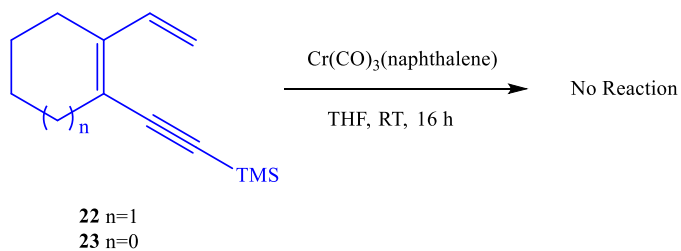
Scheme 3-7: **93** mediated electrocyclization of **66**.

Cyclization was again successfully achieved for a bulk substituted dienyne **32**. Unfortunately, we were not able to obtain a neat NMR spectrum of the metal coordinated arene product **67** likely due to the multiple arene binding sites available for Cr coordination. However, after exposing it to atmosphere and sunlight for 72 hours, organic arene product **68** was isolated at a 27 % yield.



Scheme 3-8: $\text{Cr(CO)}_3(\eta^6\text{-dienyne})$ mediated electrocyclization of **32**.

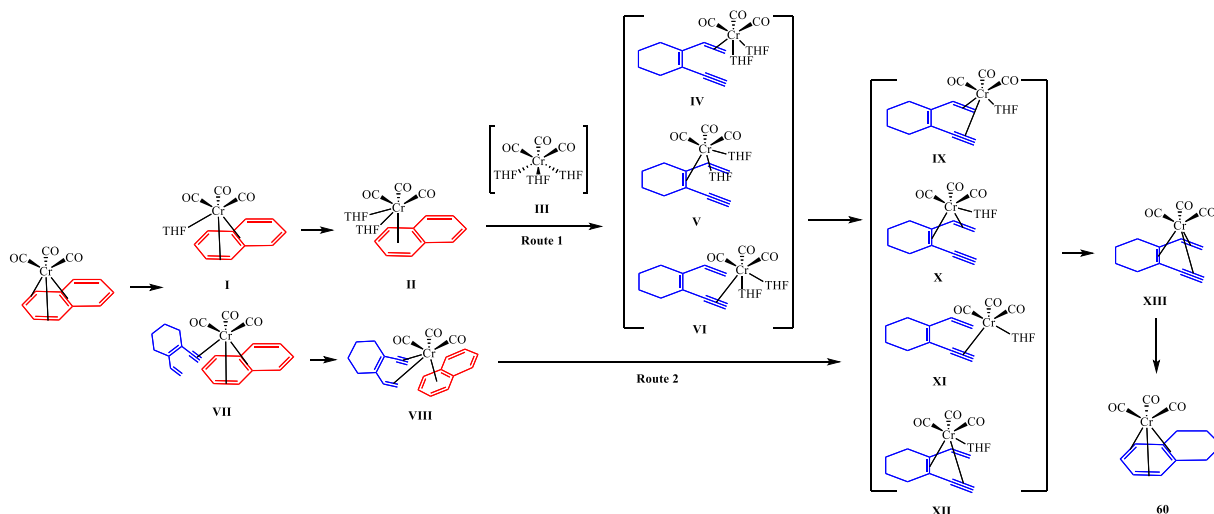
22 and **23** were not able to produce any arene products. This result was consistent with our previously reported study of reacting **22** and **23** with **92**, in which we believed the steric hindrance of TMS prohibits the formation of the arene product. Unfortunately, the attempts in isolating the possible $(\text{CO})_3\text{Cr}(\eta^6\text{-dienyne})$ complex were not successful.



Scheme 3-9: **22** and **23** failed to cyclize when reacting with $\text{Cr}(\text{CO})_3(\eta^6\text{-dienyne})$.

Reaction conditions were also examined in non-coordinating solvents such as CHCl_3 and CH_2Cl_2 . In those solvents, **95** remained in its precursor state without naphthalene dissociation. Heating to $70\text{ }^\circ\text{C}$ or exposing the reaction mixture to 252 nm ultraviolet light did not accelerate the cyclization but only resulted in the decomposition of **95**. Only unreacted substrate and free naphthalene were obtained after chromatography.

III. Mechanistic investigation and kinetic study with Fourier-transform infrared spectroscopy (FT-IR).



Scheme 3-10: Proposed mechanism routes and intermediates of Cr mediated dienyne electrocyclization.

We proposed a stepwise naphthalene dissociation and dienyne coordination mechanism during the cyclization and hoped to observe any intermediates via ^1H NMR spectroscopy (Scheme 3-10). However, precipitation resulting from minor decomposition of the **95** prohibits the

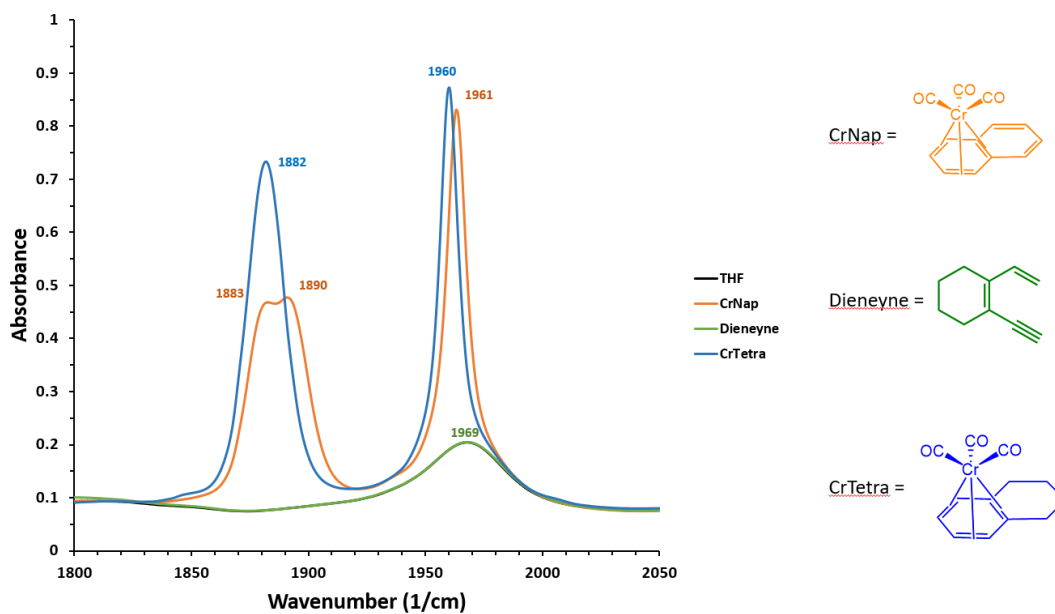


Figure 3-2: Proposed mechanism routes and intermediates of Cr mediated dienyne electrocyclization.

convenience of monitoring such reactions with ^1H NMR spectroscopy, thus we carried out a mechanistic study with FT-IR spectroscopy by monitoring the change in carbonyl stretching frequency. The IR spectra of **95** $\nu(\text{CO})$: 1883, 1890, 1961 cm^{-1} and **60** $\nu(\text{CO})$: 1882, 1960 cm^{-1} were recorded separately (Figure 3-2). Into an airtight IR cell, was injected 0.1 mL THF solution containing **95** and **54** in a 1: 10 mole ratio mixture. At 23 $^\circ\text{C}$, a dramatic increase in absorption at 1938 cm^{-1} was observed which could be due to a $\text{Cr}(\eta^6\text{-enediynes})$ intermediate (Figure 3-3). After 20 h, the IR absorption at 1938 cm^{-1} decreased with a corresponding increase in an absorption at 1690 cm^{-1} due to the formation of **60**. In addition, we observed a decomposition product with an absorption at 1978 cm^{-1} . To identify the decomposed product, we performed control samples of **54** reacting with **95** in THF under atmosphere (Figure 3-4, blue), **95** solution in THF exposed to ambient air (Figure 3-4, yellow) and a CrCO_6 solution in THF (Figure 3-4, red). All three samples had an absorption at 1978 cm^{-1} (Figure 3-4) while such an absorption peak was not observed in the case of the **95** solution sample stored under N_2 . The decomposition product exhibited absorptions

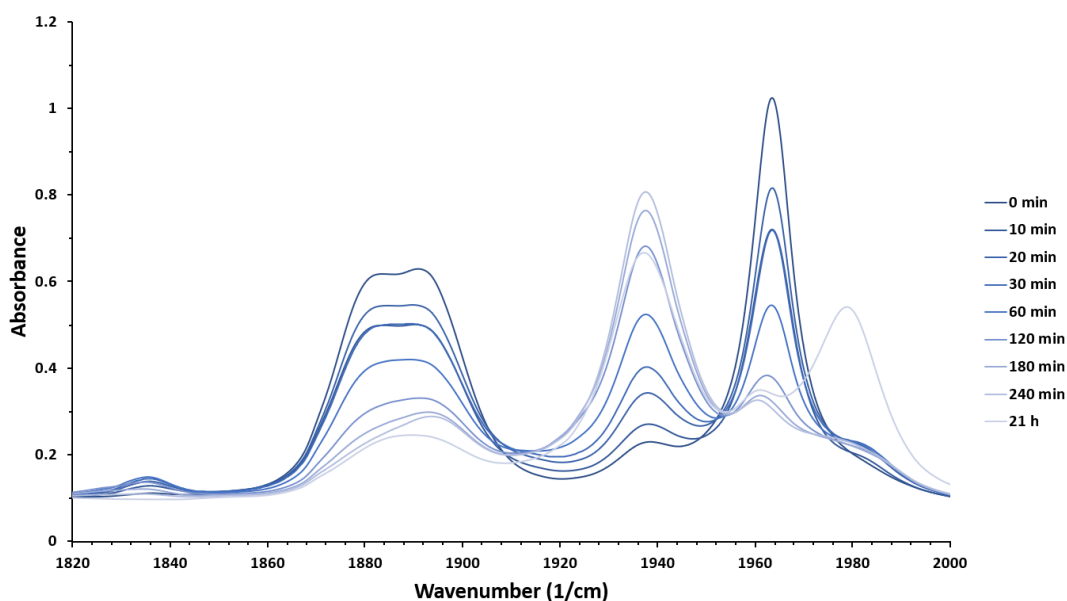


Figure 3-3: FT-IR monitored reaction of **53** with **95** in a 10:1 mole ratio in THF.

that are identical to those of $\text{Cr}(\text{CO})_6$, which suggests that **95** underwent a highly complex decomposition mechanism in solution when a leakage of air was introduced.

To confirm our hypothesis on the $\text{Cr}(\eta^6\text{-enediyne})$ intermediate as the crucial pathway towards cyclization, we again performed a reaction of **95** and **22** in the IR cell. As predicted, an intermediate IR absorption at 1938 cm^{-1} was again observed. After 20 hours, the speculative intermediate peak did not decrease in intensity, this was believed to be as a result of the failure in forming the cyclized product (Figure 3-5). Thus, the “intermediate” peak remained in this case.

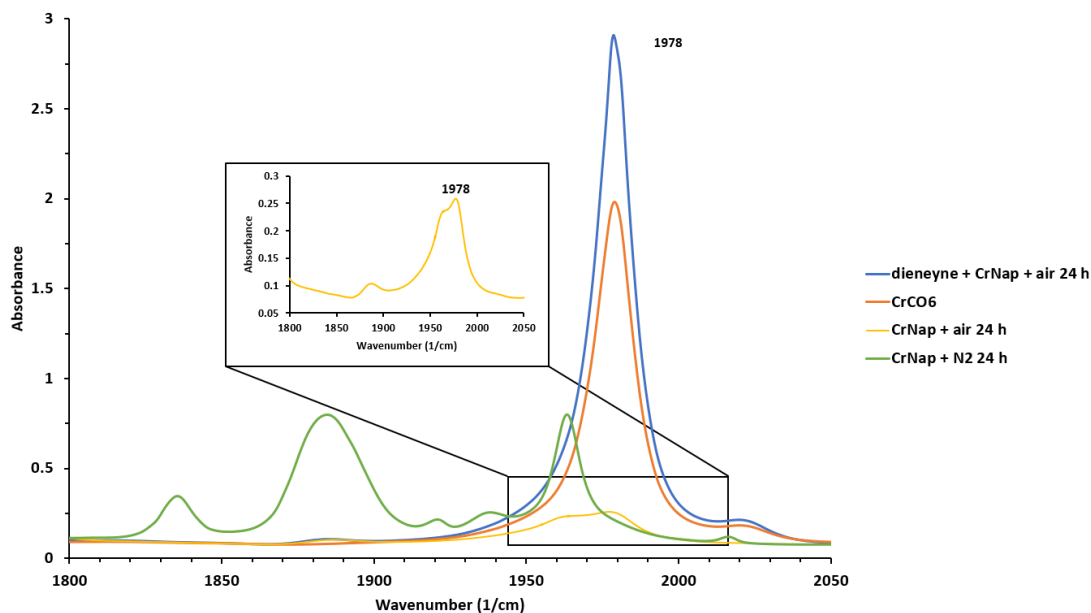


Figure 3-4: FTIR spectrum of **95** under ambient atmosphere (yellow), **95** reacting with **53** under ambient air (blue), **95** under N_2 (green) and CrCO_6 (red).

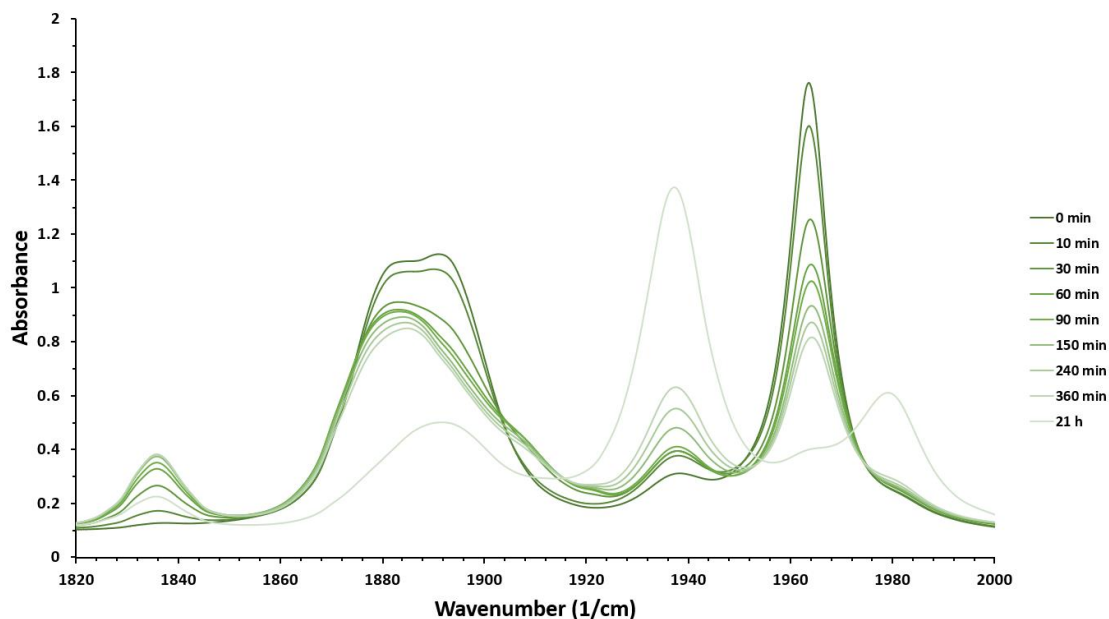


Figure 3-5: FTIR monitored reaction of **22** with **95** in a 10:1 mole ratio in THF.

Solvent influences were studied in the same manner. We believe that the formation of the $\text{Cr}(\eta^6\text{-enediyne})$ intermediate requires that it be performed in a coordination solvent. Thus, a control study in 2,5-dimethyltetrahydrofuran was carried out with **54**. Within 240 min, the peak

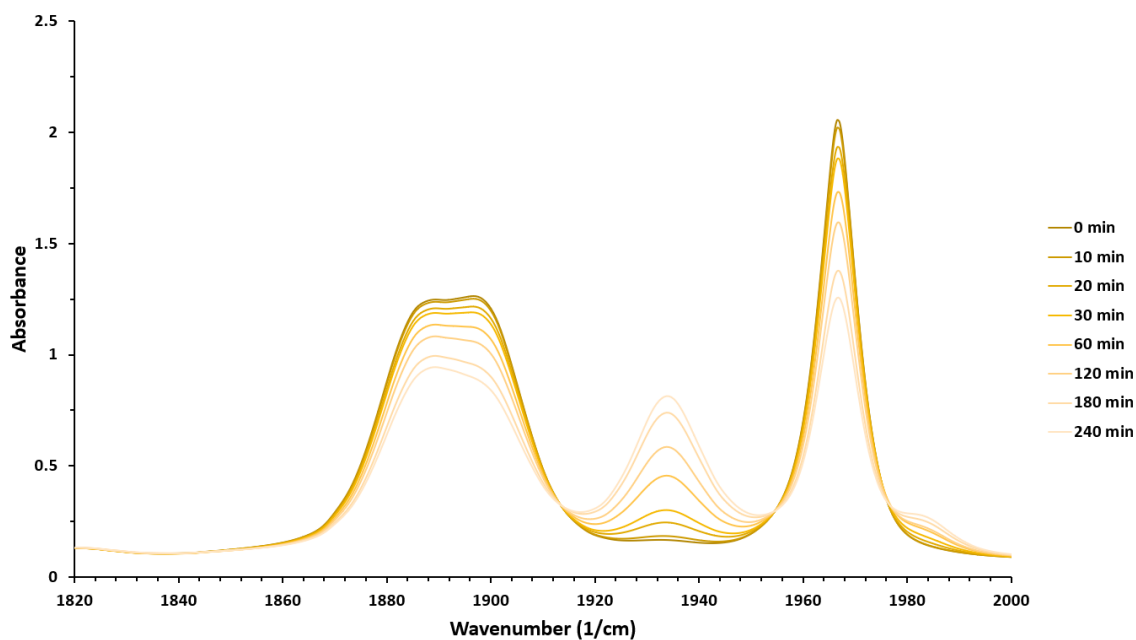


Figure 3-6: FTIR monitored reaction of **54** with **95** in a 10:1 mole ratio in 2,5-dimethyltetrahydrofuran.

intensity of an absorption at 1983 cm^{-1} relative to the starting material absorption was much lower than the case of the THF solvent, indicating that the intermediate was formed at a much slower rate (Figure 3-6) caused by the steric hindrance of the solvent.¹⁴ The retardation resulting from the bulky coordination solvent suggests that the solvent plays an important role in naphthalene dissociation and substrate re-coordination. Thus, we believe the step wise dissociation presented in route one is likely the major reaction pathway. Based on the previous experience with **93**

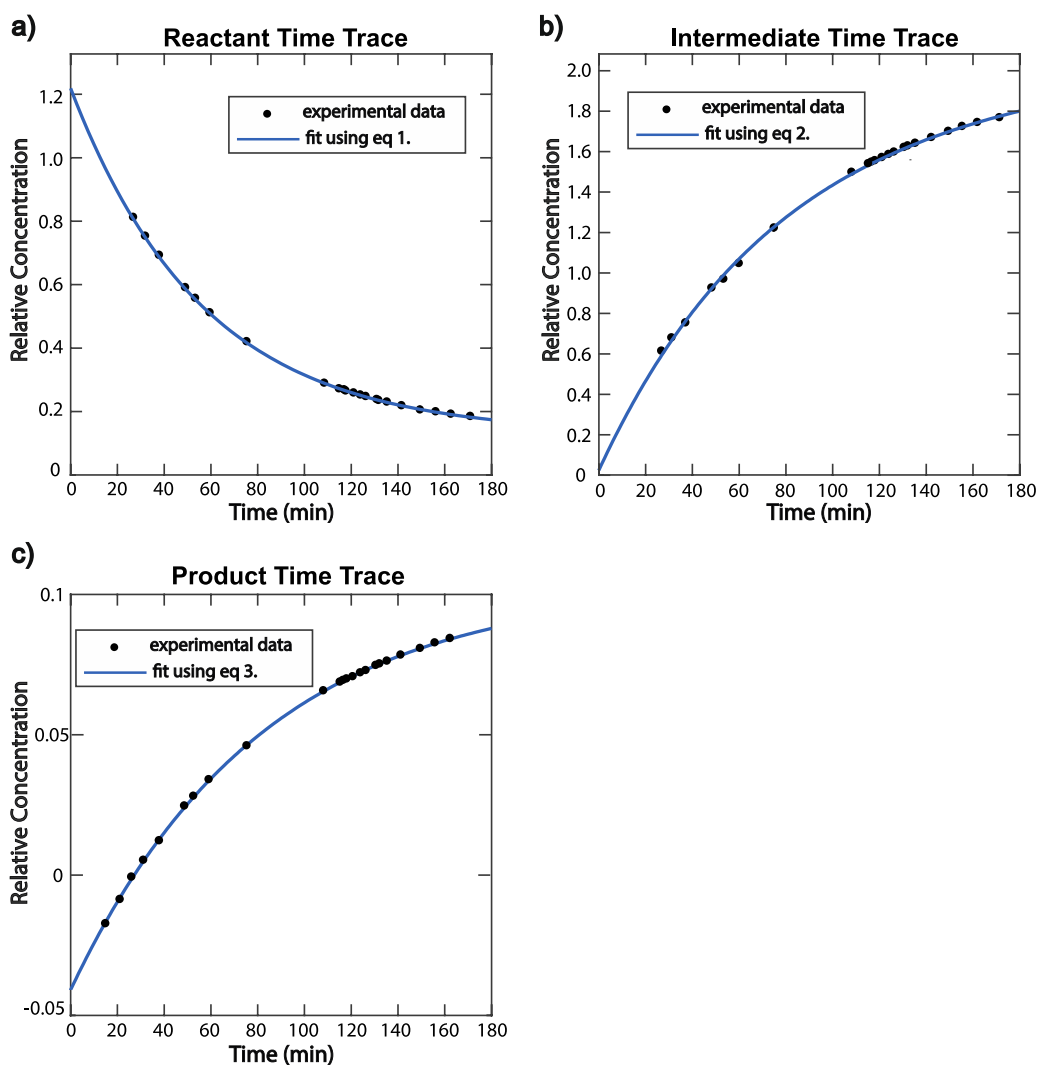
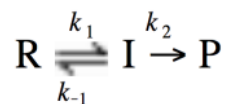


Figure 3-7: Time trace of reactant **95**, intermediate and product **60**. Each component is separated with multivariate analysis for each FTIR spectrum that taken at different time points. Experimental data is then fitted with equation 1, 2, and 3, respectively. Relative concentrations of reactant (a), intermediate (b), and product(c) are plotted as a function of time.

mediated diyne cyclization studies, the bond formation from the hexahepto to the arene product is the rate determining step as determined by calculation. It is reasonable to assume the same result can be applied in this study, in which the slow step should be the step where **XIII** converts into **60**. In another words, the intermediate we observed at 1983 cm⁻¹ likely belongs to **XIII**.

We were also able to retrieve kinetic information from the FT-IR study. Multivariate regression was applied to extract the reactant, the intermediate and the product time trace from the FT-IR spectrum (Figure 3-7). The model we use to simulate is a two-step, first-order consecutive reaction:¹⁵



The rate constant can be represented in the following expressions:

$$[R](t) = \frac{[R]_0(\lambda_2 - k_1)}{(\lambda_2 - \lambda_1)} (e^{-\lambda_1 t} + Ae^{-\lambda_2 t}) \quad (1)$$

$$[I](t) = \frac{[R]_0(k_1)}{(\lambda_2 - \lambda_1)} (e^{-\lambda_1 t} - e^{-\lambda_2 t}) \quad (2)$$

$$[P](t) = [R]_0 - [R](t) - [I](t), \quad (3)$$

Where the rate constant can be calculated with:

$$k_1 = \frac{A\lambda_2 + \lambda_1}{A+1}, k_2 = \frac{\lambda_1\lambda_2}{k_1}, \text{ and } k_{-1} = \lambda_1 + \lambda_2 - k_1 - k_2. \quad (4)$$

Fitting the experimental data to equation 1, 2 and 3 and calculating from equation 4 yields the rate constants to be:

Rate Constant	
$k_1(\text{s}^{-1})$	0.0128244
$k_2(\text{s}^{-1})$	0.0001183
$k_{-1}(\text{s}^{-1})$	0.0015329

In agreement with our expectation, the results indicated that $k_1 + k_{-1} \gg k_2$. we observed that the intermediate peak started appearing almost immediately once the reaction starts, indicating that the first step of the reaction took place rapidly. In addition, the fact that the intermediate peak grew gradually after 6 hours and finally decreased after 20 hours supported the assumption that the rate of the second step of the reaction was much slower than the first step. Therefore, the rate constants designate that the cyclization from **XIII** to **60** was more likely to be the rate determining step.

IV. 2D-IR in determining intermediates.

In order to comprehend the reaction intermediate, a 2D-IR study was performed to observe intermediate species at a higher resolution. The reactant and product 2D-IR exhibited carbonyl vibrational peaks and their corresponding overtone peaks at 1883 cm^{-1} and 1960 cm^{-1} respectively (Figure 3-8a and 3-8b). As the reaction continued, we observed that the intermediate vibrational peak and overtone peak features appeared at 1938 cm^{-1} (Figure 3-8c). Furthermore, 2D-IR allowed

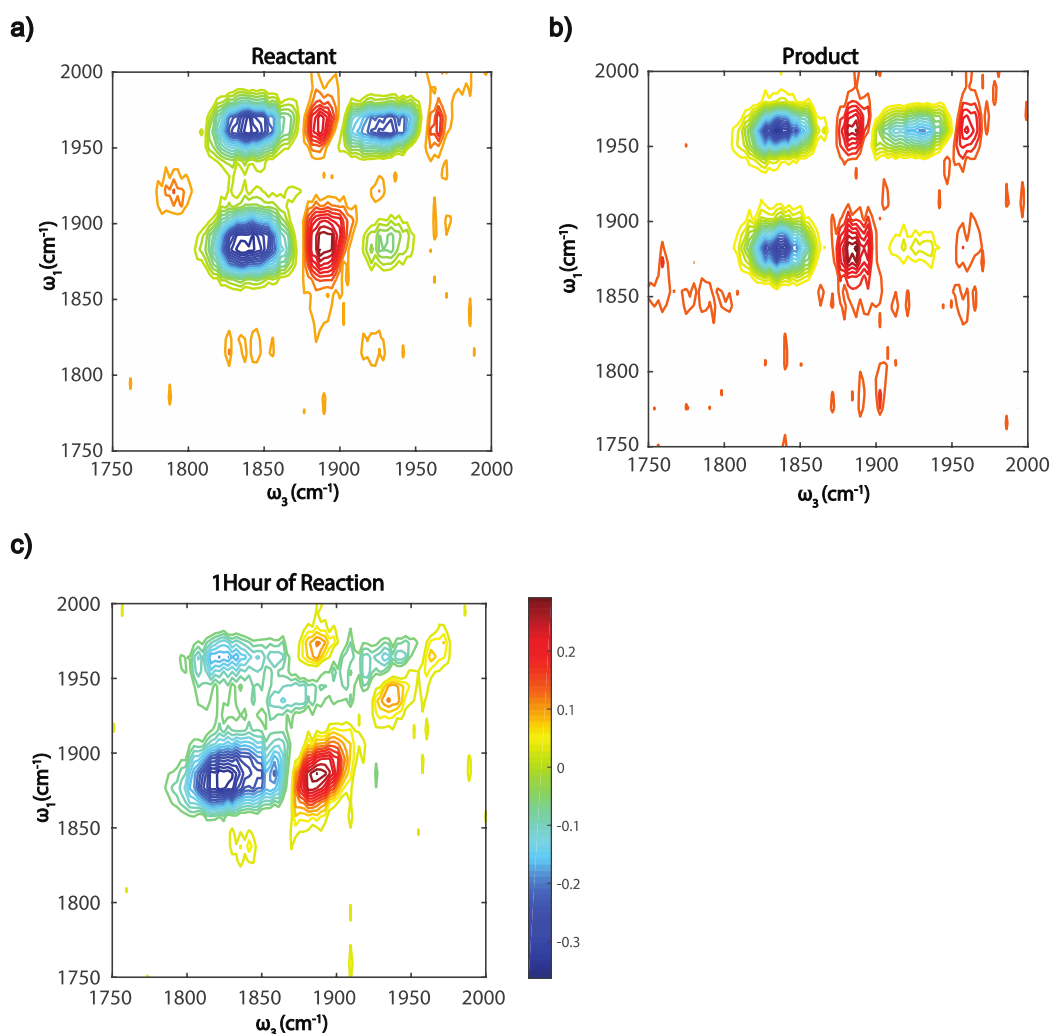


Figure 3-8: Time trace of reactant 6-H, intermediate and product 6-Cr-H. Each component is separated with multivariate analysis for each FTIR spectrum that taken at different time points. Experimental data is then fitted with equation 1, 2, and 3, respectively. Relative concentrations of reactant (a), intermediate (b), and product (c) are plotted as a function of time.

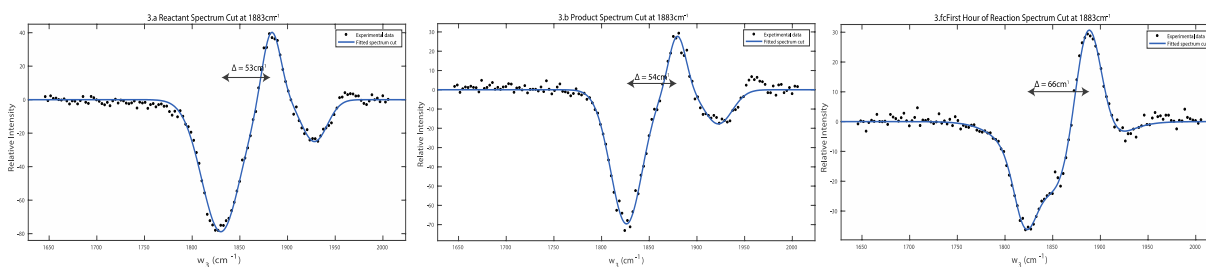


Figure 3-9: 2D-IR spectrum cut at 1883 cm^{-1} fitted with Gaussian function. Intensity as a function of wavenumber. (a) $\text{Cr}(\text{CO})_3(\eta^6\text{-naphthalene})$ peak's anharmonicity is 53 cm^{-1} ; (b) **60** peak's anharmonicity is 54 cm^{-1} ; (c) One hour of reaction peak's anharmonicity is 66 cm^{-1} .

the acquisition of the anharmonicity of molecular vibrations. We retrieved the anharmonicity by applying a cut at 1883 cm^{-1} and 1960 cm^{-1} . For the reactant and the product, the anharmonicity is of similar values at 53 cm^{-1} and 54 cm^{-1} at both 1883 cm^{-1} and 1960 cm^{-1} , respectively. However, a 13 cm^{-1} shift in anharmonicity was observed in the one-hour reaction which could not be distinguished through FT-IR at 1883 cm^{-1} (Figure 3-9) while 1960 cm^{-1} remained unchanged (Figure 3-10). This indicates that this intermediate vibrational peak overlapped with the reactant and product absorption peaks at 1883 cm^{-1} . With 2D-IR, the intermediate vibrational peak's position was further revealed.

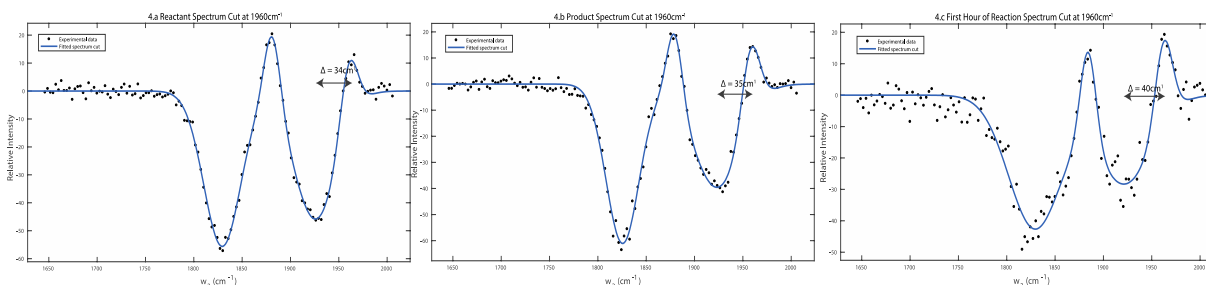
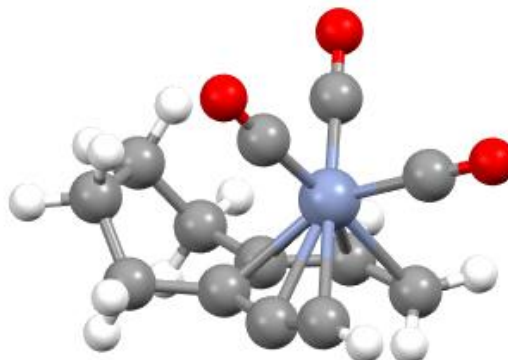
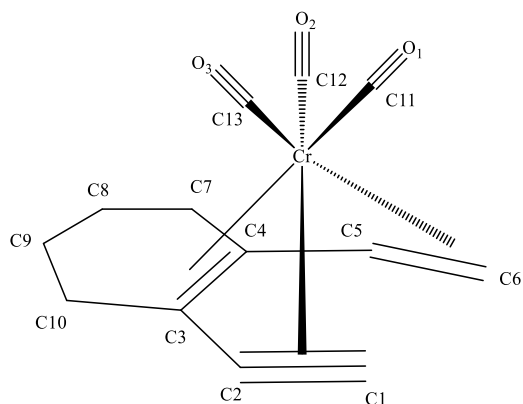


Figure 3-10: 2D-IR spectrum cut at 1960 cm^{-1} fitted with Gaussian function. Intensity as a function of wavenumber. (a) Reactant peak's anharmonicity is 34 cm^{-1} ; (b) **60** peak's anharmonicity is 35 cm^{-1} ; (c) One hour of reaction peak's anharmonicity is 40 cm^{-1} .

Our observation was supported by our collaborator Prof. Baldrige's computational study. The structure of **XIII** was established via the BP86 density function with an ultrafine grid, together

Table 3-1: Calculated bond length (Å) and bond angle (°) of Cr-dienyne intermediate **XIII**.



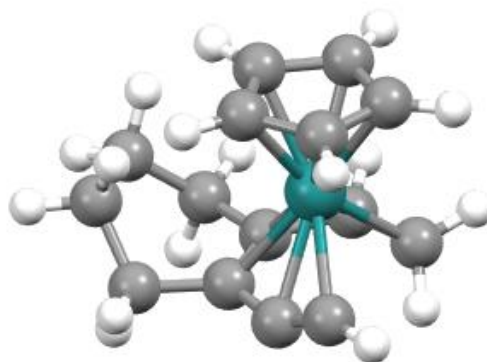
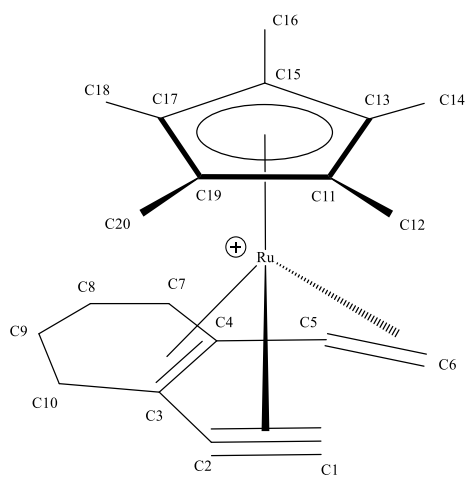
XIII

Cr carbon bond length	Bond length Å	Dienyne bond length	Bond length Å
Cr-C1	2.448	C1-C2	1.236
Cr-C2	2.224	C2-C3	1.405
Cr-C3	2.280	C3-C4	1.418
Cr-C4	2.284	C4-C5	1.440
Cr-C5	2.251	C5-C6	1.385
Cr-C6	2.374	C3-C10	1.515
Cr-C11	1.844	C10-C9	1.545
Cr-C12	1.822	C9-C8	1.553
Cr-C13	1.848	C8-C7	1.544
		C7-C4	1.510
		C1-C6	3.142

Cr carbon bond angle	Bond angle °	Dienyne bond length	Bond angle °
C1-Cr-C2	30.2	C1-C2-C3	158.3
C2-Cr-C3	36.3	C2-C3-C4	122.2
C3-Cr-C4	36.2	C3-C4-C5	125.5
C4-Cr-C5	37.0	C4-C5-C6	128.6
C5-Cr-C6	34.7	C10-C3-C4	117.6
Cr-C11-O1	177.3	C3-C4-C7	115.3
Cr-C12-O2	175.8	C4-C7-C8	112.5
Cr-C13-O3	178.9	C7-C8-C9	112.9
		C8-C9-C10	113.3
		C9-C10-C3	112.5

with the Def2-TZVPP basis set (Table 3-1). The antisymmetric $\nu(\text{CO})$ vibrational stretching

Table 3-2: Calculated bond length (Å) and bond angle (°) of Ru-dienyne intermediate **69**.



69

Ru carbon bond length	Bond length Å	Dienyne bond length	Bond length Å
Ru-C1	2.290	C1-C2	1.249
Ru-C2	2.194	C2-C3	1.405
Ru-C3	2.293	C3-C4	1.436
Ru-C4	2.309	C4-C5	1.434
Ru-C5	2.189	C5-C6	1.413
Ru-C6	2.209	C3-C10	1.512
		C10-C9	1.544
		C9-C8	1.549
		C8-C7	1.539
		C7-C4	1.509
		C1-C6	2.919

Ru carbon bond angle	Bond angle °	Dienyne bond length	Bond angle °
C1-Ru-C2	32.3	C1-C2-C3	153.5
C2-Ru-C3	36.4	C2-C3-C4	121.7
C3-Ru-C4	36.4	C3-C4-C5	124.9
C4-Ru-C5	37.1	C4-C5-C6	125.8
C5-Ru-C6	37.5	C10-C3-C4	118.1
C11-Ru-C13	36.7	C3-C4-C7	115.3
C13-Ru-C15	37.2	C4-C7-C8	113.0
C15-Ru-C17	38.2	C7-C8-C9	113.4
C17-Ru-C19	38.7	C8-C9-C10	113.7
C19-Ru-C11	38.9	C9-C10-C3	114.1

frequencies were calculated to be 1833.6 and 1859.0 cm^{-1} , the symmetric stretches in combination

with the interacting triple bond stretch were calculated to be 1934.5 cm^{-1} and 1997.5 cm^{-1} . The absorbance at 1833.6 cm^{-1} and 1934.5 cm^{-1} can be directly observed from the FT-IR spectrum (Figure 3-3c). The antisymmetric stretch absorbance at 1859 cm^{-1} was not directly obtained from the IR spectrum but a negative peak shoulder at $\sim 1855\text{ cm}^{-1}$ was observed and believed to be an overtone peak from the 1859 cm^{-1} absorbance peak. Although we speculate an absorbance peak was exhibited at $\sim 1997\text{ cm}^{-1}$ (Figure 3-4c), it was not confirmed due to its low intensity relative to noise. Combining the results obtained from the IR study and the computation, it is reasonable to believe the intermediate we observed very likely to be **XIII**.

To compare the structure difference between the ruthenium system, $\text{Cp}^*\text{Ru}^+(\eta^6\text{-dienyne})$ (**69**) was established via the same computation method. In the case of **XIII**, the Cr-dienyne bonds have an average bond length of 2.310 \AA . The alkyne bond was bent from 180° to 158° due to metal coordination. On the other hand, **69** exhibits a shorter average Ru-dienyne bond length, 2.247 \AA and the alkyne was bent to 153° , in which case is more twisted in **XIII**. Due to this, **69** vs. **XIII** C1-C6 nonbonding distance is 3.14 \AA vs. 2.92 \AA , which might explain the lower yield chromium mediated cyclization.

V. Proposed Mechanism.

With the evidence given by IR studies and the model given by previous studies with $[\text{Cp}^*\text{Ru}(\eta^6\text{-dienyne})]\text{PF}_6$, we speculate the mechanism shown in scheme 3-10 as the most probable reaction pathway. The coordination solvent promotes the dissociation of naphthalene from **95** to generate $\text{Cr}(\text{CO})_3\text{L}_3$. A fast equilibrium is then established between $\text{Cr}(\text{CO})_3\text{L}_3$ and the $\text{Cr}(\text{CO})_3(\eta^6\text{-dienyne})$ intermediate, which is believed to be the contributor of the intermediate peak observed in IR at 1938 cm^{-1} . The formation of the product may undergo two pathways, a [1,3] hydride shift or a [1,2] hydride shift, as suggested by the previous O'Connor cyclization reported by our group.

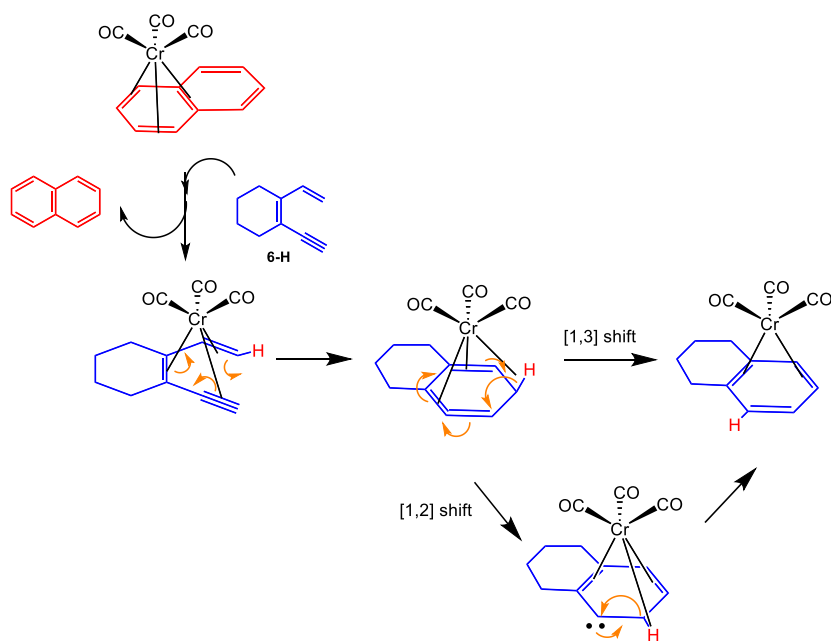


Figure 3-11: Speculative mechanism of **95** mediated dienyne cyclization.

VI. Conclusions and Future work.

Here we report that an oxygen and moisture stable complex $\text{Cr}(\text{CO})_3(\eta^6\text{-naphthalene})$ promotes the diyne cyclization under ambient temperature in moderate yield; thereby demonstrating that the prior observation of the ruthenium-mediated cyclization may also work with other metals. Bulky coordinating solvents and bulky alkyne substituents, such as TMS, prohibited the cyclization due to the steric hindrance which matches what we observed in the previous ruthenium study. The IR spectroscopic studies provided evidence for the formation of the observable intermediate. We speculate it to be the $\text{Cr}(\text{CO})_3(\eta^6\text{-diyne})$ intermediate based on the previously reported ruthenium-mediated diyne cyclization. However, the information we obtained from the 2D-IR studies did not give a concrete identification of the intermediate. We are currently conducting calculations in order to verify the best explanation for the complex that was observed in IR studies.

VII. Experimental.

1. General procedures

Standard Schlenk technique or a nitrogen-filled glovebox are applied in all NMR reactions between dienyne substrates and metal complexes. Flash column chromatographic purifications were performed using silica gel (60 Å, particle size 43-60 µm, 230-400 mesh, EMD Chemicals). ¹H and ¹³C NMR spectra were recorded on Varian Mercury 400 MHz or Varian VX 500 MHz instruments. ¹H and ¹³C NMR chemical shifts (δ) are reported in parts per million (ppm). Spectra were referenced to the residual solvent peak. Chloroform was dried by refluxing with CaH₂ overnight and THF was dried over activated molecular sieves followed by distillation under static vacuum. The structural and energetic analyses of the molecular systems described in this study were carried out using the BP86 density functional, with an ultrafine grid, together with the Def2-TZVPP basis set. Effects of solvent were included by the continuum solvation model based the original COSMO theory of Klamt modified for *ab initio* theory, with a dielectric for THF. Full geometry optimizations were performed and uniquely characterized via second derivative (Hessian) analysis to establish stationary points and effects of zero point energy and thermal corrections. Visualization and analysis of structural was carried out using Avogadro and WebMO.

2. FT-IR and 2D-IR.

To monitor the reaction, 0.1 mL reaction mixture was injected into an airtight IR flow cell equipped with Teflon caps and infrared spectra were obtained on a Nicolet iS10 FT-IR. High/low resolution mass spectra analyses were performed at the mass spectrometer facility at UC San Diego. Two-dimensional infrared (2D IR) spectroscopy is applied to investigate the mechanism of the reaction. The setup scheme is shown in Figure 3-10. 800-nm laser pulses (~ 35 fs, ~ 5 W, 1 kHz) generated by an ultrafast Ti:Sapphire regenerative amplifier (Astrella, Coherent) are sent into an optical parametric amplifier (OPA) (TOPAS, LightConversion) which outputs tunable near-IR pulses. The near-IR pulses are converted to mid-IR pulses through a difference frequency generation (DFG) process by a type II AgGaS₂ crystal (Eksma). After DFG, a CaF₂ wedge splits the mid-IR pulse into two parts: the 95 % transmitted part is sent into a Ge-Acoustic Optical Modulator based mid IR pulse shaper (QuickShape, PhaseTech) and is shaped to double pulses, which forms the pump beam arm; the 5 % reflected is the probe beam. Both pump (~ 1.1 μ J) and probe (~ 0.2 μ J) are focused by a parabolic mirror ($f = 10$ cm) and overlap spatially at the sample. The output signal is collimated by another parabolic mirror ($f = 10$ cm) at a symmetric position. The pulse sequence is shown in Figure 3-12. Two pump pulses and a probe pulse (pulse duration of 100~150 fs) interact with samples at delayed times (t_1 , t_2 and t_3). After the first IR pulse, a

vibrational coherence is generated, which is converted into a subsequent state by the second IR pulse and is characterized by scanning t_1 (0 to 4000 fs with 20 fs steps) using the mid IR pulse shaper. A rotating frame at $f_0 = 1583 \text{ cm}^{-1}$ is applied to shift the oscillation period to 80 fs and to make the scanning step meet the Nyquist frequency requirement. After waiting for t_2 , the third IR

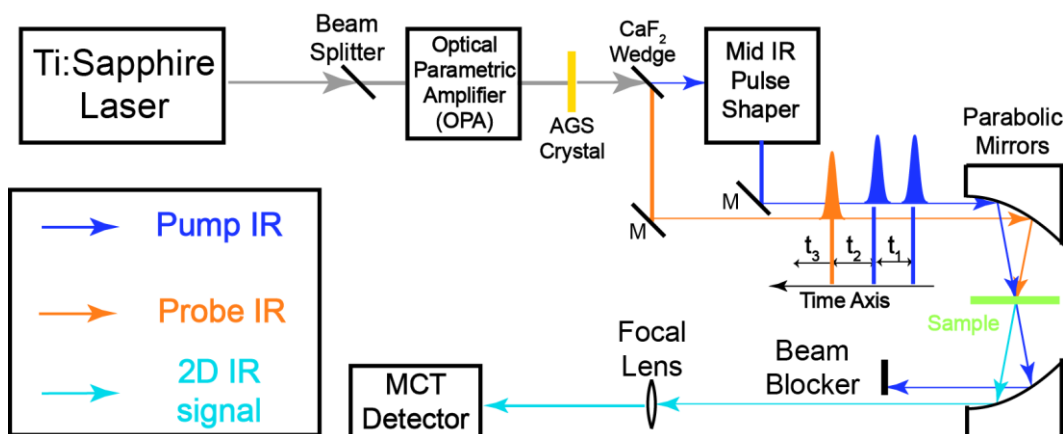
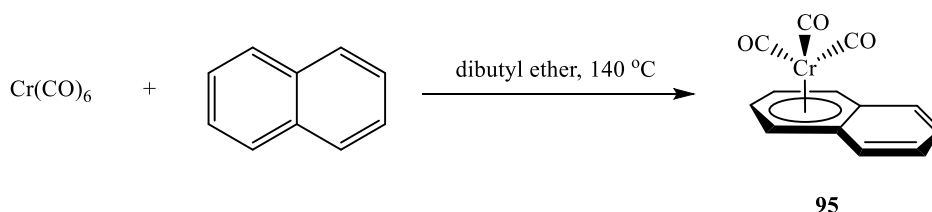


Figure 3-12: Scheme of the 2D-IR setup in this study.

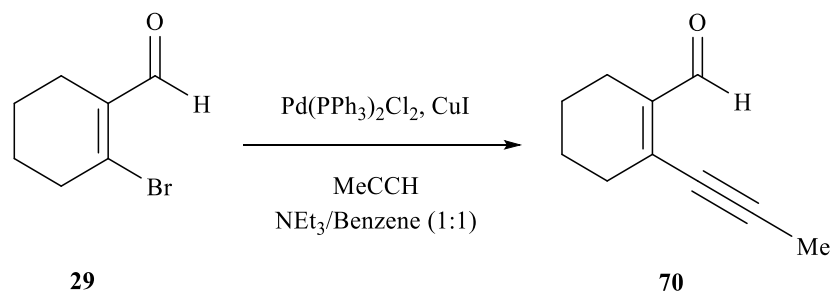
pulse (probe) is impinged on the sample, and the resulting macroscopic polarization emits an IR signal. The monochromator and MCT (Mercury-Cadmium-Telluride) IR (infrared) Detector (PhaseTech) experimentally Fourier transform the signal, thus generating a spectrum along the ω_3 axis. Numerical Fourier transform of the signal along the t_1 axis is required to obtain the spectrum along ω_1 . The resulting 2D-IR spectra are plotted against ω_1 and ω_3 . The t_2 time delay is controlled by a computerized delay stage and fixed at 500 fs. The whole data collection process is done by home-written LabVIEW programs. 2D-IR spectra were obtained at designated markers in the timelines to characterize the kinetics of the chemical reaction.

3. Synthesis and Characterization Data

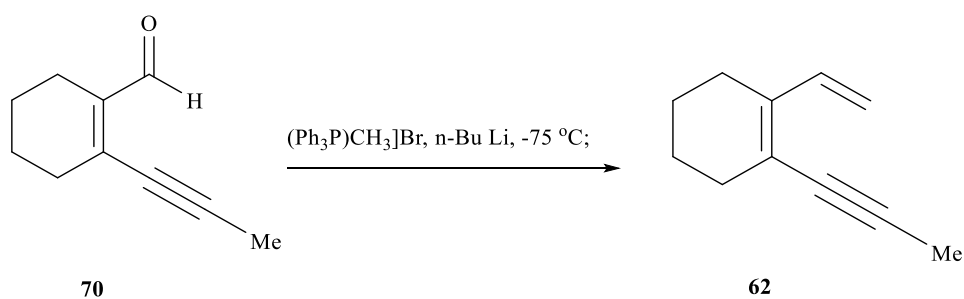
Cr(CO)₃(η^6 -naphthalene) (95): Cr(CO)₆ (3.0 g, 13.6 mmol) and naphthalene (3.0 g, 23.4 mmol) were added to a solution containing THF and dibutyl ether (1:10 v/v). Then the mixture was refluxed at 140 °C for 3 days under inert atmosphere and the solution turned red. The solvent was removed under rotavapor and the solute was placed on top of a flash silica gel column. Hexanes (300 mL) was used to collect the unreacted naphthalene and the product was collected with toluene. Removing volatiles yields **95** as a red solid (3.3 g, 12.5 mmol, 91.9 %).



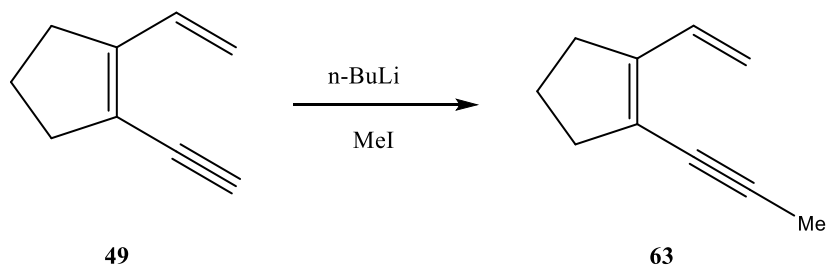
2-(prop-1-yn-1-yl)cyclohex-1-ene-1-carbaldehyde (70): To a propyne saturated triethylamine/benzene (1:1, 70 mL) solution of compound of **29** (6.0 g, 31.5 mmol), PdCl₂(PPh₃)₂ (0.8 g, 1.1 mmol) and CuI 0.3 g, 1.5 mmol) were added at 23 °C. The solution was stirred for 8 h and concentrated in vacuo. The mixture was then diluted with DCM and extracted with ether (1 x 100 mL). The organic substract was then washed with 1 M aq. HCl (2 x 100 mL) / H₂O (2 x 100 mL) / Brine (2 x 100 mL), dried over anhydrous MgSO₄ and concentrated under reduced pressure. The residue was purified through silica gel column (98:2, hexanes / EtOAc) to afford compound **70** as yellow oil (3.7 g, 25.6 mmol, 81 %). ¹H NMR δ : 1.58 – 1.67 (m, 4H, -CH₂), 2.04 (s, 3H, Me), 2.19 – 2.24 (m, 2H, -CH₂), 2.33 - 2.38 (m, 2H, -CH₂), 10.15 (s, 1H, CHO). The product exhibited identical spectroscopic properties to those reported in literature.



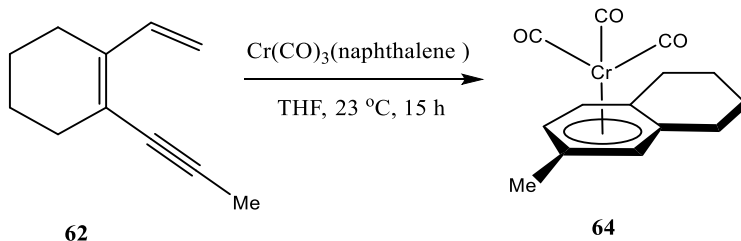
1-(prop-1-yn-1-yl)-2-vinylcyclohex-1-ene (62): N-Butyllithium (7.8 mL, 18.6 mmol, 2.4 M in hexanes) was added dropwise to a stirring mixture of methyltriphenylphosphonium bromide (7.3 g, 20.5 mmol) in anhydrous THF (70 mL) at $-78\text{ }^\circ\text{C}$. The solution then was stirred at $23\text{ }^\circ\text{C}$ for 1 h followed by the addition of **70** (2.0 g, 13 mmol). After stirring at $23\text{ }^\circ\text{C}$ for 1 h, the reaction was quenched with sat. aq. NH_4Cl (200 mL) and extracted with Et_2O (2 x 200 mL, 1 x 100 mL). The organic extract was washed with H_2O (3 x 200 mL) / brine (3 x 100 mL), dried over anhydrous MgSO_4 , concentrated and purified by flash column chromatography (hexanes) to afford **62** as colorless oil (1.6 g, 10.9 mmol, 84 %). The product exhibited identical spectroscopic properties to those reported in literature.



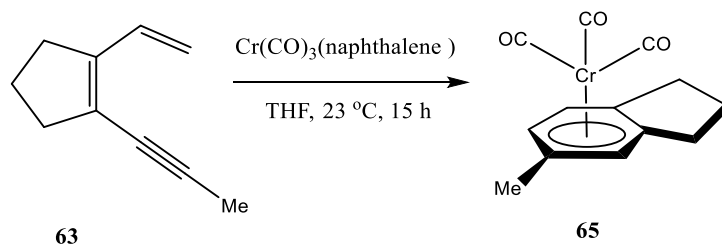
1-(prop-1-yn-1-yl)-2-vinylcyclopent-1-ene (63): N-Butyllithium (8.0 mL, 19.2 mmol, 2.4 M in hexanes) was added dropwise to a stirring mixture of **49** (2.0 g, 16 mmol) in anhydrous THF (50 mL) at -78 °C. The solution then was stirred at 23 °C for 1 h followed by the addition of MeI (3.0 g, 21 mol). After stirring at 23 °C for 1 h, the reaction was quenched with sat. aq. NH₄Cl (200 mL) and extracted with Et₂O (2 x 200 mL, 1 x 100 mL). The organic extract was washed with H₂O (3 x 200 mL) / brine (3 x 100 mL), dried over anhydrous MgSO₄, concentrated and purified by flash column chromatography (hexanes) to afford **63** as colorless oil (1.2 g, 10.9 mmol, 77 %). The product exhibited identical spectroscopic properties to those reported in literature.



Cr(CO)₃(η⁶-6-methyl-1,2,3,4-tetrahydronaphthalene) (64): **95** (50 mg, 0.18 mmol) was mixed with **62** (31 mg, 0.21 mmol) in 1 mL anhydrous THF under inert atmosphere. After 15 h, the mixture was concentrated and diluted with hexanes, purified through flash silica column (hexanes / EtOAc 10:1) to afford **64** (30 mg, 0.12 mmol, 55 %) as light yellow solid. **64**: ¹H NMR (CDCl₃, 400 MHz) δ: 1.60 – 1.78 (m, 4H, -CH₂), 2.14 (s, 3H, arene-Me), 2.54-2.64 (m, 4H, -CH₂), 5.08 (s, 1H, arene H), 5.32 (d, *J*_{HH} = 6.8 Hz, 2H, arene H). ¹³C NMR (CDCl₃, 500 MHz) δ: 20.4, 21.9, 22.1, 27.8, 28.1, 92.3, 94.1, 95.3, 106.7, 108.4, 110.6.

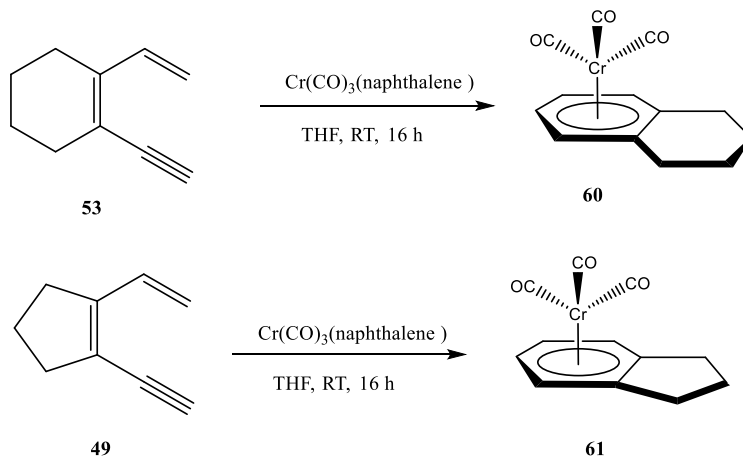


Cr(CO)₃(η^6 -5-methyl-2,3-dihydro-1H-indene)(65): **95** (1.0 g, 3.6 mmol) was mixed with **63** (5.1 g, 3.8 mmol) in 20 mL anhydrous THF under inert atmosphere. After 15 h, the mixture was concentrated and diluted with hexanes, purified through flash silica column (hexanes / EtOAc 10:1) to afford **65** (0.53 g, 1.98 mmol, 56 %) as light yellow solid. **65**: ¹H NMR (CDCl₃, 400 MHz) δ : 2.05 (m, 2H, -CH₂), 2.16 (s, 3H, arene-Me), 2.61 - 2.71 (m, 4H, -CH₂), 5.05 (d, $J_{\text{HH}} = 5.6$ Hz, 1H, arene H), 5.28 (s, 1H, arene H), 5.52 (d, $J_{\text{HH}} = 6.4$ Hz, 1H, arene H). ¹³C NMR (CDCl₃, 500 MHz) δ : 20.7, 23.8, 31.4, 31.6, 90.5, 91.7, 91.9, 108.6, 111.7, 115.9.

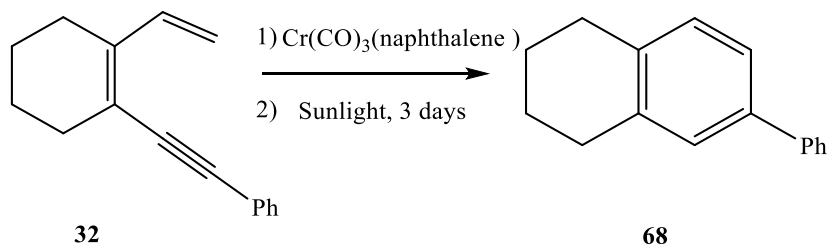


Cr(CO)₃(η^6 -1,2,3,4-tetrahydronaphthalene) (60) and Cr(CO)₃(η^6 -2,3-dihydro-1H-indene) (61): **95** (25.0 mg, 0.09 mmol) was mixed with **53** (14.7 mg, 0.12 mmol) in 20 mL anhydrous THF under inert atmosphere. After 15 h, the mixture was concentrated and diluted with hexanes, purified through flash silica column (hexanes / EtOAc 10:1) to afford **60** (12.6 mg, 0.45 mmol, 55 %) as light yellow solid. **61** was synthesized under the similar condition with a yield of 43 %. 9.8 mg. **60** ¹H NMR (CDCl₃, 400 MHz) δ : 5.47 (s, 4H, -arene H), **61** ¹H NMR (CDCl₃, 400

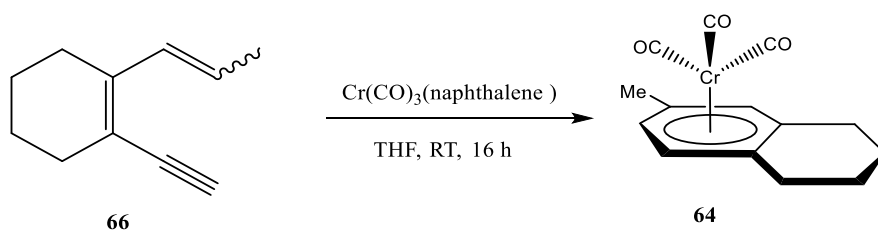
MHz) δ : 5.15 (s, 2H, -arene H), 6.58 (s, 2H, -arene H). Compounds **60** and **61** exhibited identical spectroscopic properties to those reported in literature.



6-phenyl-1,2,3,4-tetrahydronaphthalene (68): **95** (3.0 mg, 0.012 mmol) was mixed with **32** (3.1 mg, 0.014 mmol) in 20 mL anhydrous THF under inert atmosphere. After 15 h, the mixture was concentrated and diluted with hexanes, purified through flash silica column (hexanes / EtOAc 10:1) light yellow solid. Then the product was dissolved in acetone and exposed to sunlight for 72 hours, filtered and **68** was collected as color less oil (17 %). $^1\text{H NMR}$ (CDCl_3 , 400 MHz) δ : 1.74 (t, 4H, $-\text{CH}_2$), 2.70 (t, 4H, $-\text{CH}_2$), 7.11 – 7.75 (m, 8H, arene H). **68** exhibited identical spectroscopic properties to those reported in literature.



$\text{Cr}(\text{CO})_3(\eta^6\text{-6-methyl-1,2,3,4-tetrahydronaphthalene})(\mathbf{64})$: **66** (E:Z = 3: 1) (38.2 mg, 0.26 mmol) and **95** (46 mg, 0.17 mmol) were dissolved in 5 mL of anhydrous THF under inert atmosphere. After 15 h, the solution turned dark brown. The mixture was then concentrated and purified through a flash silica column. **64** was isolated as yellow solid (18.4 mg, 0.06 mmol, 27 %). (compound **64** has been characterized).



4. ^1H and ^{13}C NMR Spectroscopic Data.

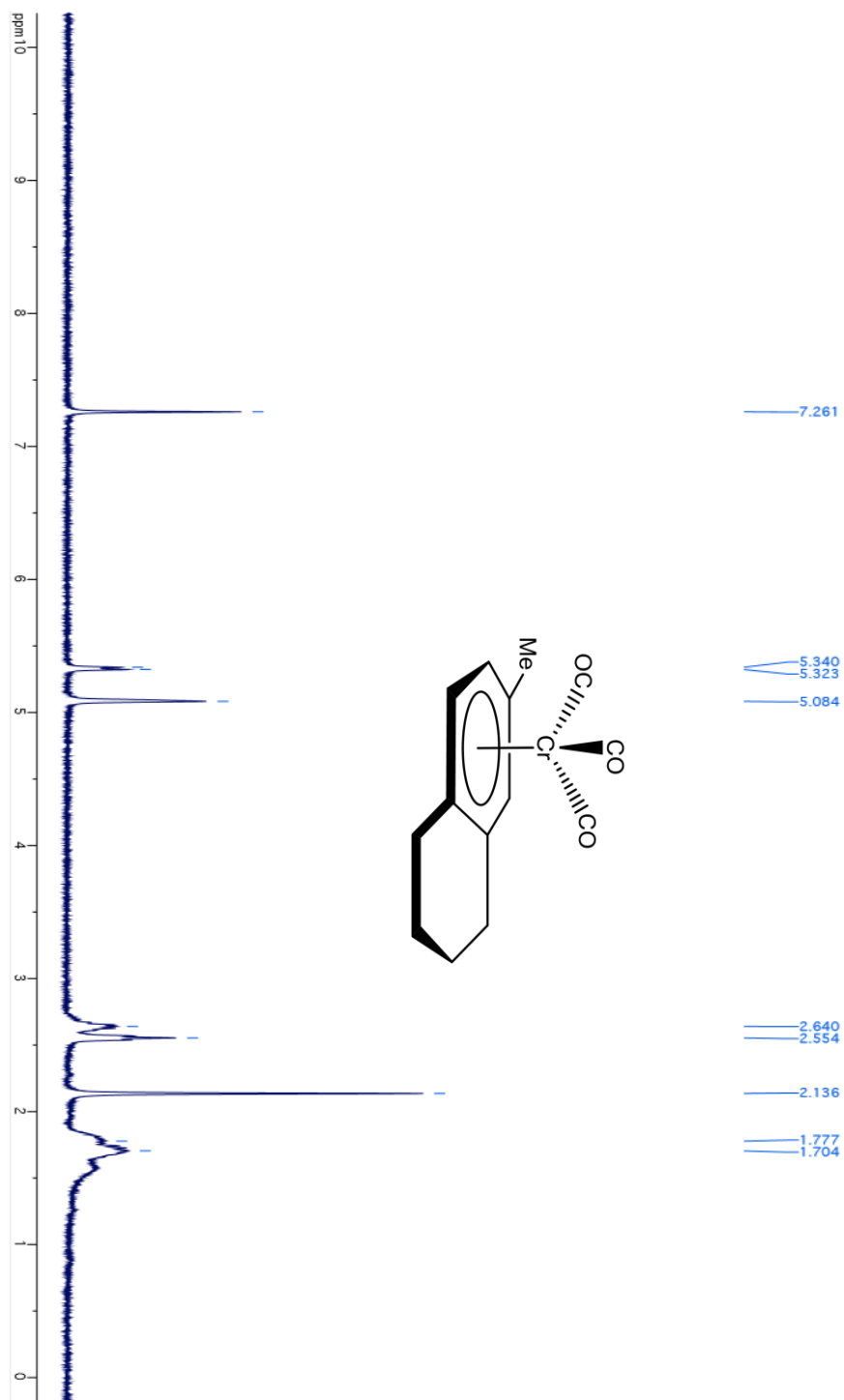


Figure 3-13: ^1H NMR spectrum of **64** (CDCl_3 , 400 MHz)

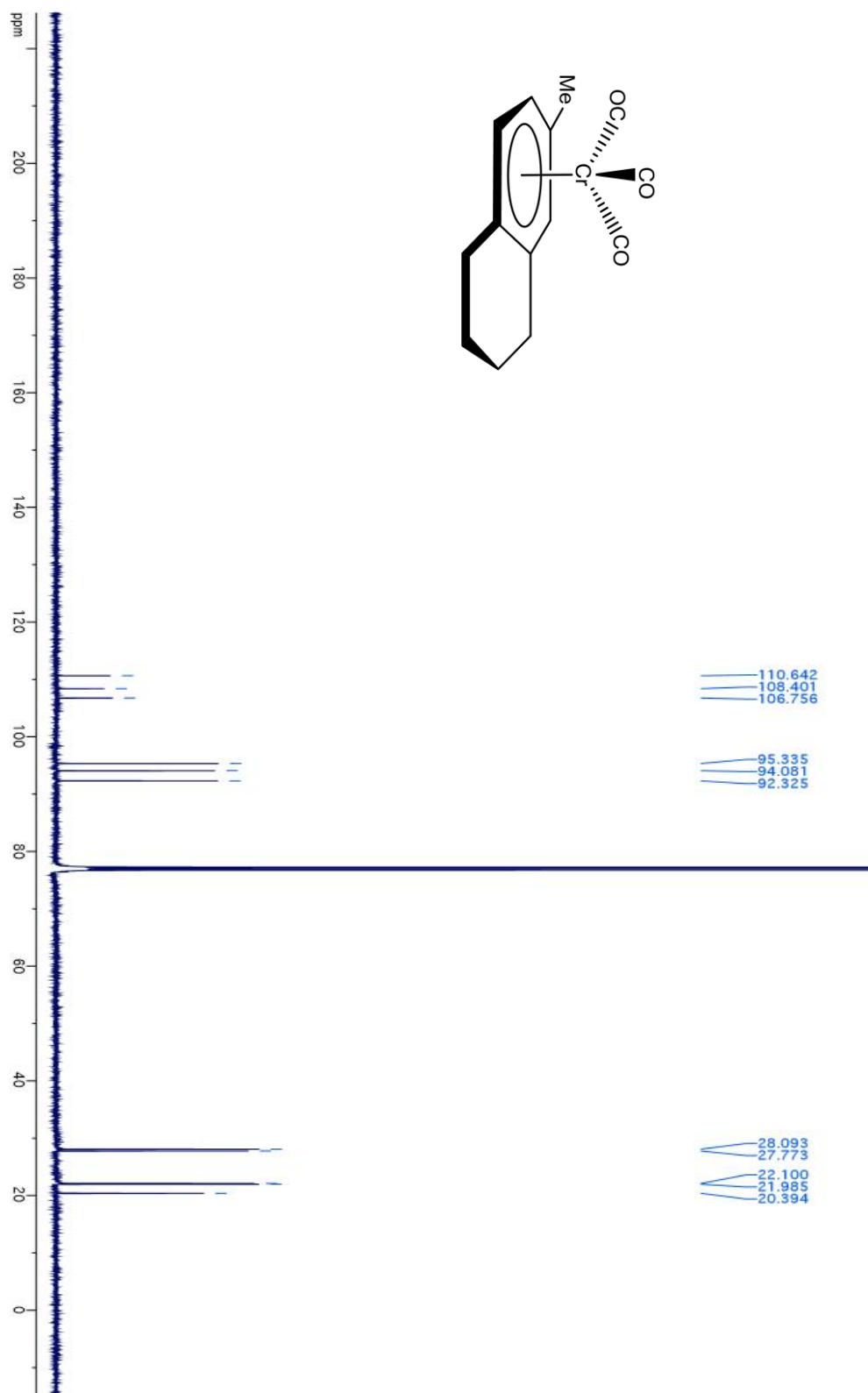


Figure 3-14: ^{13}C NMR spectrum of **64** (CDCl₃, 500 MHz)

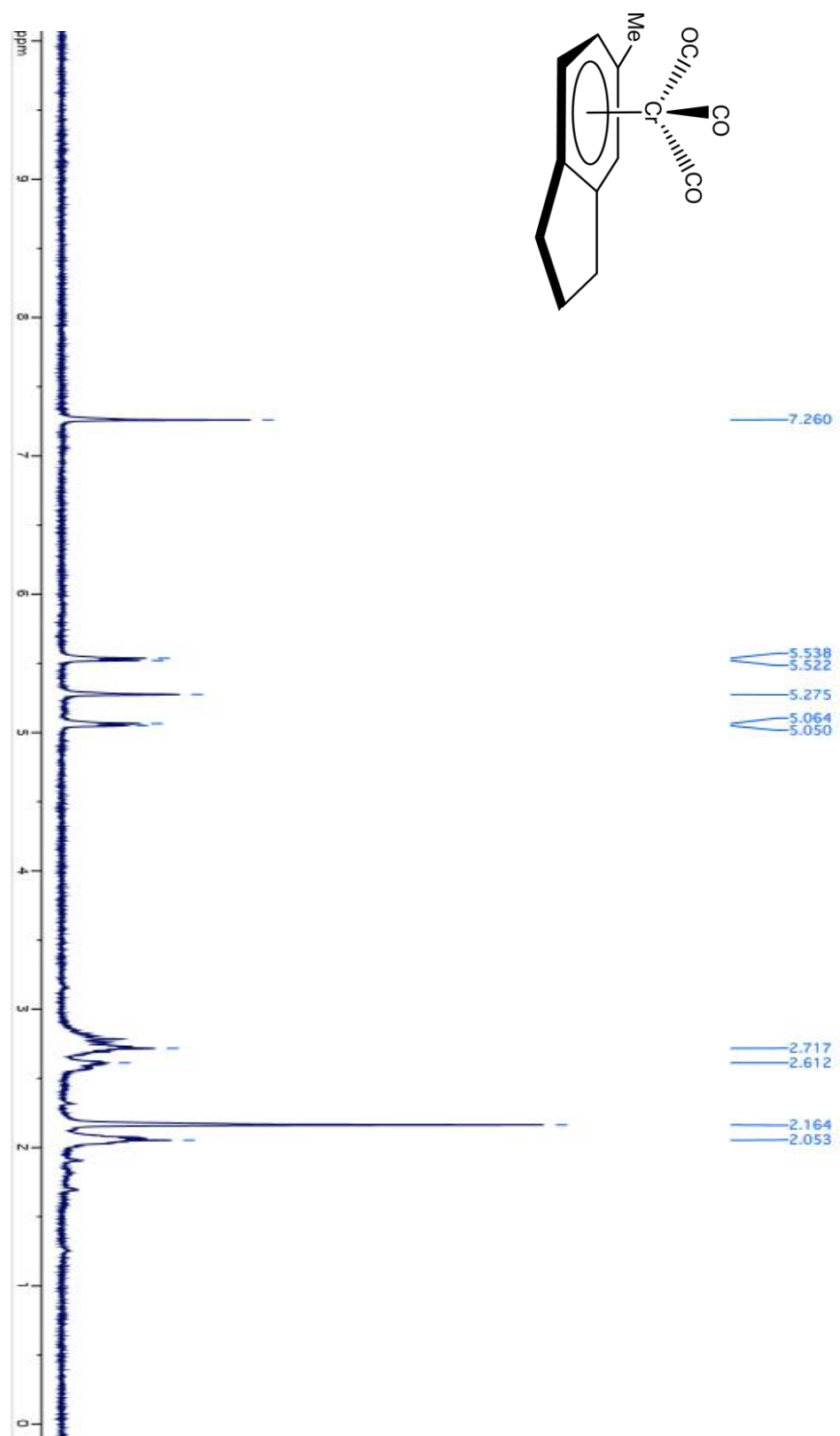


Figure 3-15: ^1H NMR spectrum of **65** (CDCl_3 , 400 MHz)

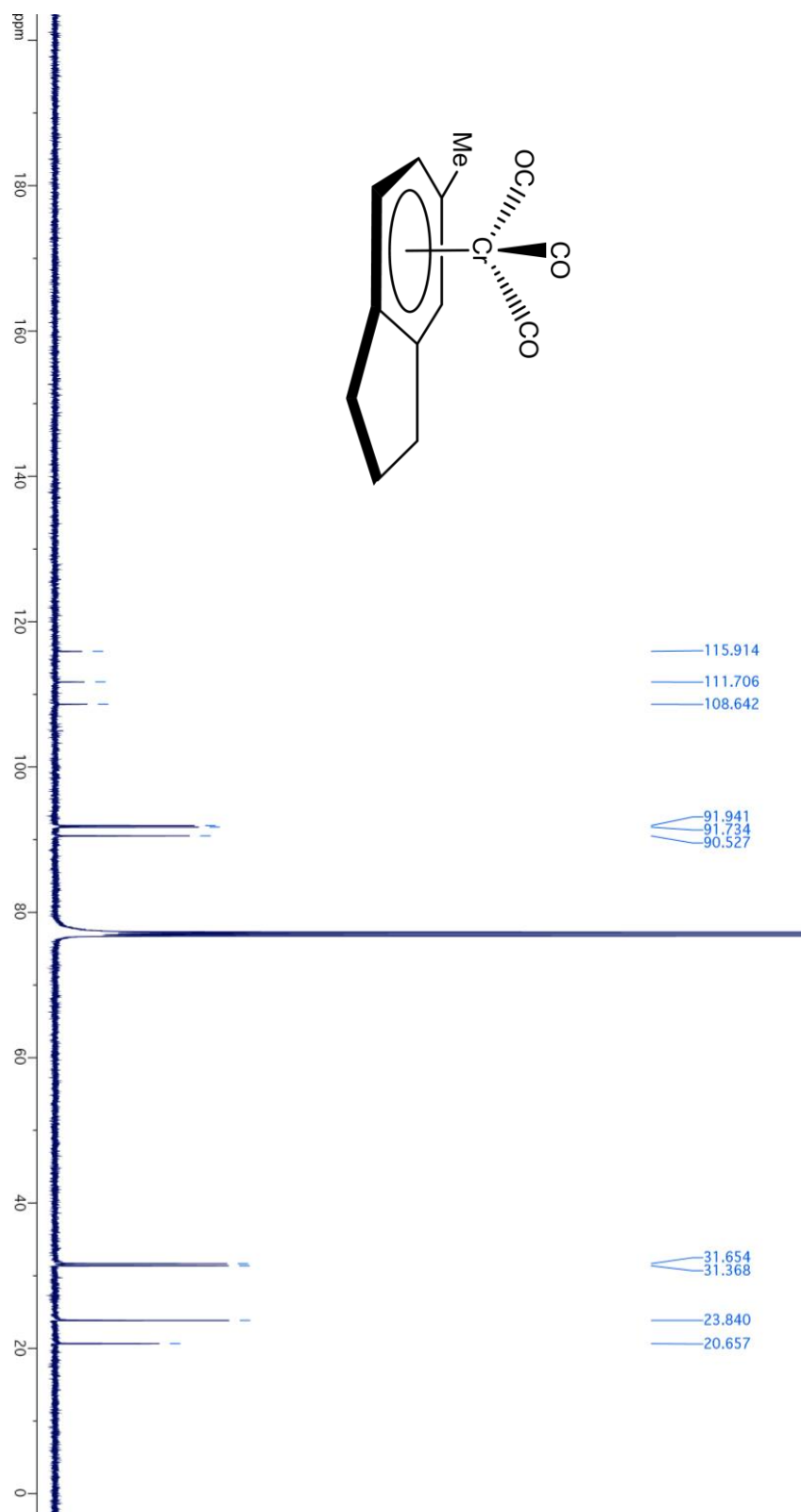


Figure 3-16: ^{13}C NMR spectrum of **65** (CDCl_3 , 500 MHz).

5. X-ray crystallographic summary and ORTEPS for characterized structures

General Experimental Procedures for X-ray Structure Determinations.

The single crystal X-ray diffraction studies were carried out on a Bruker Kappa APEX-II CCD diffractometer equipped with molybdenum $K\alpha$ radiation ($\lambda = 0.71073 \text{ \AA}$). The crystals were mounted on a Cryoloop with Paratone oil and data were collected under a nitrogen gas stream at 100 K using ω and φ scans. Data were integrated and scaled using the Bruker SAINT software program. Solution by direct methods (SHELXS) produced a complete phasing model consistent with the proposed structure. All non-hydrogen atoms were refined anisotropically by full-matrix least squares (SHELXL-97). All hydrogen atoms were placed using a riding model. Their positions were constrained relative to their parent atom using the appropriate HFIX command in SHELXL-97. Crystallographic data and structure refinement parameters are summarized in the supporting information.

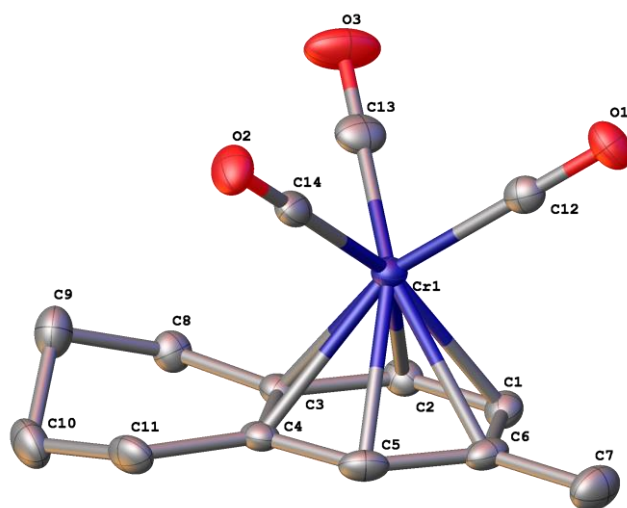


Figure 3-17: ORTEP of 64, SH22_a.

Table 3-3: Crystal data and structure refinement for **64**.

Identification code	SH22_a	
Empirical formula	C ₁₄ H ₁₄ CrO ₃	
Formula weight	282.25	
Temperature	100.0 K	
Wavelength	1.54178 Å	
Crystal system	Monoclinic	
Space group	P2 ₁ /c	
Unit cell dimensions	a = 6.8738(5) Å	a = 90°.
	b = 13.4086(10) Å	b = 103.588(2)°.
	c = 14.1563(10) Å	g = 90°.
Volume	1268.24 Å ³	
Z	4	
Density (calculated)	1.478 Mg/m ³	
Absorption coefficient	0.898 mm ⁻¹	
F(000)	584.0	
Crystal size	0.2 x 0.1 x 0.085 mm ³	
Theta range for data collection	4.242 to 54.2°.	
Index ranges	-8<=h<=8, -17<=k<=15, -17<=l<=18	
Reflections collected	1144	
Independent reflections	2794 [R(int) = 0.281]	
Completeness to theta = 67.500°	100.0 %	
Absorption correction	Semi-empirical from equivalents	
Max. and min. transmission	0.5210 and 0.4233	
Refinement method	Full-matrix least-squares on F ²	
Data / restraints / parameters	2794 / 0 / 164	
Goodness-of-fit on F ²	1.081	
Final R indices [I>2sigma(I)]	R1 = 0.0321, wR2 = 0.0766	
R indices (all data)	R1 = 0.0417, wR2 = 0.0814	
Extinction coefficient	n/a	
Largest diff. peak and hole	0.63 and -0.29 e.Å ⁻³	

Table 3-4: Fractional Atomic Coordinates ($\times 10^4$) and Equivalent Isotropic Displacement Parameters ($\text{\AA}^2 \times 10^3$) for **64**. U_{eq} is defined as 1/3 of the trace of the orthogonalized U_{IJ} tensor.

Atom	<i>x</i>	<i>y</i>	<i>z</i>	U(eq)
Cr1	4775.1(4)	4365.1(2)	6920.8(2)	15.53(10)
O1	7204(2)	3378.5(11)	5686.4(10)	26.7(3)
O2	7165(2)	3270.1(12)	8657.1(10)	28.8(3)
O3	7680(2)	6062.4(12)	7261.6(15)	43.7(5)
C12	6265(3)	3754.0(14)	6166.2(14)	19.1(4)
C13	6581(3)	5394.9(16)	7135.9(16)	25.7(4)
C7	1795(3)	2819.6(16)	5299.4(16)	29.8(5)
C2	2457(3)	5475.8(14)	6306.5(13)	18.4(4)
C5	1987(3)	3556.2(15)	6969.6(15)	20.9(4)
C1	2239(3)	4674.3(15)	5665.5(14)	20.4(4)
C6	2014(3)	3689.4(15)	5986.5(14)	20.5(4)
C3	2415(3)	5342.5(14)	7298.2(13)	17.4(4)
C4	2154(3)	4369.5(14)	7627.8(13)	17.6(4)
C14	6252(3)	3696.3(15)	7985.9(14)	19.9(4)
C8	2701(3)	6228.4(14)	7980.2(14)	20.1(4)
C11	2055(3)	4171.4(16)	8668.0(14)	24.2(4)
C10	1848(3)	5115.4(17)	9227.4(15)	29.0(5)
C9	3282(3)	5913.2(16)	9041.3(15)	26.9(5)

Table 3-5: Anisotropic Displacement Parameters ($\text{\AA}^2 \times 10^{-3}$) for **64**. The Anisotropic displacement factor exponent takes the form: $-2\pi^2[h^2a^2U_{11}+2hka^*b^*U_{12}+\dots]$.

Atom	U ₁₁	U ₂₂	U ₃₃	U ₂₃	U ₁₃	U ₁₂
Cr1	12.07(15)	17.42(16)	17.01(16)	-0.74(12)	3.23(11)	0.70(12)
O1	28.5(7)	27.6(8)	28.1(7)	0.9(6)	15.1(6)	3.7(6)
O2	26.8(7)	37.2(9)	20.4(7)	1.9(6)	2.0(6)	9.1(7)
O3	25.4(8)	26.6(9)	78.3(14)	-8.3(9)	10.3(8)	-8.1(7)
C12	18.4(9)	18.5(9)	19.9(9)	2.8(7)	3.2(7)	-0.8(7)
C13	17.9(9)	23.8(11)	35.6(12)	-2.7(9)	6.5(8)	5.2(8)
C7	25.4(10)	27.1(11)	34.6(12)	-11.0(9)	2.6(9)	-0.2(9)
C2	16.7(8)	19.0(10)	19.2(9)	4.2(7)	4.0(7)	3.4(7)
C5	13.5(8)	17.1(9)	31.6(11)	1.1(8)	3.9(8)	-2.6(7)
C1	16.3(9)	25.8(10)	18.0(9)	-0.9(8)	1.6(7)	2.9(8)
C6	12.6(8)	20.9(10)	26.0(10)	-5.0(8)	0.5(7)	0.3(7)
C3	12.8(8)	19.2(9)	20.5(9)	1.1(7)	4.7(7)	2.4(7)
C4	11.1(8)	22.5(10)	19.2(9)	1.7(8)	3.6(7)	-0.2(7)
C14	15.9(8)	23.8(10)	21.3(9)	-4.7(8)	6.9(7)	1.1(8)
C8	21.8(9)	17.9(9)	21.2(9)	-0.7(8)	6.4(7)	1.9(8)
C11	20.6(9)	30.4(11)	23.0(10)	8.0(8)	8.1(8)	-3.5(8)
C10	29.9(11)	39.1(13)	21.2(10)	4.2(9)	12.4(9)	3.7(10)
C9	33.4(11)	27.9(11)	19.5(10)	-2.7(8)	6.3(9)	2.4(9)

Table 3-6: Bond Lengths for **64**.

Ato	m	Length/Å	Ato	m	Length/Å
Cr1	C12	1.837(2)	C7	C6	1.503(3)
Cr1	C13	1.834(2)	C2	C1	1.392(3)
Cr1	C2	2.2049(18)	C2	C3	1.422(3)
Cr1	C5	2.2174(18)	C5	C6	1.408(3)
Cr1	C1	2.2163(19)	C5	C4	1.421(3)
Cr1	C6	2.2346(18)	C1	C6	1.417(3)
Cr1	C3	2.2455(18)	C3	C4	1.411(3)
Cr1	C4	2.2576(18)	C3	C8	1.514(3)
Cr1	C14	1.841(2)	C4	C11	1.513(3)
O1	C12	1.156(2)	C8	C9	1.521(3)
O2	C14	1.159(2)	C11	C10	1.517(3)
O3	C13	1.158(3)	C10	C9	1.519(3)

Table 3-7: Hydrogen Atom Coordinates ($\text{Å}\times 10^4$) and Isotropic Displacement Parameters ($\text{Å}^2\times 10^3$) for **64**.

Atom	x	y	z	U(eq)
H7A	2524.46	2957.33	4796.46	45
H7B	374.95	2715.67	4994.35	45
H7C	2342.31	2218.77	5659.54	45
H2	2638.45	6126.77	6076.44	22
H5	1852.73	2900.73	7201.05	25
H1	2242.07	4789.08	5003.61	25
H8A	1441.99	6617.09	7862.8	24
H8B	3757.08	6666.59	7839.61	24
H11A	3285.08	3815.65	9004.83	29
H11B	901.31	3729.75	8668.72	29
H10A	2134.83	4964.77	9931.2	35
H10B	456.29	5364.96	9025.28	35
H9A	4665.9	5649.45	9199.09	32
H9B	3234.42	6497.17	9463.17	32

VIII. Acknowledgments.

The material in Chapter 3, is currently under preparation for publication with the following authors: Steger, H.; Chen, L.; Baldrige, K.K.; Xiong, W.; O'Connor, J. M. The dissertation author was the primary investigator and author of this material.

IX. References.

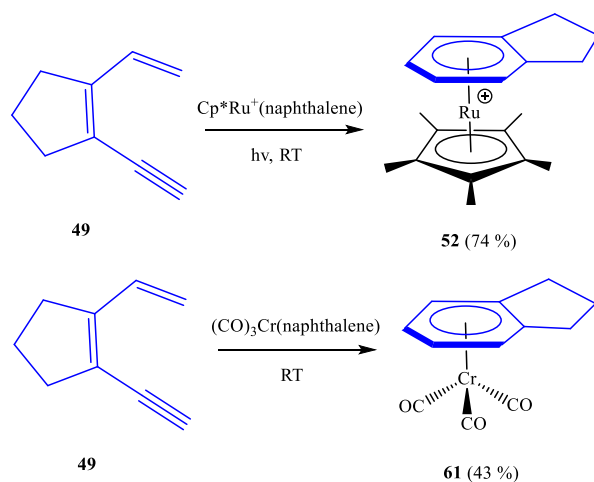
1. Hopf, H.; Musso, H. *Angew. Chem. Int. Ed. Engl.* **1969**, 8, 680. "Preparation of Benzene by Pyrolysis of cis-and trans-1,3-Hexadien-5-yne".
2. Bergman, R.G. *Acc. Chem. Res.* **1973**, 6, 25-31. "Reactive 1,4-Dehydroaromatics".
3. Mandal, S.; Basak. *Tetrahedron Letters.* **2009**, 50, 3641-3644. "Aza Hopf cyclization: synthesis and reactivity of cyclic azadienynes".
4. Wan, Y.; Zheng, X.; Ma, C. *Angew. Chem.* **2018**, 130, 5580-5584. "Conjugated Dienyne-Imides as Robust Precursors of 1-Azatrienes for 6 pi Electrocyclizations to Furo[2,3-b]dihydropyridine cores".
5. Capitani, J. F.; Gaffney, S. M.; Castaldo, L.; Mitra, A. *Current Topics in Medicinal Chemistry.* **2008**, 8, 470-486. "The Critical Distance of the Cycloaromatization Reactions of Ene-dienes".
6. O'Connor, J. M.; Friese, S. J.; Tichenor, M. *J. Am. Chem. Soc.* **2002**, 124, 3506-3507. "Ruthenium-Mediated Cycloaromatization of Acyclic Ene-dienes and Dienynes at Ambient Temperature".
7. O'Connor, J. M.; Friese, S. J.; Rodgers, B. L.; Rheingold, A. L.; Zakharov, L. *J. Am. Chem. Soc.* **2005**, 127, 9346-9347. "An η^6 -Dienyne Transition-Metal Complex".
8. Hitt, D. M.; O'Connor, J. M. *Chem. Rev.* **2011**, 111, 7904-7922. "Acceleration of Conjugated Dinyne Cycloaromatization".
9. Bland, W. J.; Davis, R.; Durrant, J. L. A. *J. Organometallic. Chem.* **1985**, 280, 95-103. "The mechanism of the addition of haloalkanes to alkenes in the presence of tricarbonyl- η^6 -naphthalenechromium(0), $[\text{Cr}(\text{CO})_3(\eta^6\text{-C}_{10}\text{H}_8)]$ ".

10. Blagg, J.; Davies, S. G.; Goodfellow, C. L.; Sutton, K. H. *J. Chem. Soc. Perkin Trans.* **1990**, 1, 1133-1144. "Regioselective nucleophilic additions to tricarbonyl(η^6 -arene)chromium(0) complexes: electronic *versus* chelation control".
11. Blagg, J.; Davies, S. G.; Goodfellow, C. L.; Sutton, H. H. *J. Chem. Soc. Perkin Trans.* **1987**, 1805-1811. "The Diastereoselective Functionalisation of Arene Tricarbonylchromium Complexes Containing a Benzylic Heteroatom Substituent".
12. Ylijoki, K. E. O.; Lavy, S.; Fretzen, A.; Kundig, P. E.; Berclaz, T.; Bernardinelli, G.; Besnard, C. *Organometallics*. **2012**, 31, 5396-5404. "A Synthetic and Mechanistic Investigation of the Chromium Tricarbonyl-Mediated Masamune–Bergman Cyclization. Direct Observation of a Ground-State Triplet *p*-Benzyne Biradical".
13. Qin, P.; Cope, S.; Steger, H.; Veccharelli, K. M.; Holland, R. L.; Hitt, D. M.; Moore, C. E.; Baldrige, K. K.; O'Connor, J. M. *Organometallic*. **2017**, 36, 3967-3973. "Photoactivated Transition-Metal Triggers for Ambient Temperature Ene-yne and Dienyne Cyclization: Ruthenium- η^6 -Naphthalene Complexes".
14. Wax, M. J.; Bergman, R. G. *J. Am. Chem. Soc.* **1981**, 103, 7028-7030. "Direct Evidence for Solvent Coordination in Migratory CO Insertion".
15. Ramachandran, B. R.; Halpern, A. M. *J. Chem. Ed.* **1997**, 74, 975-978. "A Novel Experiment in Chemical Kinetics: The A \rightarrow B \rightarrow C Reaction System".

**Chapter 4 . Selective Terminal C-C Double Bond Reduction of
Conjugated 1,3-Dien-5-yne in $\text{Cr}(\text{CO})_3(\text{CH}_3\text{CN})_3$ -Acetone Solution
Under Moderate Conditions**

I. Introduction.

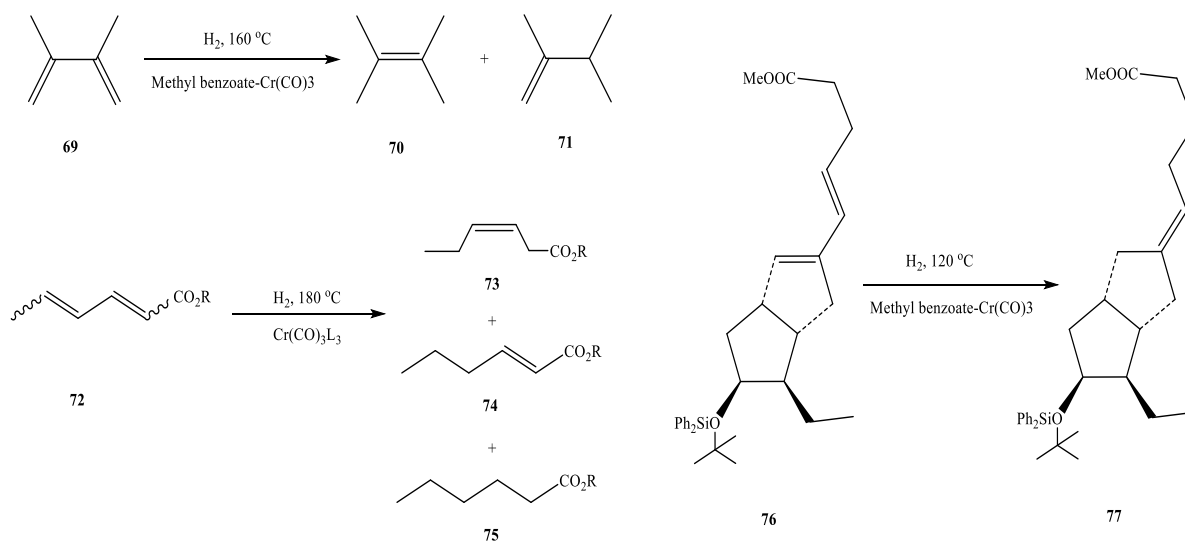
Thermal cycloaromatization of conjugated dienyne often requires high temperature,^{1, 2} which may induce thermal decomposition or polymerization of substrates.³ To overcome this issue, the O'Connor lab has been focusing on improving the dienyne aromatization reaction conditions with a series of metal-L₃ complexes.⁴⁻⁶ Our previous work has demonstrated success in establishing a Cp*Ru⁺(η^6 -naphthalene) cation system⁷ that mediates dienyne aromatization at ambient temperature with the addition of a photon. During the course of investigating the



Scheme 4-1: Dienyne cyclization triggered with Ru and Cr complex demonstrated in O'Connor lab's previous work.

possibility of using a low-cost earth-abundant metal, such as chromium, we noticed that dienyne aromatization can also be achieved with Cr(CO)₃(η^6 -naphthalene)⁸ (Scheme 4-1). However, to our great surprise, while examining another chromium complex candidate, Cr(NCMe)₃(CO)₃ (**96**), a selective terminal alkene reduction occurred. Chromium as an earth-abundant metal displays, in several of its organometallic complexes, the ability to trigger alkene hydrogenation under certain conditions. The documented methods of achieving this occur under high temperature and pressure, along with a constant stream of hydrogen gas (Scheme 4-2)⁹⁻¹¹. We have demonstrated in our lab,

that **96** promotes selective alkene reduction. We report this unprecedented reduction of the alkene moiety in the presence of a competitive alkyne within a diene substrate. In comparison to traditional hydrogenation reactions, our mechanistic study indicates that, surprisingly, acetone as

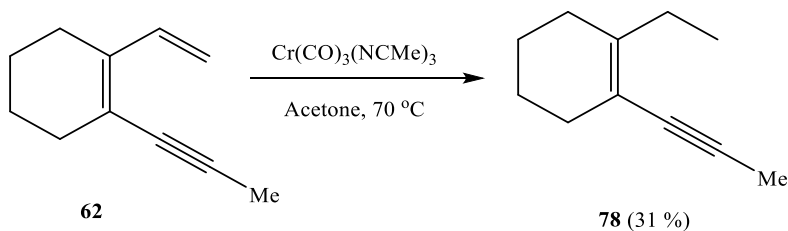


Scheme 4-2: Alkene reduction facilitated by Cr complex in previously reported work.

a solvent, provides the main source of hydrogen via an aldol condensation, due to water being generated in-situ. The study of this reaction is still in its nascence, and its highly complex mechanism is not fully disentangled. Although the fact that the product yield is not yet competitive in comparison to other catalysts, yet we consider this discovery to have merit given its potential to contribute to the current synthetic methodology of unsaturated selective alkene reductions.

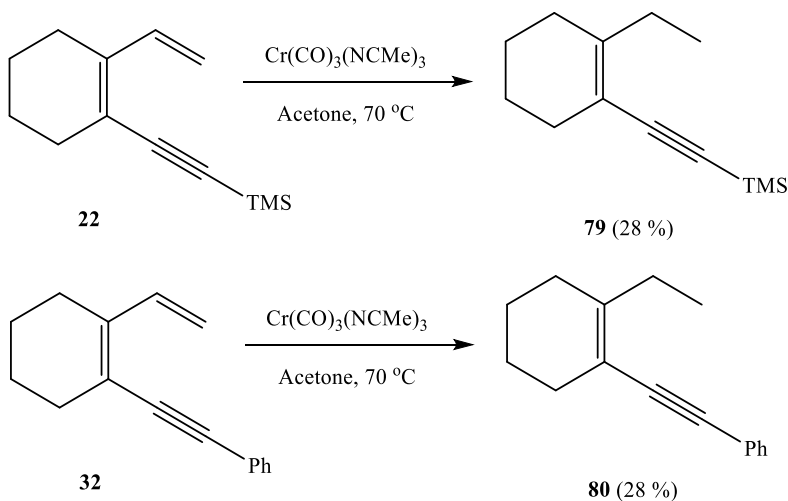
II. Hydrogenation of 1,3-Dien-5-yne.

We initiated this study by treating dienyne **62** as the parent substrate with **96** at a mole ratio of 1:2 in anhydrous acetone under an inert atmosphere. After observing no reaction at ambient temperature, the reaction temperature was increased to 70 °C. After 16 hours, we obtained **78** in 31 % yield (Scheme 4-3). We then extended the reaction time from 16 hours to 7 days expecting a higher yield. However, no increase in yield was observed except for a side thermal decomposition of the dienyne substrate which led to a significant decrease in yield from 31 % to 18 %. To further explore the generality of the reaction, dienyne **22** and **32** substrates, along with a variety of alkyne



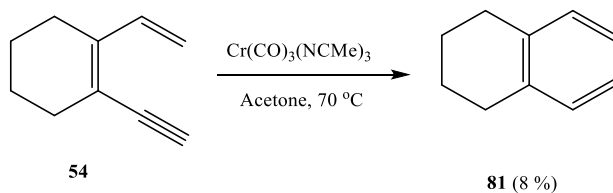
Scheme 4-3: **96** facilitates alkene hydrogenation of **62**.

substitutes were synthesized in a similar manner to **62**. As predicted, hydrogenated products **79** and **80**, were both observed at around 20 % to 30 % yield under similar reaction conditions



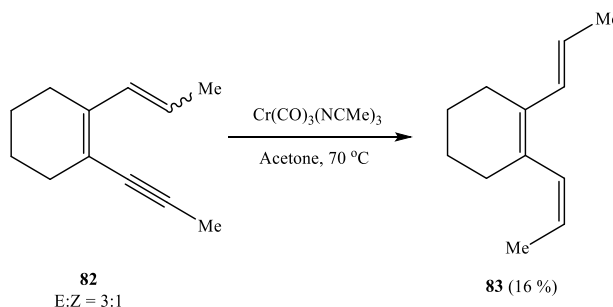
Scheme 4-4: **96** facilitates alkene hydrogenation of **22** and **32**.

(Scheme 4-4). Unfortunately, allowing the reaction to proceed longer did not increase the yield. The addition of more than 1 mole equivalence of dienyne **22** did not result in a higher yield of the



Scheme 4-5: **96** facilitates alkene hydrogenation of **54**.

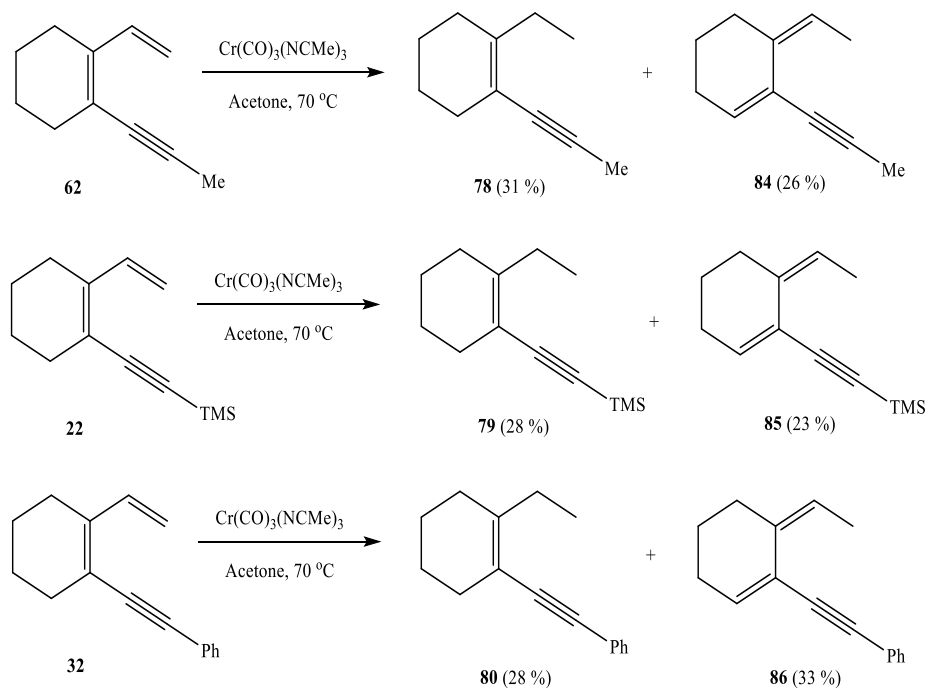
product, and from a prep scale reaction, excess unreacted **22** was either decomposed or recovered via chromatography, which supported the assumption that this reaction was not catalytic. Presumably, the selective hydrogenation was a result of the steric hindrance. To clarify this, dienyne **54** and **82** were treated with **96** under similar conditions, **54** undergoes rapid thermal decomposition at 70°C ., but at room temperature, trace yield (8 %) of the alkyne reduced product **81** was obtained (Scheme 4-5), indicating that when both alkene and alkyne were substituted in the same fashion, alkyne was hydrogenated prior to alkene, further confirming that this selectivity was directed by the steric bulkiness. Product **83** exhibits only EZ stereochemistry and it is not clear why only one stereoisomer was formed. Results confirmed that only less hindered alkenes were reduced and in case of substituted compounds **54** and **82**, more reactive alkynes were reduced to alkenes (Scheme 4-6). The reaction of each dienyne substrate including **54** and **82** with 2, 3 and 5



Scheme 4-6: **96** facilitates alkene hydrogenation of **82**.

mole equivalents of **96** were also performed. GC-MS spectrum clearly showed that, only a mono-hydrogenated product was formed with no evidence of di-hydrogenated or tri-hydrogenated products in all cases.

Studies focusing solely on the chromium complex were also carried out and while the reaction Schlenk flask and J. Young NMR tubes were tested for air seal, notable amounts of green precipitate formed throughout the course of the reaction, suspected to be Cr_2O_3 according to a previous reported **96** study.¹⁴⁻¹⁶ It was also surprising to us that $\text{Cr}(\text{CO})_6$ was formed at the same time, confirmed by ^{13}C NMR and UV-vis spectroscopy. Therefore, the reaction required mole equivalent amounts of **96** to substrate. No reactivity of CrCO_6 and Cr_2O_3 compounds for the reduction of **62** were confirmed by running the reaction under similar conditions. However, isolation of compounds from the reaction of the **62**, **22** and **32** with less than 2 mole equivalents



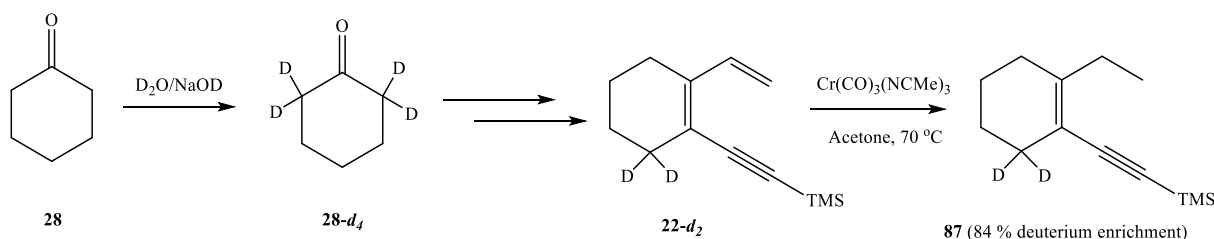
Scheme 4-7: **96** facilitates alkene hydrogenation and tautomerization of dienynes.

of **96** showed a mixture of reduced product and an isomer **84**, **85** and **86** in an almost 1:1 ratio, respectively (Scheme 4-7).

III. Investigation in hydrogenation sources.

We proposed that the hydrogenations might be from three resources: First, the trace amount of H₂ or H₂O in the solution; second, from another dienyne molecule and the third, from the solvent. We firstly ran the reaction under H₂ atmosphere but did not result a significant increase in yield. The addition of 0.1 mole equivalence of water to the reaction mixture containing dienyne and **96** rapidly decomposed to give a green precipitate.

Compound **28-d₄** was obtained by stirring **28** in D₂O contained NaOD. Substrate **22-d₂** with an 84 % deuterium enrichment was then synthesized by following the procedure mentioned in previous chapter. The ¹H NMR of the hydrogenation product did not exhibit a deuterium enrichment on the alkane (Scheme 4-8).

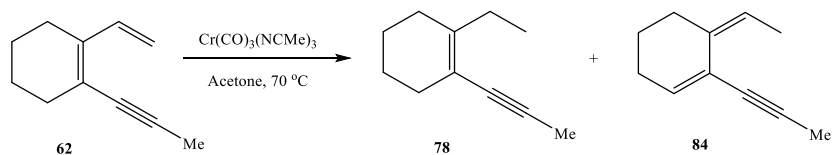


Scheme 4-8: Synthesis of **22-d₂** and **87**.

Thus, we believe water must be generated in situ to serve as the hydrogen source. To confirm this, an isotope labelling experiment was carried out in acetone-*d*₆. An ¹H NMR spectrum of isolated hydrogenation product **79-d₂** and **85-d** exhibited an 86 % and 80 % deuterium enrichment in the reduced terminal alkene (Scheme 4-9).

were detected from the reaction in benzophenone as benzophenone was not capable of undergoing self-condensation. This result provides strong support for our proposed mechanism.

Table 4-1: Product yield of **78** obtained by treating **84** and **96** with a variety of solvent. Reaction time: 16 h; Reaction temperature: 70 °C.



Solvent	Yield 78 (%)	Yield 84 (%)
2-butanone	16	18
Acetophenone	12	13
Benzophenone	0	0
CHCl ₃	0	0
DCM	1	2
DMF	3	5
NCMe	2	0
DMSO	0	0
Ethyl acetate	3	5
NO ₂ Me	0	0

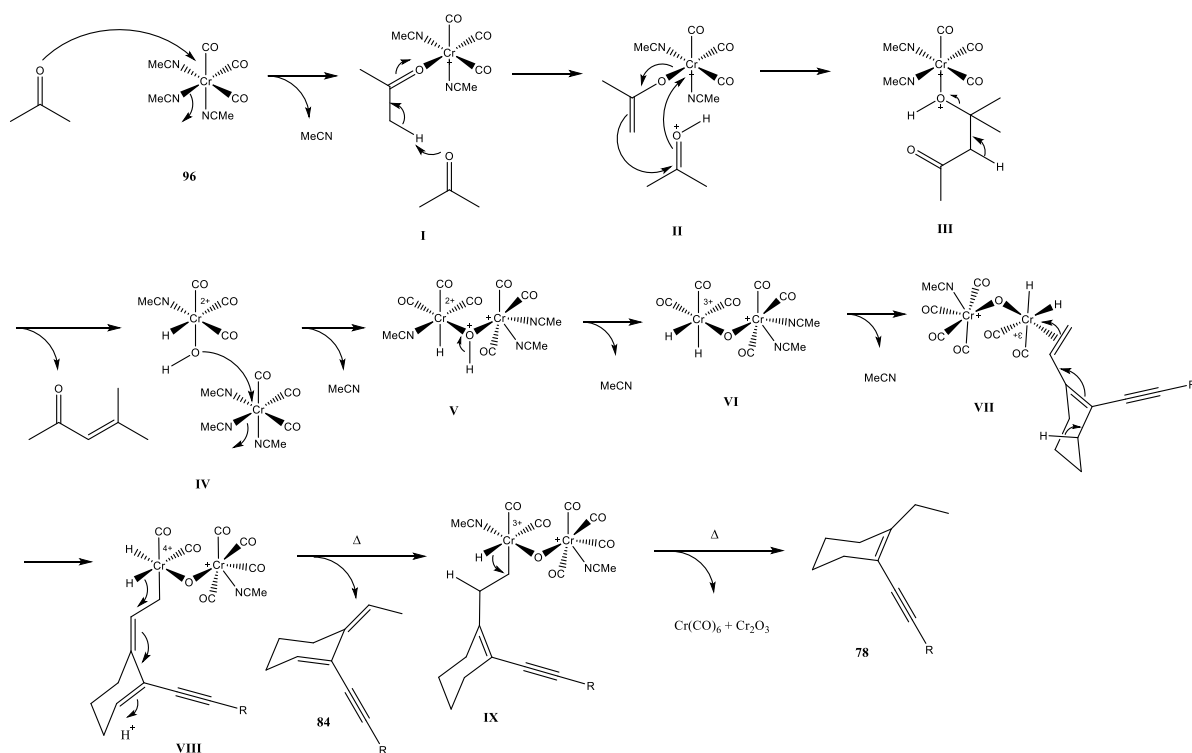
IV. Study on chromium and solvent.

Studies focusing solely on the chromium complex were also carried out. The reaction Schlenk flask and J. Young NMR tubes were tested for air seal, notable amounts of green precipitate formed throughout the course of the reaction, suspected to be Cr_2O_3 according to a previous reported $\text{Cr}(\text{NCMe})_3(\text{CO})_3$ study¹⁴⁻¹⁶. Therefore, the reaction required mole equivalent amounts of **96** to substrate. Collected green precipitate exhibited similar physical properties and IR absorbance to that previously reported for Cr_2O_3 . We performed the reaction in a customized Schlenk flask equipped with a quartz glass cuvette in order to monitor the oxidation state of chromium. **96** prior to the reaction showed a UV absorbance at 385 nm. This absorbance gradually decreased until disappeared during 16 h of reaction while the solution turned from yellow to green with the formation of green precipitate. We confirmed that chromium was oxidized within the course of the reaction.

Since our hypothesis suggests that chromium complex mediates the acetone-self condensation reaction, it was important to prove the formation of the condensed by product. A control reaction with only **96** in acetone was performed at 70 °C. The product mixture was purified via prep plate. We were pleased to observe the formation of the 4-methylpent-3-en-2-one via ¹H NMR. The above results gave us an encouraging direction in revealing its mechanism.

V. Mechanism.

Summarizing the evidence obtained from previous studies, we proposed the formation of product **78** through a highly speculative mechanism (Scheme 4-10). As shown, **96**, as the Lewis acid, undergoes a rapid ligand exchange with acetone in solution. The resulting Cr-Acetone intermediate continues to form the aldol condensed product with water generated in-situ. It is possible that a short-lived H-Cr-OH intermediate **IV** was then formed before conversion to the Cr-O-Cr dimer complex **V**. With the presence of dienyne substrate, less sterically hindered alkenes coordinate to the chromium core via ligand exchange further led to an oxidative insertion of Cr between the alkene carbon and the vinyl hydrogen **VIII**. Reductive elimination then occurred to give the tautomer product **84**. More than one equivalence of Cr will accelerate the formation of

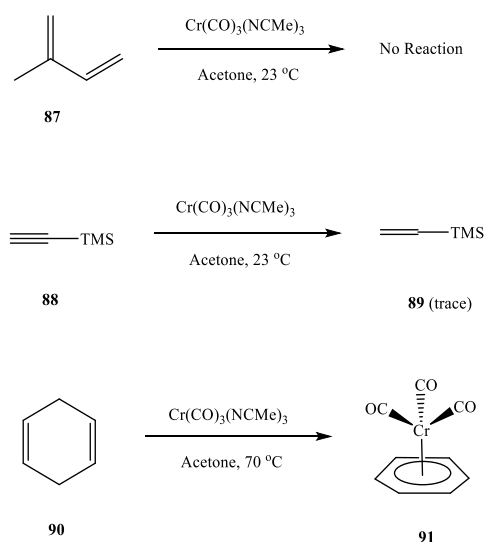


Scheme 4-10: Speculative mechanism of the hydrogenation reaction of dienyne.

the dimer intermediate causing a secondary elimination to give the hydrogenated product. The resulting Cr dimer undergoes a highly complex mechanism to yield $\text{Cr}(\text{CO})_6$ and Cr_2O_3 . In this mechanism, **84** was identified as the precursor to the hydrogenated product **78**. Finally, isolated **84** was examined by mixing with 1.0 eq of **96** in acetone under the same conditions for 16 h. GC-MS did not exhibit any notable increase in product formation. This result suggests that the intermediate that is formed between diyne and the Cr-dimer complex (**VII**) is crucial for any further alkene hydrogenation.

VI. Investigation on various alkene substrates.

We further extended the scope to other reactive alkene complexes. The examination of **96** with isoprene was unsuccessful at both ambient temperature and at 70 °C. When treated with



Scheme 4-11: Attempted reactions of treating **96** with other organic compounds with unsaturated carbon bonds.

1,4-CHD, the only cyclization which occurred gave a Cr(η^6 -benzene) product. However, a trace amount of reduced product was detected by GC-MS when reacting **96** with trimethylsilylstyrene at ambient temperature only (Scheme 4-11). We also investigated the performance of other metal complexes such as Mo and W by preparing Mo(NCMe)₃(CO)₃ and W(NCMe)₃(CO)₃ in the same fashion. Unfortunately no desired products were obtained in the two cases of Mo(NCMe)₃(CO)₃ and W(NCMe)₃(CO)₃.

VII. Conclusion.

In conclusion, a selective hydrogenation of an alkene from a conjugated dienyne was facilitated by Cr(NCMe)₃(CO)₃ under moderate conditions to form a reduced product with its intermediate tautomer uncovered. More than one mole equivalence of **96** only results in a single pi bond hydrogenation and steric hindrance seems to be the major determining factor in determining selectivity and alkyne can be protected by a bulky substituent. We found and have confirmed that traditional and expected sources of hydrogen were not those that allowed the reaction, but rather that a ketone solvent, which must have an α -hydrogens, was the source of the hydrogen. This was unexpected, novel and perhaps unprecedented. Via condensation, trace amounts of water were generated, followed by the formation of a Cr-O-Cr dihydride intermediate that further led to isomerization and hydrogenation of the alkene. On the other hand, oxidized Cr was a key byproduct as a result of consumed **96** through a complex mechanism. Although current knowledge of the mechanism of this newly discovered reaction is still in its nascence, further investigation will be carried out for an in depth understanding.

VIII. Experimental.

1. General Information.

All manipulations were carried out under an atmosphere of dry dinitrogen using standard Schlenk or glove box techniques. NMR scale reactions were performed under a dry dinitrogen atmosphere in 5 mm J. Young NMR tubes equipped with a Teflon needle-valve adapter using freshly degassed solvent. Chloroform-*d* was dried and stored over calcium hydride under vacuum. Acetone-*d*₆ was dried under activated molecule sieves and then distilled. Flash column chromatographic purifications were performed using silica gel (60 Å, particle size 43-60 µm, 230-400 mesh, EMD Chemicals).

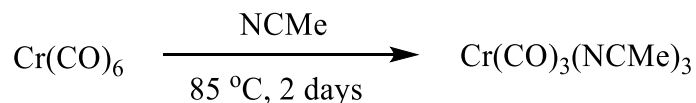
2. Instrumentation and analysis methods.

NMR spectra were recorded on Varian Mercury 400 (¹H, 400 MHz; ¹³C, 75.5 MHz) and Varian VX 500 (¹H, 500 MHz; ¹³C, 125 MHz). ¹H and ¹³C {¹H} NMR chemical shifts (δ) are reported in parts per million (ppm) relative to TMS (¹H and ¹³C, δ = 0.00 ppm), with reference to the residual proton or carbon resonance for CDCl₃ (¹H, δ = 7.26 ppm; ¹³C, δ = 77.16 ppm). IR spectra of isolated compounds were recorded on a Thermo-Nicolet iS10 FTIR spectrometer at ambient temperature. Gas chromatography and High-resolution spectra were recorded at the University of California, San Diego mass spectrometry facility on an Agilent 6230 accurate-mass TOFMS instrument by using the positive ion mode. GC analysis: General sample preparation for GC-MS analysis: Substrate **22** (2.5 mg, 0.012 mmol) were placed in an oven dried J. Young NMR tube. Under inert atmosphere, **96** (9.7 mg, 0.037 mmol) dissolved in 1.0 mL of anhydrous solvent

(acetone) was transferred into the tube. The tube was placed in an oil bath for 16 h at 70 °C. The reaction mixture was then filtered, and 0.25 mL of the filtrate was mixed with 0.25 mL of 18.7 mM benzophenone solution in acetone. The sample was then submitted for GC-MS analysis. Sample preparation for UV-vis spectrum: 0.5 mg of **96** was dissolved in 1.5 mL of anhydrous acetone in a custom made quartz cuvette with a Teflon adapter in dry box. Acetone was collected first as a blank followed by sample spectrum collection.

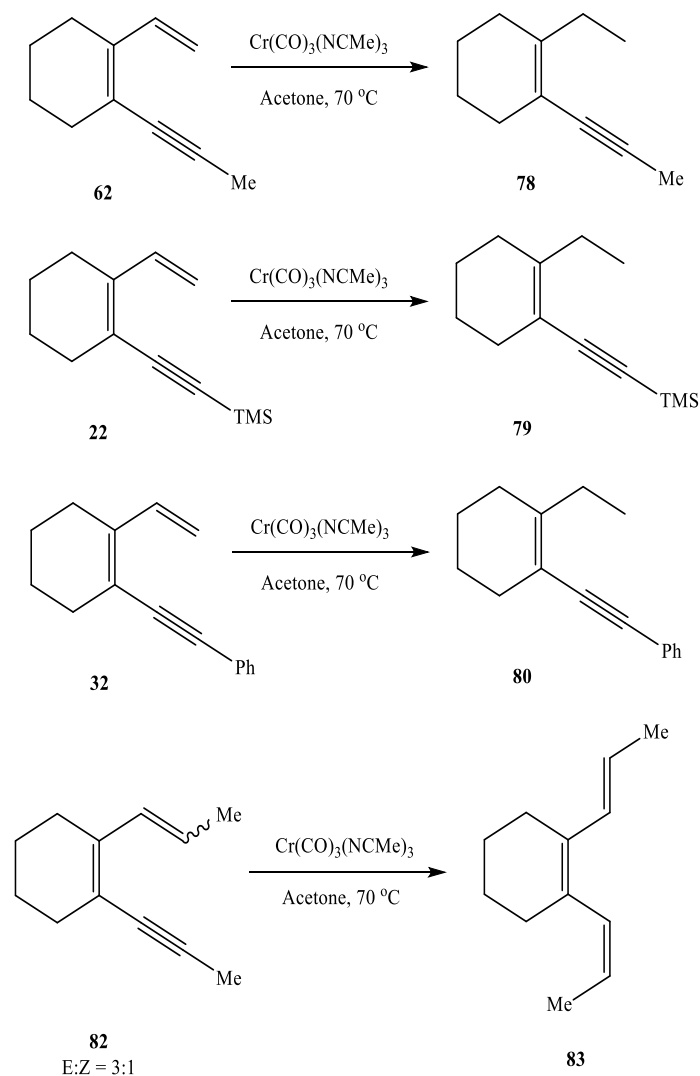
3. Synthesis and Characterization.

Cr(CO)₃(NCMe)₃(96). Cr(CO)₆ (2 g, 9.1 mmol) was added to 30 mL of anhydrous MeCN. Vacuum was then pulled and refilled the set up with N₂. After repeating the process 10 times the mixture was refluxed under inert atmosphere for 2 days and the solution gradually turned yellow. After cooling to ambient temperature, the reaction mixture was filtered in a dry box, then concentrated and dried under a Schlenk line. Cr(CO)₃(NCMe)₃ was collected as light yellow solids (2.07 g, 87.9 %).



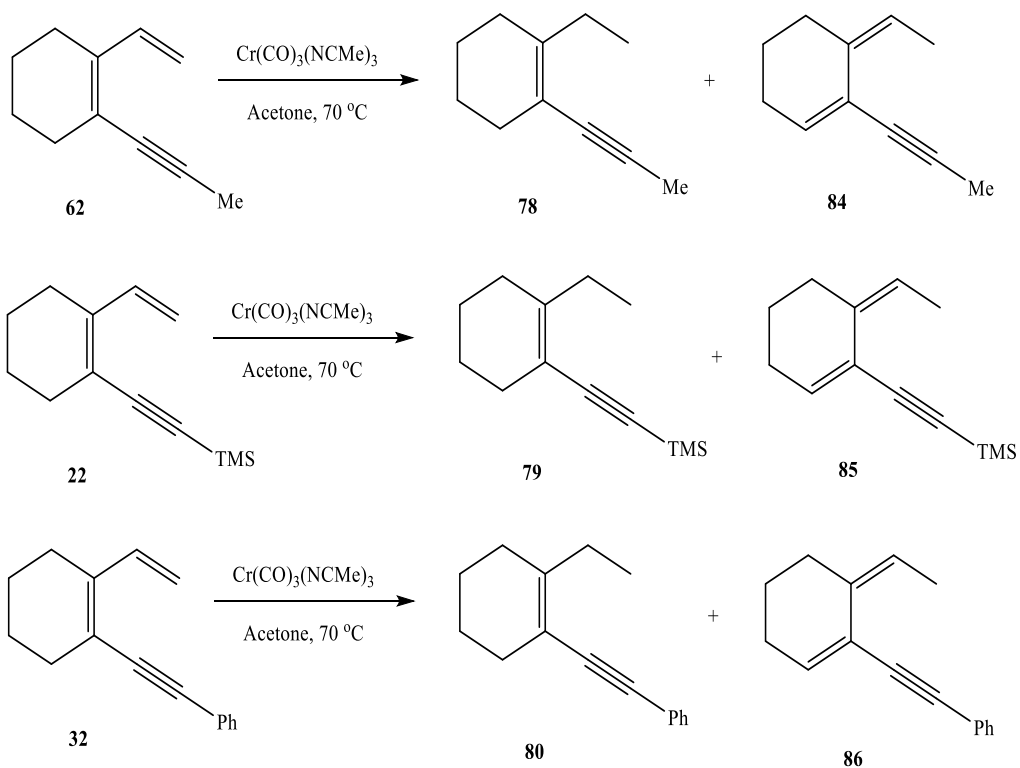
General procedure for the synthesis of **1-(prop-1-yn-1-yl)-2-vinylcyclohex-1-ene (78)**, **trimethyl((2-vinylcyclohex-1-en-1-yl)ethynyl)silane (79)**, **((2-vinylcyclohex-1-en-1-yl)ethynyl)benzene (80)** and **1-((E)-prop-1-en-1-yl)-2-((Z)-prop-1-en-1-yl)cyclohex-1-ene (83)**.

96 (2.8 g, 11.0 mmol) was added to a side-armed shrink tube containing **22** (1.0 g, 4.9 mmol) dissolved in 35 mL anhydrous acetone under inert atmosphere. The shrink tube was placed in an oil bath for 16 h at 70 °C. The mixture was then exposed to ambient air and sunlight for 1 h, diluted with hexanes, filtered, concentrated and purified through flash silica column (hexanes) to afford **79** (0.28 g, 1.3 mmol, 27.7 %). **79**: ^1H NMR (CDCl_3 , 400 MHz) δ : 0.18 (s, 9H, TMS), 1.05 (t, $J_{\text{HH}} = 7.6$ Hz, 3H, $-\text{CH}_3$), 1.57 (m, 4H, ring- CH_2), 2.04 (m, 2H, ring- CH_2), 2.14 (m, 2H, ring- CH_2), 2.28 (q, $J_{\text{HH}} = 7.6$ Hz, 2H, ethyl- CH_2). ^{13}C NMR (CDCl_3 , 500 MHz) δ : 0.2, 12.2, 22.4, 22.5, 28.5, 29.2, 29.7, 95.1, 106.2, 113.7, 149.2. HRMS (ESI) for $\text{C}_{12}\text{H}_{21}\text{Si}^+$: $[\text{M}^+]$ calculated 205.1407; found 205.1406. **80** (28.3 % yield): ^1H NMR (CDCl_3 , 400 MHz) δ : 1.06 (t, $J_{\text{HH}} = 7.6$ Hz, 3H, $-\text{CH}_3$), 1.64 (m, 4H, ring- CH_2), 2.11 (m, 2H, ring- CH_2), 2.24 (m, 2H, ring- CH_2), 2.36 (q, $J_{\text{HH}} = 7.6$ Hz, 2H, ethyl- CH_2), 7.27-7.73 (m, 5H, Ph). ^{13}C NMR (CDCl_3 , 500 MHz) δ : 12.6, 22.6, 28.6, 29.4, 29.9, 90.2, 90.9, 113.6, 124.2, 127.5, 128.2, 131.3, 147.9. HRMS (ESI) for $\text{C}_{16}\text{H}_{19}^+$: $[\text{M}^+]$ calculated 211.3203; found 211.3202. **78** (31.1 % yield): ^1H NMR (CDCl_3 , 400 MHz) δ : 0.99 (t, $J_{\text{HH}} = 7.6$ Hz, 3H, ethyl- CH_3), 1.57 (m, 4H, ring- CH_2), 1.98 (s, 3H, alkyne- CH_3), 2.02 (m, 2H, ring- CH_2), 2.10 (m, 2H, ring- CH_2), 2.25 (q, $J_{\text{HH}} = 7.6$ Hz, 2H, ethyl- CH_2). ^{13}C NMR (CDCl_3 , 500 MHz) δ : 4.4, 12.5, 22.6, 22.7, 28.2, 28.9, 30.2, 80.1, 86.7, 113.7, 145.5. HRMS (ESI) for $\text{C}_{11}\text{H}_{17}^+$: $[\text{M}^+]$ calculated 149.1425; found 149.1324. **83** (16 % yield) ^1H NMR (CDCl_3 , 400 MHz) δ : 1.53 (d, $J_{\text{HH}} = 7.2$) 1.76 (d, $J_{\text{HH}} = 6.4$, 3H, $-\text{Me}$) 6.31 (d, $J_{\text{HH}} = 15.6$, 3H, $-\text{Me}$), 5.87 (d, $J_{\text{HH}} = 15.6$, 1H, vinyl H), 5.65 (m, 1H, vinyl H), 5.55 (m, 1H, vinyl H) exhibited identical spectroscopic properties to those reported in literature.

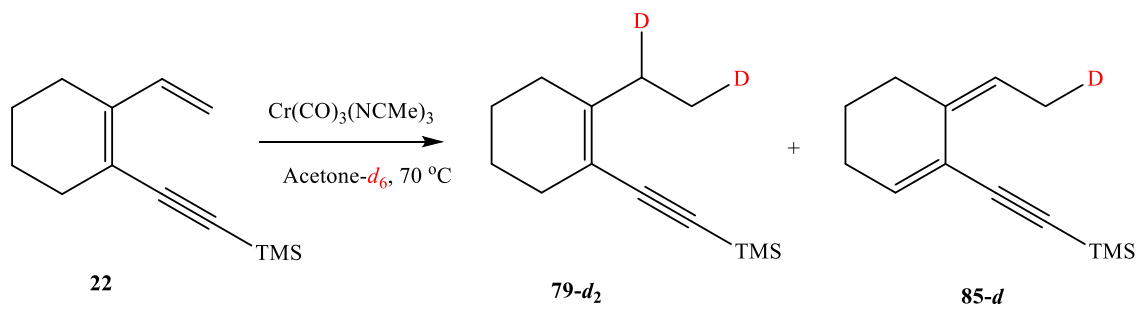


General procedure for the synthesis of **(Z)-6-ethylidene-1-(prop-1-yn-1-yl)cyclohex-1-ene (84)**, **(Z)-(((6-ethylidene-1-cyclohex-1-en-1-yl)ethynyl)trimethylsilane (85))** and **(Z)-(((6-ethylidene-1-cyclohex-1-en-1-yl)ethynyl)benzene (86))**: **96** (0.2 g, 0.79 mmol) was added to a side-armed shrink tube containing **62** (0.13 g, 0.61 mmol) dissolved in 10 mL anhydrous acetone under inert atmosphere. The shrink tube was placed in an oil bath for 16 h at 70 °C. The mixture was then exposed to ambient air and sunlight for 1 h, diluted with hexanes, filtered, concentrated and

purified through flash silica column (hexanes) to afford **78** (24 mg, 0.16 mmol, 27.7 %) and **84** (22 mg, 0.15 mmol, 25.0 %). **84** ^1H NMR (CDCl_3 , 400 MHz): δ : 1.66 (m, 2H, ring- CH_2), 1.70 (d, $J_{\text{HH}} = 7.2$ Hz, 3H, alkene- CH_3), 1.99 (s, 3H, alkyne- CH_3), 2.17 (m, 2H, ring- CH_2), 2.32 (t, 2H, $J_{\text{HH}} = 6$ Hz, 2H, ring- CH_2), 5.98 (q, $J_{\text{HH}} = 7.6$ Hz, 1H, vinyl H), 6.09 (t, $J_{\text{HH}} = 4$ Hz, vinyl H). ^{13}C NMR (CDCl_3 , 500 MHz) δ : 4.2, 13.1, 21.9, 24.8, 26.1, 30.3, 34.2, 85.5, 121.6, 125.5, 133.8. HRMS (ESI) for $\text{C}_{11}\text{H}_{15}^+$: $[\text{M}^+]$ calculated 147.1168; found 147.1168. **86** (33.1 % yield): ^1H NMR (CDCl_3 , 400 MHz) δ : 1.71 (m, 2H, ring- CH_2), 1.74 (d, $J_{\text{HH}} = 7.2$ Hz, - CH_3), 2.26 (m, 2H, ring- CH_2), 2.38 (t, $J_{\text{HH}} = 6.4$ Hz, ring- CH_2), 6.09 (q, $J_{\text{HH}} = 7.6$ Hz, 1H, vinyl H), 6.29 (t, $J_{\text{HH}} = 4.4$ Hz, vinyl H), 7.36-7.54 (m, 5H, Ph). ^{13}C NMR (CDCl_3 , 500 MHz) δ : 13.2, 21.8, 24.8, 26.3, 87.8, 89.4, 122.1, 127.8, 128.2, 128.4, 131.5, 132.5, 133.4, 135.3. HRMS (ESI) for $\text{C}_{16}\text{H}_{17}^+$: $[\text{M}^+]$ calculated 209.1305; found 209.1306. **85** (22.6 % yield): ^1H NMR (CDCl_3 , 400 MHz) δ : 0.21 (s, 9H, TMS), 1.67 (m, 2H, ring- CH_2), 1.73 (d, $J_{\text{HH}} = 6.8$ Hz, 3H, - CH_3), 2.18 (t, $J_{\text{HH}} = 5.2$ Hz, 2H, ring- CH_2), 2.32 (t, $J_{\text{HH}} = 6$ Hz, 2H, ring- CH_2), 6.00 (q, $J_{\text{HH}} = 7.6$ Hz, 1H, vinyl H), 6.25 (t, $J_{\text{HH}} = 4.4$ Hz, 1H, vinyl H). ^{13}C NMR (CDCl_3 , 500 MHz) δ : 0.1, 13.2, 21.3, 24.7, 26.1, 93.9, 103.7, 122.1, 123.2, 133.1, 136.2. HRMS (ESI) for $\text{C}_{13}\text{H}_{21}\text{Si}^+$: $[\text{M}^+]$ calculated 205.1407; found 205.1408.



((2-(ethyl-1,2-d₂)cyclohex-1-en-1-yl)ethynyl)trimethylsilane (79-d₂) and **(Z)-((6-(ethylidene-2-d)cyclohex-1-en-1-yl)ethynyl)trimethylsilane (85-d): 96** (0.15 g, 0.59 mmol) was added to a side-armed shrink tube containing **22** (0.10 g, 0.50 mmol) dissolved in 5.0 mL anhydrous acetone-*d*₆ under inert atmosphere. The shrink tube was placed in an oil bath for 16 h at 70 °C. The mixture was then exposed to ambient air and sunlight for 1 h, diluted with hexanes, filtered, concentrated and purified through flash silica column (hexanes) to afford **79-d₂** (18.7 mg, 0.09 mmol, 18.0 %, deuterium enrichment 86 %) and **85-d** (16.4 mg, 0.08 mmol, 16 %, deuterium enrichment 80 %).



4. ^1H and ^{13}C NMR Spectroscopic Data.

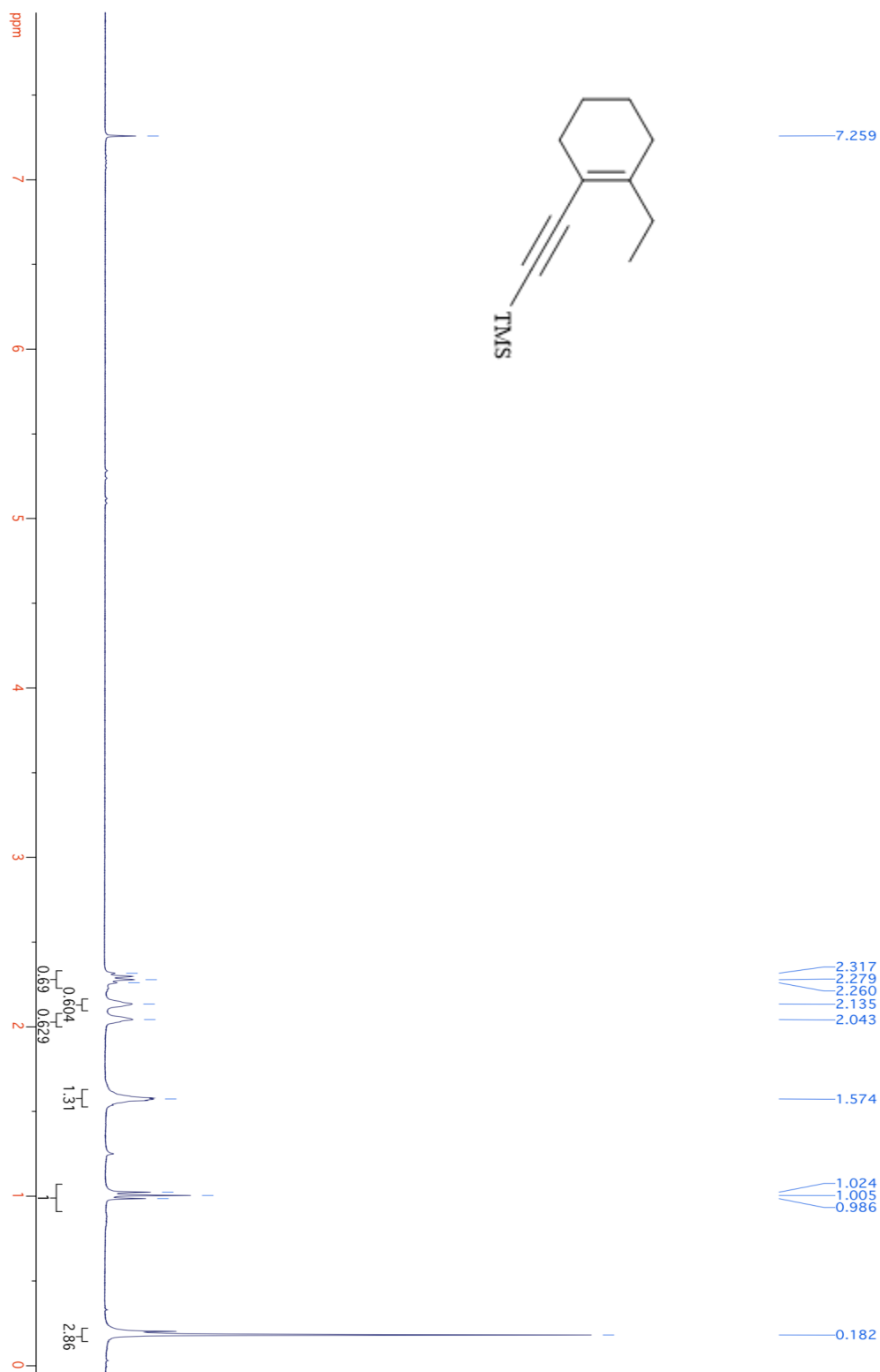


Figure 4-1: ^1H NMR spectrum of **79** (CDCl_3 , 400 MHz).

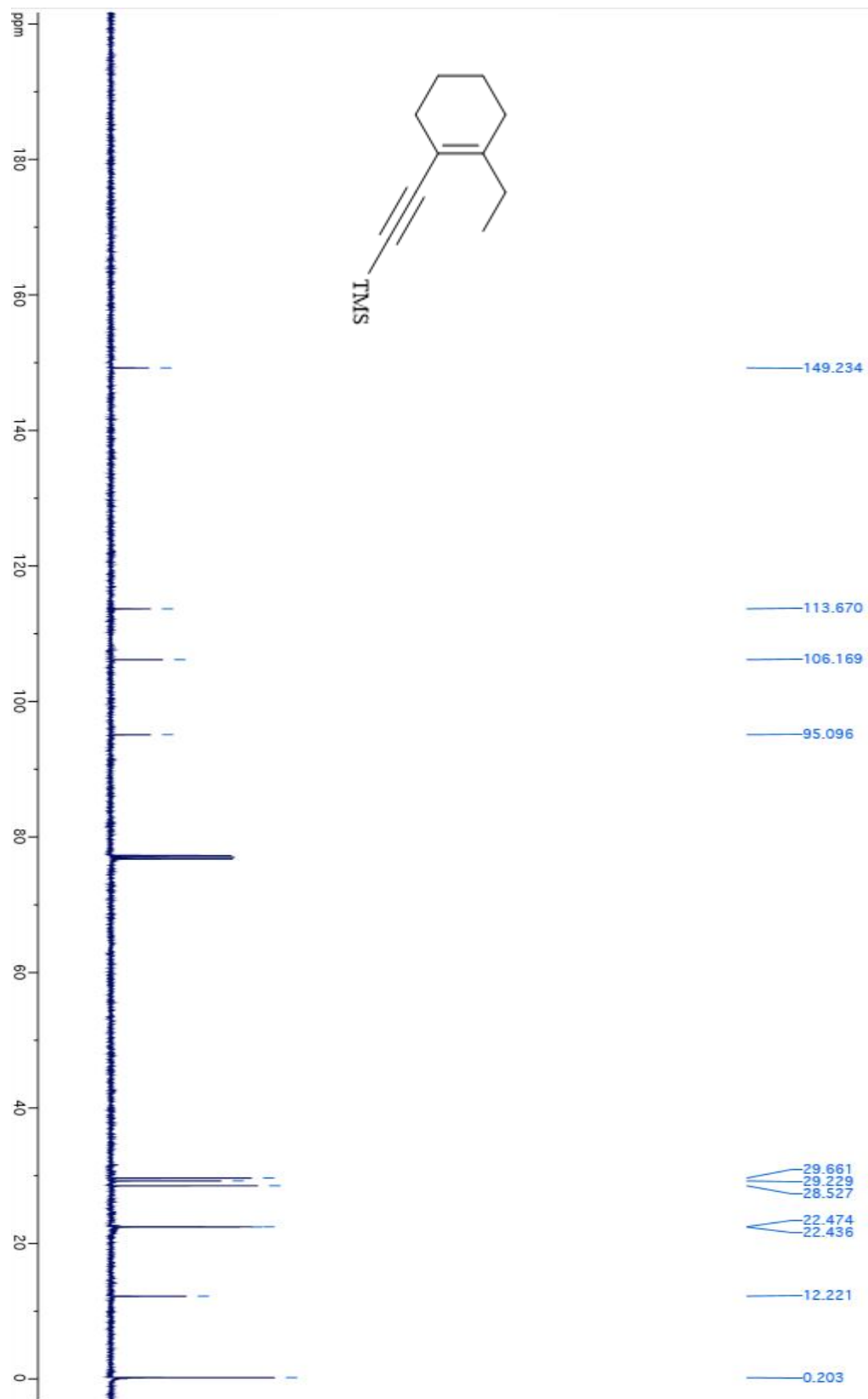


Figure 4-2: ^{13}C NMR spectrum of **79** (CDCl_3 , 500 MHz).

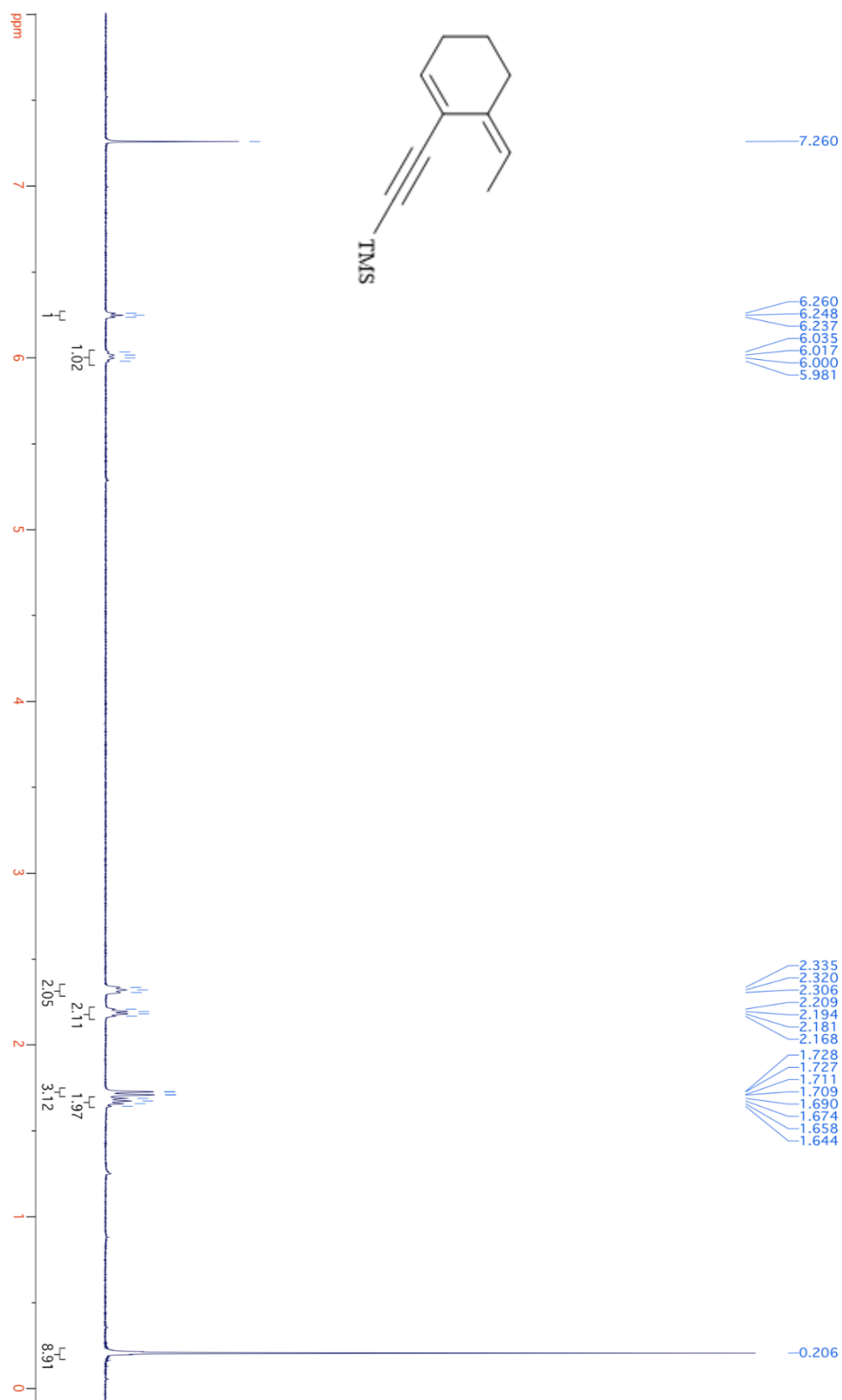


Figure 4-3: ¹H NMR spectrum of **85** (CDCl₃, 400 MHz).

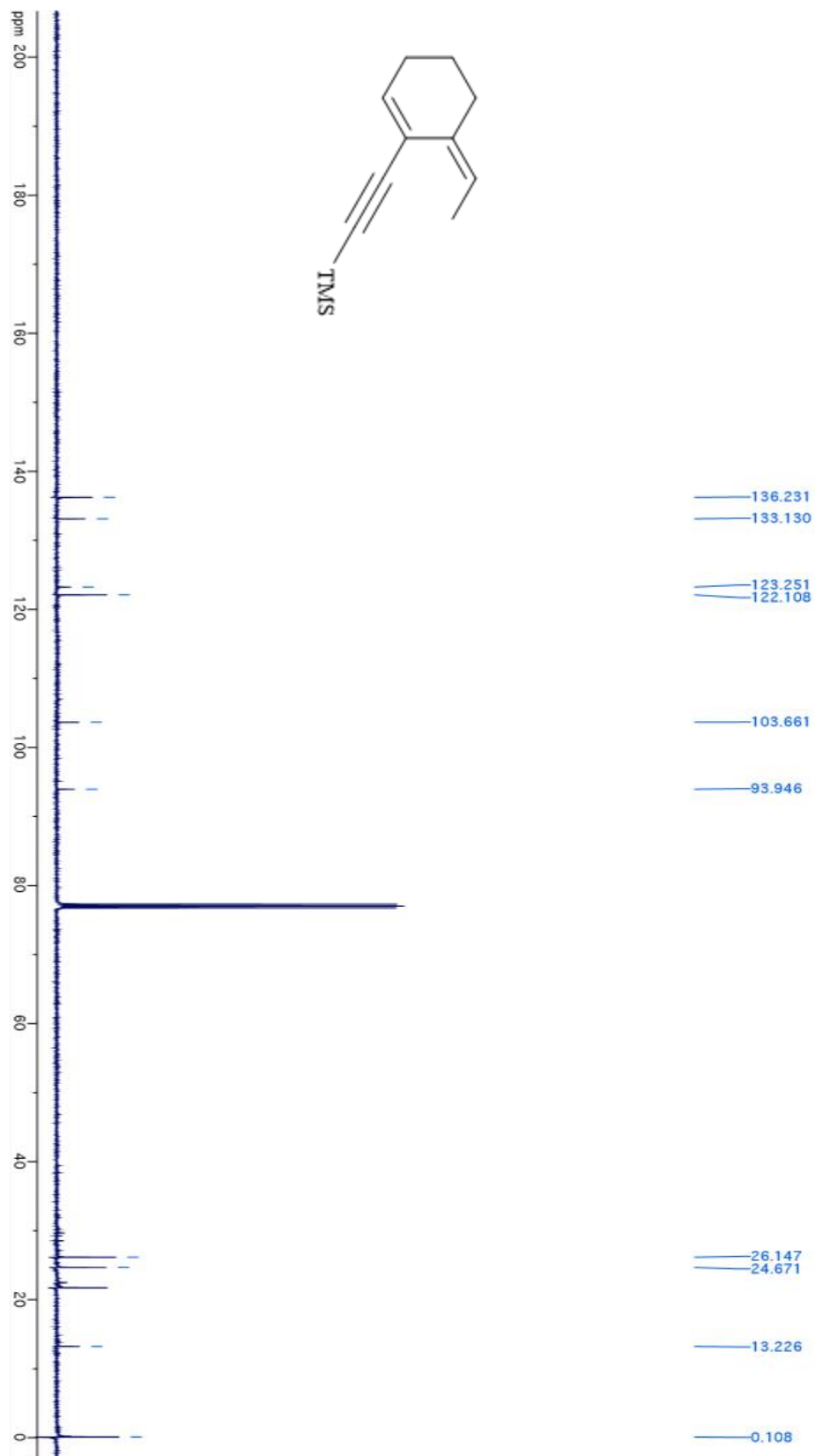


Figure 4-4: ^{13}C NMR spectrum of **85** (CDCl₃, 500 MHz).

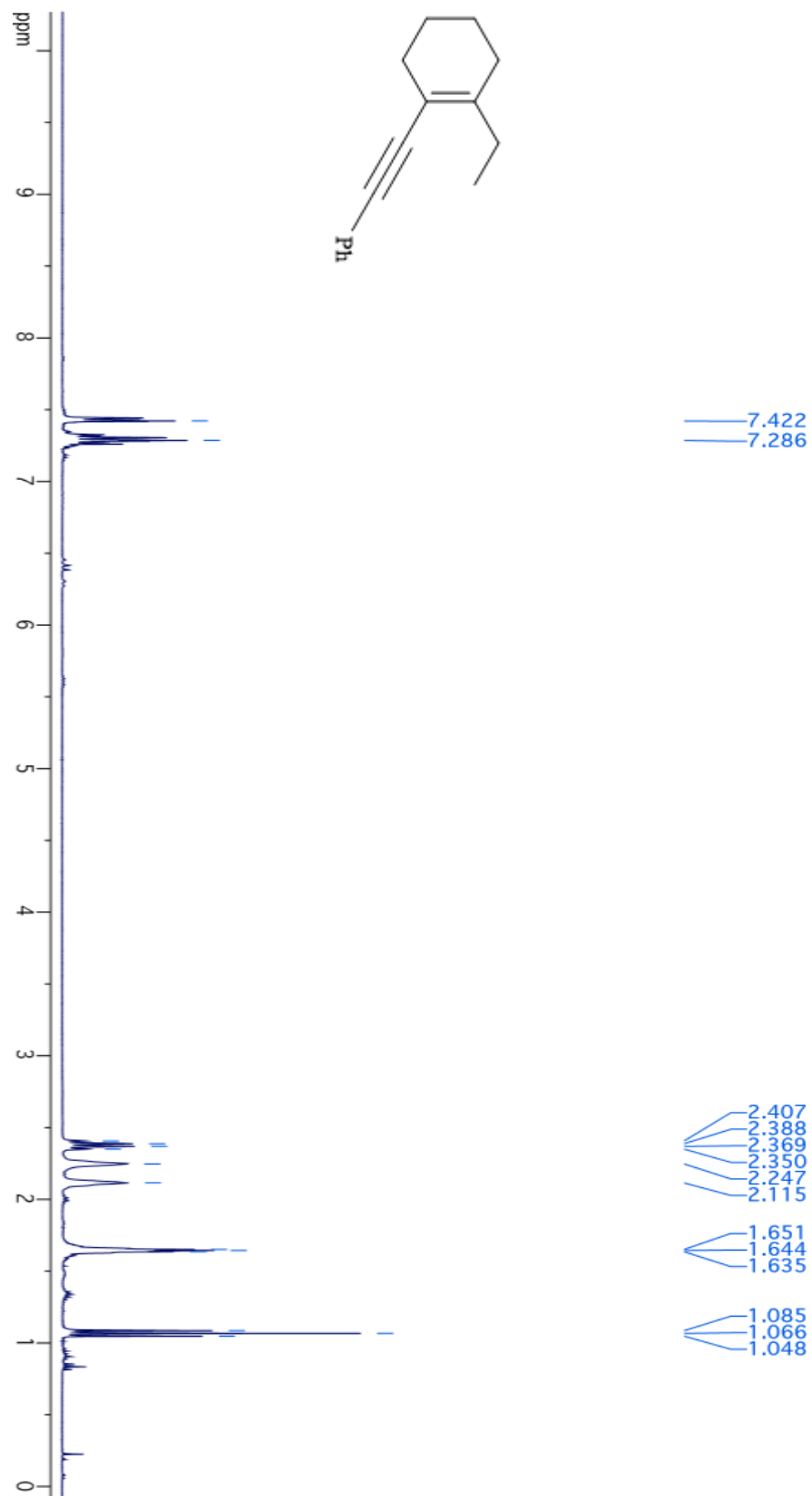


Figure 4-5: ¹H NMR spectrum of **80** (CDCl₃, 400 MHz).

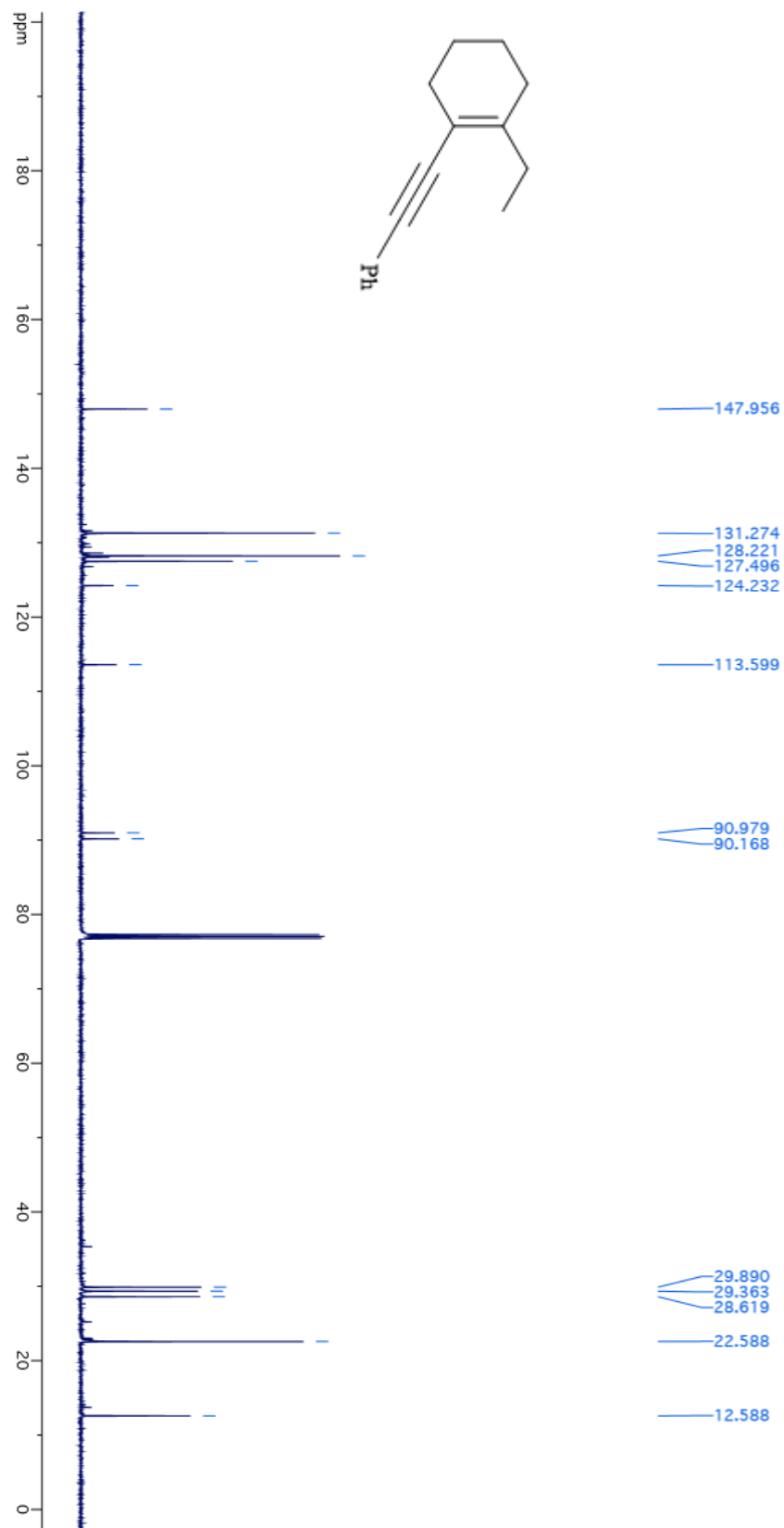


Figure 4-6: ^{13}C NMR spectrum of **80** (CDCl_3 , 500 MHz).

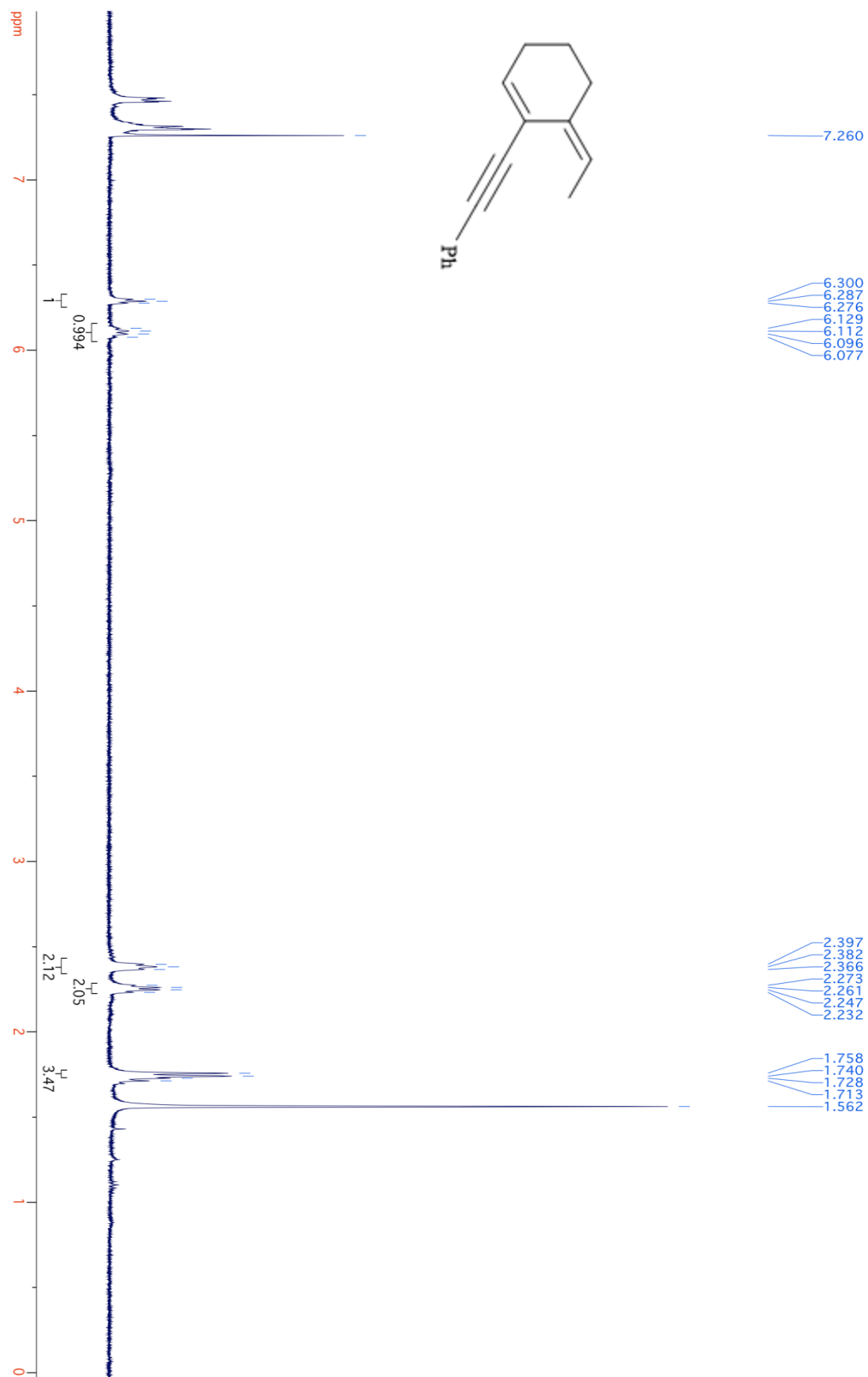


Figure 4-7: ¹H NMR spectrum of **85** (CDCl₃, 400 MHz).

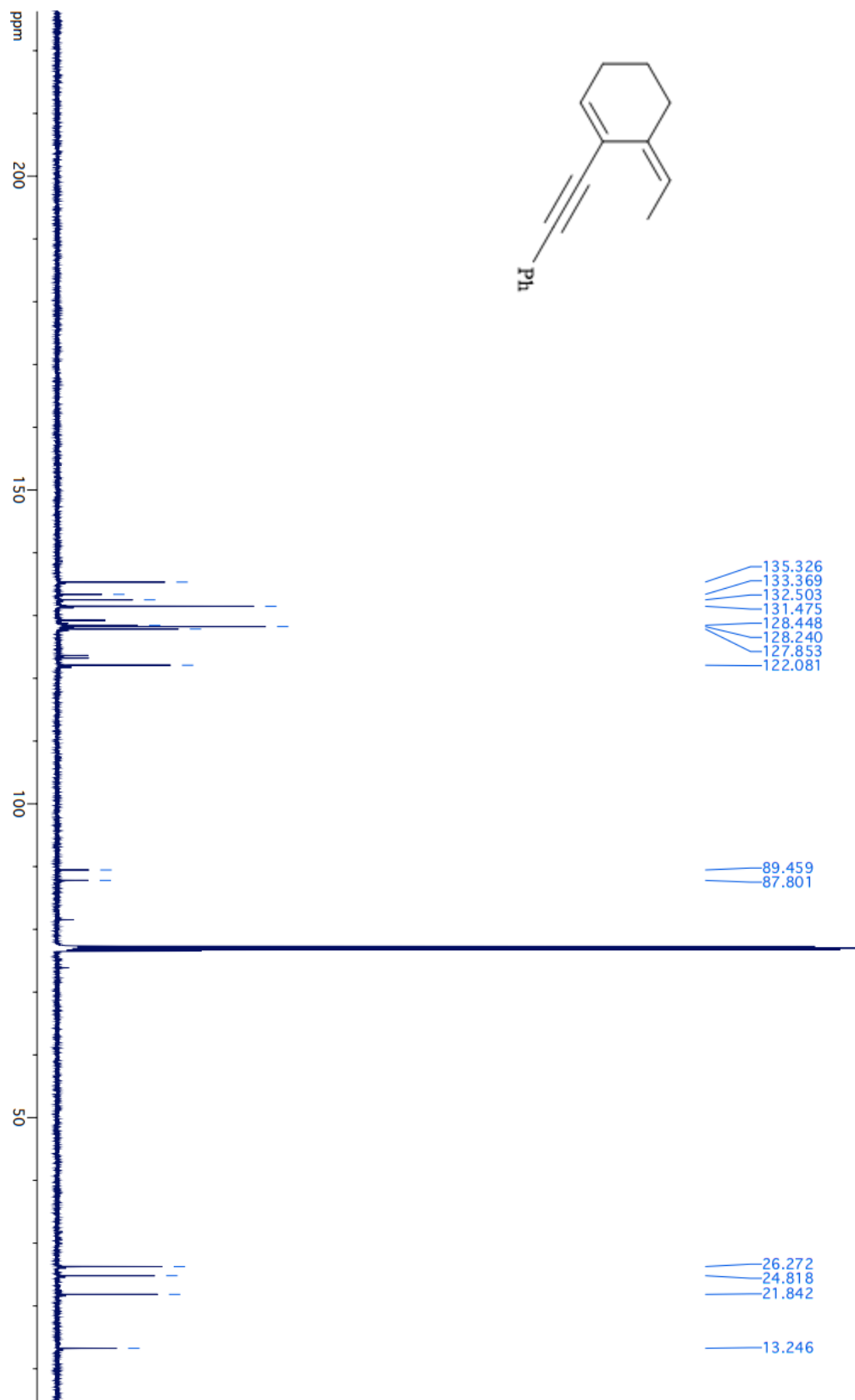


Figure 4-8: ¹³C NMR spectrum of **85** (CDCl₃, 500 MHz).

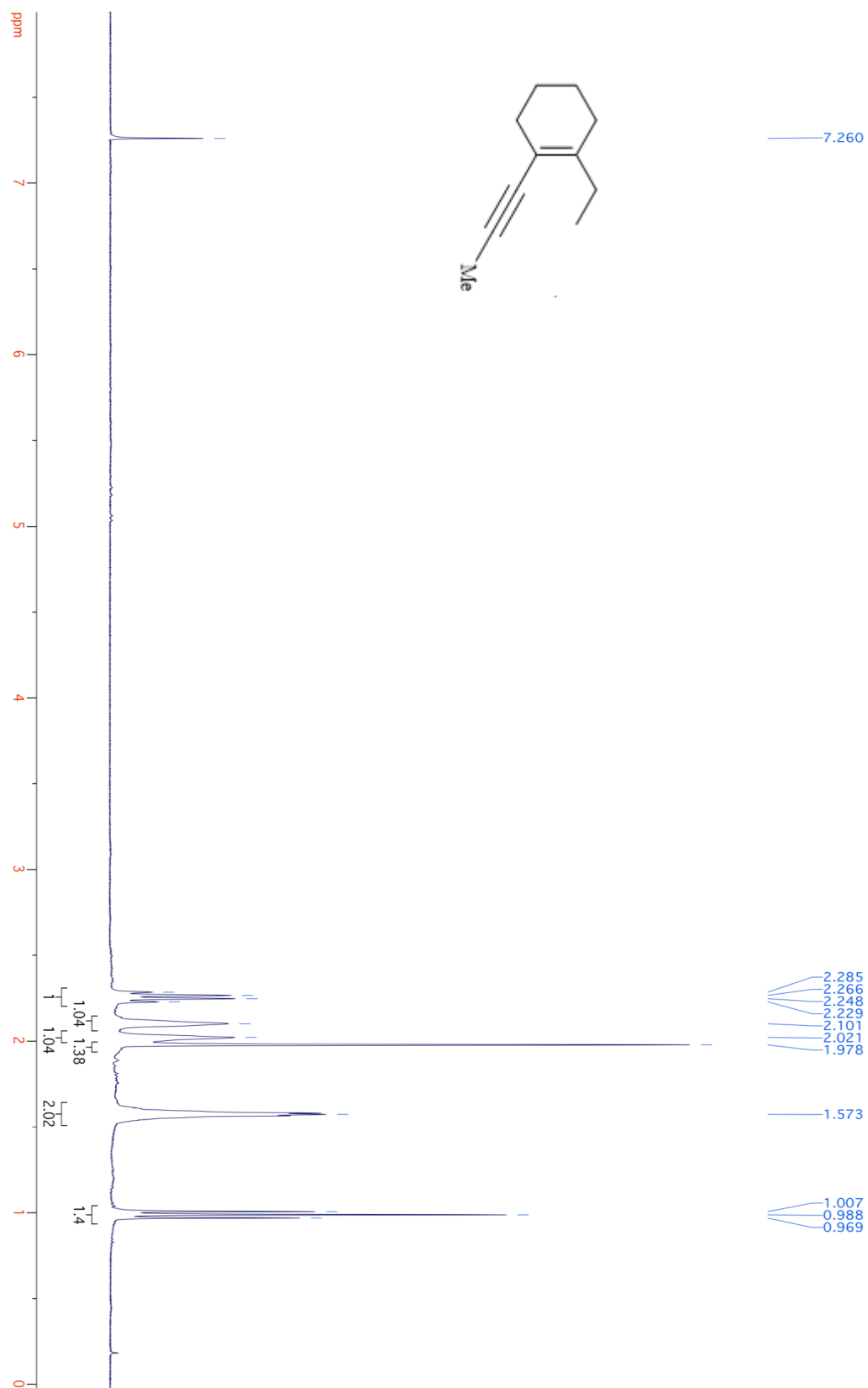


Figure 4-9: ^1H NMR spectrum of **78** (CDCl_3 , 400 MHz).

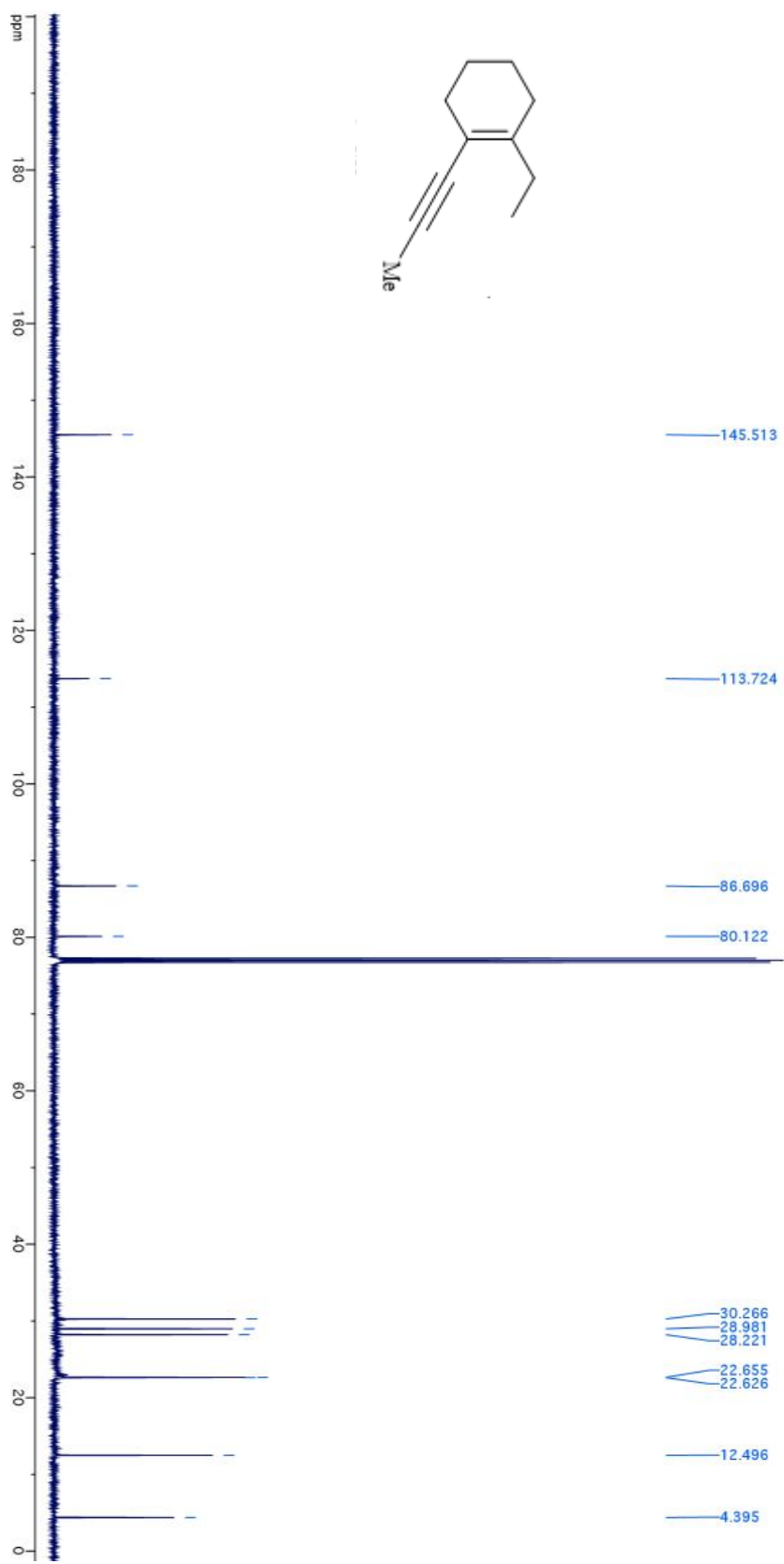


Figure 4-10: ^{13}C NMR spectrum of **78** (CDCl₃, 500 MHz).

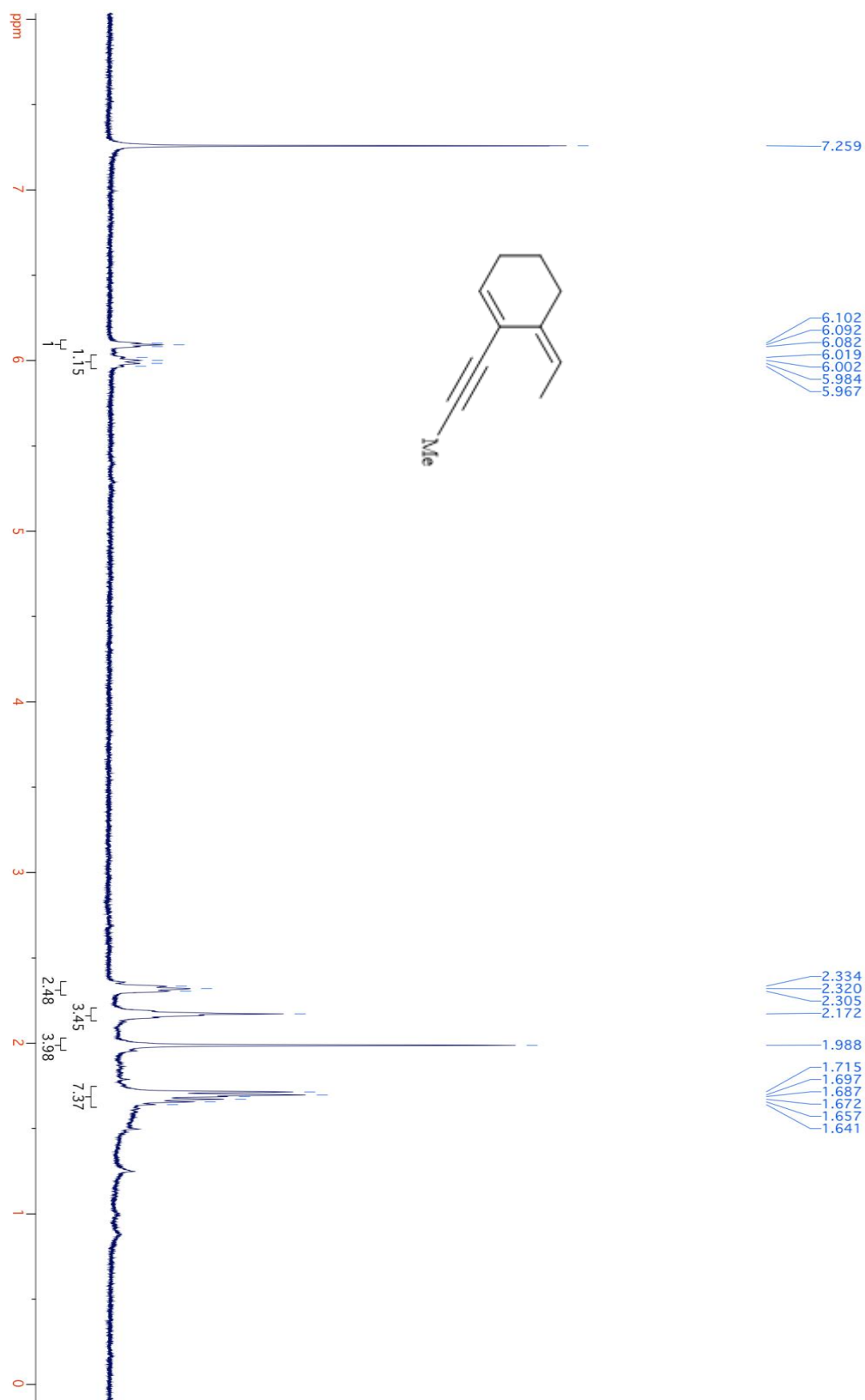


Figure 4-11: ¹H NMR spectrum of **84** (CDCl₃, 400 MHz).

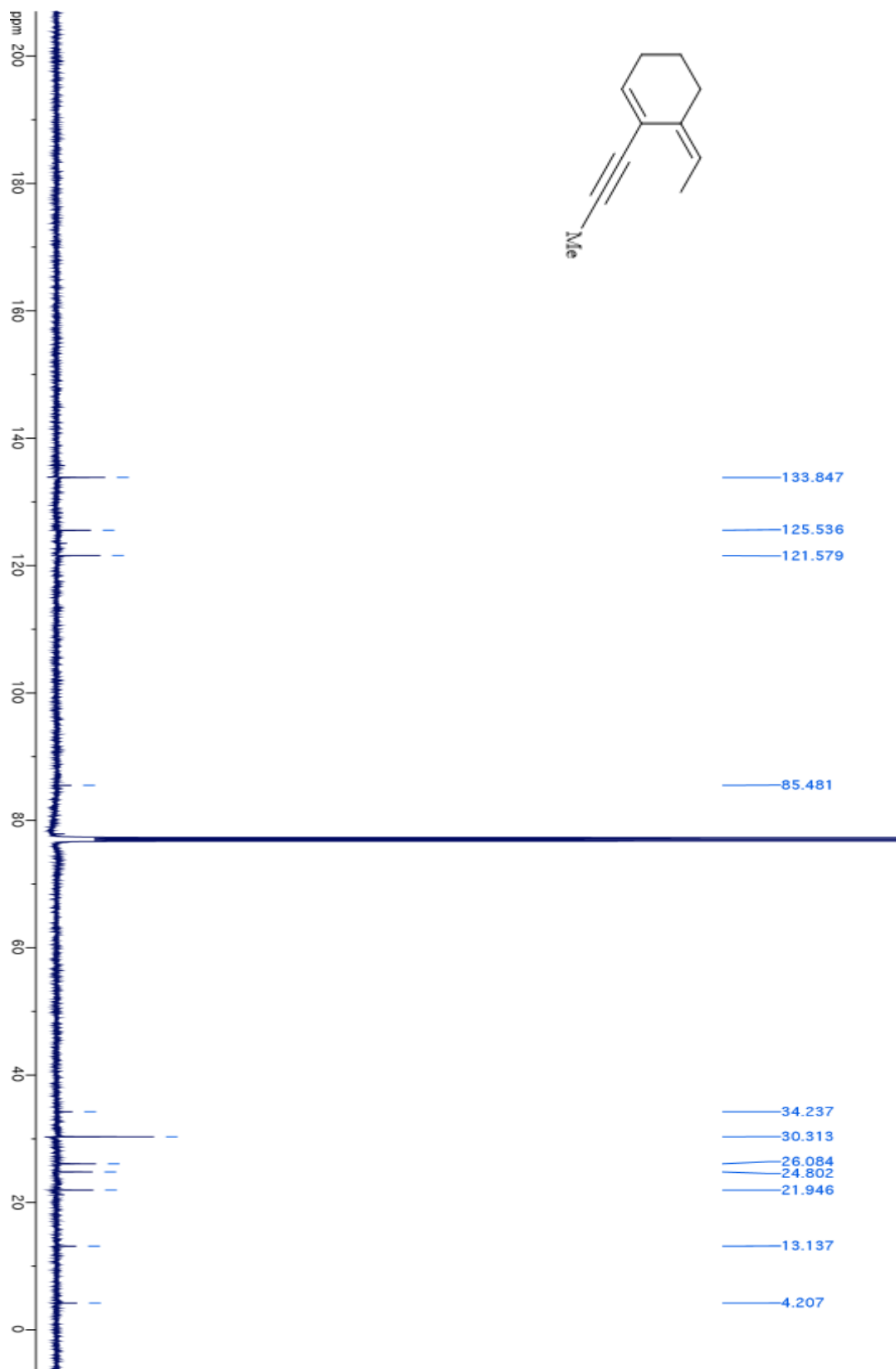


Figure 4-12: ^{13}C NMR spectrum of **84** (CDCl_3 , 500 MHz).

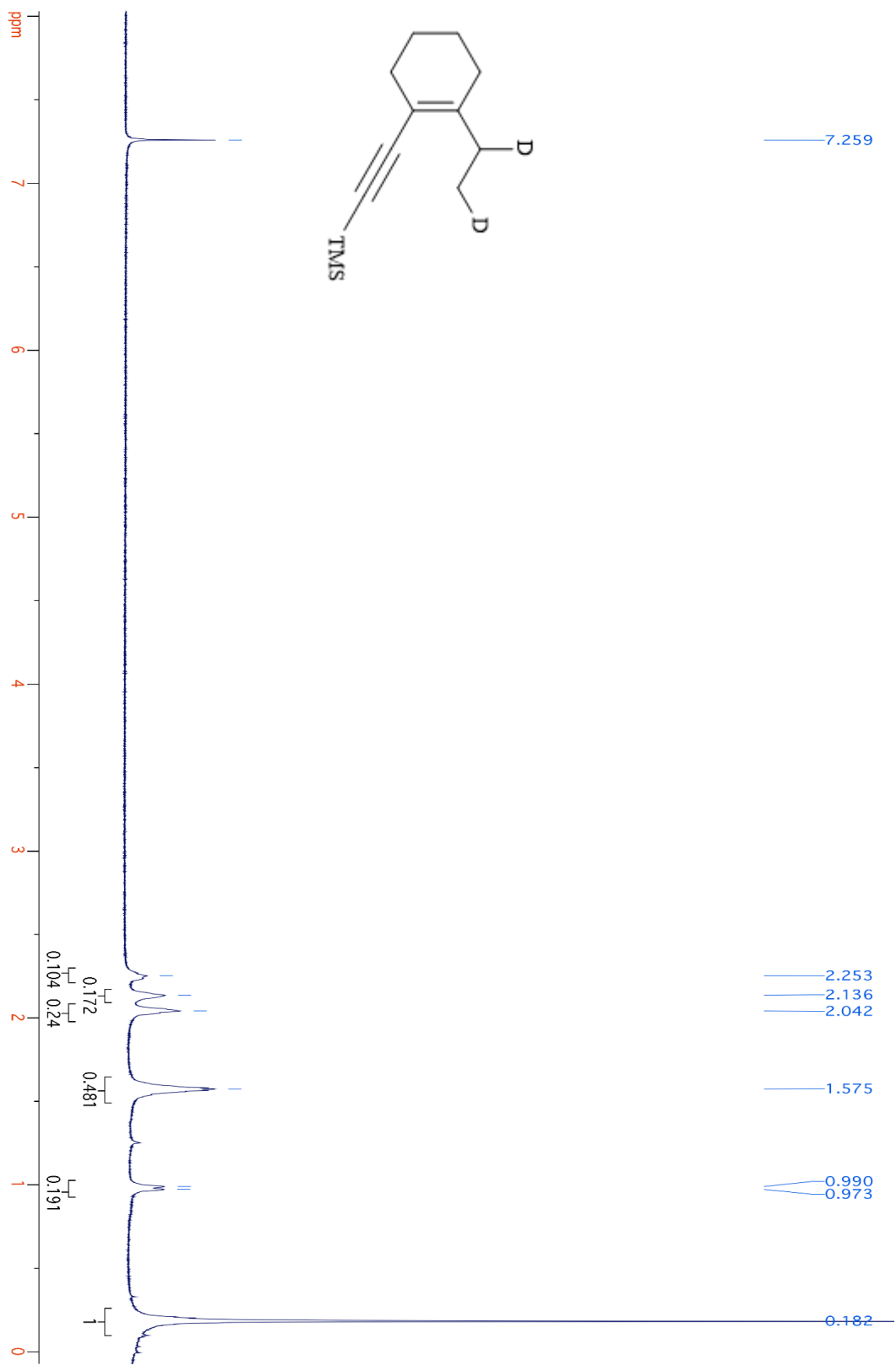


Figure 4-13: ¹H NMR spectrum of **79-d₂** (CDCl₃, 400 MHz).

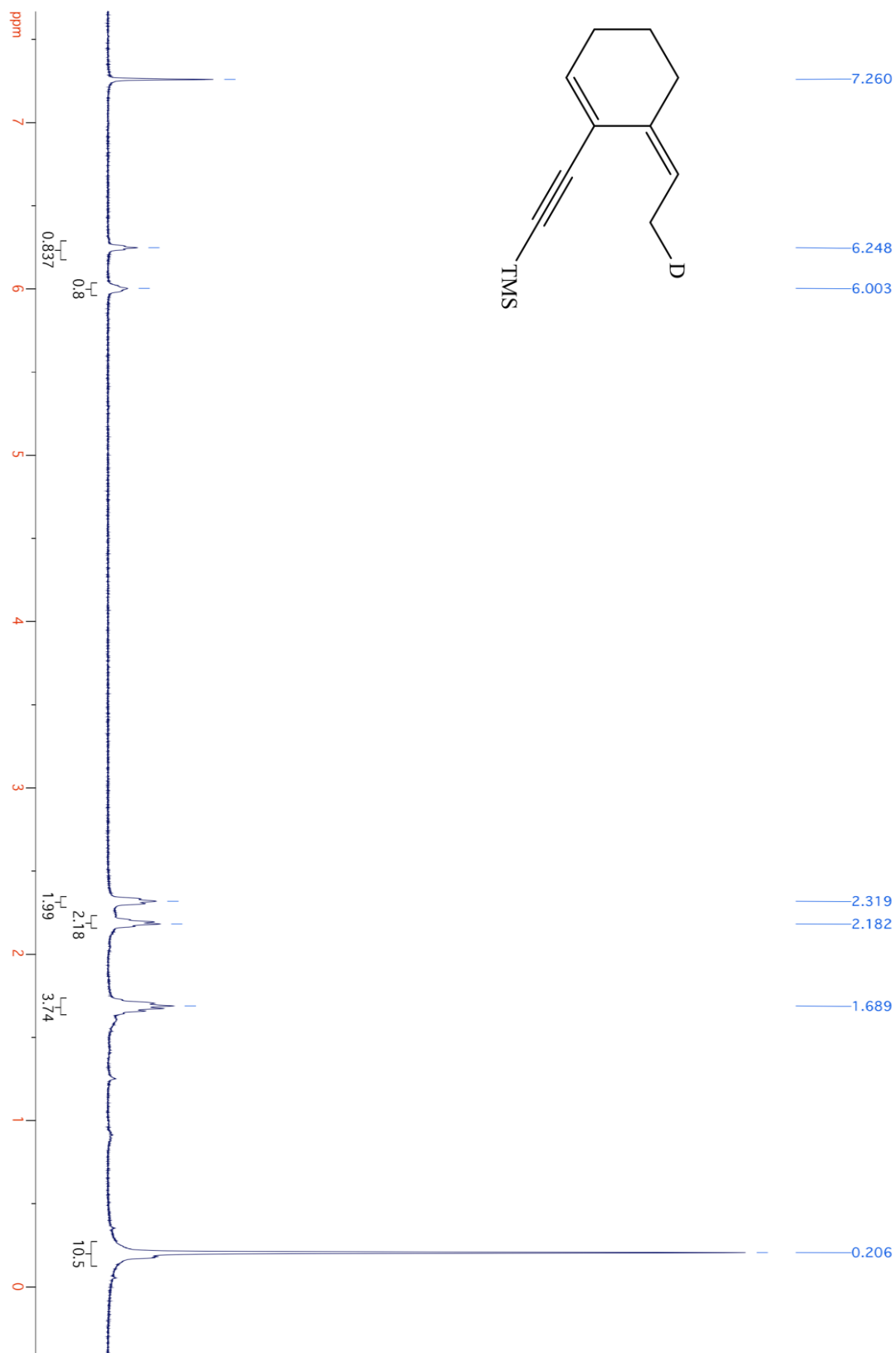


Figure 4-14: ^1H NMR spectrum of **85-d** (CDCl_3 , 400 MHz).

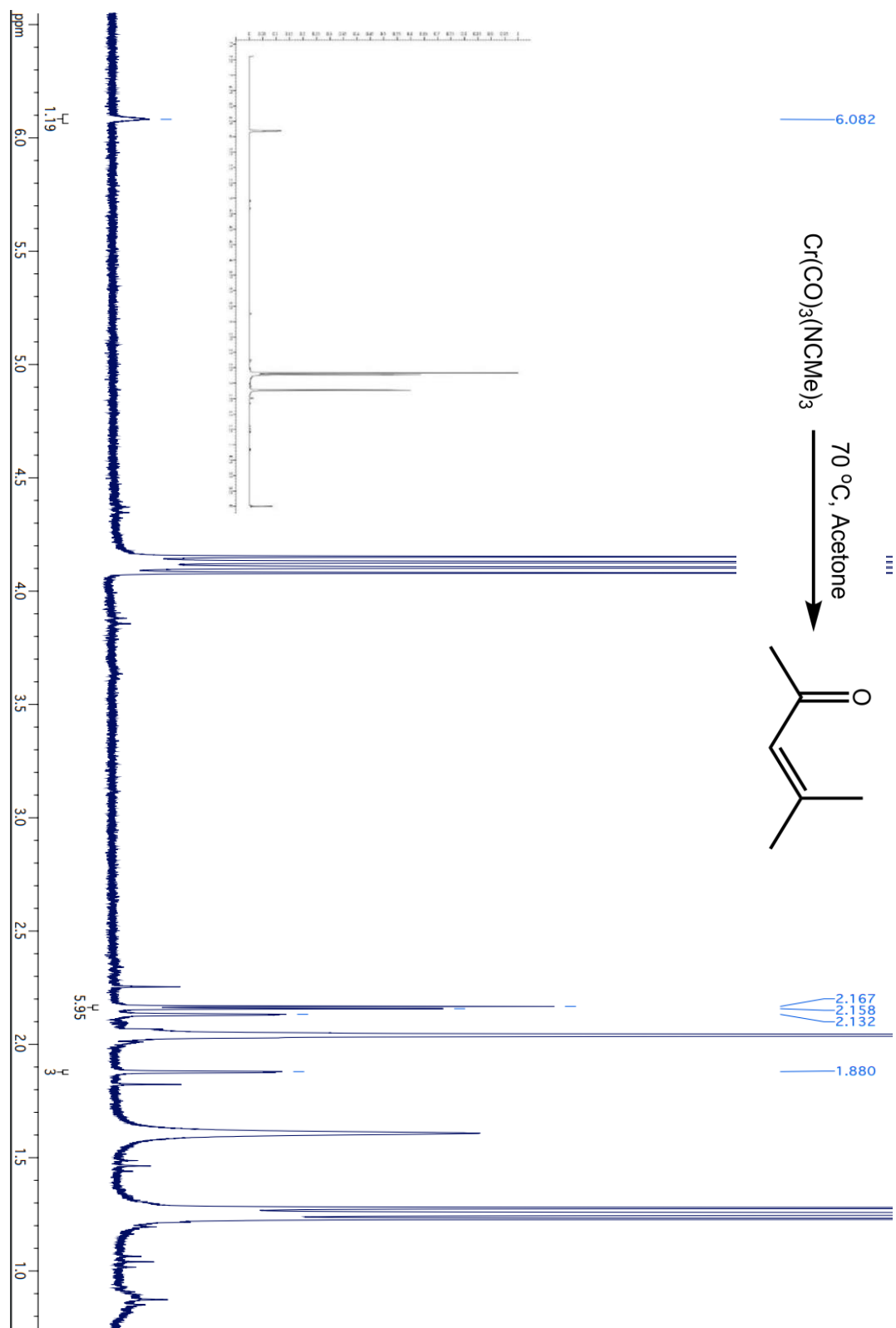


Figure 4-15: ^1H NMR spectrum of **96** heating with acetone in ethyl acetate and the comparison with reference 4-methylpent-3-en-2-one.

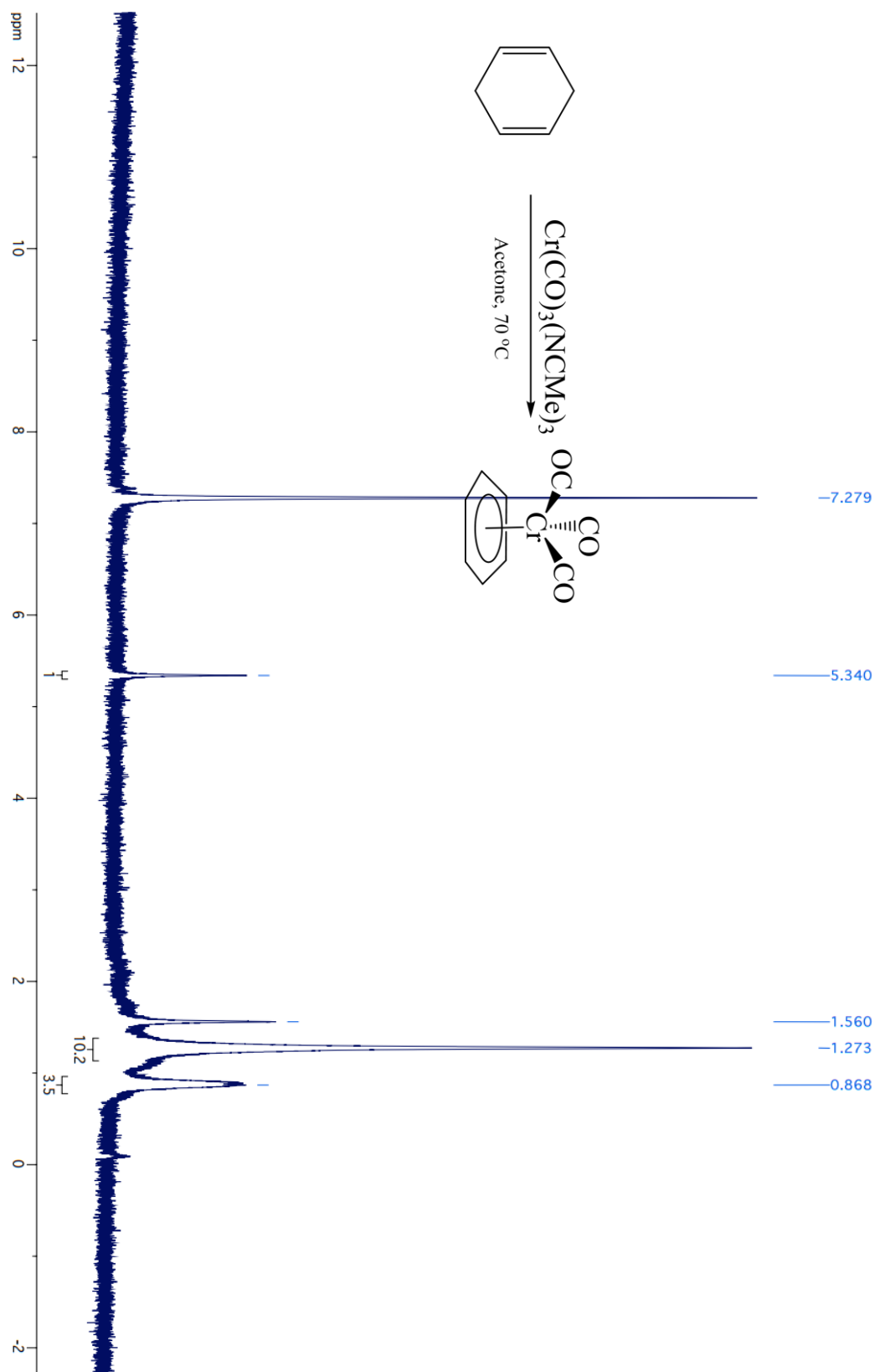


Figure 4-16: ^1H NMR spectrum of **96** reacting with 1,4-CHD.

5. Product yield under various conditions.

Table 4-2: Hydrogenation and tautomer product yield at various reaction times.

Substrate	Reaction time (h)	Hydrogenation product (%)	Tautomer product (%)
22	48	6	6
22	72	8	2
32	48	13	5
32	72	5	14
62	48	6	7
62	72	14	12
62	7 days	18	10

Table 4-3: Hydrogenation and tautomer product yield with various substrate to Cr mole ratios.

Substrate	Sub to Cr mole ratio	Hydrogenation product (%)	Tautomer product (%)
22	1:2	4	0
22	1:3	17	0
22	1:5	15	0
32	1:2	26	12
32	1:3	21	2
32	1:5	22	0
62	1:2	3	10
62	1:3	2	8
62	1:5	5	16

Table 4-4: Hydrogenation product yield with various hydrogen sources.

Substrate	Hydrogen source	Hydrogenation product (%)
22	Air	0
22	H ₂ O	0
22	H ₂	34 %

IX. Acknowledgement.

The material in Chapter 4 is currently under preparation for publication with the following authors: Steger, H.; Shrinidhi, A.; O'Connor, J. M. The dissertation author was the primary investigator and author of this material.

X. Reference.

1. Hopf, H.; Musso, H. *Angew. Chem. Int. Ed. Engl.* **1969**, 8, 680. "Preparation of Benzene by Pyrolysis of cis-and trans-1,3-Hexadien-5-yne".
2. Hopf, H.; Kruger, A. *Chem. Eur. J.* **2001**, 7, 4378-4385. "Synthesis of Cyclo-1,3-dien-5-ynes".
3. Mandal, S.; Basak. *Tetrahedron Letters.* **2009**, 50, 3641-3644. "Aza Hopf cyclization: synthesis and reactivity of cyclic azadieneynes".
4. Hitt, D. M.; O'Connor, J. M. *Chem. Rev.* **2011**, 111, 7904-7922. "Acceleration of Conjugated Dienyne Cycloaromatization".
5. O'Connor, J. M.; Friese, S. J.; Rodgers, B. L.; Rheingold, A. L.; Zakharov L. *J. Am. Chem. Soc.* **2005**, 127, 9346-9347. "An η^6 -Dienyne Transition-Metal Complex".
6. O'Connor, J. M.; Friese, S. J.; Tichenor, M. *J. Am. Chem. Soc.* **2002**, 124, 3506-3507. "Ruthenium-Mediated Cycloaromatization of Acyclic Enediynes and Dienes at Ambient Temperature".
7. Qin, P.; Cope, S.; Steger, H.; Veccharelli, K. M.; Holland, R. L.; Hitt, D. M.; Moore, C. E.; Baldridge, K. K.; O'Connor, J. M. *Organometallic.* **2017**, 36, 3967-3973. "Photoactivated Transition-Metal Triggers for Ambient Temperature Enediyne and Dienyne Cyclization: Ruthenium- η^6 -Naphthalene Complexes".
8. Steger, H.; Chen, L.; Xiong, W.; O'Connor, J. M. Manuscript under preparation. "Ambient Temperature $\text{Cr}(\text{CO})_3$ (η^6 -naphthalene)-Mediated 1,3-Dien-5-ynes Cycloaromatization".
9. Frankel, E.N.; Butterfield, R.O. *J. Org. Chem.* **1969**, 34, 3930-3936. "Homogeneous Hydrogenation of Diolefins Catalyzed by Tricarbonyl Chromium Complexes. I. Stereoselective 1,4 Addition of Hydrogen".

10. Sodeoka, M.; Ogawa, Y.; Kirio, Y.; Shibasaki, M. *Chem. Pharm. Bull.* **1991**, 39, 309-322. "Stereocontrolled Synthesis of Exocyclic Olefins Using Arene Tricarbonyl Chromium Complex-Catalyzed Hydrogenation. I. Efficient Synthesis of Carbacyclin and Its Analogs".
11. Vasil'ev, A. A.; Kuchurov, I. V.; Zlotin, S. G. *Russian Chemical Bulletin.* **2018**, 67, 923-926. "1,4-cis-Hydrogenation of butyl sorbate in supercritical carbon dioxide".
12. Bhandari, G.; Kim, Y.; McFarland, J. M.; Rheingold, A. L.; Theopold, K. H. *Organometallics.* **1995**, 14, 738-745. "Paramagnetic (Benzyl) chromium complexes as homogeneous ethylene polymerization catalysts".
13. Weckhuysen, B. M.; Schoonheydt, R. A.; Mabbs, F. E.; Collison, D. *J. Chem. Soc., Faraday Trans.* **1996**, 92, 2431-2436. "Electron paramagnetic resonance of heterogeneous chromium catalysts."
14. Ashe, A. J.; Kampf, J. W.; Kausch, C. M.; Konishi, H.; Kristen, M. O.; Kroker, J. *Organometallics.* **1990**, 9, 2944-2948. "Synthesis and molecular and crystal structure of (3-methyl-3-benzoborepin)chromium tricarbonyl".
15. Sarkar, S.; Niyogi, S.; Bekyarova, E.; Haddon, R. C. *Chem. Sci.* **2011**, 2, 1326-1333. "Organometallic chemistry of extended periodic π -electron systems: hexahapto-chromium complexes of graphene and single-walled carbon nanotubes".
16. Sarkar, S.; Zhang, H.; Huang, J.; Wang, F.; Bekyarova, E.; Lau, C. M.; Haddon, R. C. *Adv. Mater.* **2013**, 25, 1131-1136. "Organometallic hexahapto functionalization of single layer graphene as a route to high mobility graphene devices".

**Chapter 5 Chelated $[\text{Zn}(\text{cyclam})]^{2+}$ Lewis acid improves the reactivity of
the electrochemical reduction of CO_2 by Mn catalysts with bulky
bipyridine ligands.**

I. Introduction.

Greenhouse gas production from extensive fossil fuel usage and other human activities have changed the global climate over the past century. Global warming and raising sea levels have cost the world's economy, agriculture, and industry billions of dollars.¹⁻⁴ As of 2019, CO₂ content in the atmosphere has reached 415.39 ppm, and is growing alarmingly (Figure 5-1).⁵ Reduction of CO₂ by converting it to other compounds has been the focus of intense research. Sustainably manufacturing, from CO₂, alternative organic chemicals can potentially slow the accumulation of atmospheric CO₂.⁵⁻¹¹

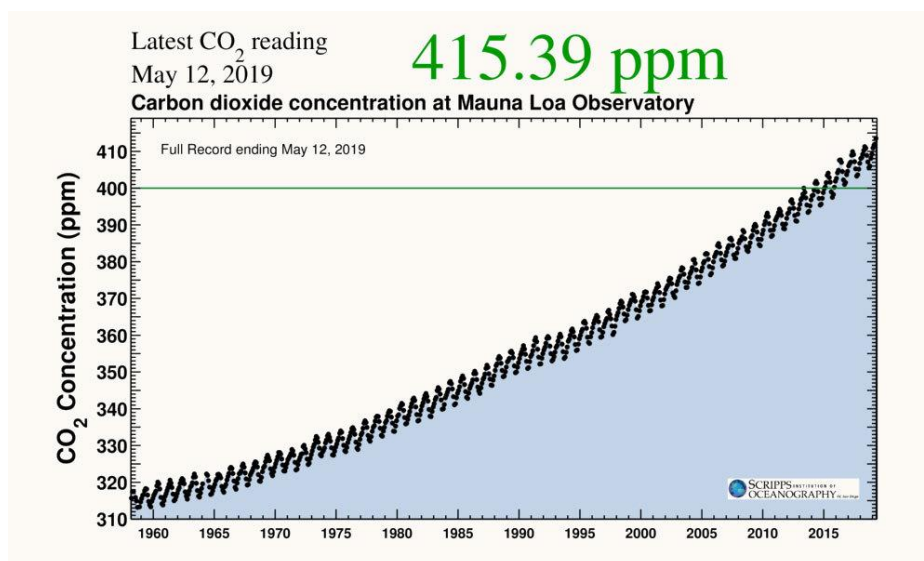


Figure 5-1: CO₂ content in atmosphere reported by Mauna Loa Observatory on May 12, 2019.

Electrochemical reduction of CO₂ has been one of the focused aspects of this effort. It can be carried out at ambient pressure and room temperature, without the production of hazardous side products. At the same time, products with high combustion energy such as methane, alcohol and carbon monoxide can be obtained. However large overpotentials are typically required because of

the kinetic barriers involved in the multi-electron, multi-proton reduction reactions (Figure 5-2).⁸⁻

12

				$E^{0'}$	
CO_2	+	e^-	\longrightarrow	$\text{CO}_2^{\cdot-}$	-1.90 V
CO_2	+	$2 \text{H}^+ + 2 e^-$	\longrightarrow	HCOOH	-0.61 V
CO_2	+	$2 \text{H}^+ + 2 e^-$	\longrightarrow	$\text{CO} + \text{H}_2\text{O}$	-0.52V
CO_2	+	$4 \text{H}^+ + 4 e^-$	\longrightarrow	$\text{HCHO} + \text{H}_2\text{O}$	-0.48 V
CO_2	+	$6 \text{H}^+ + 6 e^-$	\longrightarrow	$\text{CH}_3\text{OH} + \text{H}_2\text{O}$	-0.38 V
CO_2	+	$8 \text{H}^+ + 8 e^-$	\longrightarrow	$\text{CH}_4 + 2\text{H}_2\text{O}$	-0.24 V
2H^+	+	$2 e^-$	\longrightarrow	H_2	-0.41 V

Figure 5-2: Equilibrium potential for CO_2 reduction at pH 7 (V^0 Vs. SHE).

Prof. Clifford Kubiak's group, as one of the world's leaders in electrochemical reduction of CO_2 research, has thoroughly studied manganese catalysts of the class $\text{Mn}(\text{bpy-R})(\text{CO})_3\text{X}$ (Figure 5-3), where bpy is one of various bipyridyl ligands and X is a halide or pseudo-halide. These catalysts have been reported to catalyze the electrochemical reduction of CO_2 to CO at lower overpotential than the corresponding Re complexes without significant decrease in activity.^{13, 14}

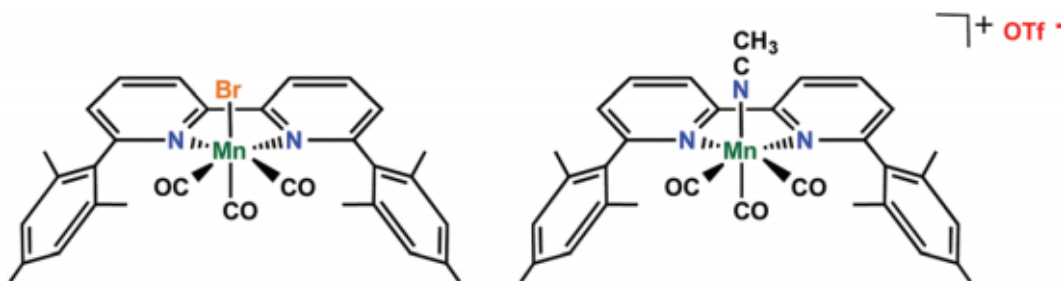


Figure 5-3: Schematic of the molecular structure of $[\text{Mn}(\text{mes-bpy})(\text{CO})_3(\text{Br})]$ and $[\text{Mn}(\text{mes-bpy})(\text{CO})_3(\text{MeCN})]^+$.

Kubiak's group previously reported that complexes $[\text{Mn}(\text{mes-bpy})(\text{CO})_3(\text{Br})]^+$ and $[\text{Mn}(\text{mes-bpy})(\text{CO})_3(\text{MeCN})]^+$ bearing the bulky mesityl-substituted bipyridine ligand, which prevents dimerization of the one-electron reduced state to Mn(0) dimer species, display even lower overpotentials for electrocatalytic reduction of CO_2 (Figure 5-4).¹⁵

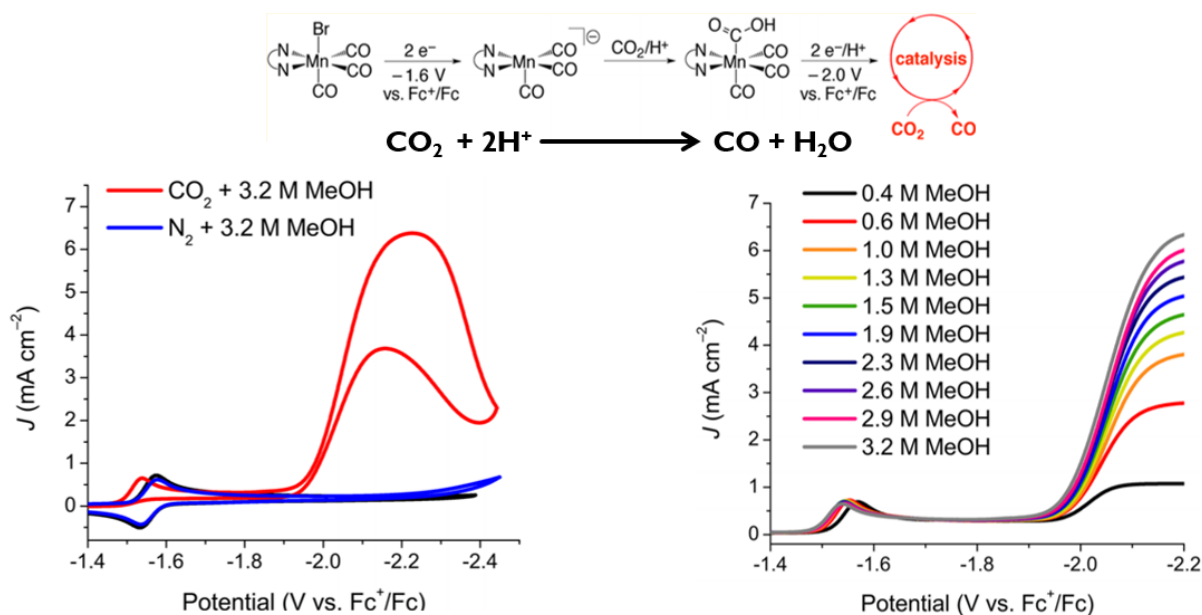


Figure 5-4: Left: Cyclic voltammograms (CVs) showing catalytic current for 1 mM $[\text{Mn}(\text{mesbpy})(\text{CO})_3(\text{MeCN})](\text{OTf})$ under CO_2 with added MeOH (red). This current increase is due solely to the electrocatalytic reduction of CO_2 to CO. Under N_2 with added MeOH, no current increase is observed (blue), which is like the CV under CO_2 with no added MeOH (black). Right: Linear scan voltammograms showing the electrocatalytic reduction of CO_2 to CO by 1 mM $[\text{Mn}(\text{mesbpy})(\text{CO})_3(\text{MeCN})]^+(\text{OTf})^-$ in 0.1 M TBAPF₆/MeCN with addition of MeOH. The solution is saturated with (~ 0.28 M), CO_2 .

In 1996, Saveant and co-workers reported that the addition of Lewis acidic metal cations increased the rate of CO_2 reduction by iron tetraphenylporphyrin catalysts. The Lewis acid was reported to promote cleavage of one C–O bond of the reduced Fe– CO_2 intermediate to generate CO and CO_3^{2-} as the side product more efficiently and improve the stability and activity of the 2-

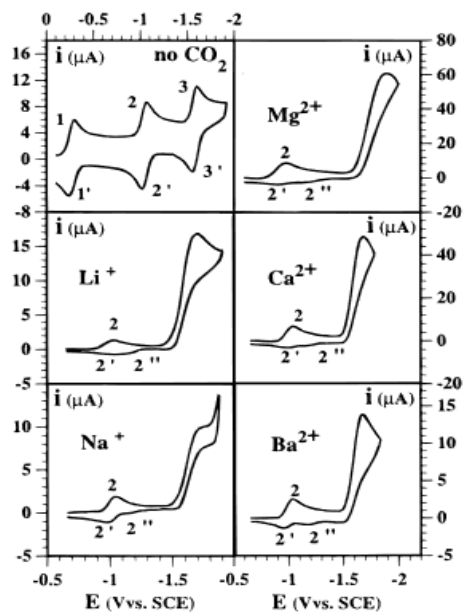


Figure 5-5: Saveant reported CVs of TPPFe(III)Cl in DMF with various Lewis acids.

electron catalytic reduction. Such behavior was observed with the presence of Mg^{2+} , Li^+ , Ca^{2+} , Na^+ and Ba^{2+} (Figure 5-5).¹⁶

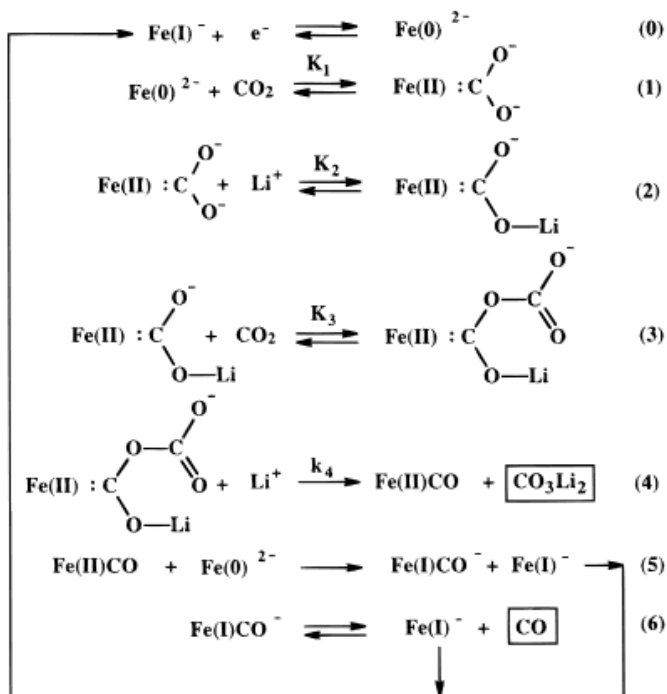


Figure 5-6: Saveant reported mechanism of TPPFe(III)Cl in DMF with various Lewis acids.

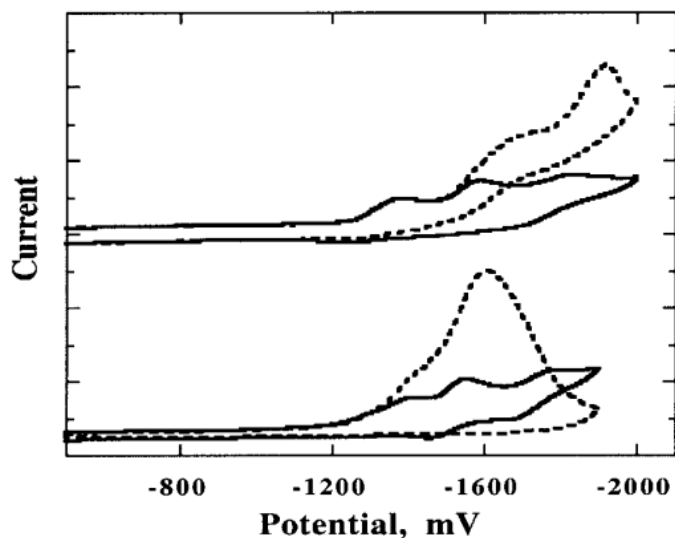


Figure 5-7: Fujita reported CV of $[\text{Ru}(\text{bpy})_2(\text{CO})\text{Cl}]^-$ in CH_3CN . Solid line: under Ar; dotted line: under CO_2 ; top: with Pr_4NClO_4 ; bottom: with LiClO_4 .

A similar observation was also observed by Fujita's group in 2002 where the presence of Ru catalyst, $[\text{Ru}(\text{bpy})_2(\text{CO})\text{Cl}]^-$ and Lewis acid, Pr_4NClO_4 and LiClO_4 lowered the overpotential and increase TOF (Figure 5-7).¹⁷

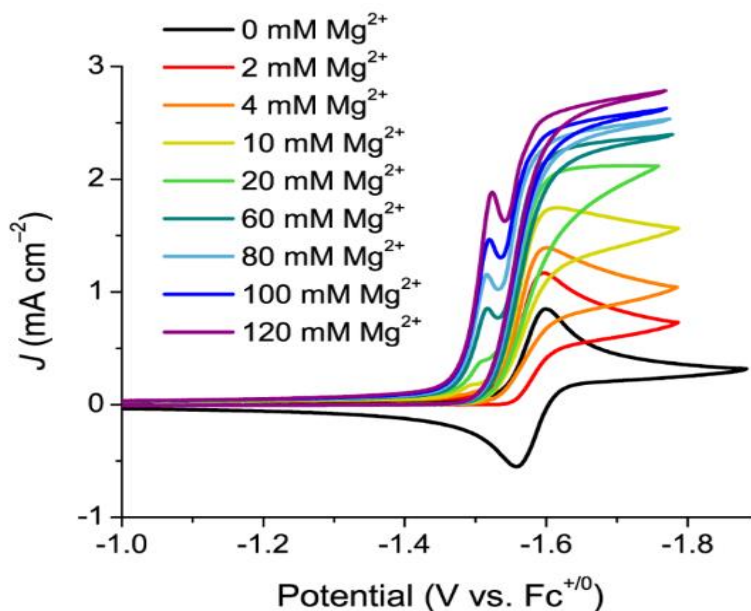


Figure 5-8: Sampson reported CVs of 1 mM $[\text{Mn}(\text{mesbpy})(\text{CO})_3(\text{MeCN})](\text{OTf})$ under CO_2 with varying concentrations of Mg^{2+} , showing electrocatalytic reduction of CO_2 .

Formal Kubiak lab member Dr. Sampson's work demonstrated that the addition of Lewis acid also provided a positive influence in $[\text{Mn}(\text{mes-bpy})(\text{CO})_3(\text{Br})]^+$ (**5-4**) and $[\text{Mn}(\text{mes-bpy})(\text{CO})_3(\text{MeCN})]^+$ (**5-5**) CO_2 reduction performance. It was observed that the reduction overpotential at $-1.6 \text{ V vs. Fc}^{0/+}$ and the catalytic current increased along with the addition Mg^+ (Figure 5-8).¹⁸ However, a significant drawback of the Mg^{2+} co-catalyzed system is the formation of insoluble MgCO_3 . Precipitation of MgCO_3 changes the overall thermodynamics of the reaction, which infers a change in the kinetics of catalysis to an extent that is difficult to determine precisely (Figure 5-9).

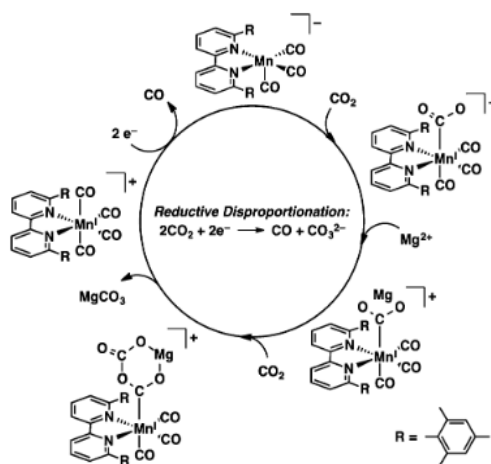
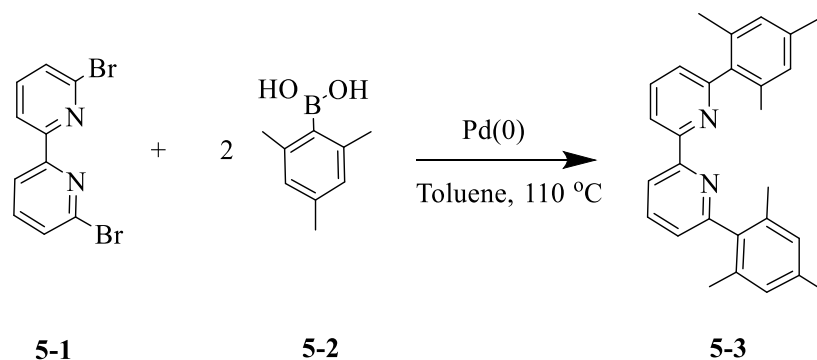


Figure 5-9: Proposed catalytic mechanism of $[\text{Mn}(\text{mesbpy})(\text{CO})_3]$ with CO_2 and Mg^{2+} at -1.5 V versus $\text{Fc}^{+/0}$, showing an overall catalytic reaction of $2\text{CO}_2 + 2e^- \rightarrow \text{CO} + \text{CO}_3^{2-}$.

One way to obviate the sacrificial use of Mg is to employ soluble Lewis acid agents that do not combine irreversibly with CO_3^{2-} . The idea is to use chelated Lewis acids that could function as the co-catalyst and disfavor the formation of precipitates with carbonate which was explored and presented in this work.

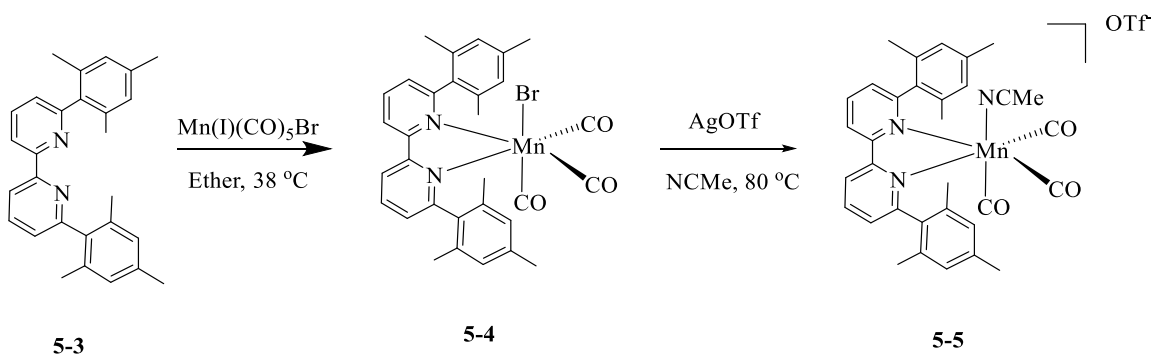
II. Synthesis of Mn complex with bulky bipyridine ligand, cyclam and cyclam chelated zinc complexes.

The importance of bulky bipyridine was verified by Dr. Sampson. One electron reduction of the $\text{Mn}(\text{bpy-R})(\text{CO})_3\text{X}$ without bulky bipyridine ligand results a rapid dimerization after the cleavage of X (X = halogen or solvent molecule with counter-anion), which limits the activity of the Mn catalyst. The reasoning was that the bulky substituent would inhibit such dimerization.¹⁵



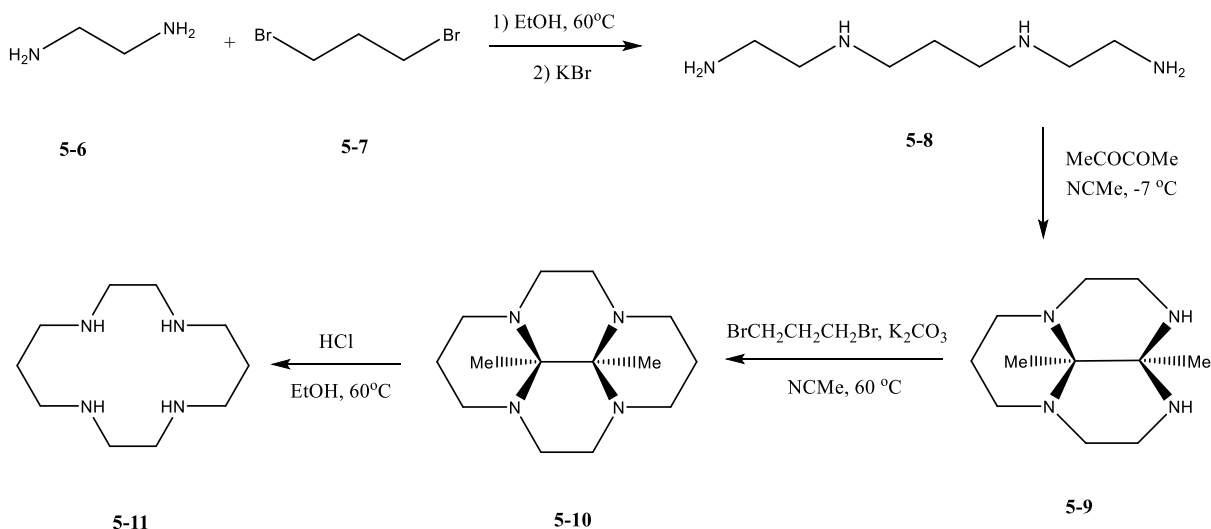
Scheme 5-1: Synthesis of 6,6'-Dimesityl-2,2'-bipyridine.

6,6'-Dimesityl-2,2'-bipyridine (mes-bpy) (**5-3**) was synthesized via a Suzuki coupling by refluxing 6,6'-dibromo-2,2'-bipyridine (**5-1**) and 2,4,6-trimethylphenylboronic acid (**5-2**) (Scheme 5-1). Complex $[\text{Mn}(\text{mes-bpy})(\text{CO})_3(\text{Br})]$ (**5-4**) was then synthesized by refluxing the ether

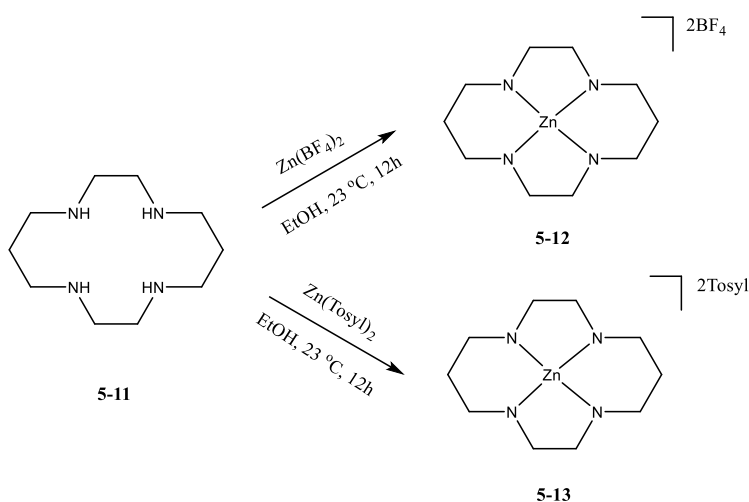


Scheme 5-2: Synthesis of $[\text{Mn}(\text{mes-bpy})(\text{CO})_3(\text{Br})]$ and $[\text{Mn}(\text{mes-bpy})(\text{CO})_3(\text{MeCN})]^+$.

solution containing **5-3** and $\text{Mn(I)CO}_5\text{Br}$. Another Mn catalyst precursor $[\text{Mn}(\text{mes-bpy})(\text{CO})_3(\text{MeCN})]^+$ (**5-5**) was then synthesized by refluxing **5-5** with AgOTf in acetonitrile (Scheme 5-2).¹⁵



Cyclam (**5-11**) was chosen as the candidate for the Lewis acid chelator due to its axially exposed coordination environment to metals and its high stability.¹⁹ Hypothetically, the Lewis acid cations in solution would stay in its chelated form with cyclam that prevents the formation of the carbonate precipitate. Cyclam was synthesized via a multistep synthetic route in 15 % yield.



Zinc, as a well-studied Lewis acid, has been reported in various reactions and catalysis.^{20,21} We synthesized cyclam chelated zinc complex by reacting **5-11** with the zinc salt in EtOH (Scheme 5-4). Two zinc complexes with different counterions were synthesized: $[\text{Zn}^{2+}(\text{cyclam})][\text{BF}_4]_2$ (**5-12**) and $[\text{Zn}^{2+}(\text{cyclam})][\text{Tosyl}]_2$ (**5-13**). Their structures were confirmed via X-ray analysis of grown crystals in an EtOH/ether mixture (Figure 5-10). Crystallographic data indicate that the Zn atoms lie at the center of an idealized octahedral geometry with the coordination of solvent molecules in the axial positions (Figure 5-10) and the four nitrogen bonded hydrogen atoms having a typical trans-SSRR configuration in both cases.²² Metal-solvent bonds in the axial position in **5-12** are 2.331 Å, which indicates an expectedly weak binding interaction between the Zn center and the solvent molecules. However, the metal solvent bonds seemed to be much stronger in the case of **5-13** with a length of 2.158 Å.

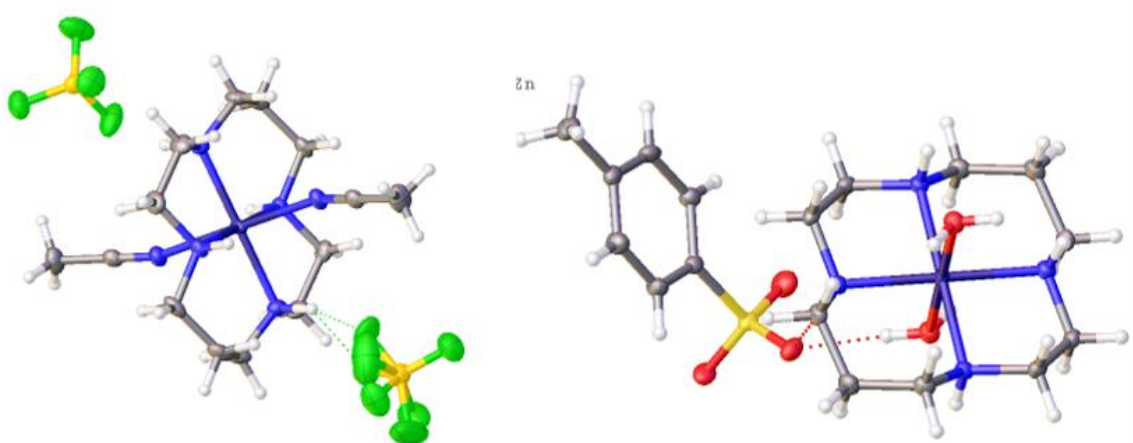


Figure 5-10: X-Ray crystal structure of the main isomers of **5-12** (left) and **5-13**(right).

III. Cyclic voltammetry study of Zn catalyzed Mn CO₂ electroreduction system.

In this study, polished glassy carbon was chosen as the working electrode, a platinum rod served as the counter electrode and the reference electrode was Ag / AgCl. The ferrocene redox peak was recorded manually as reference. We used degassed dry acetonitrile as solvent because its reduction potential does not interference with the catalysis region. The solution also contained 0.1 M of TBAPF₆ as electrolyte. In the case of **5-13**, No redox activity was observed within the catalysis region under argon or CO₂ (Figure 5-11 left), indicating that **5-12** alone does not facilitate CO₂ reduction or Zn²⁺ to Zn reduction.

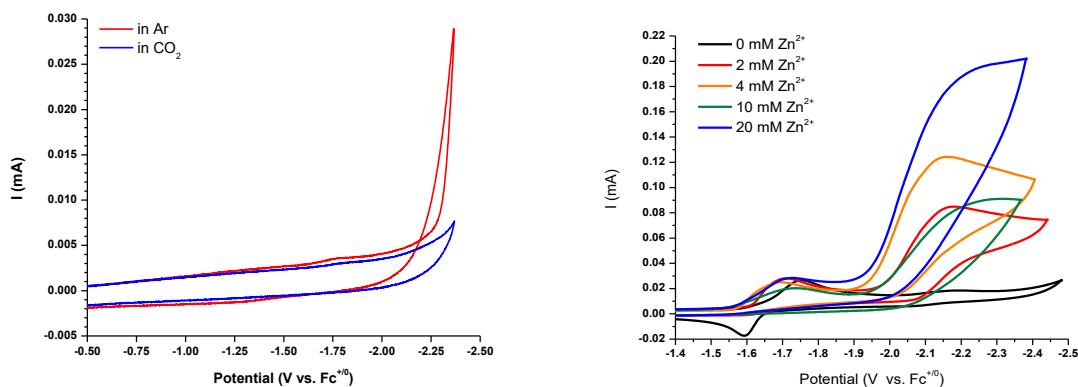


Figure 5-11: Left: CVs of 10 mM of **5-13** under Ar (blue), under CO₂ (red) in acetonitrile. Right: CVs of 1 mM **5-4** under CO₂ with varying concentrations of **5-13**, showing electrocatalytic reduction of CO₂.

We then introduced **5-13** in a variety of concentrations as cocatalyst with 0.1 M **5-4** in CO₂ saturated acetonitrile solution. Although a decrease in CO₂ reduction potential was observed at -1.7 V vs. Fc⁺⁰, the catalytic current was not amplified with the increase in **5-13** concentration (Figure 5-11 right). This was believed to be due to the poor solubility of **5-13** in acetonitrile. Thus, we do not believe that **5-13** may serve as the cocatalyst as we expected.

A much more encouraging result was given using **5-12**. Under a CO₂ atmosphere and without **5-12**, **5-4** showed a response similar to that observed under Ar without a proton source or Lewis acid, previously reported by Sampson. With the addition of **5-12**, a significant increase of current occurs at -1.6 V vs. Fc⁺⁰ which corresponds to the electrocatalytic reduction of CO₂ to CO as verified by controlled potential electrolysis *vide infra*. There were also no reductive features within this potential window for **5-12** in the absence of Mn catalyst under either Ar or CO₂ atmosphere, indicating that **5-12** alone does not mediate CO₂ reduction (Figure 5-12 left). Furthermore, the critical role of the cyclam ligand was verified by examining the CV behavior of

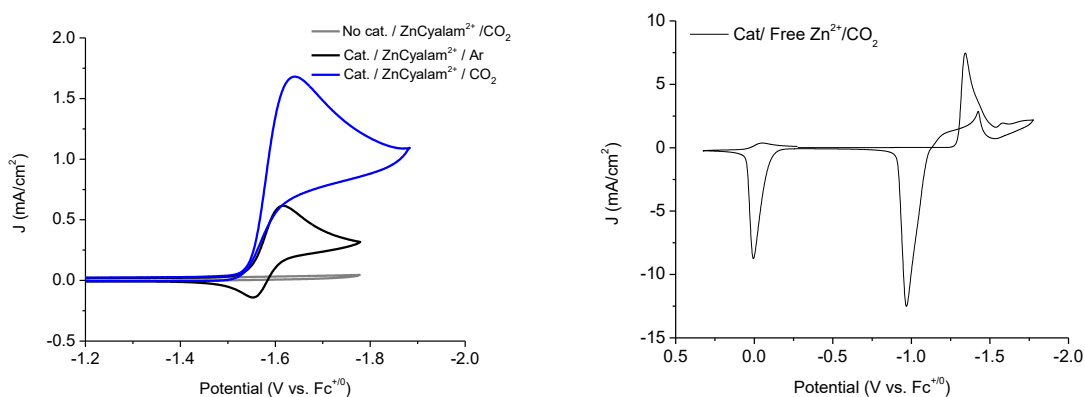


Figure 5-12: Left: CVs of 1 mM **5-4** with 10 mM of **5-12** under Ar (black), with 10 mM of **5-12** under CO₂ (blue). 10 mM **5-12** under CO₂ is shown in gray. Right: CVs of 1 mM **5-4** under CO₂ with free Zn²⁺ (Zn(BF₄)₂).

5-4 with free Zn²⁺, added to solution as Zn(BF₄)₂. Without the chelating ligand, Zn²⁺ was reduced to Zn metal at -1.35 vs. Fc⁺⁰, more positive than the CO₂ binding potential (Figure 5-12 right).

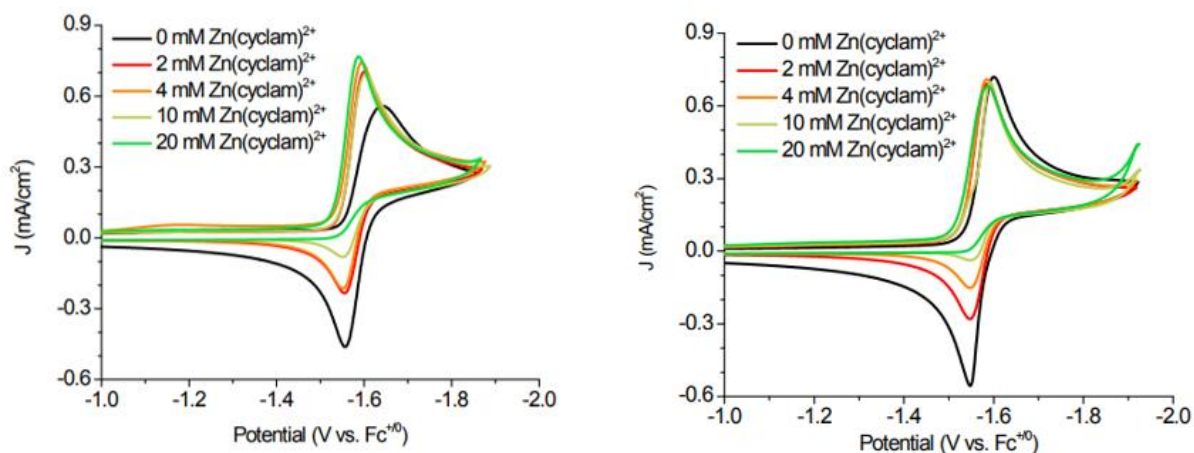


Figure 5-14: CVs of 1 mM **5-4** (left) and **5-5** (right) under Ar with varying concentrations of **5-12**.

Further addition of **5-12** up to 30 mM with the presence of **5-4** or **5-5** resulted in greater catalytic current densities at the same potential under CO₂ atmosphere (Figure 5-14). Linear dependence between the catalytic current and the concentration of **5-12** was observed with the current saturation at 30 mM, above which no additional increase in current density occurred. This behavior is indicative of saturation kinetics. No catalytic current was observed at the same conditions under inert atmosphere.

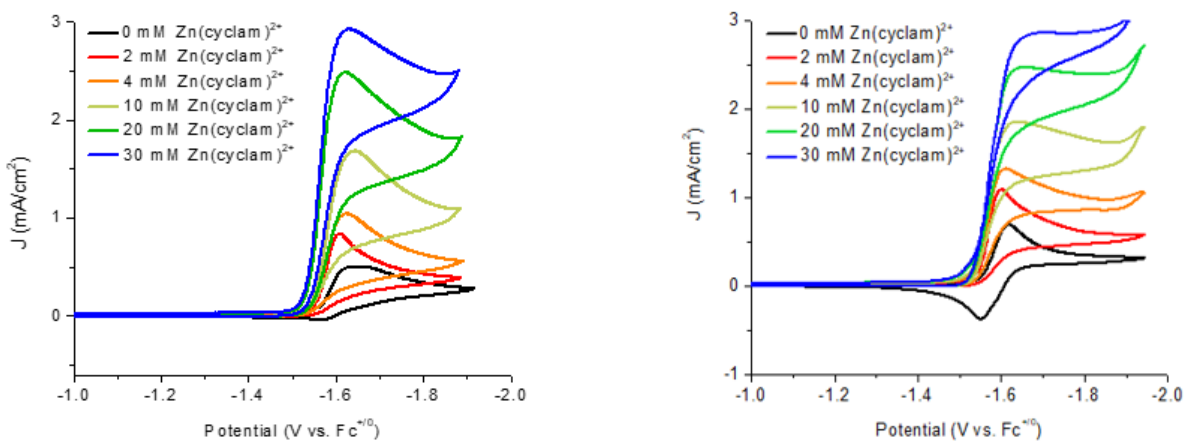


Figure 5-13: CVs of 1 mM **5-4** (left) or **5-5** (right) under CO₂ with varying concentrations of **5-12**, showing electrocatalytic reduction of CO₂.

There was no current enhancement under argon in the presence of **5-12**, neither with catalyst **5-4** nor **5-5**. Furthermore, as the concentration of **5-12** increased, the anodic wave gradually decreased until a full loss of reversibility above 20 mM **5-12**. This finding is consistent with the previously described binding that occurred between Mg^{2+} and the catalysts **5-4** or **5-5** once the catalyst was doubly reduced under N_2 atmosphere.

The turnover frequency (TOF) for electrocatalytic CO_2 reduction can be estimated from the catalytic current enhancement i_{cat}/i_p , the ratio of the maximum catalytic current i_{cat} to the peak current i_p in absence of a substrate. With 30 mM of **5-12**, i_{cat}/i_p is determined to be 1.5, at a scan rate 3.2 V s^{-1} from which the catalytic TOF is estimated to be 105 s^{-1} (Figure 5-15),^{23,24} calculated from the formula:

$$TOF = 0.1992 \frac{Fv}{RT} \frac{n_p^3}{n_{\text{cat}}^2} \frac{i_{\text{cat}}^2}{i_p^2}$$

In the previous study of **1** and **2** with Mg^{2+} as the Lewis acid additive a lower catalytic rate for CO_2 reduction was achieved, with the addition of 120 mM Mg^{2+} (TOF = 20 s^{-1}).¹⁸ This further supports that the **5-12** in this study behaves as a co-catalyst, and not as a sacrificial additive.

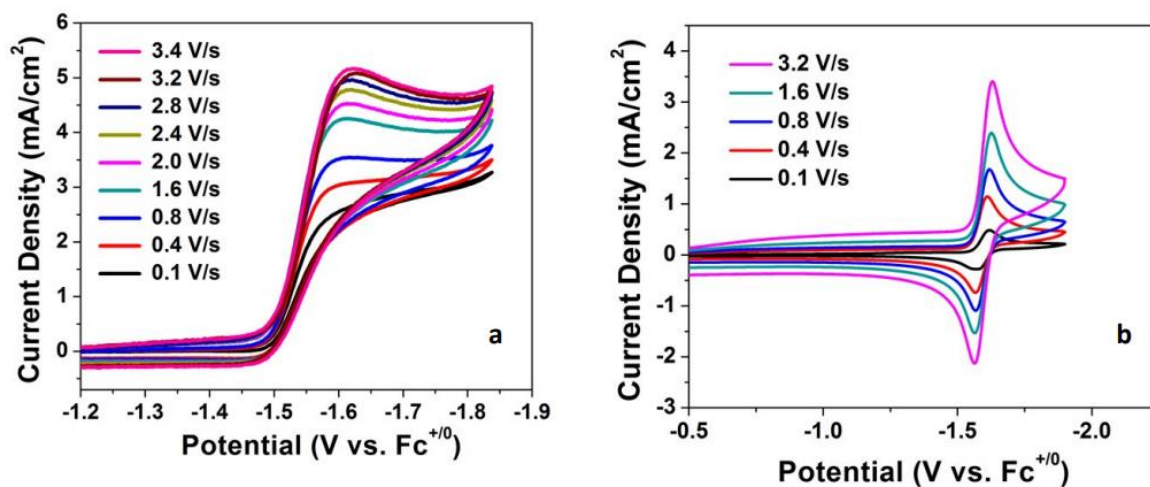


Figure 5-15: CV of 1 mM of **5-5** with 30 mM of **5-12** under CO_2 (left) and under N_2 without a substrate (right) in 0.1 M TBAPF₆/MeCN at various scan rates (0.1 – 3.4 V/s).

IV. Controlled potential electrolysis (CPE) study.

Controlled potential electrolysis (CPE) was used to confirm that the origin of the catalytic current enhancement is indeed electrocatalytic CO₂ reduction to CO. CPE studies were performed with 0.5 mM of catalyst **5-4** or **5-5** and 30 mM of **5-12** at -1.6 V versus Fc⁺⁰ in dry acetonitrile under CO₂ atmosphere. Gas chromatography analysis was performed after 6 h of electrolysis and indicated that CO gas was generated with a Faradaic efficiency of 84 % and 80 % for complex 1 and 2, respectively (Table 5-1). During 6 hours of electrolysis under these conditions, no insoluble

Table 5-1: Result of CPE experiments with **5-12** added. Performed under CO₂ with 1 mM of cat. **5-4** or **5-5** and 30 mM of **5-12**. Potentials are reported vs. Fc⁺⁰.

	Potential (V vs. Fc)	TON	FE CO
1 mM 5-4 /30 mM 5-12	-1.6	22	80 %
1 mM 5-5 /30 mM 5-12	-1.6	32	84 %
30 mM 5-12	-1.6	0	0

precipitate was observed (Figure 5-16), and no sacrificial Zn electrode was needed to maintain electrocatalysis. Additional Controlled Potential Electrolysis (CPE) experiments were performed

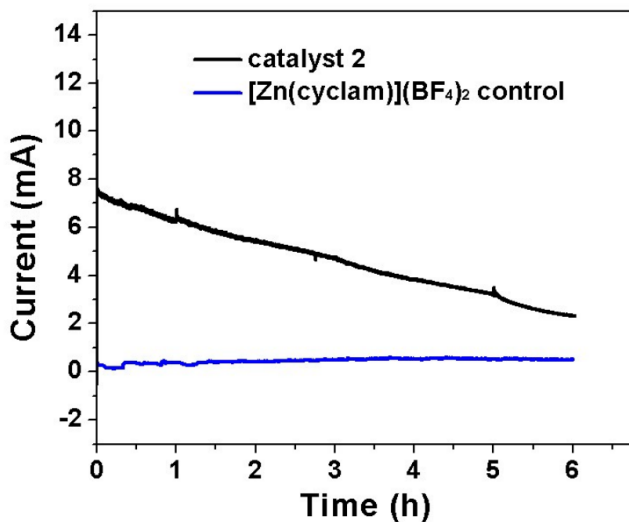


Figure 5-16: CPE current density over time for 0.5 mM of **5-5** under CO₂ with 30 mM of **5-12**. Conditions: potential = -1.6 V vs. Fc⁺⁰.

without the Mn catalyst but in the presence of 30 mM **5-12**. No CO gas was detected after 6 h of electrolysis in this experiment.

V. Examinations on other cyclam chelated Lewis acid with Mn catalyst.

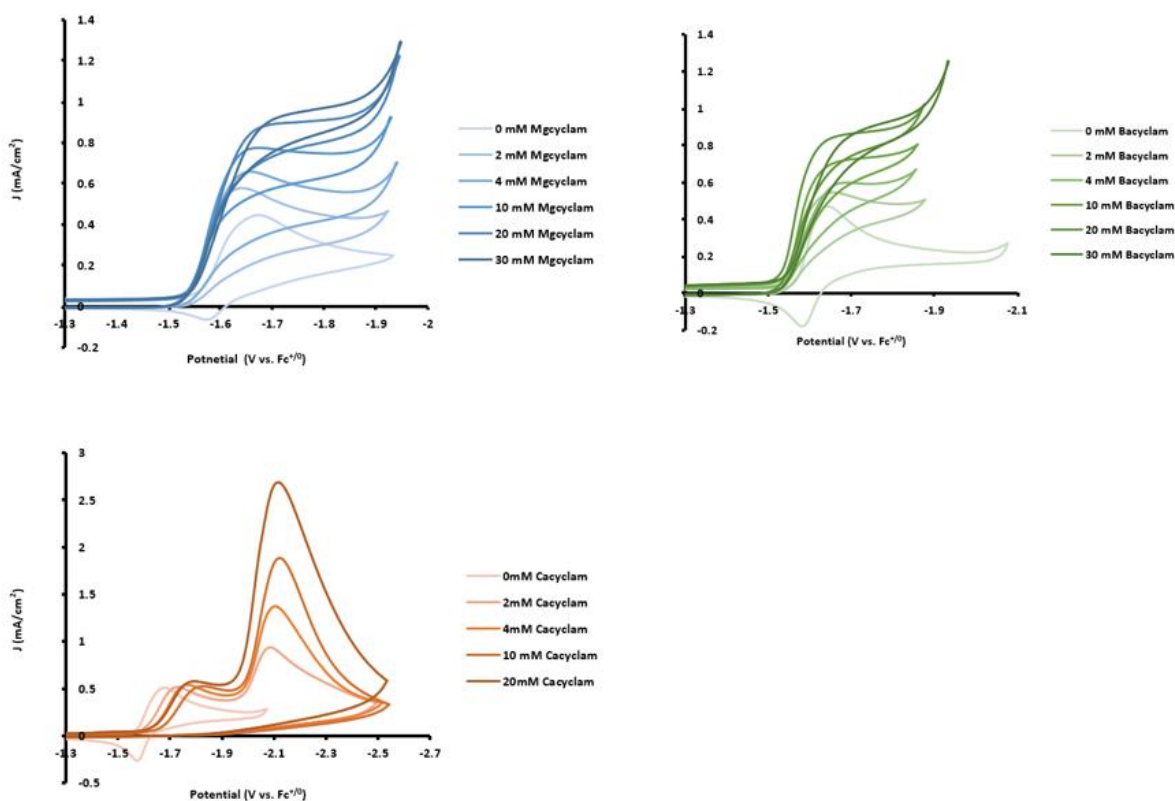


Figure 5-17: CVs of 1 mM **Mgcyclam** (top left), **Bacyclam** (top right) or **Cacyclam** (bot) under CO₂ with varying concentrations of **5-12**, showing electrocatalytic reduction of CO₂.

Although Zn cyclam yielded a promising cocatalyst application, we were still interested in investigating other possibilities in other Lewis acid candidates. Mg(cyclam), Ca(cyclam) and

Ba(cyclam) were synthesized in a similar fashion. CV studies were performed within a 0.1 M Cat **5-4** in acetonitrile solution with various concentrations (Figure 5-17).

As expected, in all three cases we observed a co-catalysis activity in current. However, a large quantity of precipitate was formed, these we believed to be the carbonate side products. This indicated the weak binding between the metal center and the cyclam ligand. On the other hand, current densities were significantly lower than the case of **5-12** indicating a much weaker catalytic activity. Thus, based on these investigations, we believe that **5-12** in Mn catalyst/Lewis acid co-catalyst gives the most satisfying performance.

VI. Conclusions and Future Outlook

In this work we described an improved system for the homogeneous reduction of CO₂ to CO by Mn mes-bipyridine catalyst and Lewis acid. Utilization of [Zn(cyclam)]²⁺ as a Lewis acid enhanced catalytic performance of catalysts **5-4** and **5-5** under CO₂ in anhydrous conditions. The strong chelating properties of cyclam prevented the formation of metal carbonate that precipitated from the solution in the previously reported system. CPE experiments showed that CO was the only gaseous product even without the implementation of a sacrificial anode. These findings show that the use of co-catalysts to activate CO₂ during electrochemical reduction is a viable strategy for lowering overpotential and maintaining selectivity.

VII. Experimental.

1. General procedures and instrumentals.

Electrochemistry (CV): Electrochemical experiments were carried out using a BASi Epsilon potentiostat. A glassy carbon electrode was used as a working electrode (3 mm in diameter), with a Pt wire as a counter electrode and Ag/AgCl wire with the vycor tip as a reference electrode. Ferrocene was added as an internal reference. All electrochemical experiments were performed with 0.1 M TBAPF6 electrolyte solution in MeCN. The cell was shielded from light with aluminum foil during all the electrochemical experiments and the solutions were degassed with Ar or CO₂. CO₂ electrocatalysis experiments were carried out with CO₂ at gas saturation, 0.28M. All electrochemical data were compensated for the iR drop.

Control potential electrolysis (CPE): CPE experiments were carried out in a 64 mL 4 neck electro cell designed by Gamry. A carbon rod electrode was used as a working electrode, a Pt wire in the form of a spool with high surface area was used as a counter electrode and was separated from the solution by a porous glass frit and the Ag/AgCl reference electrode was separated from the solution by a Vycor tip. The electrocatalyst and the Lewis acid were dissolved in 30 mL of 0.1 M TBAPF6 solution in dry acetonitrile, and purged with CO₂ for at least 20 min. The cell was wrapped with aluminum foil and stirred throughout the entire experiment. A Hewlett-Packard 7890A series gas chromatograph and 1 ml glass syringe were used for gas analysis for all CPE experiments.

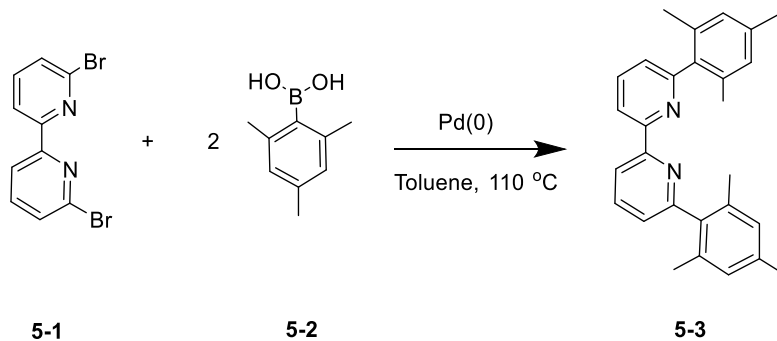
X-ray diffraction: The single crystal X-ray diffraction studies were carried out on a Bruker Kappa APEX-II CCD diffractometer equipped with molybdenum K α radiation ($\lambda = 0.71073 \text{ \AA}$). The crystals were mounted on a Cryoloop with Paratone oil and data were collected under a nitrogen gas stream at 100 K using ω and ϕ scans. Data were integrated and scaled using the Bruker

SAINT software program. Solution by direct methods (SHELXS) produced a complete phasing model consistent with the proposed structure. All non-hydrogen atoms were refined anisotropically by full-matrix least squares (SHELXL-97). All hydrogen atoms were placed using a riding model. Their positions were constrained relative to their parent atom using the appropriate HFIX command in SHELXL-97. Crystallographic data and structure refinement parameters are summarized in the supporting information.

Nuclear magnetic resonance (NMR), mass spectrum and microanalyses: ^1H NMR spectra were collected on Varian 300 MHz instruments. ^1H NMR chemical shifts (δ) were reported in parts per million (ppm) and referenced to the residual solvent peak. High/low resolution mass spectra analyses were performed at the mass spectrometer facility at UC San Diego. Microanalyses were performed by NuMega resonance lab, LLC (San Diego, CA) for C, H, and N.

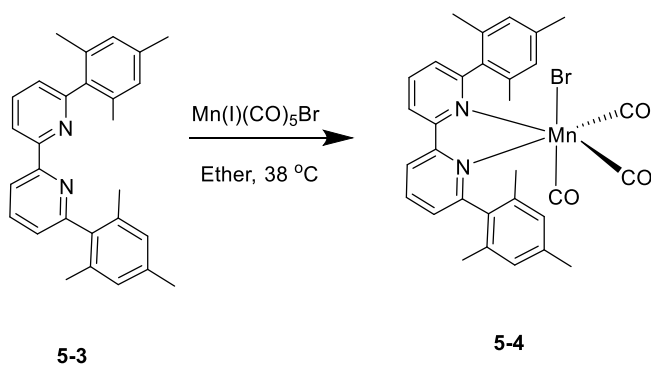
2. Synthesis and characterizations.

6,6'-Dimesityl-2,2'-bipyridine (5-3): 6,6'-dibromo-2,2'-bipyridine (1.00 g, 3.18 mmol) and 2,4,6-trimethylphenylboronic acid (1.50 g, 9.19 mmol) were added to 50 mL degassed dry

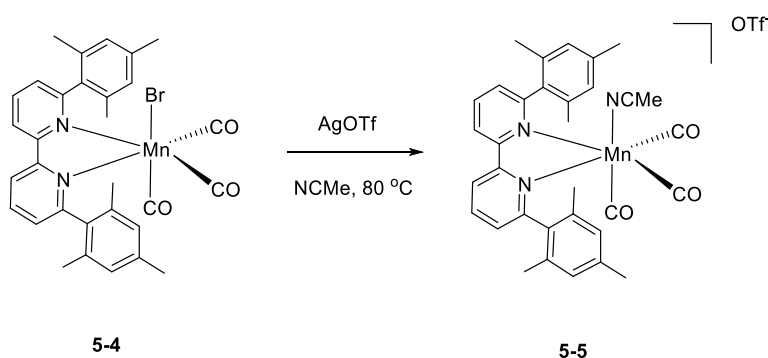


toluene. Na_2CO_3 and $\text{Pd}(\text{PPh}_3)_4$ (2.3% mol cat.) were then added to the reaction mixture. Then the mixture was refluxed for 72 h under argon. After cooling to ambient temperature, the organic layer containing the product was washed with brine, and the aqueous layer was washed with chloroform. The organic fractions were combined, and all the volatiles were removed via rotary evaporation. The resulting crude solid was dissolved in a minimal amount of hot chloroform and filtered. Methanol was added until a white precipitate was formed from the filtrate. The white precipitate was filtered and dried overnight under vacuum at 80 °C. The yield of pure product was 0.51 g (59%). ^1H NMR resonances exhibited results identical to those of previous reports.¹⁵

Mn(mesbpy)(CO)₃ Br (5-4): $\text{Mn}(\text{CO})_5\text{Br}$ (100 mg, 0.35 mmol) and **5-3** (100 mg, 0.25 mmol) was added to a 50 mL of diethyl ether. After refluxing for 2 hours, the precipitate had formed. The mixture was cooled to room temperature, and the precipitate was filtered off and washed with diethyl ether. The product was dried overnight under vacuum obtained at a yield of 50% (79.7 mg). ^1H NMR resonances exhibited results identical to those of previous reports.¹⁵

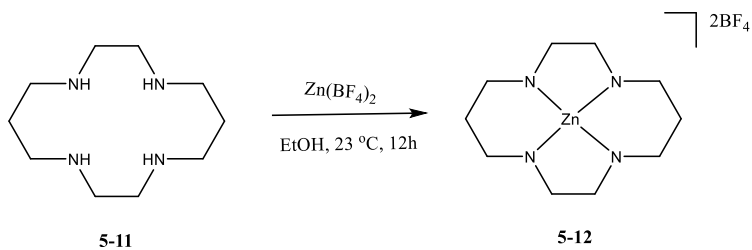


[Mn(mesbpy)(CO)₃(MeCN)](OTf) (5-5): **5-4** (150 mg, 0.25 mmol) and AgOTf (70.0 mg, 0.29 mmol) were refluxed in 10 mL of dry MeCN under an inert atmosphere for 20 h in the dark. The brown solid formed during reflux was then removed, filtered, and dried under rotary evaporation, followed by flash chromatography with a Teledyne CombiFlash Rf by passing the mixture through a basic alumina column with MeCN as the eluent. Product was collected at a yield of 70% (120 mg). ¹H NMR resonances exhibited results identical to those of previous reports.¹⁵



[Zn(cyclam)]²⁺ (BF₄)₂ (5-12): 0.41 g of 1,4,8,11-tetraazacyclotetradecane (2.05 mmol) was dissolved in 15 mL of ethanol (solution 1) and 0.48 g of zinc tetrafluoroborate (2.01 mmol) was dissolved in 20 mL of ethanol (solution 2). Solution 2 was added to the solution 1 dropwise and the combined solution was stirred overnight under reflux. Ethanol was removed under rotary evaporation. The white solid was then dissolved in acetonitrile and filtered. Diethyl ether was added to the filtrate until the white precipitate was evident. The resulting white solid (74% yield) was then dried under vacuum overnight. Crystal for X-ray diffraction analysis was obtained by vapor diffusion of ether into the product contained in ethanol solution. ¹H NMR (300 MHz, CD₃CN) δ : 1.56 ppm (s, 4H, NH), 4.00-2.51 ppm (m, 20H, CH₂). ¹⁵N NMR (300 MHz, CD₃CN) δ : 4.56

ppm (s, 4N). Anal. Calcd for **5-12**, C₁₃H₂₈N₄Zn₁: C, 27.37; H, 5.56; N, 12.77. Found: C, 27.34; H, 5.51; N, 12.75. LRMS (EI): Calcd for (C₁₃H₂₈N₄Zn₁): 304.16, found 303.17.



3. ^1H and ^{13}C NMR Spectroscopic Data.

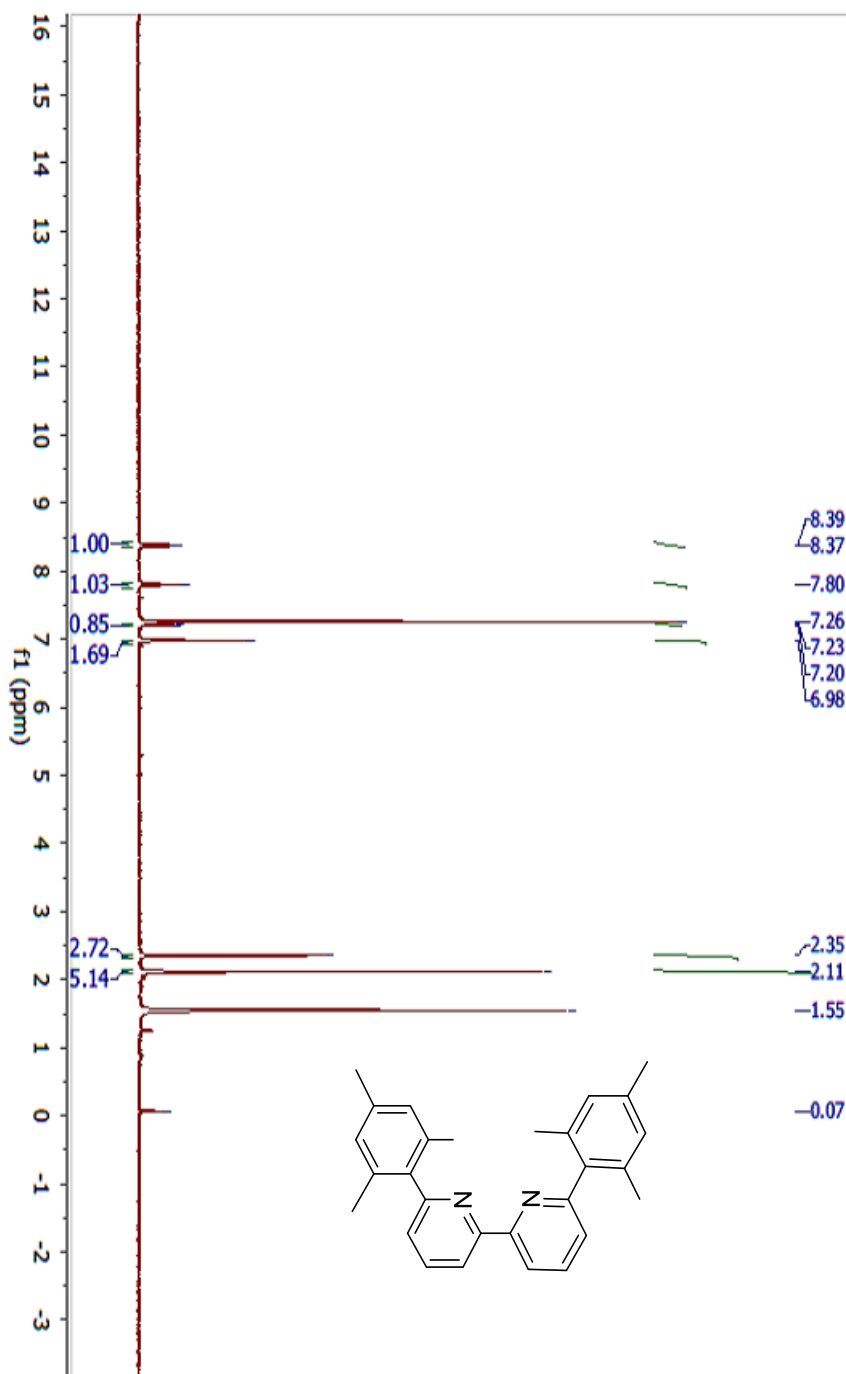


Figure 5-18: 5-3 ^1H NMR spectrum (CDCl_3 , 300 MHz).

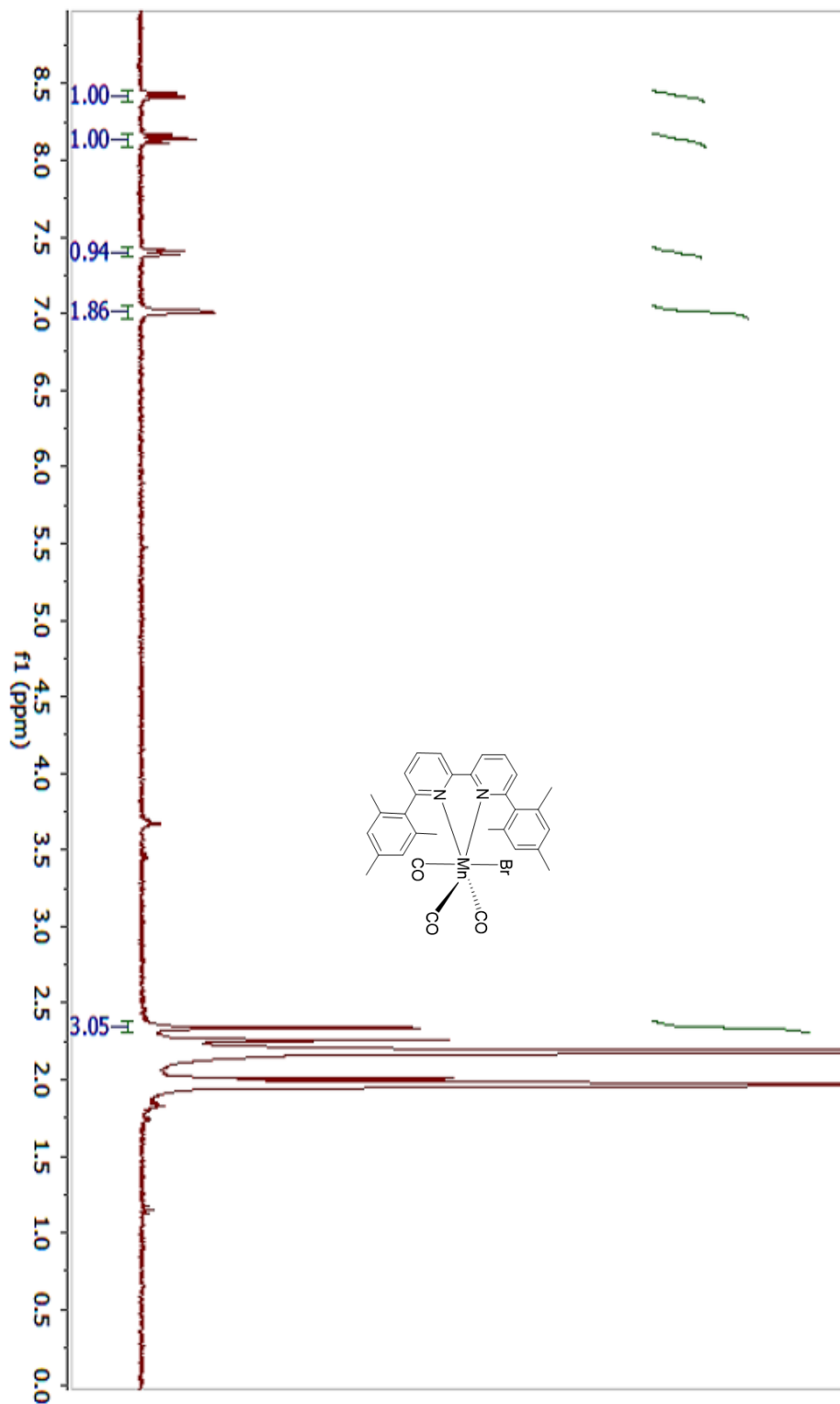


Figure 5-19: 5-4 ^1H NMR spectrum (CD_3CN , 300 MHz).

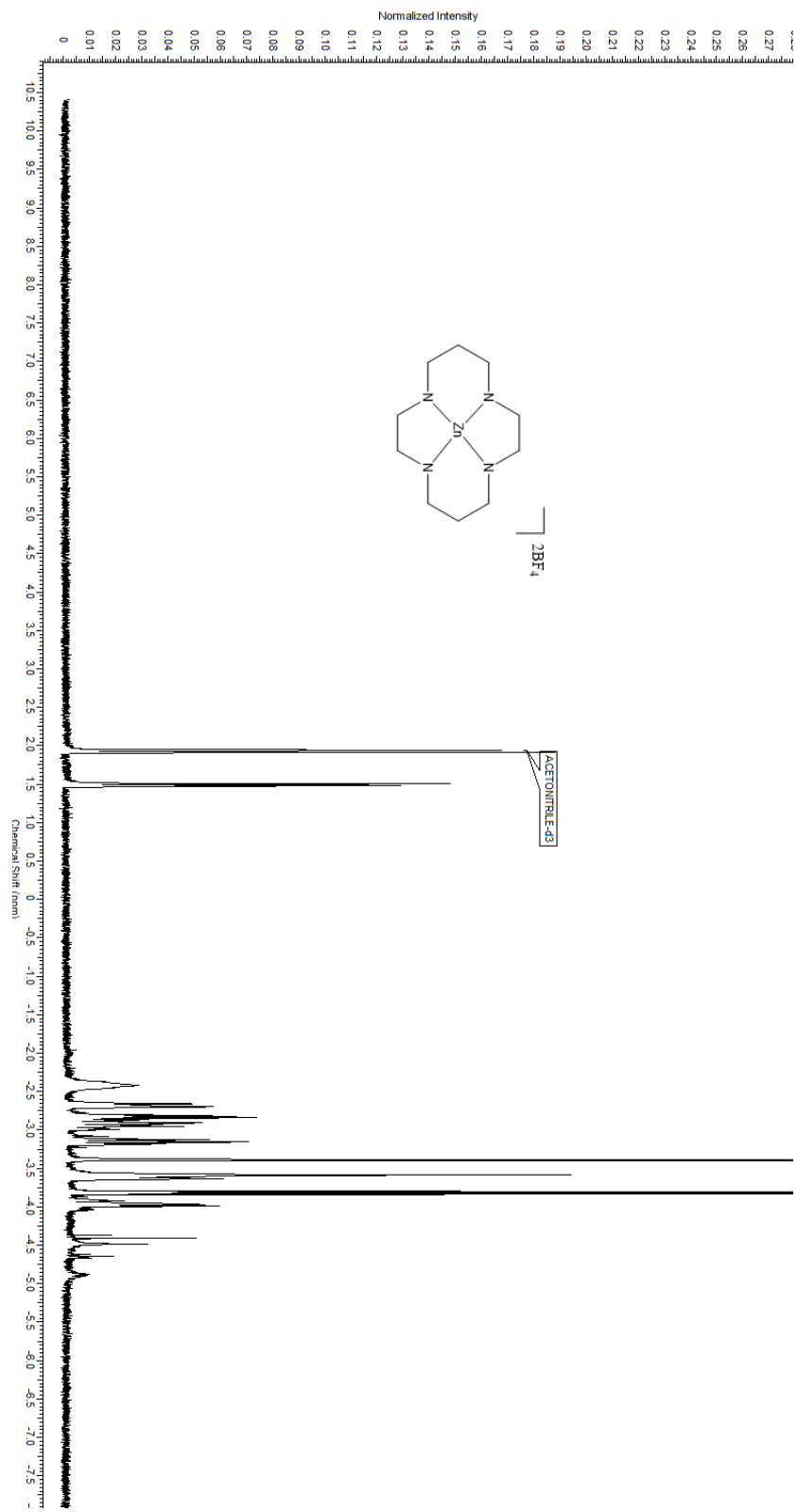


Figure 5-20: 5-12 ¹H NMR spectrum (CD₃CN, 300 MHz).

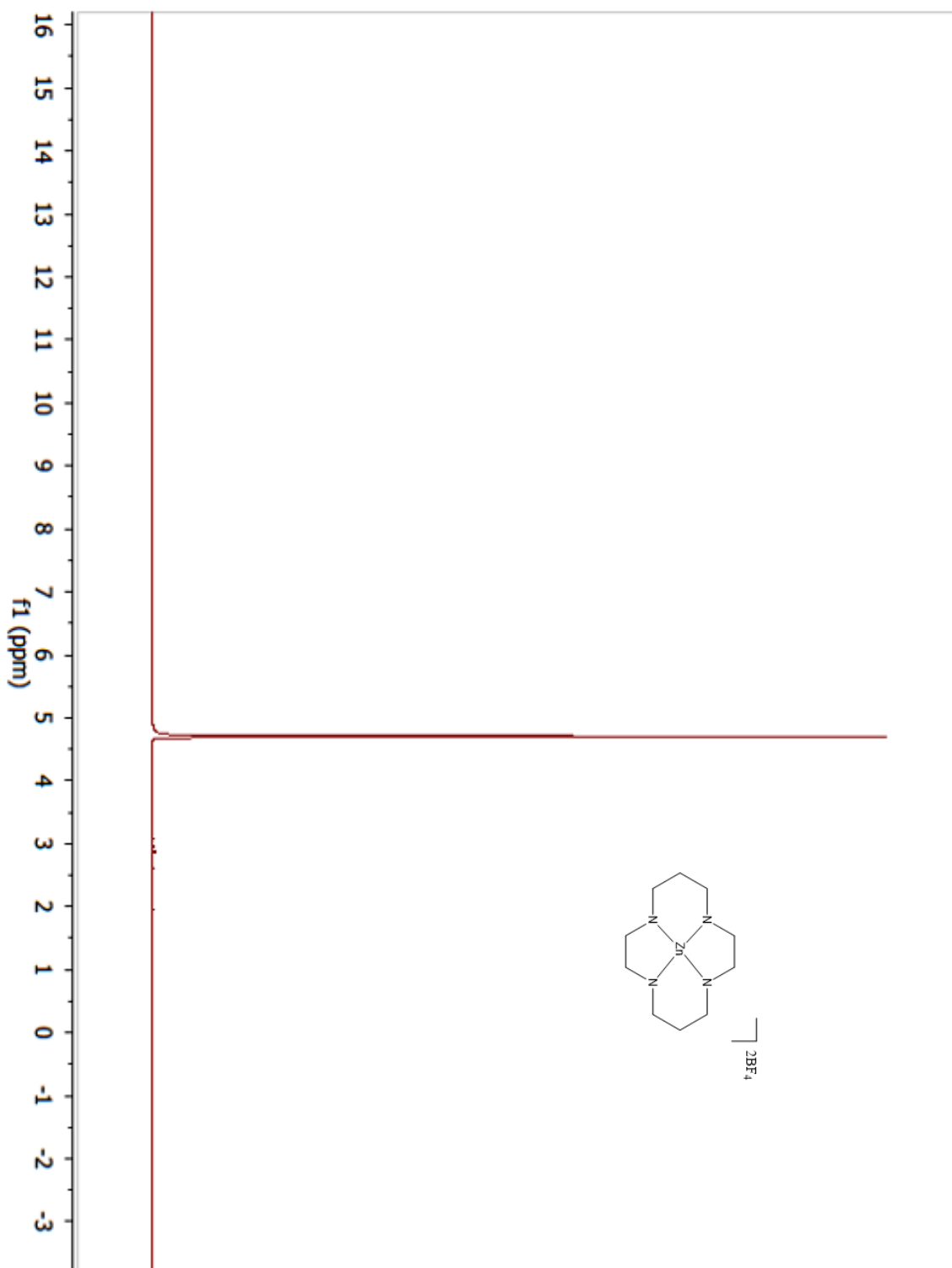


Figure 5-21: 5-12 ^{15}N NMR spectrum (CD_3CN , 300 MHz).

4. X-ray crystallographic summary and ORTEPS for characterized structures

General Experimental for X-ray Structure Determinations.

The single crystal X-ray diffraction studies were carried out on a Bruker Kappa APEX-II CCD diffractometer equipped with molybdenum K α radiation ($\lambda = 0.71073 \text{ \AA}$). The crystals were mounted on a CryoLoop with Paratone oil and data were collected under a nitrogen gas stream at 100 K using ω and ϕ scans. Data were integrated and scaled using the Bruker SAINT software program. Solution by direct methods (SHELXS) produced a complete phasing model consistent with the proposed structure. All non-hydrogen atoms were refined anisotropically by full-matrix least squares (SHELXL-97). All hydrogen atoms were placed using a riding model. Their positions were constrained relative to their parent atom using the appropriate HFIX command in SHELXL-97. Crystallographic data and structure refinement parameters are summarized in the supporting information.

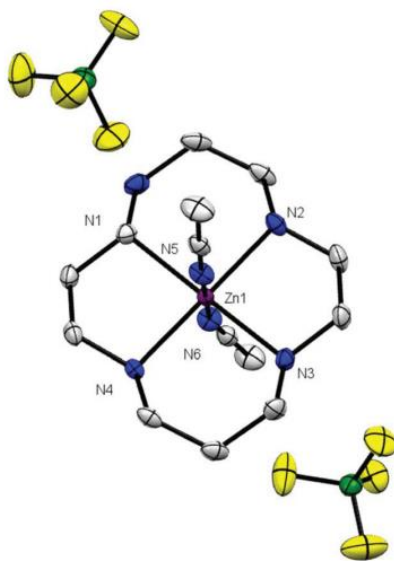


Figure 5-22: ORTEP of 5-12.

Table 5-2: Crystal data and structure refinement for **5-22**.

Identification code	p21n	
Empirical formula	C ₁₄ H ₃₀ B ₂ F ₈ N ₆ Zn	
Formula weight	521.43	
Temperature	100.0 K	
Wavelength	1.54178 Å	
Crystal system	Monoclinic	
Space group	P 1 21/n 1	
Unit cell dimensions	a = 17.4835(5) Å	a = 90°.
	b = 7.9463(2) Å	b = 114.5920(10)°.
	c = 18.0503(5) Å	g = 90°.
Volume	2280.25(11) Å ³	
Z	4	
Density (calculated)	1.519 Mg/m ³	
Absorption coefficient	2.223 mm ⁻¹	
F(000)	1072	
Crystal size	0.15 x 0.15 x 0.05 mm ³	
Theta range for data collection	2.957 to 68.268°.	
Index ranges	-21 ≤ h ≤ 21, -9 ≤ k ≤ 9, -21 ≤ l ≤ 21	
Reflections collected	36573	
Independent reflections	4171 [R(int) = 0.0470]	
Completeness to theta = 67.500°	100.0 %	
Absorption correction	Semi-empirical from equivalents	
Max. and min. transmission	0.5210 and 0.4233	
Refinement method	Full-matrix least-squares on F ²	
Data / restraints / parameters	4171 / 72 / 310	
Goodness-of-fit on F ²	1.028	
Final R indices [I > 2σ(I)]	R1 = 0.0297, wR2 = 0.0760	
R indices (all data)	R1 = 0.0325, wR2 = 0.0781	
Extinction coefficient	n/a	
Largest diff. peak and hole	0.478 and -0.426 e.Å ⁻³	

Table 5-3: Atomic coordinates ($\times 10^4$) and equivalent isotropic displacement parameters ($\text{\AA}^2 \times 10^3$) for **5-22**. $U(\text{eq})$ is defined as one third of the trace of the orthogonalized U^{ij} tensor.

	x	y	z	$U(\text{eq})$
Zn(1)	4961(1)	4888(1)	7356(1)	16(1)
N(1)	3940(1)	4975(2)	7678(1)	20(1)
N(2)	5528(1)	2819(2)	8108(1)	20(1)
N(3)	5994(1)	4803(2)	7050(1)	16(1)
N(4)	4386(1)	6953(2)	6609(1)	20(1)
N(5)	4214(1)	3124(2)	6260(1)	23(1)
N(6)	5692(1)	6601(2)	8449(1)	22(1)
C(1)	3599(1)	3324(2)	7779(1)	26(1)
C(2)	4276(1)	2204(2)	8387(1)	27(1)
C(3)	4926(1)	1510(2)	8108(1)	25(1)
C(4)	6174(1)	2220(2)	7835(1)	24(1)
C(5)	6621(1)	3737(2)	7682(1)	23(1)
C(6)	6324(1)	6473(2)	6964(1)	21(1)
C(7)	5652(1)	7580(2)	6340(1)	25(1)
C(8)	4985(1)	8262(2)	6602(1)	25(1)
C(9)	3756(1)	7571(2)	6897(1)	27(1)
C(10)	3308(1)	6067(2)	7064(1)	27(1)
C(11)	3734(1)	2639(2)	5651(1)	20(1)
C(12)	3113(1)	2029(3)	4875(1)	31(1)
C(13)	5966(1)	7152(2)	9089(1)	21(1)
C(14)	6301(1)	7873(3)	9903(1)	36(1)
F(1)	3911(1)	5981(2)	4648(1)	50(1)
F(2)	3098(1)	7844(2)	4938(1)	44(1)
F(3)	3413(1)	8300(2)	3862(1)	56(1)
F(4)	2536(1)	6177(2)	3809(1)	39(1)
B(1)	3238(1)	7078(3)	4313(1)	24(1)
F(5)	7048(1)	4031(2)	11123(1)	54(1)
B(2)	6431(1)	2924(2)	10668(1)	28(1)
F(6)	6871(2)	1455(3)	10699(2)	56(1)
F(7)	5812(2)	2655(4)	10926(2)	49(1)
F(8)	6157(2)	3577(5)	9890(1)	54(1)
F(6')	6486(4)	1542(5)	11152(3)	103(3)
F(7')	5690(2)	3713(9)	10591(3)	81(2)
F(8')	6282(2)	2339(6)	9902(2)	44(1)

Table 5-4: Bond lengths [Å] and angles [°] for **5-22**.

Zn(1)-N(1)	2.0963(14)
Zn(1)-N(2)	2.0987(14)
Zn(1)-N(3)	2.0981(14)
Zn(1)-N(4)	2.0965(14)
Zn(1)-N(5)	2.3314(15)
Zn(1)-N(6)	2.2973(15)
N(1)-H(1)	1.0000
N(1)-C(1)	1.483(2)
N(1)-C(10)	1.477(2)
N(2)-H(2)	1.0000
N(2)-C(3)	1.480(2)
N(2)-C(4)	1.484(2)
N(3)-H(3)	1.0000
N(3)-C(5)	1.476(2)
N(3)-C(6)	1.482(2)
N(4)-H(4)	1.0000
N(4)-C(8)	1.479(2)
N(4)-C(9)	1.483(2)
N(5)-C(11)	1.137(2)
N(6)-C(13)	1.139(2)
C(1)-H(1A)	0.9900
C(1)-H(1B)	0.9900
C(1)-C(2)	1.522(3)
C(2)-H(2A)	0.9900
C(2)-H(2B)	0.9900
C(2)-C(3)	1.526(3)
C(3)-H(3A)	0.9900
C(3)-H(3B)	0.9900
C(4)-H(4A)	0.9900
C(4)-H(4B)	0.9900
C(4)-C(5)	1.524(3)
C(5)-H(5A)	0.9900
C(5)-H(5B)	0.9900
C(6)-H(6A)	0.9900
C(6)-H(6B)	0.9900
C(6)-C(7)	1.524(3)
C(7)-H(7A)	0.9900
C(7)-H(7B)	0.9900
C(7)-C(8)	1.529(3)
C(8)-H(8A)	0.9900
C(8)-H(8B)	0.9900
C(9)-H(9A)	0.9900
C(9)-H(9B)	0.9900
C(9)-C(10)	1.526(3)

Table5-4: Bond lengths [Å] and angles [°] for **5-22**. Continued.

C(10)-H(10A)	0.9900
C(10)-H(10B)	0.9900
C(11)-C(12)	1.452(3)
C(12)-H(12A)	0.9800
C(12)-H(12B)	0.9800
C(12)-H(12C)	0.9800
C(13)-C(14)	1.453(3)
C(14)-H(14A)	0.9800
C(14)-H(14B)	0.9800
C(14)-H(14C)	0.9800
F(1)-B(1)	1.385(2)
F(2)-B(1)	1.391(2)
F(3)-B(1)	1.380(3)
F(4)-B(1)	1.385(3)
F(5)-B(2)	1.369(3)
B(2)-F(6)	1.387(2)
B(2)-F(7)	1.362(2)
B(2)-F(8)	1.382(2)
B(2)-F(6')	1.382(2)
B(2)-F(7')	1.393(2)
B(2)-F(8')	1.377(2)
N(1)-Zn(1)-N(2)	94.30(6)
N(1)-Zn(1)-N(3)	179.27(6)
N(1)-Zn(1)-N(4)	85.19(6)
N(1)-Zn(1)-N(5)	90.81(6)
N(1)-Zn(1)-N(6)	88.65(6)
N(2)-Zn(1)-N(5)	91.42(6)
N(2)-Zn(1)-N(6)	87.99(6)
N(3)-Zn(1)-N(2)	85.30(6)
N(3)-Zn(1)-N(5)	89.80(5)
N(3)-Zn(1)-N(6)	90.73(5)
N(4)-Zn(1)-N(2)	179.48(5)
N(4)-Zn(1)-N(3)	95.22(6)
N(4)-Zn(1)-N(5)	88.59(6)
N(4)-Zn(1)-N(6)	91.99(6)
N(6)-Zn(1)-N(5)	179.17(5)
Zn(1)-N(1)-H(1)	107.1
C(1)-N(1)-Zn(1)	115.87(11)
C(1)-N(1)-H(1)	107.1
C(10)-N(1)-Zn(1)	105.58(11)
C(10)-N(1)-H(1)	107.1
C(10)-N(1)-C(1)	113.51(14)
Zn(1)-N(2)-H(2)	107.8
C(3)-N(2)-Zn(1)	113.93(11)

Table5-4: Bond lengths [\AA] and angles [$^\circ$] for **5-22**. Continued.

C(3)-N(2)-H(2)	107.8
C(3)-N(2)-C(4)	114.41(14)
C(4)-N(2)-Zn(1)	104.89(10)
C(4)-N(2)-H(2)	107.8
Zn(1)-N(3)-H(3)	107.8
C(5)-N(3)-Zn(1)	105.00(10)
C(5)-N(3)-H(3)	107.8
C(5)-N(3)-C(6)	113.50(14)
C(6)-N(3)-Zn(1)	114.52(10)
C(6)-N(3)-H(3)	107.8
Zn(1)-N(4)-H(4)	108.0
C(8)-N(4)-Zn(1)	113.83(11)
C(8)-N(4)-H(4)	108.0
C(8)-N(4)-C(9)	113.67(14)
C(9)-N(4)-Zn(1)	105.13(11)
C(9)-N(4)-H(4)	108.0
C(11)-N(5)-Zn(1)	162.09(15)
C(13)-N(6)-Zn(1)	161.42(14)
N(1)-C(1)-H(1A)	109.2
N(1)-C(1)-H(1B)	109.2
N(1)-C(1)-C(2)	112.00(15)
H(1A)-C(1)-H(1B)	107.9
C(2)-C(1)-H(1A)	109.2
C(2)-C(1)-H(1B)	109.2
C(1)-C(2)-H(2A)	108.3
C(1)-C(2)-H(2B)	108.3
C(1)-C(2)-C(3)	115.78(15)
H(2A)-C(2)-H(2B)	107.4
C(3)-C(2)-H(2A)	108.3
C(3)-C(2)-H(2B)	108.3
N(2)-C(3)-C(2)	111.96(15)
N(2)-C(3)-H(3A)	109.2
N(2)-C(3)-H(3B)	109.2
C(2)-C(3)-H(3A)	109.2
C(2)-C(3)-H(3B)	109.2
H(3A)-C(3)-H(3B)	107.9
N(2)-C(4)-H(4A)	109.9
N(2)-C(4)-H(4B)	109.9
N(2)-C(4)-C(5)	108.96(14)
H(4A)-C(4)-H(4B)	108.3
C(5)-C(4)-H(4A)	109.9
C(5)-C(4)-H(4B)	109.9
N(3)-C(5)-C(4)	108.76(14)
N(3)-C(5)-H(5A)	109.9

Table5-4: Bond lengths [Å] and angles [°] for **5-22**. Continued.

N(3)-C(5)-H(5B)	109.9
C(4)-C(5)-H(5A)	109.9
C(4)-C(5)-H(5B)	109.9
H(5A)-C(5)-H(5B)	108.3
N(3)-C(6)-H(6A)	109.1
N(3)-C(6)-H(6B)	109.1
N(3)-C(6)-C(7)	112.33(14)
H(6A)-C(6)-H(6B)	107.9
C(7)-C(6)-H(6A)	109.1
C(7)-C(6)-H(6B)	109.1
C(6)-C(7)-H(7A)	108.4
C(6)-C(7)-H(7B)	108.4
C(6)-C(7)-C(8)	115.43(15)
H(7A)-C(7)-H(7B)	107.5
C(8)-C(7)-H(7A)	108.4
C(8)-C(7)-H(7B)	108.4
N(4)-C(8)-C(7)	112.75(15)
N(4)-C(8)-H(8A)	109.0
N(4)-C(8)-H(8B)	109.0
C(7)-C(8)-H(8A)	109.0
C(7)-C(8)-H(8B)	109.0
H(8A)-C(8)-H(8B)	107.8
N(4)-C(9)-H(9A)	109.9
N(4)-C(9)-H(9B)	109.9
N(4)-C(9)-C(10)	109.10(15)
H(9A)-C(9)-H(9B)	108.3
C(10)-C(9)-H(9A)	109.9
C(10)-C(9)-H(9B)	109.9
N(1)-C(10)-C(9)	108.87(14)
N(1)-C(10)-H(10A)	109.9
N(1)-C(10)-H(10B)	109.9
C(9)-C(10)-H(10A)	109.9
C(9)-C(10)-H(10B)	109.9
H(10A)-C(10)-H(10B)	108.3
N(5)-C(11)-C(12)	179.3(2)
C(11)-C(12)-H(12A)	109.5
C(11)-C(12)-H(12B)	109.5
C(11)-C(12)-H(12C)	109.5
H(12A)-C(12)-H(12B)	109.5
H(12A)-C(12)-H(12C)	109.5
H(12B)-C(12)-H(12C)	109.5
N(6)-C(13)-C(14)	178.9(2)
C(13)-C(14)-H(14A)	109.5
C(13)-C(14)-H(14B)	109.5

Table5-4: Bond lengths [\AA] and angles [$^\circ$] for **5-22**. Continued.

C(13)-C(14)-H(14C)	109.5
H(14A)-C(14)-H(14B)	109.5
H(14A)-C(14)-H(14C)	109.5
H(14B)-C(14)-H(14C)	109.5
F(1)-B(1)-F(2)	108.96(16)
F(1)-B(1)-F(4)	108.75(17)
F(3)-B(1)-F(1)	110.19(18)
F(3)-B(1)-F(2)	109.12(17)
F(3)-B(1)-F(4)	109.27(16)
F(4)-B(1)-F(2)	110.55(17)
F(5)-B(2)-F(6)	103.32(18)
F(5)-B(2)-F(8)	102.9(2)
F(5)-B(2)-F(6')	107.5(2)
F(5)-B(2)-F(7')	103.8(3)
F(5)-B(2)-F(8')	126.3(2)
F(7)-B(2)-F(5)	115.81(18)
F(7)-B(2)-F(6)	111.1(2)
F(7)-B(2)-F(8)	114.7(2)
F(8)-B(2)-F(6)	108.0(2)
F(6')-B(2)-F(7')	103.7(4)
F(8')-B(2)-F(6')	107.5(3)
F(8')-B(2)-F(7')	105.8(3)

Symmetry transformations used to generate equivalent atoms:

Table 5-5: Anisotropic displacement parameters ($\text{\AA}^2 \times 10^3$) for **5-22**. The anisotropic displacement factor exponent takes the form: $-2p^2 [h^2 a^{*2} U^{11} + \dots + 2 h k a^* b^* U^{12}]$

	U11	U22	U33	U23	U13	U12
Zn(1)	14(1)	13(1)	22(1)	1(1)	10(1)	1(1)
N(1)	18(1)	18(1)	28(1)	-5(1)	13(1)	-4(1)
N(2)	24(1)	16(1)	19(1)	0(1)	10(1)	2(1)
N(3)	14(1)	18(1)	18(1)	-3(1)	8(1)	-1(1)
N(4)	20(1)	15(1)	24(1)	1(1)	9(1)	3(1)
N(5)	23(1)	22(1)	22(1)	-5(1)	8(1)	-4(1)
N(6)	22(1)	23(1)	23(1)	-7(1)	11(1)	-6(1)
C(1)	26(1)	22(1)	37(1)	-9(1)	22(1)	-11(1)
C(2)	40(1)	20(1)	32(1)	-2(1)	24(1)	-10(1)
C(3)	36(1)	14(1)	29(1)	4(1)	17(1)	0(1)
C(4)	25(1)	22(1)	26(1)	4(1)	10(1)	10(1)
C(5)	15(1)	28(1)	24(1)	-1(1)	7(1)	5(1)
C(6)	20(1)	23(1)	26(1)	-7(1)	14(1)	-9(1)
C(7)	33(1)	20(1)	28(1)	0(1)	19(1)	-6(1)
C(8)	32(1)	14(1)	33(1)	4(1)	18(1)	1(1)
C(9)	24(1)	21(1)	37(1)	2(1)	15(1)	9(1)
C(10)	16(1)	28(1)	39(1)	-3(1)	13(1)	4(1)
C(11)	22(1)	18(1)	25(1)	-1(1)	14(1)	-2(1)
C(12)	29(1)	41(1)	23(1)	-10(1)	10(1)	-9(1)
C(13)	20(1)	21(1)	27(1)	-2(1)	14(1)	-4(1)
C(14)	40(1)	46(1)	24(1)	-12(1)	15(1)	-8(1)
F(1)	39(1)	50(1)	43(1)	-12(1)	-1(1)	19(1)
F(2)	54(1)	51(1)	32(1)	-12(1)	24(1)	5(1)
F(3)	93(1)	42(1)	42(1)	-2(1)	38(1)	-22(1)
F(4)	31(1)	43(1)	38(1)	-10(1)	10(1)	-4(1)
B(1)	29(1)	25(1)	19(1)	-1(1)	11(1)	4(1)
F(5)	48(1)	49(1)	58(1)	-5(1)	15(1)	-14(1)
B(2)	32(1)	30(1)	21(1)	-3(1)	12(1)	3(1)
F(6)	52(2)	28(1)	89(2)	-4(1)	29(2)	12(1)
F(7)	48(2)	67(2)	47(2)	-15(2)	35(1)	-16(2)
F(8)	53(2)	81(3)	20(1)	9(1)	6(1)	5(2)
F(6')	152(6)	70(3)	58(3)	27(2)	16(3)	-44(4)
F(7')	36(2)	129(5)	76(4)	-54(3)	22(2)	6(2)
F(8')	50(2)	57(3)	28(2)	-16(2)	21(1)	-7(2)

Table 5-6: Hydrogen coordinates ($\times 10^4$) and isotropic displacement parameters ($\text{\AA}^2 \times 10^3$) for **5-22**.

	x	y	z	U(eq)
H(1)	4136	5572	8213	24
H(2)	5828	3244	8678	23
H(3)	5813	4203	6517	19
H(4)	4077	6532	6039	24
H(1A)	3347	2747	7245	31
H(1B)	3148	3508	7967	31
H(2A)	3997	1243	8523	33
H(2B)	4575	2855	8894	33
H(3A)	5238	581	8474	30
H(3B)	4633	1045	7551	30
H(4A)	5903	1553	7329	29
H(4B)	6585	1490	8259	29
H(5A)	6904	4388	8192	27
H(5B)	7053	3357	7498	27
H(6A)	6792	6317	6796	26
H(6B)	6553	7049	7498	26
H(7A)	5365	6921	5833	30
H(7B)	5932	8545	6209	30
H(8A)	5268	8752	7155	30
H(8B)	4669	9175	6226	30
H(9A)	3342	8304	6478	32
H(9B)	4039	8239	7401	32
H(10A)	2895	6462	7268	33
H(10B)	3004	5428	6555	33
H(12A)	3000	2902	4459	46
H(12B)	2592	1753	4928	46
H(12C)	3328	1019	4714	46
H(14A)	6753	8664	9964	54
H(14B)	6523	6972	10307	54
H(14C)	5852	8469	9985	54

Single Crystal X-ray structural data for $[\text{Zn}(\text{cyclam})](\text{BF}_4)_2$ is deposited under CCDC number **CCDC 1562780**.

VIII. Acknowledgements.

The material in Chapter 5, has been published in *Dalton Trans* in 2017 with the following authors: Zhanaidarova, A.; Steger, H.; Reineke, H. M.; Kubiak, C. P. The dissertation author was the primary investigator and author of this material.

IX. References

1. Diffenbaugh, N. S.; Burke, M. *PNAS*. **2019**, 116, 9808-9813. “Global warming has increased global economic inequality”.
2. Hughes, T. P.; Kerry, J. T.; Baird, A. H. et al. *Nature*. **2019**, 568, 387-390. “Global warming impairs stock-recruitment dynamics of corals”.
3. Meehl, G. A.; Washington, W. M.; Collins, W. D.; Arblaster, J. M.; Hu, A. *Science*. **2005**, 18, 1769-1772. “How much more global warming and sea level rise?”.
4. Mendelsohn, R.; Nordhaus, W. D.; Shaw, D. *The American Economic Review*. **1994**, 84, 753-771. “The impact of global warming on agriculture: a Ricardian analysis”.
5. Gunathilake, C. A.; Ranathungem G. G. T. A.; Dassanayake, R. S.; Illesinghe, S.D.; Manchanda, A. S.; Kalpage, C. S.; Rajapakse, R. M. G.; Karunaratune, D. G. G. P. *Environ. Sci.: Nano*. **2020**, 7, 1225-1239. “Emerging investigator series: synthesis of magnesium oxide nanoparticles fabricated on a graphene oxide nanocomposite for CO₂ sequestration at elevated temperatures”.
6. Mikkelsen, M.; Jorgensen, M.; Krebs, C. F. *Energy Environ. Sci.* **2010**, 3, 43–81. “The teraton challenge. A review of fixation and transformation of carbon dioxide”.
7. Yu, C. H.; Huang, C. H.; Tan, C. S. *Aerosol Air Qual. Res.* **2012**, 12, 745–769. “A review of CO₂ capture by absorption and adsorption”.
8. Hori, Y. “Modern Aspects of Electrochemistry”, *Springer*, New York, **2008**, vol. 42, ch. 3, pp. 89–189.
9. Spall, S. J. P.; Keane, T.; Tory, J.; Cocker, D. C.; Adams, H.; Fowler, H.; Meijer, A. H. H. M.; Hartl, F.; Weinstein, J. A. F. *Inorg. Chem.* **2016**, 55, 12568–12582. “Manganese tricarbonyl complexes with asymmetric 2-iminopyridine ligands: Toward decoupling steric and electronic factors in electrocatalytic CO₂ reduction”.

10. Cook, R. E.; Phelan, B. T.; Shoer, L. E.; Majewski, M. B.; Wasielewski, M. R. *Inorg. Chem.* **2016**, *55*, 12281–12289. “Effect of perylene photosensitizer attachment to [Pd(triphosphine)L]²⁺ on CO₂ electrocatalysis.
11. Barton, E. E.; Rampulla, M. D.; Bocarsly, B. A. *J. Am. Chem. Soc.* **2008**, *130*, 6342–6344. “Selective solar-driven reduction of CO₂ to methanol using a catalyzed p-GaP based photoelectrochemical cell”.
12. Benson, E. E.; Kubiak, C. P.; Sathrum, J. A.; Smieja, J. M. *Chem. Soc. Rev.* **2009**, *38*, 89–99. “Electrocatalytic and homogeneous approaches to conversion of CO₂ to liquid fuels”.
13. Fei, H.; Sampson, M. D.; Lee, Y.; Kubiak, C. P.; Cohen, S. M. *Inorg. Chem.* **2015**, *54*, 6821–6828. “Photocatalytic CO₂ reduction to formate using a Mn(I) molecular catalyst in a robust metal-organic framework”.
14. Smieja, J. M.; Sampson, M. D.; Grice, K. A.; Benson, E. E.; Froehlich, J. D.; Kubiak, C. P. *Inorg. Chem.* **2013**, *52*, 2484–2491. “Manganese as a substitute for rhenium in CO₂ reduction catalysis: The importance of acids”.
15. Sampson, M. D.; Nguyen, A. D.; Grice, K. A.; Moore, C. E.; Rheigold, A. L.; Kubiak, C. P. *J. Am. Chem. Soc.* **2014**, *136*, 5460–5471. “Manganese Catalysts with Bulky Bipyridine Ligands for the Electrocatalytic Reduction of Carbon Dioxide: Eliminating Dimerization and Altering Catalysis”.
16. Bhugun, I.; Lexa, D.; Saveant, J. *J. Am. Chem. Soc.* **1996**, *118*, 19981–19985. “Catalysis of the electrochemical reduction of carbon dioxide by iron (0) porphyrins. Synergistic effect of Lewis acid cations”.
17. Fujita, E.; Chou, M.; Tanaka, K. *Appl. Organomet. Chem.* **2000**, *14*, 844–846. “Characterization of Ru(bpy)₂(CO)(COO) prepared by CO₂ addition to Ru(bpy)₂(CO) in acetonitrile”.
18. Sampson, M. D.; Kubiak, C. P. *J. Am. Chem. Soc.* **2016**, *138*, 1386–1393. “Manganese electrocatalysts with bulky bipyridine ligands: Utilizing Lewis acids to promote carbon dioxide reduction at low overpotentials”.
19. Tripiper, F. R.; Chuburu, F.; Baccon, M. L.; Handel, H. *Tetrahedron*, **2003**, *59*, 4573–4579. “Phenylglyoxal for polyamines modification and cyclam synthesis”.
20. Penzien, J.; Abraham, A.; Bokhoven, J. A.; Jentys, A.; Muller, T. E.; Siever, C.; Lercher, J. A. *J. Phys. Chem. B*, **2004**, *108*, 4116–4126. “Generation and Characterization of Well-Defined Zn²⁺ Lewis Acid Sites in Ion Exchanged Zeolite BEA”.
21. Evans, D. A.; Kozlowski, M. C.; Tedrow, J. S. *Tetrahedron Lett.* **1996**, *37*, 7481–7484. “Cationic bis (oxazoline) and pyridyl-bis (oxazoline) Cu (II) and Zn (II) Lewis acid catalysts. A comparative study in catalysis of Diels-Alder and aldol reactions”.

22. Liang, X.; Weishaupl, M.; Parkinson, J. A.; Parsons, A.; McGregor, P. A.; Sadler, P. J. *Chem. Eur. J.* **2013**, *9*, 4709–4717. “Selective recognition of configurational substates of zinc cyclam by carboxylates: implications for the design and mechanism of action of anti-HIV agents”.
23. Saveant, J. M.; Vianello, E. *Electrochim. Acta*, **1962**, *8*, 905–923. “Potential-sweep chronoamperometry theory of kinetic currents in the case of a first order chemical reaction preceding the electron-transfer process”
24. Bard, A. J.; Faulkner, R. L. *Electrochemical Methods*, Wiley, New York, **1980**.